UNIVERSITY OF HULL

Investigating the impact of interstitial fluid flow on cancer biology

Being a Thesis Submitted for the Degree of

Doctor of Philosophy

at the University of Hull

by

Emily Seton Pyne

BSc, MSc

November 2022

Abstract

Despite major advances in our understanding of cancer progression mechanisms, cancer remains a leading cause of death in the UK and globally. Solid tumours are complex, and heterogeneous, existing in a dynamic microenvironment subjected to a variety of biomechanical cues. Conventional cancer research methods have long relied on two-dimensional (2D) static cultures which neglect the dynamic, three-dimensional (3D) nature of the tumour microenvironment (TME), especially the role of interstitial fluid (ISF) and the impact of interstitial fluid flow (IFF). In order to address this, we have developed and optimised a spheroid-on-chip microfluidic platform which allows 3D cancer spheroids to be integrated into extracellular matrices (ECM)-like hydrogels and exposed to continuous perfusion, mimicking IFF in the TME. Our platform enables clear imaging of spheroids, analysis of effluent media, and harvesting of spheroids for further analyses. Where many studies have focused on perfusion as a tool mainly for high-throughput methods, we aim to identify how perfusion, mimicking IFF in the TME, alters the biology of cancer spheroids.

Spheroids exposed IFF-like or static conditions were harvested, and gene and protein expression analysis was performed. These data indicated that gene expression was altered by flow when compared to static conditions, but clear functional patterns were not identifiable. Subsequently, a large-scale transcriptomic analysis by RNA-sequencing was used to conduct an unbiased analysis, revealing robust gene expression changes in genome preservation pathways and leading to the identification of a potential biomarker of IFF in cancer.

Our spheroid-on-chip flow platform has revealed that exposure to IFF-like conditions in a 3D environment significantly altered the transcriptome of spheroids after just 24 hours, leading to changes in the expression of key factors involved in various aspects of tumour progression. These results will direct our future work on further elucidating the role of ISF flow in cancer biology and spread.

Acknowledgements

Isabel and Nicole, I'll never be able to truly thank you enough for your supervision during my PhD. You are two of the most brilliant people I know, and certainly two of the kindest. It has been a pleasure working with you both and I consider myself extremely lucky to have had the opportunity to work in your labs. Thank you for everything.

Thank you as well to Dr Alex Iles and Dr Martin Christensen for their invaluable contributions to this work. Alex, this project truly would not have been possible without your microfluidics wisdom and design knowledge. I am very grateful to have had the opportunity to work with such talented researchers.

I would like to say thank you to all my lab colleagues of past and present for making my time doing research in the lab an enjoyable experience. Moving to a new country to start my PhD was a challenging experience, but I can honestly say it was made better by the welcome I received from everyone at that time and the continued kindness of colleagues today.

Most especially, Leah and Kelly – I'm so grateful to have gained your friendship through this experience. Kelly, you truly made commutes to and from the lab more bearable but also a lot more fun.

To my partner Chris, I can't thank you enough for your steadfast support and love. And my sweet Winnie: I know you can't read this, but I want everyone to know that there are so many days I would have fallen apart if it weren't for your unconditional love. Brenda and Collin, thank you too for your love and support throughout this process.

And finally, to my family, I want to say the biggest thank you of all. I love you all very much. Mom and Dad, I wouldn't have been able to do this or accomplish so many other things in my life if it weren't for you. I am deeply grateful for this and all the other opportunities you've provided for me. Beth, you've always been a guiding force in my life and the best big sister I could ask for. In many ways your pursuit of knowledge has inspired my own, leading me to this journey. Thank you for forging the path ahead and always being there when I need you.

Contents

List of Figures

List of Tables

List of Abbreviations

2D: two dimensional

3D: three dimensional

ATCC: American Type Culture Collection

ATR: ataxia telangiectasia and Rad3-related

B2M: β-2-microglobulin

bp: base pair

BRCA1: breast cancer 1, early onset

BRCA2: breast cancer 2, early onset

BSA: bovine serum albumin

°C: degree Celsius

CA9: carbonic anhydrase IX

CAFs: cancer-associated fibroblasts

cDNA: complementary DNA

CDX: cell-derived xenograft

CNC: computer numerical control

CO_2: carbon dioxide

DEG: differentially expressed gene

DFS: disease-free survival

DMEM: Dulbecco's Modified Eagle Medium

DMFS: distant metastasis-free survival

DMSO: dimethyl sulfoxide

DNA: deoxyribonucleic acid

dNTP: deoxynucleotide triphosphate

ECM: extracellular matrix

EDTA: ethylenediaminetetraacetic acid

ELISA: enzyme-linked immunosorbent assay

EMT: epithelial to mesenchymal transition

ER: oestrogen receptor

FBS: fetal bovine serum

FDA: fluorescein diacetate

FDR: false discovery rate

G: gram

x *g*: gravity acceleration

h: height

h: hour

HER2: human epidermal growth factor receptor

HIF: hypoxia inducible factor

HK2: hexokinase 2

HNSCC: head neck squamous cell carcinoma

HR: hazard ratio

ID: inner diameter

IFF: interstitial fluid flow

IS-ECM: interstitial extracellular matrix

ISF: interstitial fluid

kDa: kilodalton

L: litre

l: length

LOC: lab-on-a-chip

LOX: lysyl oxidase

M: molar

Min: minutes

Mm: millimetre

MMP: matrix metalloproteinase

mRNA: messenger ribonucleic acid

NTC: no template control

O2: oxygen

OS: overall survival

PBS: phosphate-buffered saline

PDMS: polydimethylsiloxane

pH: potential of hydrogen

PR: progesterone receptor

PTFE: polytetrafluoroethylene

PVDF: polyvinylidene difluoride

qPCR: quantitative polymerase chain reaction

RNA: ribonucleic acid

ROS: reactive oxygen species

rpm: rotations per minute

RPMI: Roswell Park Memorial Institute medium

SDS-PAGE: sodium dodecylsulfate polyacrylamide gel electrophoresis

Sec: second

SEM: standard error mean

TBS: Tris-buffered saline

TEMED: tetramethylethylenediamine

TME: tumour microenvironment

TNBC: triple negative breast cancer

ULA: ultra low adherence

UTB: Urea Tris buffer

V: volt

v: volume

VEGF: vascular endothelial growth factor

w: width

Chapter 1 General Introduction

1.1 Cancer overview

Cancer is a diverse family of over 100 diseases that are all characterised by uncontrolled growth and division of cells in a particular region of the body (Hanahan & Weinberg, 2011). It continues to be a major health issue facing modern society and receives substantial research attention and funding each year around the world (Love, 2010). It is a global issue with 19.3 million new cancer cases as well as 10 million cancer deaths worldwide in 2020 (excluding nonmelanoma skin cancer) (Sung et al., 2021). In the United Kingdom alone, it is estimated that 50% of individuals born after 1960 will develop cancer (Ahmad et al., 2015). Indeed, with the increasingly aging population it is expected that the global cancer burden will escalate, highlighting how it has and will continue to be a major health burden

The biology of cancer is recognised as having a set of key characteristics, or hallmarks, which are essential to development of the disease. These hallmarks have been identified and assessed over decades of research, culminating in the following list outlined by Hanahan and Weinberg (Hanahan & Weinberg, 2011):

Growth signal self-sufficiency: Normal cells are dependent on external growth signals for proliferation. In contrast, cancer cells are able to generate most of the necessary growth signals themselves. Cancer cells are capable of increasing the expression of growth factor receptors on their surface, becoming hypersensitive to growth signalling ((Velu et al., 1987; Gullick, 1991). Additionally, some cancer cells have been shown to send signals to normal cells in the area to induce growth factor suppression in the normal cells (Gleave et al., 1993). This reduces and, in some cases, even eliminates their dependency on external stimuli.

Evasion of growth suppressors: In normal tissues, homeostasis is maintained by multiple antiproliferative signals. These signals direct normal cells out of the cell cycle into either a terminal, post-mitotic differentiation state or a temporary quiescent state. Cancer cells have the capacity to evade such antiproliferative signals and therefore overcome normal growth limitations such as contact inhibition and induction of apoptosis (Amin et al., 2015).

Evasion of programmed cell death: Cell proliferation and death are tightly monitored and finely balanced processes in normal cells. These processes are regulated by complex signalling pathways involving pro- and anti-apoptotic factors. Cancer cells are able to disrupt this signalling balance through mutations in key genes connected to survival regulation to evade cell death regulation mechanisms and thus live longer (Paul-Samojedny et al., 2005).

Replicative immortality: Hand in hand with evasion of growth suppressors and programmed cell death, cancer cells are able to overcome senescence and escape apoptosis, becoming essentially

immortal. In most normal cells, telomeres are also shortened after each cycle of cell division (Jiang et al., 2007). This results in a limited number of cell divisions that a normal cell can undergo. In cancer cells, however, modification to telomerase activity (the enzyme responsible for maintenance of telomere length) contributes to unlimited cell division (Akincilar et al., 2016; Kulic et al., 2016).

Angiogenesis induction: It has been established that tumours are able to release pro-angiogenic signals to trigger the formation of new vasculature. In normal conditions, vasculature is quiescent except during wound-healing or the female menstrual cycle (Schlereth et al., 2018). Tumours manage to hijack angiogenic signalling to meet their increased need for oxygen and nutrients as they expand (Carmeliet et al., 1998). Tumour vasculature is unorganised and chaotic compared to normal vasculature which often results in poorly oxygenated areas, also known as hypoxic regions. (Brown & Giaccia, 1998; Brown & Wilson, 2004).

Invasion and metastasis activation: Normal cells are anchorage-dependent and are reliant on cell-cell interactions and adhesion to survive. Without the ability to adhere and form junctions with other cells, normal cells would not survive. Cancer cells, on the other hand, are able to overcome anchorage-dependence to live without attachment to a matrix or other cells (Wirtz et al., 2011). In fact, cancer cells are capable of degrading matrices to invade tissue and ultimately disseminate to other tissues in the body, a process known as metastasis (Nistico et al., 2012). Importantly, metastasis is responsible for the vast majority of cancer deaths. Metastasis and the series of events leading up to it, known as the metastatic cascade, will be detailed more in the following section (1.2).

Energy metabolism reprogramming: In aerobic conditions, oxidative phosphorylation (OX-PHOS) is the most common energetic pathway used by cells. However, the increased cell populations present in tumours create an increase in energetic needs. Anaerobic conditions also mean that oxygen resources are scarce, so glycolysis is used to form pyruvate and lactate. Even when cancer cells are in an aerobic environment though, they are able to use this anaerobic metabolism, a process known as the Warburg effect (Warburg, 1956). It frees them from the constraints of O_2 availability and also increases their need for glucose which in turn results in overexpression of glucose transporters (Denko, 2008). This mechanism is technically less efficient but it is faster and produces intermediate precursors used by cancer cells as building blocks to make proteins, DNA, and lipids to support fast proliferation (Zheng, 2012).

Evasion of immune system: In some studies, immunosuppressed mice were found to develop more tumours compared to wild type counterparts following exposure to carcinogenic compounds. Furthermore, mice that lacked cytotoxic and helper T cells or natural killer cells

grew tumours faster (Teng et al., 2008). Observations such as these lead to hypotheses that some cancer cells were more immunogenic than others and the more discreet cells with less immunogenicity were able to evade detection by the immune system. These cancer cells could grow undetected by immune surveillance, contributing to increased survival rates of cancer cells compared to normal cells.

1.2 Metastasis

Metastasis is a crucial step in cancer progression which radically affects clinical outcomes. Cancers found prior to metastasis are easier to treat, and patients have a better chance of survival (Mehlen & Puisieux, 2006b). Most research has focused on the oncogenic transformations that lead to the occurrence of a primary tumour while there is a lack of comprehensive understanding around the metastatic process, despite the clinical relevance of metastasis (Gupta & Massague, 2006). Metastasis as a general term refers to the spread of cancer from a primary tumour to distant sites in the body. More specifically though, it is a complex series of events known as the metastatic cascade which occur as a cumulative progression over time and ultimately result in systemic spread. Less than 0.1% of cancer cells that leave a primary tumour site successfully develop a distal metastasis (Fidler, 1970). In order to beat the odds and successfully metastasize, tumour cells must locally invade the adjacent tissue, intravasate via transendothelial migration into vessels, survive in the circulatory system, extravasate, and finally they must proliferate at the distant site to colonize and survive (Hanahan & Weinberg, 2011).

It is well understood that cancer is a major cause of death, and most cancer deaths are caused by metastasis. The importance of metastasis and the early changes that occur in tumour progression are recognised as crucial areas of research. Identifying how to prevent a permissive niche which allows cancer to progress, rather than trying to treat it after it has advanced and spread to other areas of the body, is a pertinent research question that could lead to clinically relevant therapeutics.

1.2.1 The metastatic cascade

The metastatic cascade is the specific set of steps in which tumour cells from a primary tumour site become motile and invasive and ultimately, spread throughout the body (Mehlen & Puisieux, 2006a). The steps include: 1) primary tumour formation, 2) local invasion, 3) intravasation, 4) survival in circulation, 5) arrest at distant site, 6) extravasation, 7) development of micrometastases, and 8) colony formation. These steps are visually summarised in Figure 1.1.

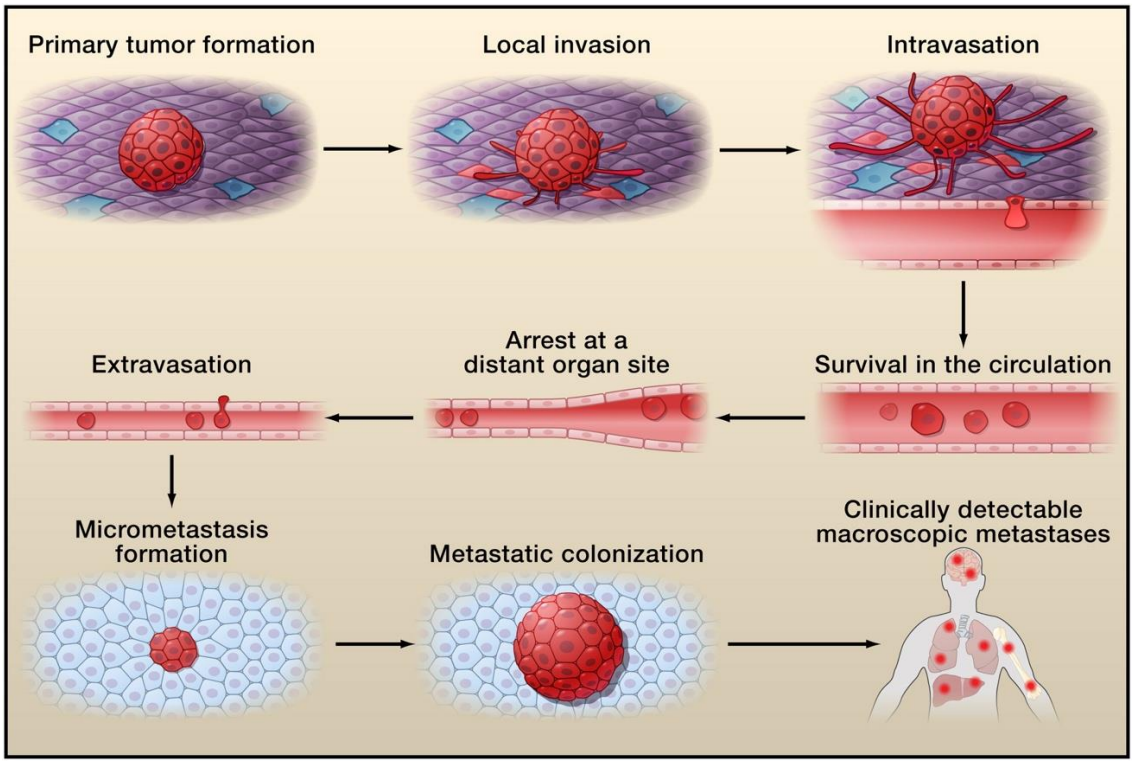

Figure 1.1: The metastatic cascade

The series of cell-biological events comprising the metastatic cascade are summarised above. Tumour cells (primary tumour formation) leave primary sites of growth (local invasion and intravasation) and travel to other areas of the body (survival in the circulation and arrest at a distant organ site) where they infiltrate foreign microenvironments (extravasation) and adapt to their new surroundings (micrometastasis formation and metastatic colonization) to ultimately survive and grow there. Cancer cells are depicted in red. Figure from (Valastyan & Weinberg, 2011).

During this cascade of events cancer cells experience a change in phenotype where they lose epithelial characteristics such as intercellular junctions and apico-basal polarity and develop a more flexible mesenchymal phenotype. This is known as the epithelial to mesenchymal transition (EMT) and is crucial to the motility of cancer cells, contrasting with their anchored, epithelial counterparts.

EMT has long been recognised as a crucial step in metastasis. However, our current understanding of EMT in metastasis is mainly based on single-cell motility; we now know that when metastasis is caused by cancer cell clusters, or spheroids, EMT is not necessary (Fang et al., 2015; Lu et al., 2015). Indeed, clusters are better at surviving in circulation and more aggressive in colonizing distant metastatic sites than single cells are (Aceto et al., 2014; Herath et al., 2020). Now that our understanding of the metastatic process is changing, our research models must start to reflect what we've learned. Incorporating new 3D techniques, as will be discussed in a later section, is an excellent way to begin examining metastasis in this new light.

1.3 Breast cancer

Breast cancer is the most common cancer type affecting women in the UK and represents 30% of cancer cases in women (source: Cancer Research UK 2022). Factors contributing to the causes of breast cancer include age, family history, lifestyle, and most notably, mutations of specific genes. *BRCA1* (breast cancer 1, early onset) and *BRCA2* (breast cancer 2, early onset) are two such genes who have strongly established links to breast cancer occurrence (Miki et al., 1994; Wooster et al., 1995). Breast cancer is also one of the most hypoxic cancer types and is known to metastasise to the lungs, bones, and liver most often (Leong et al., 2006; McKeown, 2014)).

Breast cancer subtypes have been identified and classified as a way to tailor therapeutic approaches chosen for patients (Onitilo et al., 2009; Prat et al., 2015). Subtypes are determined by the expression status of three receptors which play roles in determining a tumour's metabolism and responsiveness to chemotherapeutics, as well as predicting patient survival rates (Heldring et al., 2007; Haque et al., 2012). The three receptors are: ER (oestrogen receptor), PR (progesterone receptor), and HER2 (human epidermal growth factor receptor). Table 1.1 outlines the main breast cancer subtypes according to receptors expression status.

Table 1.1: Main breast cancer subtypes according to receptors expression status

Breast cancer subtype	ER status	PR status	HER2 status
Luminal A	+	+	−
Luminal B	+	+	+
HER2	−	−	+
Basal/ triple negative	−	−	−
ER: oestrogen receptor; PR: progesterone receptor; HER2: human epidermal growth factor receptor			

1.4 Tumour microenvironment

Our understanding of tumours has shifted over decades of research, from thinking of a tumour as an isolated, somewhat foreign, entity in the body to an integrated, albeit abnormal, structure in a dynamic, heterogeneous environment. Thus, research has shifted away from thinking of a tumour as an isolated entity and towards recognising the complexity of it both internally and externally (Xu et al., 2014). A tumour is not a homogeneous mass of cancer cells but rather a highly heterogeneous community. It is comprised of various cell types that also interact with surrounding cells, tissues, and fluids (Figure 1.1) (Joyce & Pollard, 2009). A tumour is complex in both its internal diversity and its dynamic nature. The interactions that occur between a tumour and the stromal microenvironment are important for progression of cancer, including initiation of metastasis (Fan et al., 2017). Therefore, in order to understand the occurrence of metastasis it is critical to understand the tumour microenvironment (TME) and its role.

One of the most common cell types found to interact with cancer cells in the TME is fibroblasts (Orimo et al., 2005). These cancer-associated fibroblasts (CAFs) play an active role in promoting tumour growth and support the tumour in numerous capacities, such as structure, angiogenesis, and invasion (Bhowmick et al., 2004). Various studies have demonstrated that CAFs produce factors that directly contribute to the transformation of epithelial cells (Olumi et al., 1999; Gaggioli et al., 2007). Fibroblasts can influence carcinogenesis by producing growth factors, mostly stimulators of proliferation, which are involved in both the initiation of a tumour and its progression (Bhowmick et al., 2004). Additionally, CAFs can inhibit immune cell access to the TME and inhibit their functions within the tumour. In effect this means that the CAFs are not only working with the cancer cells, but they are working *against* other cells that may be trying to prevent tumour growth (Denton et al., 2018)

When immune cells are not working against the cancer (or being inhibited by CAFs), they too can be reprogrammed to support the cancer. It is thought that under the influence of the TME, immune cells such as macrophages and neutrophils can be activated to favour tumour growth

and progression (Kim & Bae, 2016). Indeed, neutrophils are a strong example of how the TME can dramatically alter the normal function of a tissue. Although neutrophils are generally considered the first line of defence against infections and other foreign invasions to the body, it is now known that they are also involved in various cancer biology mechanisms. Some studies suggest that they promote metastatic arrest at distant sites, and others suggest that they support angiogenesis (Tazzyman et al., 2013; Wculek & Malanchi, 2015). Regardless of their specific role in permitting or promoting tumour growth, it is evident that neutrophils and other immune cells are key players in a thriving TME and must be considered in the heterogeneity of a tumour.

1.5 Tumour interstitium and interstitial fluid

In recent years there has been an elevated interest in ISF, a component that was largely ignored for many decades. The composition of ISF in normal stroma vs tumour stroma varies greatly, and indeed it has been shown to play a crucial role in the development of a tumour. Now there is a focus on trying to understand the ways that it permits, or promotes, metastasis. Specifically, foundational work has been done on the role of IFF and the impact it may have on EMT and early changes in tumour progression. Up to 20% of the body's mass is estimated to be interstitial fluid (ISF), occupying the interstitium; the spaces outside the blood/lymphatic vessels and parenchymal cells where the connective and supporting tissues of the body reside (Wiig & Swartz, 2012; Brinkman & Sharma, 2019). ISF is synonymous with extracellular fluid, or extracellular medium. Additionally, 'interstitial extracellular matrix' (IS-ECM) describes the structural molecules in the interstitial space and its community of cells such as fibroblasts, dendritic cells, and other stromal cells. The traditional perspective of the interstitium does not include a role for cells, but more recently they have been established as an integral component (Aukland & Nicolaysen, 1981; Aukland & Reed, 1993; Freitas et al., 1997). The stromal cells present in the interstitium play crucial roles in initiating immune responses, regulating fluid volume, and continuously communicating with the ECM to regulate the microenvironment (Randolph et al., 2005; Reed & Rubin, 2010). It follows that in the context of a tumour, the IS-ECM and ISF are highly involved in the abnormal pathology that occurs, and a better understanding of their roles in cancer progression could lead to better treatment insights.

Indeed, tumour ISF and the resulting pressure accumulated in the TME has already been implicated in disrupting the delivery of chemotherapy to a tumour (Jain, 1990). Pressure builds as a result of abnormal vasculature and the abnormal tumour stroma. A drug must migrate through this altered interstitium to reach cancer cells in solid tumours. Normally, ISF pressure in a tissue is close to 0 mmHg (considered subatmospheric) (Iversen et al., 2001). In tumours though, it is significantly elevated and has been shown as high as 10 to 100 mmHg in human and

animal tumour tissues (Nathanson & Nelson, 1994; Milosevic et al., 2004). One study even found pressure from ISF to be an independent predictor of cervical cancer recurrence, suggesting a crucial role of the fluid in treatment success (or lack thereof) (Milosevic et al., 2004).

In addition to pressure, other biomechanical forces are at work in the interstitium. *Stress* refers to an applied force per unit area, whereas *strain* is the deformation of a structure under mechanical stress. Pressure plays a role in all of these mechanical components of the interstitium. In fact, because interstitial space is porous, elastic, and has a medium (ISF), both fluid and solid stresses are present and furthermore, are intrinsically coupled. If a tissue is perfused, this causes increased (local) pressure. That pressure will exert tensile forces on the ECM, or mechanical solid stress. The change in pressure also changes the pressure gradient, resulting in fluid interstitial flow (IFF) (Wiig & Swartz, 2012). As discussed in the above section, the tumour stroma is altered and this abnormal pathology results in the biomechanical stresses and strains described here. The velocity of interstitial fluid *in vivo* is generally accepted as being in the range of 1×10^{-4} – 10 mm s^{-1}, although it is still poorly characterised (Wiig & Swartz, 2012; Wagner & Wiig, 2015).

1.6 Cancer research models

Given the many complexities of cancer, researchers have accordingly developed numerous models for studying it over the years. There are a range of established models, with the most common being *in vivo* animal models, such as mice or zebrafish, and *in vitro* cell lines (Galuschka et al., 2017). An assortment of other models exist on the spectrum between 2D *in vitro* and 3D animal models, and each model has pros and cons that must be considered.

2D monocultures involve culturing a cell line on flat and rigid substrate surfaces, effectively ignoring the 3D components of an *in vivo* environment (Figure 1.2). This method has provided the advantage of simple, cost-effective approaches to research, but over time have been revealed to often produce nonpredictive or even misleading results (Mehta et al., 2012). The interactions between the ECM of cells in 2D is vastly reduced and this has downstream effects on other aspects such as transport of molecules and binding of integrins (Mehta et al., 2012). Indeed, it has been shown that due to the flat morphology of cells in 2D, genetic aberrations can occur over time. These differences from the tissue origin in genetic and protein expression in 2D are likely the cause of the exponential growth exhibited in 2D cultures (Edmondson et al., 2014). The traditional use of homogeneous 2D cell models neglects the complex dynamics of a tumour and especially the 3D interactions with its environment. In sum, there are many ways that 2D culture vastly oversimplifies the 3D TME and these models best serve for answering simple, baseline questions

On the other end of the spectrum from 2D cultures, there are *in vivo* models which use animals to study cancer. Animal models can be used for drug screening, invasion, growth kinetics, and migration studies (Nunes et al., 2019a). There are variations of the *in vivo* model such as the cell derived xenograft (CDX) and the patient derived xenograft (PDX). In CDX, human tumour cells are subcutaneously implanted into an immunocompromised mouse and the tumour can be studied, but only at advanced disease stages (Holen et al., 2017). Similarly, a PDX uses human tumour fragments implanted into an immunocompromised mouse, inducing the mouse stroma to replace the human cells over time. While these models are 3D and can better replicate some facets of the TME, they are expensive, require ethics, and are relatively low throughput (depending on financial constraints). PDX models also poorly simulate the initial formation of the TME, and they rarely produce successful metastasis (Hidalgo et al., 2014).

Further to 2D cultures but not at the level of *in vivo* models there are 3D multicellular spheroids. Spheroids have been used in cancer research more frequently in recent years due to the characteristics they share with mammalian tumours. They contain distinct zones – a core, a quiescent layer of cells, and an external layer of proliferative cells – which is important especially in drug testing (Hamilton, 1998; Mehta et al., 2012). The zones result in a heterogeneous acquisition of nutrients and oxygen diffusion throughout the spheroid, which is similar to what is seen in tumours (Grimes et al., 2014). Another advantage of spheroids in research is that they can be seeded and formed at different sizes, and through certain methods can be uniformly reproduced. This is especially advantageous for high-throughput needs, such as in drug efficacy testing. The genotype and protein expression of spheroids also more closely resemble *in vivo* tumours than 2D cultures (Katt et al., 2016). Another interesting aspect of spheroids is that they naturally occur in some cases of cancer in the body, usually known as cancer cell clusters in those scenarios (Hong et al., 2016). This further demonstrates the relevance of using them in laboratory research with the goal of translating that research to clinical use. Spheroids also do not require complex ethics like *in vivo* animal models, and they are less expensive than animal research (Edmondson et al., 2014)

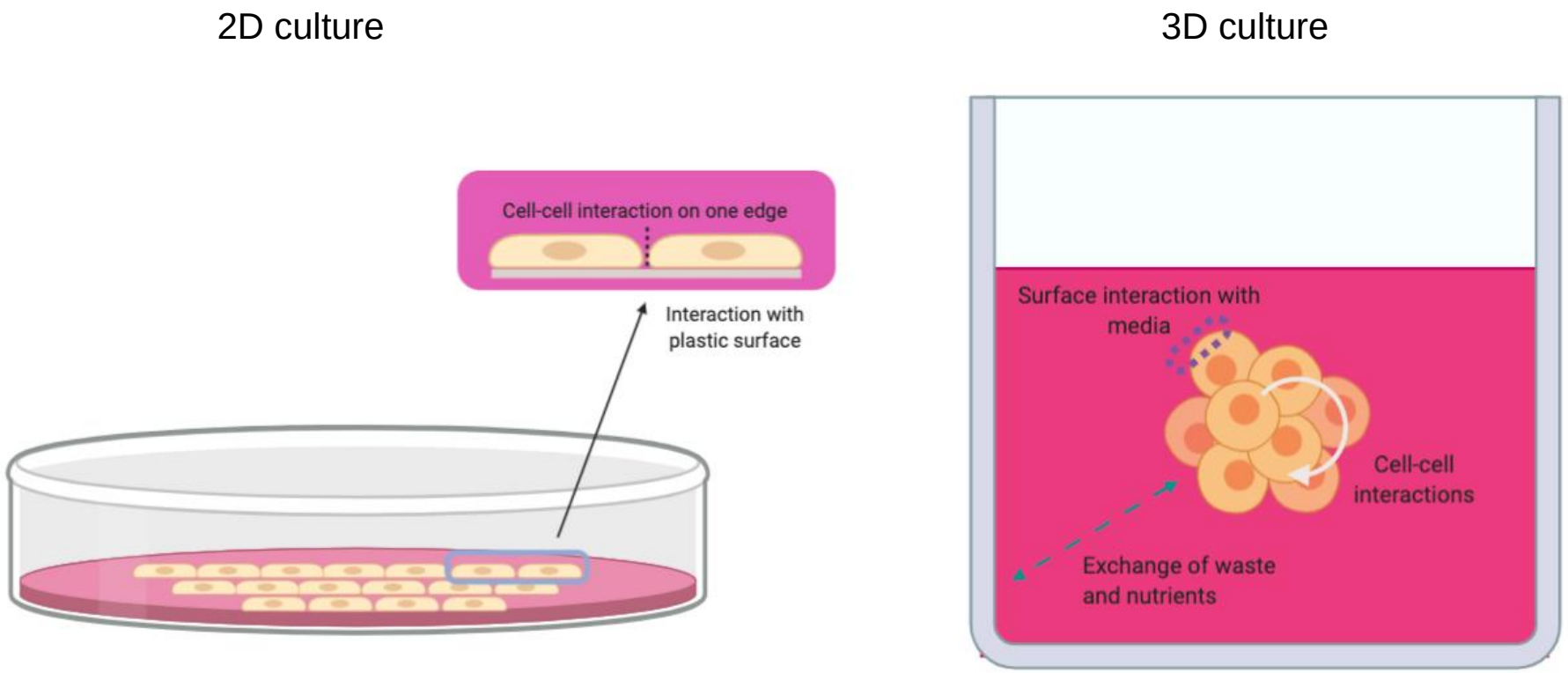

Figure 1.2: 2D vs. 3D culture

Cells cultured in 2D exist in a monolayer resulting in cell-cell interactions only on one edge and predominantly interaction with a plastic surface. In 3D culture, there is increased surface interaction with the surrounding media, cell-cell interactions in multiple dimensions, and a gradient for exchange of waste and nutrients through the 3D cell mass. Figure created in Biorender.com.

The complexities of cancer are inherently difficult to fully replicate in a research setting. Research models ranging from 2D monocultures to animal models provide an array of choice for experimental setup, but each has pros and cons. 3D spheroids are a useful medium given that they are better at recapitulating the TME than 2D cultures, but less costly and difficult than animal models. Furthermore, they are reproducible and efficient for high throughput testing. Spheroids share important characteristics with mammalian tumours that are helpful in capturing the complexities of the dynamic, 3D TME. The question of how a tumour progresses to the point of metastasis cannot be answered without addressing the complex nature of the TME, and more research is needed which aims to better reproduce the dynamic network comprising the TME. Indeed, in recent years, questions have been raised about the models used to study cancer and especially the TME.

1.7 Microfluidics for cancer research

Research models have changed substantially in attempts to better mimic the TME and its complex interactions, such as with the use of microfluidic models. Microfluidic lab-on-a-chip (LOC) devices offer a multitude of advantages for cancer cell biology research such as precise control over nutrients, internal and external control of temperature, and the ability to induce laminar flow and/or shear stress to reproduce important biophysical forces (Whitesides, 2006). Many approaches to studying cancer on-chip have been employed in recent years, and some studies have also used spheroids, hydrogels/matrices, spheroids, and co-culture techniques on-chip. Various studies have also attempted to model the TME on-chip by exploiting the precise control microfluidic devices offer over local gradients and composition of the small chambers. Microfluidic devices offer another important advantage over the use of 2D or 3D cultures off-chip: continuous flow. While spheroids have been a great advancement from 2D monoculture practices, they are generally still housed in static conditions. As discussed above in section 1.4, the reality of the TME is that it is dynamic, heterogeneous, and it experiences a constant array of biomechanical fluid and solid forces. Microfluidic devices offer a solution to bridging the gap between 3D culture and the dimension of biomechanical forces with their control of fluid flow.

To address the question of heterogeneity, LOC approaches have looked at CAFs, tumour-associated macrophages, and stromal cells. Indeed, one study used continuous media supplementation on-chip to examine migration speeds of lung cancer cells when influenced by stromal cells. They identified the role of TGF-B1 in this interaction and the increased migration speeds observed when stromal cells were present (Xu et al., 2013). Another study observed mutual interactions between CAFs and 3D tumour spheroids embedded in hydrogels on-chip, but did not use continuous media flow (Jeong et al., 2016). An earlier study used collagen patterned within microfluidic channels to study invasion of MDA-MB-231 cells with and without

tumour-associated macrophages. In this case, the macrophages invaded the gels with the cancer cells (Huang et al., 2009). Whilst strides have been made towards better replicating the heterogeneity of the TME *in vitro*, there remains a need for better models.

There are also numerous studies that investigated the phenomenon of metastasis on-chip, but these are largely focused on cancer cell transmigration through the endothelial cell lining, not other events in the metastatic cascade (Xu et al., 2016; Chen et al., 2017). For example, one study recreated 3D tumour vasculature on-chip to characterise tumour cell migration efficacy and endothelial permeability (Zervantonakis et al., 2012). While this is valuable for understanding that specific stage of metastasis, it ignores the earlier steps leading up to intravasation. A better understanding of the earlier stages could provide earlier targets for treatments.

There have also been studies that focus on the tumour-ECM interactions by using gels on-chip, but not all of these used 3D spheroids, and none used continuous flow to induce biomechanical forces in the chip (Song & Munn, 2011; Sung et al., 2011; Jeon et al., 2013; Kim et al., 2013). Additionally, microfluidics have been used to study chemotaxis and the gradients that govern tumours (Torisawa et al., 2010). Another use for microfluidics in cancer exploits the high throughput capabilities of LOC devices to do drug efficacy testing. An example of this which also integrated co-culture aspects used a LOC platform to test how stromal cells affected drug resistance in spheroids. The inclusion of stromal cells was found to significantly increase drug resistance, demonstrating the importance of both co-culture and 3D techniques (Xu et al., 2013).

Microfluidics is fast becoming a common cancer research tool thanks to the advantages it confers over traditional 2D and monoculture techniques. However, while many studies have started to use LOC to study the TME, few have incorporated major critical components governing a tumour: IFF (continuous perfusion of media or fluid shear stresses), 3D structures (multicellular spheroids), and 3D environment (hydrogel matrices).

1.8 Microfluidic models of flow in cancer

Studies in recent years have started to outline the relationship between IFF and cancer progression and have laid the foundations of a strong association between the two. A large proportion of microfluidic IFF studies have focused on the role of IFF in cell invasion and motility. One such study showed early on that IFF can guide tumour cell invasion along the flow direction (Munson et al., 2013). Other labs have used methods such as computational modelling to examine the spatial gradients in ISF that influence the direction of tumour cells as they invade (Shields et al., 2007). IFF has even been shown to promote tumour cell invasion via stromal cell

mediated matrix remodelling within the TME, again demonstrating a direction relationship between IFF and the TME (Shieh et al., 2011).

More recent approaches have built on these findings to expand the evidence for IFF promoting progression of cancer. For example, IFF was examined in the context of glioblastoma multiforme and the evidence outlined a chemokine receptor-mediated mechanism which stimulated invasion of cancer cells and cancer stem cells in this form of the disease (Kingsmore et al., 2016). In contrast, another study looked at glioma cells suspended in collagen and exposed to fluid shear stresses and found suppression of MMP-mediated migration in some cells. The results indicated that flow may heterogeneously regulate invasive potential (Qazi et al., 2011). More recently, a study used simulation techniques in addition to cancer cell spheroids in 3D collagen matrices with oriented microfluidic flow. In this case the orientation of the aligned fibers produced the microfluidic flow and according to the simulations, showed invasion to be strongly influenced by the properties of the ECM and directional flow of the fibers (Geiger et al., 2022). Another recent study used one-directional flow in a microfluidic platform to investigate how cancer cells could exert influence over fibroblasts. In this semi co-culture environment where flow facilitated communication between the cancer cells and fibroblasts, fibroblasts were activated and even migrated towards the cancer cells (Kim et al., 2022). This demonstrated not only the impact of IFF on the cancer cells and their progression but also the capacity it had to influence the surrounding environment.

In breast cancer specifically, a few models have investigated the role of fluid and flow in various forms. Notably, Tchafa et al. reported that IFF induced invasion of breast cancer cells via a chemokine receptor CXCR4-PI3K pathway in HER2 positive cells (2015). In another case, fluid shear stress – not specific to ISF – was administered to breast cancer cells within a 3D matrix by using a bioreactor. Researchers found that cells exposed to the shear stress condition exhibited a motile phenotype and concluded that shear stress promoted breast cancer cell proliferation, invasive potential, and chemoresistance (Novak et al., 2019). Another study focused again on fluid flow without specifying the role of ISF and demonstrated that flow promoted EMT in breast cancer cells (not spheroids) via the upregulation of EMT markers Snail and Vimentin at both the gene and protein level (Fuh et al., 2021). These studies are examples of how breast cancer in particular may be influenced by flow and demonstrate the need for a better understanding of flow in breast tumours.

Taken together, these findings from a variety of microfluidic models and forms of flow are indicative of a significant influence that ISF could have over the TME and over cancer progression at large. Given that metastasis is a critical turning point in the disease for clinical outcomes, it

would be beneficial to know how ISF and specifically IFF could be manipulated to prevent it. Whilst preliminary work has been done, few studies have successfully replicated IFF or have neglected the use of 3D spheroids in the experimental design. More research is needed using accurate models with 3D masses to explore the intricate relationship between IFF and cancer progression.

1.9 Project aims and objectives

Despite the recent advances in cancer research models, voids remain in our understanding of the relationship between IFF and the progression of cancer in the TME leading to metastasis. The project described here aims to fill this gap in understanding by using modern research models to mimick the TME and IFF. Multicellular 3D cancer spheroids will be integrated into a microfluidic LOC device to recapitulate the TME. Continuous media flow over the spheroid in the LOC will reproduce biomechanical forces of fluid flow that are seen in a tumour. Using this platform, the aims of the project will be to:

1. Refine a spheroid-on-chip microfluidic system for investigating interstitial flow effects on spheroid biology.
2. Investigate the effects of interstitial flow on cancer cell biology in the TME.
3. Identify potential interstitial flow biomarkers and evaluate their clinical relevance.

Chapter 2 Materials and Methods

2.1 Cell culture

2.1.1 Cell lines

Several human cell lines were used for the experiments in this study: MCF7 (pleural effusion of metastatic adenocarcinoma), MDA-MB-231 (pleural effusion of metastatic adenocarcinoma), HEK293T (human embryonic kidney) and U-87 MG (glioblastoma). Table 2.1 summarises the characteristics of each cell line. Cell lines were obtained from ATCC (Teddington, UK) and ECACC (Salisbury, UK). Cell culture media was tested regularly for mycoplasma infection with consistently negative results.

2.1.2 Subculture

Cells were cultured in high glucose complete Dulbecco's Modified Eagle Medium (DMEM (Corning, Amsterdam, Netherlands) supplemented with 10% v/v (volume/volume) heat inactivated FBS (Gibco, Life Technologies, Loughborough, UK) in an incubator (Nuaire, USA) at 37°C with a humidified atmosphere of 5% CO_2.

To keep cell populations in an exponential growth state, cells were passaged after reaching 70-80% confluency and seeded into T75 cm^2 filter cap tissue culture flasks (Greiner, Bio-One UK). To passage cells, spent medium was removed and cells were washed with 1X PBS (Phosphate-Buffered Saline; VWR, USA) to remove any non-adherent cells. Cells were then incubated for 5 minutes at 37°C in 1X Trypsin (Lonza) to detach cells. Once cells were detached, they were re-suspended in complete media and a fraction (dependent on splitting ratio) was transferred to a new culture flask with fresh media. Cell lines were not passaged more than 30 times (Masters & Stacey, 2007).

Table 2.1 Characteristics of cell lines used in this study (information from ATCC, ECACC, and Holliday *et al.*)

Cell Line	**MCF7**	**MDA-MB-231**	**HEK293T**	**U-87 MG**
Disease/Tumour type	Adeno-carcinoma	Adeno-carcinoma	Not applicable (N/A)	Glioblastoma; astrocytoma
Development	Metastatic	Metastatic	Not applicable (N/A)	Primary
Origin	Pleural effusion	Pleural effusion	Embryonic kidney	Brain
Classification	Luminal A	Claudin-low	N/A	IV

2.1.3 Viable cells counting

Cells were counted before experimental setups to ensure seeding at a constant number. The cell suspension was diluted 1:1 or 1:2 in a 0.4% w/v (weight/volume) trypan blue solution (Corning, USA) and loaded into a haemocytometer (Heinz Herenz Hamburg, Germany). Viable cells were counted in the four large quadrants using a light microscope (Olympus CKX41, 10X magnification). To determine the number of cells per millilitre, the average cell count per quadrant was multiplied by the dilution factor, and then by 10^4.

2.1.4 Freezing and thawing of cells

To maintain a cell stock for long term storage, cells were frozen at an early passage and stored in liquid nitrogen. For this, the cells were trypsinsed as detailed in section 2.1.2 and washed with 1X PBS when at 70-80% confluence in a T175 cm^2. The cell suspension was then transferred to a 50 mL centrifuge tube and centrifuged for 5 minutes at 300 x *g* to create a cell pellet. The pellet was washed with 1X PBS after medium supernatant was removed. Cells were then re-suspended in freezing media, a solution comprised of 90% FBS and 10% dimethyl sulfoxide (DMSO). The cell suspension was aliquoted into cryovials (Nunc, ThermoFisher Scientific, Loughborough, UK) and vials were placed into a freezing container (ThermoFisher Scientific) with isopropanol. The container was stored at -80°C for gradual cooling (1°C /minute) for no more than 72 hours, and then transferred into liquid nitrogen (-196°C) for long term storage.

To revive frozen cells, a cryovial was brought to room temperature quickly and cell solution was transferred to a T25 cm^2 flask with pre-warmed complete medium (containing 10% FBS). Cells were allowed to attach (with media changed after 18 – 24 hours) and to reach 70-80% confluence before being passaged (usually after 24 hours) to a T75 cm^2 flask for normal growth/maintenance.

2.2 Spheroid biology

2.2.1 Spheroid formation

Cells were seeded in ultralow adherence (ULA), round bottom, 96-well plates (Costar, Sigma-Aldrich, UK) at varying densities. Seeding density depended on experiment and was typically between 3.0 x 10^4 to 1.5 x 10^5 cells per well. Wells on the outermost columns and rows were filled with 200μL of PBS to seal moisture into the plate and prevent media evaporation. Once the cell suspension and PBS were added to microwells, the plate was transferred to an incubator (37 °C, 5% CO_2) to allow cells to aggregate. The plate was left undisturbed for 96 hours, after which time spheroids could be used for experiments. This procedure followed the protocol established by Vinci *et al.* (Vinci et al., 2012).

2.2.2 Measurement of spheroid diameter

Spheroid diameter was determined from images obtained on a GelCount scanner (Oxford Optronix, Oxford, UK). Using ImageJ analysis software (National Institutes of Health, Maryland, USA; (Haque et al., 2012)), spheroid diameter was measured using the software's 'measurement tool'. The longest diameter of each spheroid was recorded (excluding cell debris) and used for analysis (Pires et al., 2012).

2.2.3 Measurement of spheroid growth curve

Spheroids were generated as described above in section 2.2.1 from cell lines (Table 2.1). Spheroids were seeded at 5 different densities: 3.0×10^4, 6.0×10^4, 9.0×10^4, 1.2×10^5 and 1.5×10^5 to demonstrate a range of sizes. For record purposes, t = 0 hours was considered the time of seeding cell suspensions, and t = 96 hrs (day 4 of growth; aggregation complete) was used for the first measure. Images were taken on days 4, 7, 10, 12, and 14. On the days that images were taken, spheroid media was also refreshed using complete DMEM in order to maintain nutrient levels. A logistic growth curve (nonlinear regression) was generated using GraphPad Prism software version 9 (San Diego, California, USA).

2.2.4 Fluorescein diacetate (FDA) staining for live cells

To assess spheroid viability in all spheroid-based experiments, a fluorescence live staining assay was used. The assay employs fluorescein diacetate (FDA) (Thermo Fisher Scientific) to stain viable cells. FDA is converted into a green fluorescent metabolite (known as fluorescein) via an esterase dependent reaction in viable cells, and the intensity of the green fluorescent signal produced can be detected/measured. (Decker, 2001).

To conduct the stain on spheroids, media was carefully pipetted off and discarded, and spheroids were washed 3 times with 1x PBS to remove all traces of media, as phenol red interferes with the fluorescent imaging. Spheroids were then stained with an FDA (5 mg mL^{-1}) solution in phenol red-free DMEM. After a 5-minute incubation at 37°C and 5% CO_2 in the dark, the staining solution was discarded and spheroids were washed again 3 times with 1x PBS to fully remove the staining solution. Fresh PBS was added to each well and spheroids were imaged using an inverted epifluorescence microscope (Zeiss, Germany). Pre-set filters on the microscope allowed for imaging FDA using the 'fluorescein isothiocyanate' setting (excitation 495 nm/emission 517 nm).

2.2.5 Fluorescence quantification

The fluorescent signal produced by FDA was quantified using ImageJ analysis software with a method adapted from (McCloy et al., 2014). The 'area', 'integrated density' and 'mean grey value' options were selected in the ImageJ 'analyse' tool bar menu. Using greyscale images of

spheroids stained with FDA, the 'polygon' tool was then used to draw around the spheroid, marking this as the region of interest (ROI). The selections that were pre-set in the analyse tool bar could then be used to take automatic measures of those parameters. Additionally, a background signal measurement located away from the ROI was taken at the same size as the ROI. If a background signal area was not large enough to match the size of the ROI, a sample without interference was taken and the value was divided by the area taken. This value could then be multiplied by the total area of the ROI and be used as the matched background signal. To produce the corrected total spheroid fluorescence (CTSF), the background fluorescent signal was subtracted from the integrated density value, and this was represented as relative levels between two conditions.

2.3 Microfluidic protocols

2.3.1 Flow cell 1 chip

The microfluidic device design used in initial experiments was developed by Dr Thomas Collins and designed in collaboration with Dr Alex Iles at the University of Hull (Collins et al., 2021). Dr Collins adapted a previously established microfluidic design used at the University of Hull for the purpose of housing spheroids on-chip. It will herein be referred to as the "flow cell 1" chip. The flow cell 1 chip featured three microwells connected by a straight channel which was 0.6 mm deep and 1.5 mm wide. The chip was made from Schott B270 glass and the features described were milled into the material as described in section 2.3.3. The channel on the outlet side of the spheroid microwell was narrowed for a short distance of 2 mm - a 70 µm shallow weir - a design feature intended to trap the spheroid from flowing out of the well and down the outlet channel. The key dimensions of the flow cell 1 chip are depicted in Figure 2.1. The spheroid microwell, at the centre of the chip, was made by drilling through completely to leave a cylindrical access port 3 mm deep and 2 mm wide. A glass coverslip was glued to the bottom to create the spheroid microwell. Previous imaging optimisation conducted by Dr Collins in the development of the flow cell 1 chip showed that use of a milled glass slide as the bottom of the microwell produced difficulties with imaging due to light refraction of the milled surface. Therefore, a coverslip was best suited for optical purposes. The wells at each end of the chip were designed to interface with a standard plastic syringe (for cleaning protocols). A polydimethylsiloxane (PDMS) plug was also designed to fit into the port above the spheroid well, allowing for a spheroid to be transferred into the well with a pipette, and then covered with the plug to prevent leakage. PDMS is gas permeable so it permits oxygen exchange to maintain spheroid viability.

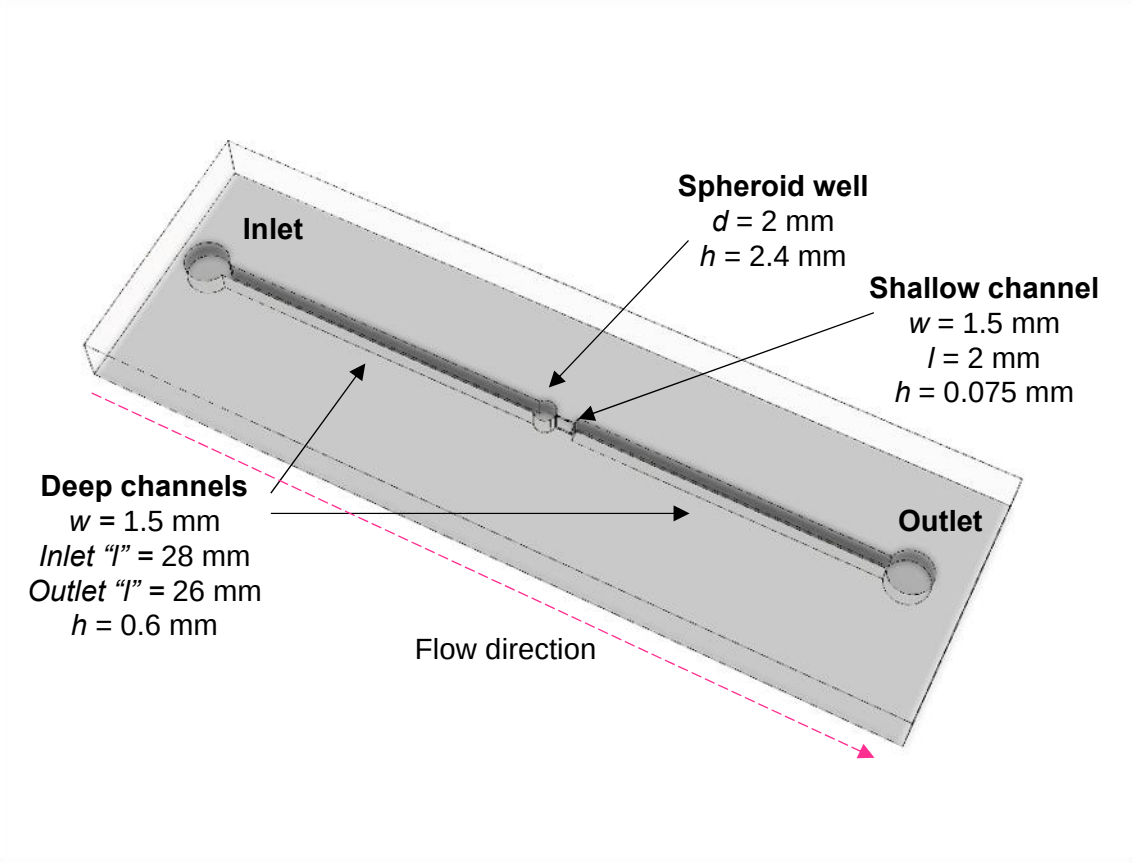

Figure 2.1: 3D rendering of the flow cell 1 chip and key internal features

AutoCAD was used to render a 3D representation of the channels and spheroid well in the flow cell 1 device. The device was made from 2 thermally bonded pieces of glass, with channels milled into the bottom piece. The key internal features included a deep channel of 0.6 mm depth which lead to a spheroid microwell 2 mm in diameter, a shallow channel or "weir" 0.075mm deep on the outlet side of the spheroid well, and another deep channel leading to the outlet port

2.3.2 Flow cell 2 chip

After initial experiments with the flow cell 1 chip revealed the system's failure to harbour the volumes of Matrigel and size of spheroids required for prospective studies, it was decided that a newer version of the chip would be produced featuring a larger spheroid microwell. In collaboration with Dr Iles, the flow cell 2 chip was designed and fabricated (fabrication is described in section 2.3.3). The general structure of the chip (2 thermally bonded glass slides), wells (1 inlet, 1 spheroid chamber, and 1 outlet), and channel systems remained the same as in the flow cell 1 design but with a few significant design differences: the diameter of the spheroid microwell was increased, the weir (shallow channel) on the outlet side was removed, and where the channels met the spheroid microwell a teardrop shape was used for the interface rather than a direct junction of a straight channel to a circular well. The channels remained 0.6 mm deep and 1.5 mm wide. The key dimensions of the flow cell 2 chip are summarised in Figure 2.2. The justifications for the optimisation of flow cell 1 and the work comprising the evolution to the flow cell 2 chip are described in detail in results Chapter 3.

2.3.3 Fabrication

Chips (both flow cells 1 and 2) were designed in collaboration with Dr Alex Iles at the Lab on a Chip Fabrication Facility at the Department of Chemistry and Biochemistry (University of Hull). Chips were fabricated at this facility by Dr Iles by thermally bonding two glass slides (Schott B270) together. Channels and wells were milled using a Computer Numerical Controlled (CNC) machine (Datron, Germany) with a diamond milling tool of 1 mm diameter (Eternal Tools, UK). To create a base that allows imaging on the chip (see section 2.3.1), a borosilicate glass coverslip was glued to the bottom of the device where the spheroid resides.

2.3.4 Polydimethylsiloxane (PDMS) plug casting

PDMS "plugs" were used to seal the open port which comprised the top of the spheroid microwell in the flow cell 1 and flow cell 2 devices. PDMS is a gas permeable, silicon-based organic polymer. Therefore, it allowed oxygen exchange to help maintain spheroid viability. A polytetrafluoroethylene (PTFE) mould was fabricated by Dr Alex Iles to allow x 8 plugs to be cast simultaneously at the appropriate size determined for sealing the top of the spheroid chamber. The PTFE mould was cleaned using 70% ethanol prior to plug casting. Plugs were cast by combining PDMS with a catalyst curing agent (Sylgard) at a 10:1 ratio and centrifuging for 3 min at 1700 x *g.* A glass slide was used to remove excess, smooth the surface, and seal the mould shut. This was left to set for a minimum of 2 days before plugs could be gently removed from the glass/mould with a scalpel.

2.3.5 Microfluidic device cleaning

Microfluidic devices were cleaned routinely between uses. For routine maintenance cleaning, chip channels and the spheroid well were filled with virusolve and allowed to soak for 3-5 min before the system was flushed with 70% ethanol. Chips were then flushed with 70% ethanol, DI water, and air using syringes. The flushing process was done a minimum of 3 times or until all debris and bubbles were cleared. Once chips were clean and dry, they were autoclaved and then stored in a sealed container until the next use. Chips were also periodically (after 3-4 uses) deep cleaned using acetone.

2.3.6 Microfluidic interfacing and setup

Most experiments in this study used comparisons between "static" and "flow" conditions, unless other experimental designs were specified. The general workflow for these experiments is depicted in Figure 2.3. In the flow condition, spheroids were grown as described in section 2.2.1 before being transferred to a chip. Before transferring, approximately 150 μL of media was gently removed from the spheroid well on the ULA plate. Then, using a 200 μL cut pipette tip the spheroid was retrieved in a volume of ≈ 45 μL and gently pipetted into the spheroid microwell of the chip. A volume of 45 μL of ice cold Matrigel was added to the chip microwell with the spheroid and allowed to set for 3-5 min. Before inserting the PDMS plug into the microwell opening to seal it, culture media was pipetted into the system (channels) to fill it. This reduced the formation of air bubbles in the spheroid microwell by eliminating dead air space in the well. Up to 6 chips could be prepared in this manner and used in the setup described below.

The chips were then attached to an electronic syringe pump set to 3 μL min^{-1} (Harvard Apparatus) to produce a continuous flow rate. A plastic syringe (BD, Oxford, UK) filled with culture media was secured in the syringe pump and attached to Tygon tubing with a 200μL pipette tip, which had been cut to fit securely over the syringe nozzle. The tubing had an outer diameter of 2.29 mm and inner diameter of 1.27 mm. At the outlet end of the chip, the interface was the same except that the tubing lead to a centrifuge tube (Falcon, Thermo Fisher Scientific) which served as a collection pot for effluent media. For this, centrifuge tubes were sealed with parafilm and tubing was inserted through the parafilm. To maintain a stable temperature of 37°C, the chip was housed in an egg incubator (Covatutto, Novital, Italy). However, the egg incubator was not CO_2 regulated. An image of a typical flow setup is depicted in Figure 2.4. In parallel, spheroids were maintained in static conditions in a ULA plate housed in a standard cell culture incubator. Media was replenished at t = 0 timepoint, equivalent to the start of perfusion in flow experiments. To replenish media, 100μL of spent media was gently removed from each well and 100 μL of fresh media was added. DMEM in both conditions was supplemented with 1% Penicillin-Streptomycin (Lonza) to mitigate risk of infections.

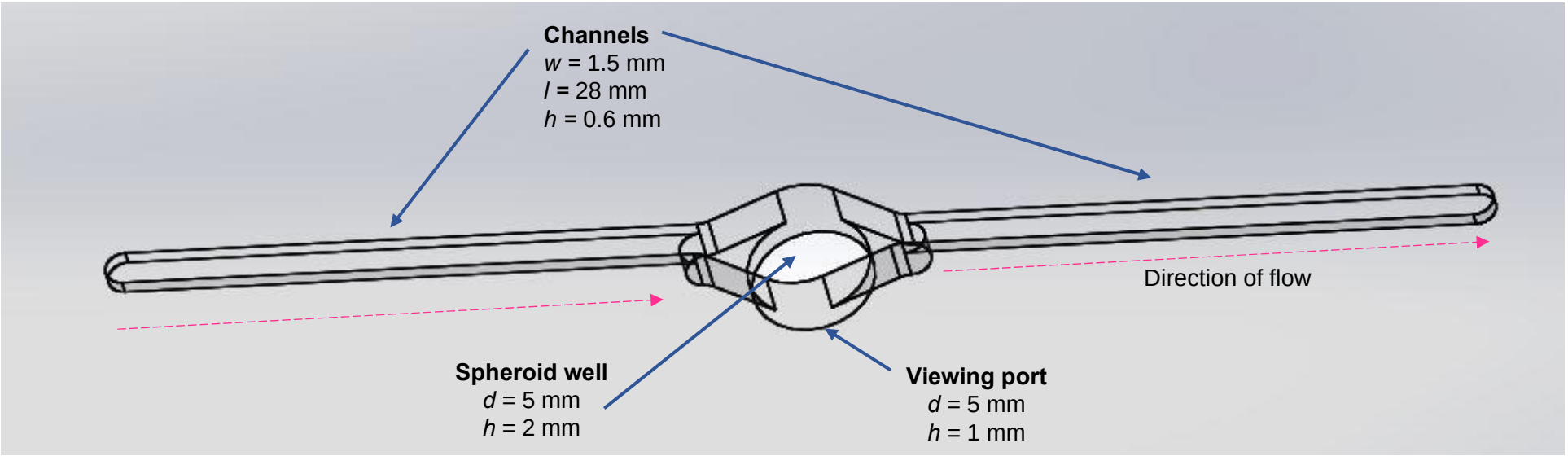

Figure 2.2: 3D rendering of the flow cell 2 device internal structures

AutoCAD was used to render a 3D representation of the internal elements of the flow cell 2 device design. The device featured a single channel 0.6 mm in depth with a spheroid well in the middle of the device. The spheroid well was 5 mm in diameter. There was a viewing port made by a 1 mm deep circular recess at the bottom of the well. Above the viewing port, the shape of the well was a “teardrop” to prevent the formation of bubbles in the well.

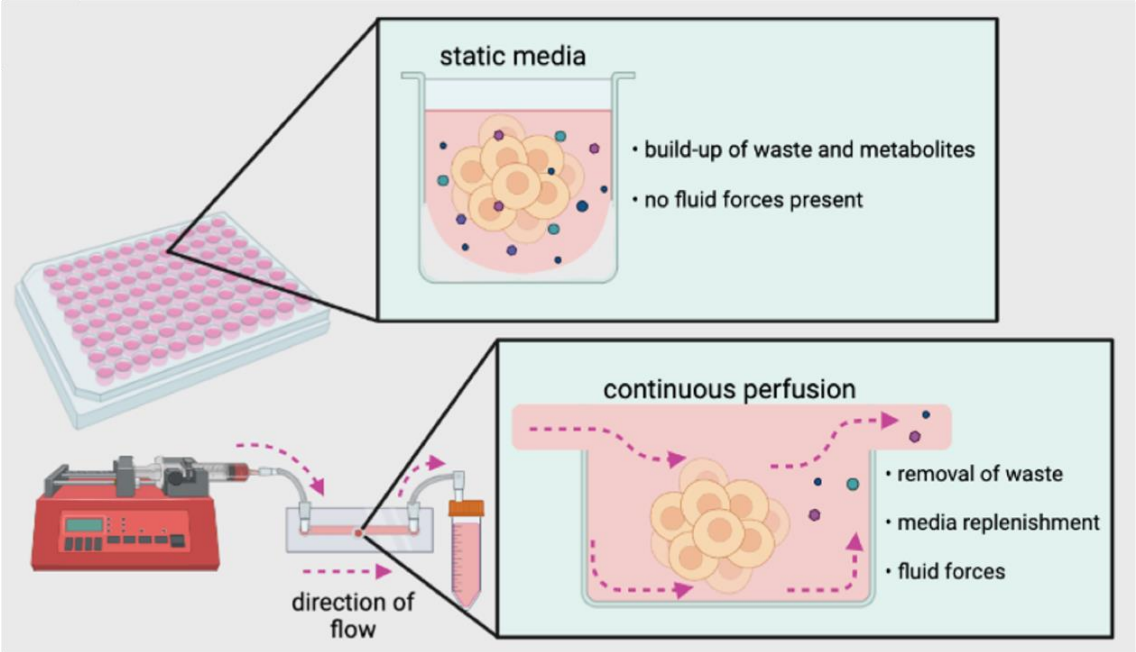

Figure 2.3: Schematic of static v. flow experimental setup

A schematic drawing of the static and flow experimental setups. Static used the plate that spheroids were formed in to house them, whereas the flow system used a syringe pump to produce continuous perfusion of media over spheroids in the microfluidic device. Experiments could be conducted in Matrigel by adding it to the static wells and to the spheroid microwell in the device. Image was created in Biorender.com.

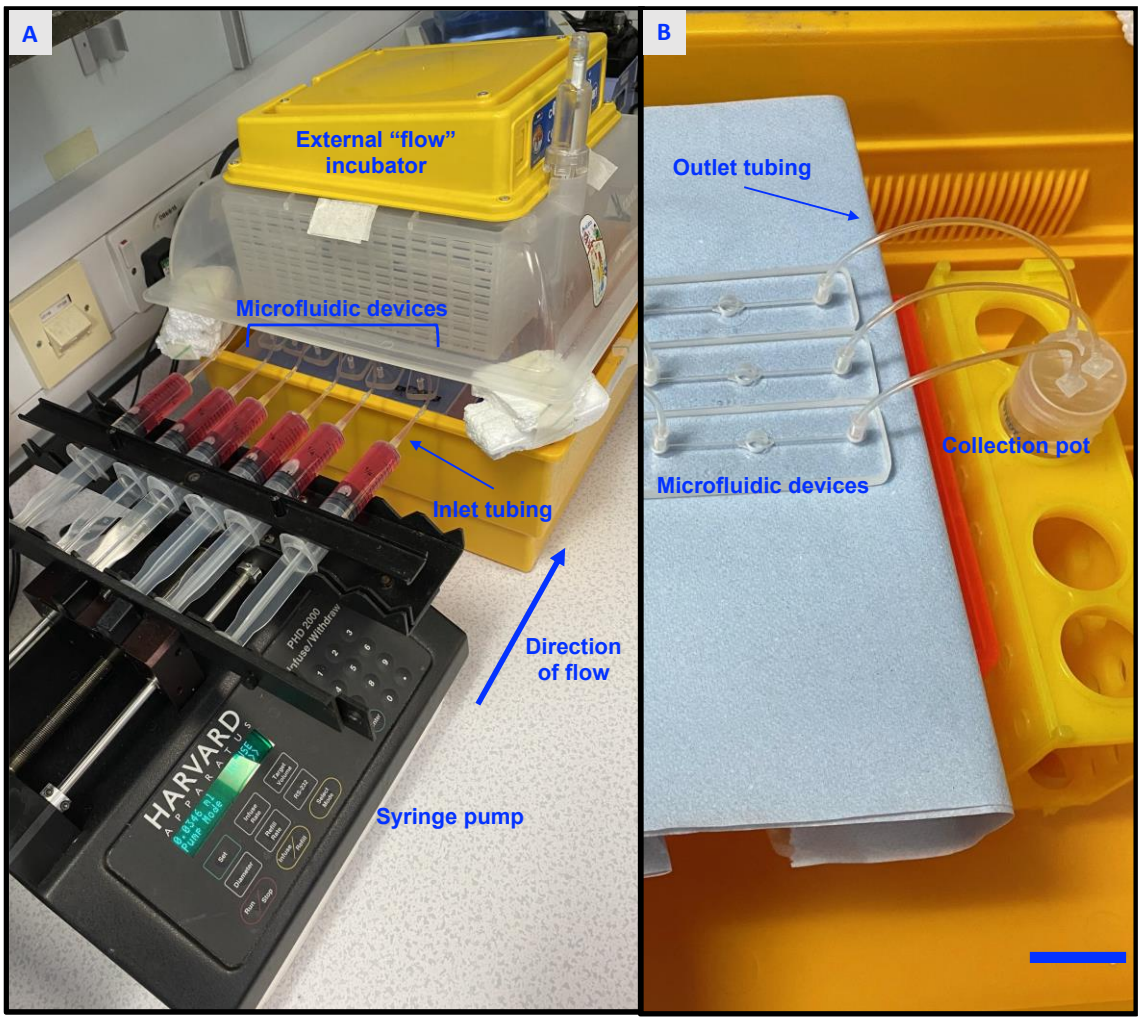

Figure 2.4: Microfluidic device setup for flow condition

Disposable, plastic syringes filled with complete DMEM were connected to microfluidic devices placed inside an egg incubator (A). The egg incubator was not humidified or CO_2 regulated. The flow rate on a Harvard Apparatus syringe pump was set to 3 µL min^{-1} and DMEM was continuously perfused through the system for a set amount of time. Effluent media was collected in a centrifuge tube sealed with parafilm (B). Scale bar = 30 mm (B).

2.3.7 Extracellular matrices on-chip

Previous studies in our lab were conducted to optimise the use of hydrogels on-chip with our microfluidic device design (Collins, 2019b). Following from the results of that work, it was determined that Matrigel (Matrigel Basement Membrane Matrix, Corning) would be used as the hydrogel of choice. Matrigel is commonly used to study migration and invasion and has been used with 3D cell cultures previously (Vinci et al., 2012). Prior to hydrogel incorporation into the device, the chip was cleaned and all air was flushed from the channels using empty syringes. Chilled pipette tips (stored in -20°C) were used to load Matrigel into the spheroid microwell. It was then allowed to set before a spheroid was transferred into the matrix with a pipette.

2.3.8 Effluent media collection

Effluent media samples were collected at appropriate time points for both static and flow conditions. In the static experimental setup, 100μL of media was removed from each spheroid well and collected into a microcentrifuge tube. Media from 3 wells was collected into 1 tube, for a total volume of approximately 300μL. In the flow condition, effluent media from 3 chips was collected into a centrifuge tube as described in section 2.3.8.

Conditioned media from both static and flow experiments was spun for 5 min at 2000 rpm to remove debris and floating cells. The cleared conditioned supernatant was collected and immediately stored at -20°C until use in subsequent analyses.

2.4 Exposure to hypoxic conditions

A H35 Hypoxistation hypoxia chamber (Don Whitley Scientific, UK) was used for achieving hypoxic conditions of 1% O_2. Humidity (75%), CO_2 (5%), and temperature (37°C) were monitored and maintained. Hypoxic samples were collected in the chamber and lysed immediately after retrieval.

2.5 Transcript analysis

2.5.1 Total RNA extraction

The Aurum Total RNA mini Kit (Biorad, UK) was used for RNA extraction. The manufacturer's instructions were followed with minor adaptations relevant to spheroids. Briefly, 3 spheroids/sample were collected into microcentrifuge tubes (Eppendorf, Sigma-Aldrich, UK). Tubes were centrifuged briefly to pellet the spheroids and allow for removal of media. In cases where extracellular-like matrices (ECM) were used, cell recovery solution (Corning, Sigma Aldrich, UK) was first added to tubes and allowed to work for 15-20 min on ice. Spheroid pellets were gently washed with ice cold 1X PBS and spun down before removing PBS, and this process repeated another 2 times for a total of 3 washes. Once all media and PBS was removed, pellets

were re-suspended in lysis solution and one equivalent volume of 70% ethanol was added and thoroughly mixed to render cell lysates. The lysates were loaded into an RNA binding column to be washed and centrifuged several times. Lysates in the column membranes were also incubated in 1X DNAse I solution for 15 min at room temperature to remove any traces of genomic DNA (deoxyribonucleic acid). Lastly, columns were transferred to fresh microcentrifuge tubes to collect final samples, which were eluted in 30 – 50 µL of elution solution.

Total RNA samples were stored at -80°C to prevent degradation of RNA material. Samples were quantified using a Nanodrop Light (Thermo Scientific) and assessed for purity by using the 260/280 absorbance reading. A ratio of ~2 suggested a pure RNA yield, and only ratios between 1.8 – 2.1 were accepted for use in subsequent experiments.

2.5.2 cDNA synthesis

Reverse transcription of mRNA into cDNA from total RNA extracts was conducted using the RevertAid H Minus First Strand cDNA Synthesis Kit (Thermo Scientfic), per the manufacturer's instructions. In brief, a master mix containing 1 mM dNTP, 10 µm oligo d(T), 1 U/µL RNAse inhibitor, 10 U/µL reverse transcriptase, and 1X reaction buffer was prepared in DEPC water (diethyl pyrocarbonate-treated water). The master mix was distributed into small PCR tubes each containing 1 µg of template RNA. To check for contamination during the synthesis process a no-template control (NTC) was also prepared in parallel where DEPC water was substituted for the RNA template in a tube including all other components of the mastermix. Samples were mixed and briefly centrifuged before being placed into a thermal cycler (TC3000 Thermal Cycler, Techne, UK). A reaction program on the cycler was used to heat the samples for 1h at 42°C and 5 min at 70°C. Samples were then either kept on ice for immediate use or stored at -20°C for future use.

2.5.3 Quantitative PCR

Relative mRNA expression was analysed with real time quantitative PCR (qPCR) using Quantifast SYBR Green assay (Qiagen, UK), and QuantiTECT (Qiagen, UK) or in-house designed qPCR primers (synthesised by Sigma-Aldrich, UK). In-house designed primers were developed and optimised by previous lab members. See Table 2.2 for a list of the primers used in all experiments.

To perform the qPCR reaction, a mastermix was prepared with 1X SYBR Green, 1X ROX reference dye, and cDNA sample diluted 1:10 in RNAse-free DEPC water. 2 µL of primer was first added to wells in a 96-well reaction plate (Applied Biosystems). Where custom designed probes were used, 1 µL of forward and 1 µL of reverse paired primers were pipetted into the well for a 2 µL final primer volume at a final concentration of 0.1µM, diluted from 100µM stocks. 18 µL of cDNA mastermix was then added for a final reaction volume of 20 µL per well. Reaction plates were

sealed with optically clear adhesive covers (Applied Biosystems) and briefly centrifuged to pool well contents. The PCR machine (Step One Plus Real Time PCR System, Applied Bioscience, USA) was programmed to perform an initial denaturation for 2 min at 95°C followed by 40 two-step cycles of denaturation at 95°C for 5 sec and annealing/extension at 60°C for 10 sec. A melt curve stage was added for first-time runs with new primers to check for primer-dimers and nonspecific products. All samples were assayed in triplicate and each primer assay included NTC wells with water substituted for cDNA. StepOne Plus software (Applied Biosciences, USA) was used to generate the cycle threshold (C_T) values by adjusting the baselines of each amplification plot to intersect with the start of the exponential phase. The mean C_T values were used to calculate the relative expression of gene targets using the $2^{-\Delta\Delta CT}$ method (Livak & Schmittgen, 2001). β_2 microglobulin (*B2M*) was used as the housekeeping gene for all qPCR experiments due to the consistent expression across systems (Dydensborg et al., 2006).

2.6 RNA sequencing

mRNA (messenger RNA) samples were obtained following the protocol outlined in section 2.5.1. 23 µL of each sample (in elution buffer) was transferred into a fresh 1.5 mL microcentrifuge tube and sealed with parafilm, ensuring that a minimum of 400 ng per sample was provided. Samples were kept on ice until being packaged in dry ice and shipped to Novogene (Cambridge, UK) for sequencing. Quality control was conducted by Novogene and these results can be found in Appendix figure 1 - 6. The sequenced reads/raw reads for RNA-seq often contain low quality reads or reads with adapters, which can affect the analysis quality and reliability. To avoid this, it is necessary to filter the raw reads to get the clean reads. Raw reads were filtered as follows, according to Novogene:

- Remove reads containing adapters;
- Remove reads containing N > 10% (N represents base that could not be determined);
- (3) Remove low quality reads: The Qscore (Quality value) of over 50% bases of the read is <= 5.

Table 2.2 List of primers used for SYBR Green qPCR

Target gene symbol	Amplicon length	Catalogue reference or sequences 5' →3'	Supplier
ABCA8	98bp	QT00011095	Qiagen
ACTL8	122bp	QT00199934	Qiagen
ASF1B	79bp	QT00007224	Qiagen
B2M	98bp	QT00088935	Qiagen
BARHL1	150bp	QT00214599	Qiagen
BLM	89bp	QT00027671	Qiagen
BNIP3	73bp	QT00024178	Qiagen
BRCA1	60bp	QT00039305	Qiagen
BRCA2	93bp	QT00008449	Qiagen
CA9	160bp	F: GGAAGGCTCAGAGACTCA R: CTTAGCACTCAGCATCAC	Sigma-Aldrich
CDH1	104bp	QT00019418	Qiagen
E2F1	73bp	QT00016163	Qiagen
EXO1	150bp	QT00080717	Qiagen
FEN1	77bp	QT00064722	Qiagen
LOX	174bp	F: GTTCCAAGCTGGCTACTC R: GGGTTGTCGTCAGAGTAC	Sigma-Aldrich
MCM6	70bp	QT00059570	Qiagen
MMP1	103bp	QT00014581	Qiagen
MT-MMP1	144bp	F: CCCCGAAGCCTGGCTACA R: GCATCAGCTTTGCCTGTTACT	Sigma-Aldrich
PTGS2	68bp	QT00040586	Qiagen
RAB6C	92bp	QT00219366	Qiagen
RAD51	83bp	QT00031493	Qiagen
RRM1	103bp	QT00066717	Qiagen
RRM2	79bp	QT00039480	Qiagen
SNA1L (SNAIL)	69bp	F: GACCACTATGCCGCGCTCTT R: TCGCTGTAGTTAGGCTTCCGATT	Sigma-Aldrich
VEGFA	121bp	F: CTACCTCCACCATGCCAAGT R: CTCGATTGGATGGCAGTAGC	Sigma-Aldrich
VIM	94bp	QT00095795	Qiagen
WEE1	118bp	QT00038199	Qiagen

WSB1	107bp	QT00064127	Qiagen

2.6.1 RNA-sequencing results

The results of the RNA-sequencing were presented in an Excel spreadsheet listing all of the transcripts detected in the samples. Differential expression analysis was performed (by Novogene) between two conditions (static and flow) with 3 biological replicates for each using the DESeq2 R package. Differential expression of genes was determined using statistical routines in the software based on a negative binomial distribution. Resulting *p* values were adjusted using the Benjamini and Hochberg's approach for controlling the False Discovery Rate (FDR). Only genes with an adjusted p value < 0.05 determined by DESeq2 were assigned as differentially expressed in the resulting dataset provided. However, all transcript data was provided, including non-differentially expressed genes. The fold change between static and flow samples expressed as log2(fold change) were provided for each transcript. Log-transformed expression were used to better model proportional changes between conditions, which is more biologically relevant (Feng et al., 2014).

2.7 *In silico* analysis of RNA-sequencing data

2.7.1 Heat map generation

The software NetworkAnalyst (Xia Lab, McGill University, Canada; networkanalyst.ca), was used to produce the heatmap of differentially expressed genes. Transcript names and corresponding log2(fold change) values were entered in the software database. The software automatically allocated colour gradient according to the range of values entered.

2.7.2 Pathway enrichment analysis

Ingenuity pathway analysis (IPA; Qiagen) was used to perform pathway enrichment analyses. A full list of gene names from RNA-sequencing – including genes upregulated, downregulated, or unchanged – along with ENSEMBL IDs, log2(fold changes), fold changes, and *p*-values were uploaded to IPA for the software to process and analyse, free from bias. In a limited number of cases, uploaded items were not recognized by the software's database and therefore removed from the list of "analysis-ready" molecules.

2.7.3 Online tools for biomarker validation

2.7.3.1 TNMplot for gene expression comparisons in normal and tumour tissues

The online tool TNMplot was used to compare expression of target genes in normal and tumour tissues (tnmplot.com/analysis; (Bartha & Gyorffy, 2021)). A target gene of interest was entered into the tool and analyses were conducted using gene chip array-based data as well as RNA-seq based data. Unpaired and paired tissue samples from publicly available breast cancer patient databases were used for the analyses performed. Unpaired samples were normal tissue samples

of the breast compared to tumour samples of the breast, from different patients. Paired samples were taken from breast tumours and adjacent normal tissue of a patient. Statistical significance was computed using Mann-Whitney tests for gene chip array-based data and Wilcoxon tests for RNA-seq based data.

2.7.3.2 Kaplan-Meier plot generation for patient survival analysis

Kaplan-Meier plots were generated using the publicly available online tool KMplot to assess the correlation between expression of target genes and patient survival (Lanczky & Gyorffy, 2021). Affymetrix probes in the tool were selected for each gene and all patient criteria were included in the analysis unless otherwise noted. The median was used to split patient cohorts into groups determined by “high” and “low” expression values of genes of interest. This generated a Kaplan-Meier survival plot with hazard ratios with 95% confidence intervals and logrank P values calculated by the database.

2.7.3.3 cBioPortal

The online platform cBioPortal was used to map expression of a gene of interest against clinical attributes integrated into the online analysis tool. The clinical attribute used for this project was hypoxia score, and two forms were used: the Winter hypoxia score and the Buffa hypoxia score (Buffa et al., 2010; Ye et al., 2019)). The patient database used was the TCGA (The Cancer Genome Atlas) Pan-cancer atlas for breast invasive carcinoma (Liu et al., 2018)).

2.7.3.4 ROCplotter

The online tool ROCplotter was used for evaluation of a gene of interest as a predictive biomarker for breast cancer (rocplot.org). The tool generated a ROC (receiver operating characteristic) plot with AUC (area under the curve) computed to assess the prognostic power of the input gene. This process is described in more detail in the experimental design section of chapter 5, where it was used for analysis.

2.8 Protein analysis

2.8.1 Cell lysis and protein extraction

Cells or spheroids were collected from experimental conditions for protein harvest. For monolayer cells seeded in plastic dishes (Nunc, Thermo Scientific), media was removed, and cells were gently washed with 1X PBS at room temperature. Cells were then scraped from the dish in 1X PBS and the cell suspension was transferred to a microcentrifuge tube. For 3D experiments, spheroids were collected from a 96-well ULA plate (static) or from the microfluidic device (flow) into a microcentrifuge tube. The samples were spun and washed with cold 1X PBS to remove any traces of Matrigel or other debris.

At this stage, both static and flow samples were resuspended in a volume of urea/Tris-HCl (UTB) lysis buffer (9M Urea; 75mM Tris-HCl pH 7.5; 0.15M β-mercaptoethanol). Sample lysates were then sonicated using a Bioruptor (Diagenode, Belgium) for 5 min on high setting. Next, sample lysates were centrifuged for 15 min at 20,000 x *g* at a temperature of 4°C to pellet sheared material. The clarified sample supernatants were transferred to fresh microcentrifuge tubes and stored at -20°C.

2.8.2 Protein quantification and sample preparation

Whole cell lysates collected as described in section 2.8.1 were quantified using a Nanodrop Light (Thermo Scientific) before being diluted to a set volume and concentration such that each sample contained 30 µg of protein, for equal loading in subsequent experiments. Sample buffer (3.3% SDS; 6M Urea; 17 mM Tris-HCl pH 7.5; 0.01% bromophenol blue; 0.07 M β-mercaptoethanol) was then added to each sample, and sample mixtures were heated on a heat block (Techne Dri-Block DB-3D, Sigma Aldrich, UK) for 5 min at 95°C. Finally, sample tubes were briefly centrifuged to pool all sample material at the bottom of each tube before loading.

2.8.3 SDS-PAGE

Prior to Western blotting, protein samples were separated using sodium dodecyl sulfate-polyacrylamide gel electrophoresis (SDS-PAGE). Electrophoresis was used to run negatively charged proteins through a polyacrylamide gel to differentiate proteins based on mass. Gels were hand cast as per the established recipes outlined in Table 2.3. Protein samples and a molecular weight ladder (Blue Easy Pre-stained Protein Ladder, Geneflow, UK) were loaded into gels assembled in an electrophoresis tank filled with 1X running buffer (see Table 2.4). The gel was then run at 100-120V for 1.5h or until the dye migration front approached the end of the gel. All equipment used in the casting of gels and running of SDS-PAGE was supplied as part of the Mini-Protean Tetra Cell system (BioRad, UK), unless noted otherwise.

Table 2.3 Composition of polyacrylamide gels for SDS-PAGE (volumes given for casting two 1mm-thick gels)

Reagent	10% Resolving gel	15% Resolving gel	Stacking gel
MilliQ water	6.07mL	3.75mL	6.1mL
0.5M Tris pH 6.8	--	--	2.5mL
1.5M Tris pH 8.8	3.75mL	3.75mL	N/A
Acrylamide	4.95mL	7.25mL	1.3mL
10% SDS	150µL	150µL	100µL
10% APS	75µL	75µL	100µL
TEMED	18µL	18µL	40µL

Table 2.4 Composition of running and blotting buffers used for SDS-PAGE and Western blotting (volumes for 10X concentrated stocks)

Reagent	Running buffer	Blotting (transfer) buffer	TBS (pH 7.4)
Tris base	30.2g	30.2g	24g
Glycine	144g	144g	--
SDS (pellets)	10g	--	--
NaCL	--	--	88g
MilliQ water	Top up to 1L	Top up to 1L	Top up to 1L

2.8.4 Western blotting

Once electrophoresis was stopped, proteins were transferred onto a PVDF (polyvinylidene difluoride; GE Healthcare) membrane that had been activated in methanol for 5 sec. The transfer was performed in 1X transfer buffer with 20% methanol (see Table 2.4) for 1h at 100V. Once complete, the PVDF membrane was removed from the transfer assembly and blocked for 1h in milk solution (5% non-fat powdered milk in TBST) to prevent non-specific binding of antibodies. Then the membrane was washed in TBST (10% 10X TBS (Tris-Buffered Saline; see Table 2.4) and 0.1% Tween 20 diluted in MilliQ water) before overnight incubation at 4°C with primary antibody diluted in a solution of 1% milk-TBST or a solution of BSA (bovine serum albumin), in accordance to the datasheet provided by the manufacturer (refer to Table 2.5 for primary antibodies used). Following incubation with the primary antibody, membranes were thoroughly washed in 1X TBST (3 x 10 min) and then incubated for 1h at room temperature with the appropriate secondary antibody (Dako, Denmark) diluted 1:2000 in 1% milk-TBST. Then the membrane was washed with 1X TBST again before imaging. A ChemiDoc XRS+ System and Image Lab software (BioRad) were used to image blots. Membranes were briefly incubated with chemiluminescence substrate (Clarity Western ECL Substrate, BioRad) before transfer to an acetate sheet for imaging on the ChemiDoc. Densitometry analyses of blots could then be performed using ImageJ software (NIH, USA). Bands were quantified as relative expression of the control, with beta actin as the loading control for all blots.

Table 2.5 List of antibodies used for Western blotting

Target	Manufacturer	Reference or Cataloge No.	Dilution	Origin	Expected band size (kDa)
β-Actin	Santa Cruz	sc-47778	1:200	M	42
E-cadherin	Cell Signaling	3195	1:1000	R	135
HIF-1α	Becton Dickinson (BD) Biosciences	610958	1:500	M	120
HK2	Cell Signaling	2867	1:1000	R	102
p53 (DO-1)	Santa Cruz	sc-126	1:2000	M	53
RPA32	Cell Signaling	2208	1:1000	Rat	32
M = mouse; R = rabbit					

2.9 VEGF (vascular endothelial growth factor) ELISA (enzyme-linked immunosorbent assay)

To quantify levels of VEGF secreted from spheroids a sandwich ELISA for VEGF was conducted per manufacturer's instructions (Quantikine, R&D Systems). In brief, conditioned media samples from spheroid experiments were collected (see section 2.3.8) and added to wells of the ELISA plate. Immobilised monoclonal antibodies specific to VEGF at the bottom of the wells caused antigens present in the media samples to bind and become immobilised. Washing was used to remove any unbound substances before an enzyme-linked polyclonal antibody specific to human VEGF was added. Wells were washed again to remove any unbound antibody-enzyme reagent before adding a substrate solution which developed colour in proportion to the amount of VEGF bound in the well. The intensity of the colour signal was measured using a FLUOstar Omega plate reader (BMG Labtech) set to a wavelength of 450 nm.

2.10 Statistical analysis

All experiments were replicated at least three times to yield three independent biological replicates, unless otherwise stated. Within a biological replicate, inter-experimental triplicates were used unless noted otherwise in following results chapters. In general, observable differences between spheroids kept in static and flow conditions were assessed using suitable statistical tests. Paired *t*-tests with were used to compare two groups (e.g. static and flow conditions). Where more than two groups were compared with one another, ANOVA followed by Kruskal-Wallis testing was used. The standard error of means (SEM) were calculated and

reported on graphs as error bars. GraphPad Prism software version 9 (California, USA) was used for statistical analyses unless stated otherwise in figure legends or chapter methods.

Chapter 3 Refinement of a spheroid-on-chip microfluidic system for investigating interstitial flow effects on spheroid biology

3.1 Introduction

The TME is subjected to a variety of biomechanical forces due to the altered stroma created by abnormal vasculature and matrix stiffness in many tumours. Whilst these biomechanical cues have been acknowledged as playing important roles in the biology of the TME, they are still poorly understood. One such biomechanical cue is fluid flow, which in the case of the TME refers to interstitial fluid flow (IFF). Microfluidics are well suited to fluid flow investigations given their tight control of flow rates and command of the experimental environment.

3.1.1 Spheroid-on-chip models

3D spheroids are better at recapitulating the TME than conventional cell culture models where cells are grown in 2D on plastic (Luca et al., 2013). Spheroids include complex architecture creating dynamic cellular interactions in 3 dimensions that are closer to those seen *in vivo*. A number of diverse platforms have arisen for both the formation and use of spheroids including microfluidics, often referred to as spheroid-on-chip models (Ro et al., 2022).

Spheroids on-chip broadly fall into two main categories: spheroids generated on-chip for high throughput applications or spheroids on-chip for the study of the TME. An example of a high throughput spheroid-on-chip application was reported by Chen and colleagues (Chen et al., 2015). They developed a microfluidic platform with the purpose of "sphere" formation, or spheroid formation. 3D spheroid cultures were generated uniformly across the microfluidic plate and it could house 1024 spheroids simultaneously. The platform was used to test the effects of photodynamic therapy on cancer cells in the 3D cultures, with a focus on the high throughput capability of the system. Other similar examples exist such as a study by Sakai and colleagues where they developed a microfluidic chip to form and culture spheroids under perfusion with multiple spheroid array chambers on the chip, allowing for culture conditions to be tested simultaneously (Sakai et al., 2014). These represent only a couple of the ways spheroids on-chip have been recruited into the high throughput market, but demonstrate the variety of methods that can be created using spheroids and microfluidics for these purposes.

The other category of TME-on-chip is also a rapidly growing field, and the combination of 3D spheroids and microfluidic models are often utilised in combination to replicate the TME (Mehta et al., 2022). In fact, "tumour-on-a-chip" is a well recognised term now, reflecting the growing interest in the use of such models. Similar to the high throughput applications described above (and indeed sometimes even overlapping with them), tumours on-chip rely on microfluidics to provide continuous perfusion to sustain spheroids for longer durations of time (Trujillo-de

Santiago et al., 2019). Notably, many of the studies that use microfluidics in either of these broad categories don't investigate perfusion, or flow, but simply use it as a feature of their chip design. In contrast, other studies have emerged citing changes in expression patterns of cells exposed to fluid flow on-chip. A limited number have used 3D spheroids, but many rely on 3D cell culture suspensions where single cells are seeded into hydrogels (Fuh et al., 2021). Without the union of flow *and* spheroids in a system, these models often fail to fully recapitulate the TME. Whilst it is difficult to reproduce all the environmental components and biomechanical cues present in the TME, fluid flow effects on 3D spheroids appear to have been largely overlooked in the literature.

3.1.2 Chapter specific hypothesis, aims and objectives

To address the need for a better understanding of how fluid flow affects the biology of 3D spheroids we sought to use our lab's microfluidic device to examine this relationship. Previous work in our lab developed a microfluidic device capable of housing viable spheroids for up to 72h in continuous perfusion to study the effects of flow. However, to achieve reproducible and meaningful results, some adjustments were required to the design of the chip. We hypothesized that by refining and advancing the previous design, known as flow cell 1, we could conduct investigations into molecular and cellular changes occurring as a result of fluid flow. Therefore, the following aims were identified for this chapter:

1. Identify areas of improvement in the flow cell 1 chip design.
2. Develop a new chip design, the flow cell 2, incorporating the improvements identified in the flow cell 1 design.
3. Establish viability of spheroids in the flow cell 2 system.
4. Optimise the protocols for extracting cellular components, such as RNA and protein, from static and flow spheroid lysate samples.

3.2 Experimental design

3.2.1 Identification of areas needing improvement in the flow cell 1 chip design

Preliminary experiments were conducted using the flow cell 1 system. The flow cell 1 chip was described in detail in section 2.3.1. Calculations of features such as well volume, shear stress, residence time of media in the system, and flow velocities were used to characterise the system. These were compared against the needs of future experiments and modified accordingly, as described in the results portion of this chapter.

3.2.2 Design and fabrication of the flow cell 2 chip

The flow cell 1 chip was refined to better accommodate the experimental setup desired for our investigations. In collaboration with Dr Iles, the flow cell 2 chip was designed and fabricated (fabrication was described in section 2.3.3). The general structure of the chip (2 thermally bonded glass slides), wells (1 spheroid chamber), and channel systems (1 inlet and 1 outlet) remained the same as in the flow cell 1 design but with four significant design differences. First, the diameter of the spheroid microwell was increased from 2 mm to 5 mm. Second, the weir on the outlet channel side was removed. Additionally, where the channels met the spheroid well a teardrop shape was used for the connection rather than a direct junction of a straight channel to a circular well. And lastly, rather than creating a teardrop shape for the entire spheroid chamber, a 1 mm circular recess remained at the bottom of the well where the microscope cover slip was positioned for optimal viewing at the bottom of the well. The overall rectangular shape of the chip remained the same as well which made the chip approximately the size of a microscope slide and therefore easily permitted imaging. The justifications for these changes and details of the modifications are discussed in more detail in results section 3.3.1..

3.2.3 Microfluidic protocols

Microfluidic protocols were conducted as described in section 2.3. Where modifications or improvements were made, they will be described in the results portion of this chapter.

3.2.4 Brilliant blue visualisation of chip components

Matrigel was selected as the hydrogel of choice for extracellular-like matrices (ECM) in the work conducted previously by Dr Thomas Collins with the flow cell 1 chip. However, with the diameter of the spheroid chamber enlarged in the flow cell 2 design and the teardrop shape feature added, it was necessary to confirm that Matrigel would still stay in the spheroid chamber as it had in the flow cell 1 design. To test this, Brilliant Blue dye was mixed into ice-cold, liquid Matrigel in a 1:1 dilution. The mixed solution was then loaded into a flow cell 2 chamber (using the volume determined appropriate for experiments) and allowed to settle for 3-5 min. Then, microscope images were taken of the interface between the chamber and channels to visually inspect where the Matrigel settled using an Olympus microscope with a 2x objective (total 20x magnification).

Brilliant blue (undiluted) was also used to visualise the flow of fluid through the system and to ensure no leaks were present. Images were taken with a handheld camera.

3.2.5 Spheroid growth characterisation

Patterns of spheroid growth were characterised by seeding 3 cell lines, known to produce varying spheroid shapes, at 5 different densities. The cell lines used were 1) U-87 MG, a glioblastoma line which has been well characterised previously in forming tight, uniform

spheroids; 2) MCF7, an ER (+)/PR(+)/HER2(-) breast cancer cell line which forms tight spheroids and; 3) MDA-MB-231, a triple negative breast cancer cell line that forms compact but irregular spheroids (Holliday & Speirs, 2011). Cells were seeded and grown as described in detail in section 2.2.1. A growth analysis curve was generated to identify logarithmic growth patterns in each line. This was aimed at determining an optimal seeding density for spheroids, ideally identifying a density that would be suitable for both MCF7s and MDA-MB-231s.

3.2.6 Determining viability of spheroids in the flow cell 2 system

3.2.6.1 FDA staining of spheroids

Spheroid viability was assessed over a period of 72h. MCF7 cells were used to form spheroids by seeding 9.0 x 10^4 cells per well in a ULA plate. After formation for 96h in a cell culture incubator undisturbed, spheroids were either kept in the ULA plate (static condition) or incorporated into the spheroid chamber of the flow cell 2 chip (flow condition). Spheroids were kept in these conditions for 72h to represent the maximum duration that would be used in subsequent experiments. FDA staining was performed at the end point of experiments as described in section 2.2.4.

3.2.6.2 VEGF ELISA

Our lab previously demonstrated that secretion of the protein VEGF was significantly increased by spheroids housed in the flow cell 1 system compared to static spheroids (Collins et al., 2021). Additionally, U-87 MG cells have been well described as secreting high levels of VEGF (Mentlein et al., 2004). Therefore, we used U-87 MG spheroids exposed to static and flow conditions in our flow cell 2 device to test whether this outcome would be reproduced in our system.

3.2.7 Optimisation of RNA and protein extraction techniques

An aim of this project was to examine how interstitial flow impacted the cell biology of cancer spheroids. In order to investigate these types of changes it was envisioned that RNA and protein could be harvested from spheroids in both static and flow conditions to make direct comparisons between the two. This would require RNA and protein to be collected in quantities sufficient to be used for downstream analyses such as qPCR and Western blotting. A series of optimisation experiments for collection of RNA were conducted to ascertain the best methods for consistently, successfully harvesting material from spheroids.

3.2.8 Evaluation of incubator effects

The use of the external flow incubator for housing microfluidic devices during experiments introduced a variation between the static and flow experimental setups. To assess whether the use of different incubators would significantly influence the biology of spheroids, static vs. flow experiments were setup as described in section 2.3.6, but with the addition of a static plate of

spheroids kept in the flow incubator during the experiment. 72h experiments were conducted to test the maximum time plates or chips would be in a given condition. qPCR analysis was used to determine relative *VEGFA* transcript levels in 2 modes of comparison:

- Static plate in the flow incubator vs. flow
- Static plate in regular incubator vs. flow

3.3 Results

3.3.1 Advancement from flow cell 1 to flow cell 2 system

The flow cell 1 chip had been used by our lab previously for preliminary work investigating the effects of fluid flow on spheroids (Collins et al., 2021). That work laid the foundation for the use of a spheroid-on-chip system to investigate changes in spheroids exposed to flow. However, to advance the utility of the device, improve user accessibility, and optimise it for the experimental designs envisaged for future work, changes to certain design features of the chip were needed. The identification of those changes, the justifications for them, and the design advancements resulting in a flow cell 2 system are described here.

3.3.1.1 Characterisation of the flow cell 1 system for identification of necessary advancements

The dimensions of the chip were outlined in section 2.3.1 and depicted in Figure 2.1. The physical characteristics of the chip were described by calculating key features of the system. Specifically, flow velocities and residence times were calculated to describe the chip and characterise some of the biomechanical forces in the system.

Flow velocities were calculated for each component of the system; tubing, deep channels, and the shallow channel. The approximate flow velocity, or the internal speed of the media flowing through each component, was calculated by dividing the volume flow rate set on the syringe pump by the cross-sectional area of a given component. Therefore, the cross-sectional area of a rectangle was used for channels and the cross-sectional area of a circle for the tubing. The cross-sectional area of a rectangle is equal to w x h, and for a circle it is equal to πr^2. The inner diameter (ID) of the PTFE tubing used for the interfacing between the flow cell 1 chip and the syringe pump was 0.5 mm. In all experiments, the volume flow rate on the syringe pump was set to 3 $\mu L\ min^{-1}$, or 5 x $10^{-11}\ m^3\ s^{-1}$. The calculations did not take into account the entry speed of the fluid at each component, but approximated velocity based on the flow rate set on the syringe

pump. The flow velocities for components in the flow cell 1 system are summarised below in Table 3.1 and presented in mm min^{-1}, m min^{-1}, m s^{-1}, and μm s^{-1}.

Table 3.1: Flow velocities (speeds) of flow cell 1 components

	Flow speed			
	mm min^{-1}	**m min^{-1}**	**m s^{-1}**	**μm s^{-1}**
Tubing	15.28	15.28 x 10^{-3}	15.28 x 10^{-5}	152.8
Deep channels	3.33	3.33 x 10^{-3}	5.55 x 10^{-5}	55.5
Shallow channels	26.6	0.026	4.44 x 10^{-4}	444

Next, residence time of fluid in the flow cell 1 system components was calculated and the results are summarised below in : . Residence time was calculated by using the flow velocity and dimensions (length or volume) for each component. Dividing the length of the channel/tubing by the velocity in mm min^{-1} yielded the number of minutes the media spent in each component, referred to as the residence time. The dimensions of each component of the flow cell 1 chip can be found in Figure 2.1. An example is shown below in **Equation 1** where the length of the tubing was equal to 150 mm (per the flow cell 1 protocols used) and the flow velocity was 15.2 mm min^{-1}, resulting in a total of 9.8 min in that component of the system.

Equation 1: Residence time of fluid in tubing in flow cell 1 system

$$Tubing\ length\ (mm) \div flow\ velocity\ (mm\ min^{-1}) = \boldsymbol{Residence\ time}$$

$$150\ mm\ \div 15.2\ mm\ min^{-1} = \mathbf{9.8}\ \boldsymbol{min}$$

Table 3.2: Residence time of fluid in flow cell 1 components

	Residence time (min)
Tubing (syringe to chip)	9.8
Deep channel (inlet)	8.3
Deep channel (outlet)	7.5
Shallow channel	0.07 (or 4.2 s)
Spheroid microwell	2.5

The total volume of the spheroid microwell was also calculated to be 7.54 mm^3 (using the equation for volume of a cylinder – the approximate shape of the flow cell 1 spheroid microwell). This volume was used to approximate the residence time for the spheroid microwell by dividing the volume by the flow velocity in the inlet channel. The flow velocity in the inlet channel would be approximately the speed of the fluid entering the well.

The spheroid microwell volume in flow cell 1 also conflicted with the loading volumes of Matrigel in the range of 10 – 20 μL that were used for flow cell 1 protocols. Loading a volume larger than that of the spheroid well caused Matrigel to spill into the channel components of the system. Furthermore, in static wells on the ULA plate, with total volume capacities of 300 μL, standard 3D cell culture protocols called for a volume of 100 μL Matrigel to be added to spheroid wells and an additional 100 μL of "replenishment" media to be added on top (Vinci et al., 2012). This meant that for the static condition, the ratio of Matrigel to spheroid media in the well was 1:1 when Matrigel was added to the static wells. In order to mimic this 1:1 ratio in the flow cell 1 microwell (with a total volume of just under 8 μL) no more than 4 μL of Matrigel could be loaded and a spheroid would need to be transferred into the well in 4 μL or less. Loading a volume of Matrigel that small was not possible due to the viscosity of the hydrogel. Furthermore, transferring a spheroid in such a small volume of media was not possible without causing damage to the spheroid or losing it during transfer. Indeed, a method using only air to transfer spheroids was attempted, where no media was used in the transfer to ascertain whether spheroids could be moved into the spheroid well with no media to reduce the liquid volume in the restricted space of the flow cell 1 spheroid chamber. A representative image of a spheroid transferred in air is shown in Figure 3.1. Ridged structures were evident on the surface of the spheroid, indicated by the darkened topographical features. This was different to the smooth, undisturbed surface seen using liquid transfers, indicating that the air only transfer was altering the shape of the spheroids. The issue of transferring in a larger volume supported the need for a larger spheroid microwell.

Figure 3.1: MCF7 spheroid transferred in air

MCF7 spheroids were formed by seeding 3.5 x 10^4 cells per well in a ULA plate. After 96h of undisturbed formation, spheroids were transferred to a plastic dish by removing all media from the static well surrounding the spheroid and cutting a 200 μL pipette tip to pick up the spheroid with air suction. Once transferred to the plastic surface, microscope images were taken of spheroids to inspect spheroid morphology. The image above is representative of *n*=3 transfer attempts. All images were taken at 50x magnification. Scale bar = 200 μm.

3.3.1.2 Development of the flow cell 2 design and characterisation of the system

Identified areas of improvement in the flow cell 1 chip included reducing the flow velocity in the tubing connecting the syringe to the chip enlarging the diameter of the spheroid well. Firstly, the tubing was changed from the previous PTFE tubing to silicon tygon tubing (Cole-Parmer, Tygon Microbore). This tubing was chosen as it was better suited to the interfacing with syringes and barbed connectors. It also had a wider inner diameter of 1.6 mm which would produce a slower fluid velocity. The widened diameter resulted in a flow velocity of 1.49 mm min^{-1} in the tygon tubing compared to 15.2 mm min^{-1} in the PTFE tubing. The length of tubing from the syringe to chip was also shortened from 150 mm to 90 mm to reduce the distance that the media needed to travel. It was also decided that the weir feature of the flow cell 1 chip was no longer required, as this was originally intended for entrapment of spheroids that were flown into the chip through the channels. The flow cell 1 design had already been optimised to include the overhead loading port on the spheroid chamber, negating the need for spheroids to be incorporated through the channels. A 3D rendering of the internal channels and chamber structures of the flow cell 2 design was shown in Figure 2.2 . The flow velocities in the flow cell 2 channels and tubing are summarised below in Table 3.3.

Table 3.3: Flow velocities (speeds) of flow cell 2 components

	Flow speed			
	mm min^{-1}	**m min^{-1}**	**m s^{-1}**	**μm s^{-1}**
Tubing	1.49	1.49 x 10^{-3}	2.45 x 10^{-5}	24.8
Channels	3.33	3.33 x 10^{-3}	5.55 x 10^{-5}	55.5

The other main need identified for the next generation of the chip was a larger spheroid microwell. The diameter of the well was increased from 2 mm to 5 mm, yielding an area of 30.52 mm^2. The chamber was 3 mm deep (2 mm deep plus 1 mm viewing port recess) giving a total volume of approximately 90 μL. Another feature added to the well area of the flow cell 2 chip was a teardrop shape connecting it to the channels. This shape mitigates the formation of bubbles in the system by reducing corners and dead ends where channels join with the chamber. Figure 3.2(A) shows a microscope image of the flow cell 2 spheroid well with Matrigel (infused with Brilliant blue™) incorporated. The teardrop shape of the well is shown in the image and also demonstrates that the Matrigel did not enter the channel. A total of approximately 90 μL of DMEM and Matrigel were used in experiments (section 2.3.7) so 90 μL total was used for the Brilliant blue test. Figure 3.2(B) shows the interfacing between the device and the tubing, connected by a syringe tip with the tubing directly inserted. Brilliant blue was used to ensure that no leaks were present in the system from inlet to outlet end.

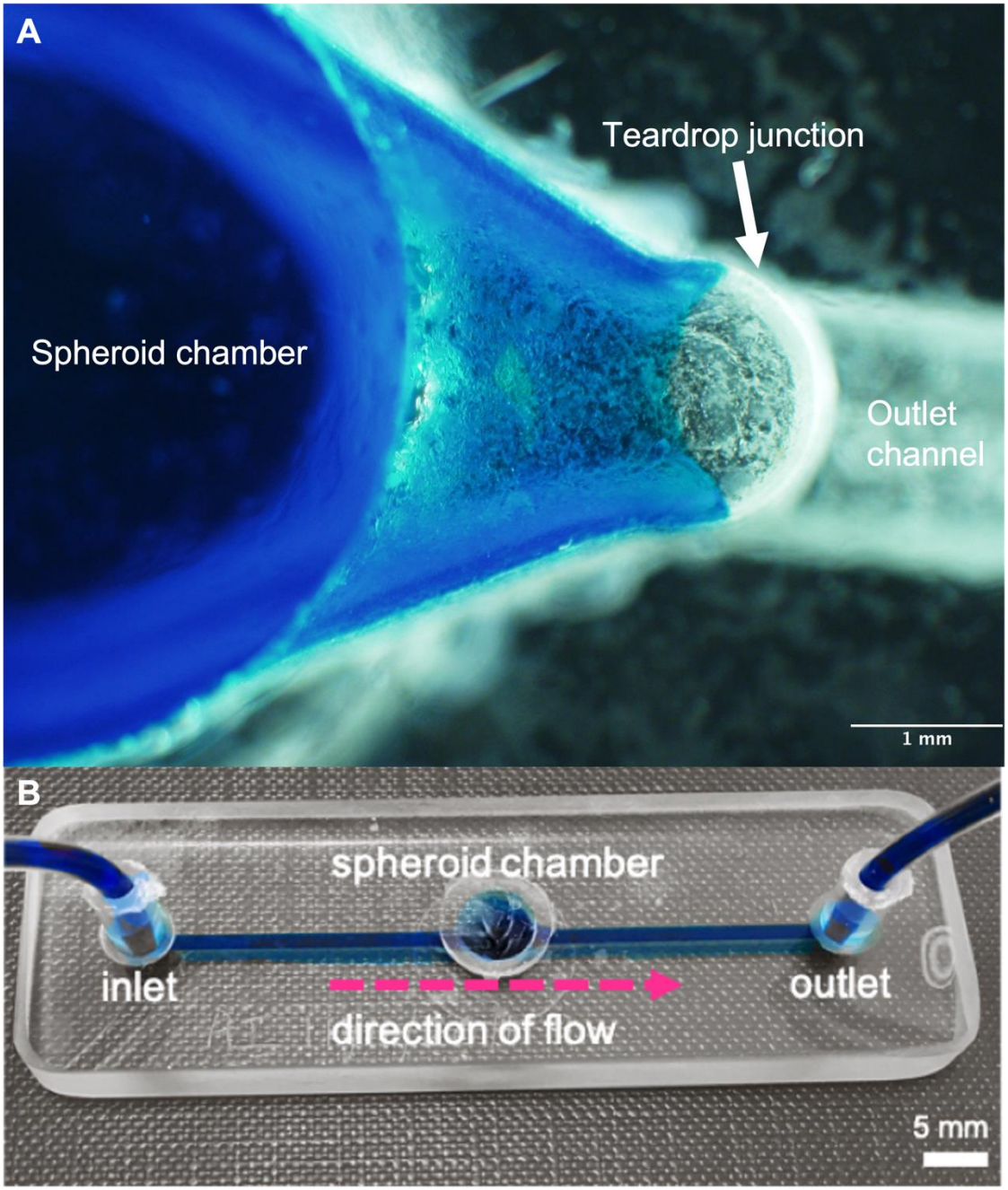

Figure 3.2 Brilliant blue™ Matrigel in flow cell 2 spheroid chamber Flow cell 2 interfacing with Brilliant blue™

(A) Brilliant blue™ dye was used to visualise the dispersion of Matrigel in the flow cell 2 spheroid chamber. Brilliant blue was mixed 1:1 with Matrigel and loaded into the spheroid well. After settling for 3-5 min at room temperature, microscope images were taken at 20x magnification. Scale bar = 1 mm. (B) Brilliant blue dye was pumped by hand with a disposable syringe through the flow cell 2 system. The syringe (not pictured) was connected to the inlet tubing of a clean flow cell 2 device and dye was pumped through the inlet tubing, the channel, the spheroid chamber, and the outlet to ensure no leaks were present. Scale bar = 5 mm.

One notable design feature of the flow cell 1 device that was kept in the flow cell 2 design was the use of a glass coverslip glued to the bottom of the spheroid well, comprising the "floor" of the well. This feature was incorporated into the flow cell 1 design as part of its optimisation and advancement process (see section 2.3.1). The glass coverslip permitted clear imaging of spheroids on-chip using an inverted microscope. As this feature was not identified as an area in need of improvement in the flow cell 1 design it remained in the flow cell 2 design. However, to facilitate further ease of imaging in flow cell 2 a viewing port was also added. This was a 1 mm deep circular recess at the bottom of the spheroid well (refer to Figure 2.2).

Following the changes to the dimensions of the device, the residence times were calculated to characterise the time fluid spent in each component of the flow cell 2 system. Due to the volume increased volume of the spheroid microwell and the shorter length of tubing with a wider inner diameter, it was important to describe how this would affect residence times. Residence times were calculated using Equation 1 and are summarised in Table 3.4.

Table 3.4: Residence time of fluid in flow cell 2 components

	Residence time (min)
Tubing (syringe to chip)	60
Spheroid microwell	27
Channels	8.3

The shear stresses in the flow cell 1 system had been previously characterised by Dr Collins (Collins, 2019a). The shear stress was then calculated for the flow cell 2 microwell to approximate the fluid shear stresses imposed on a spheroid in the chip environment. The shear stress was calculated using equation 2 where: μ = viscosity of the medium (DMEM with 10% FBS) = 0.94 x 10^{-3} Ns m^2, Q = flow rate = 3 μL min^{-1} = 5 x 10^{-11} m^3 s^{-1}, and d = 5 mm = 5 x 10^{-3} m (Frohlich et al., 2013). The shear stress in the flow cell 1 spheroid microwell was 1.34 x 10^{-3} dyne cm^2 and in the larger flow cell 2 microwell it was less, at 3.83 x 10^{-6} dyne cm^2.

Equation 2: Shear stress

$$\boldsymbol{\tau} = 32\mu Q/\pi d^3$$

Table 3.5: Shear stress in the flow cell 1 and flow cell 2 spheroid microwells

	Shear stress (dyne cm^2)
Flow cell 1 spheroid microwell	1.34 x 10^{-3}
Flow cell 2 spheroid microwell	3.83 x 10^{-6}

Lastly, the Reynolds number was calculated for the flow cell 2 system to verify the presence of laminar flow in the system channels. The Reynolds number, derived from the Navier-Stokes equation, provides a mathematical quantity to express the ratio between inertial and viscous forces acting on a liquid. The Reynolds number equation is shown in Equation 2. For the flow cell 2 system, ρ = density of medium = 1007 kg m^3, u = velocity of liquid in the channel = 5.55 x 10^{-5} m s^{-1}, d = channel diameter = 1.5 x 10^{-3} m, and μ = dynamic viscosity of medium (DMEM with 10% FBS) = 0.94 x 10^{-3} Ns m^2 (Freund et al., 2012; Frohlich et al., 2013; Poon, 2022). This yielded a Reynolds number of 8.92 x 10^{-2}, indicating laminar flow because it was below the 1000 value threshold (Freund et al., 2012).

Equation 3: Reynolds number

$$Re = \frac{forces\ of\ inertia}{forces\ due\ to\ viscosity} = \frac{\rho \cdot u \cdot d}{\mu}$$

$$Re = \frac{(1007\ kg\ m^3)(5.55\ x\ 10^{-5}\ m\ s^{-1})(1.5\ x\ 10^{-3}\ m)}{(0.94\ x\ 10^{-3}\ Ns\ m^2)} = \mathbf{8.92\ x\ 10^{-2}}$$

In summary, design modifications were made to the flow cell system design to accomplish the experimental setup required for future work. Table 3.6 summarises the differences in physical characteristics between the flow cell 1 and flow cell 2 chips. The velocity of the media in the tubing from the syringe to chip was decreased from 152.8 μm s^{-1} to 24.8 μm s^{-1}. It remained the same in the channel component because the dimensions of the deep channel in flow cell 1 were kept for the channels in flow cell 2. Residence times in the flow cell 2 system were increased in the flow cell 2 system, except for the in the channels due to remaining the same (other than the removal of the shallow channel on the outlet side). The time fluid spent in the tubing in flow cell 2 increased by just over 50 min, whilst it increased by 24.5 min in the spheroid microwell. And finally, the shear stress in the spheroid microwell was substantially reduced in the flow cell 2 spheroid well compared to flow cell 1.

Table 3.6: Comparison of physical characteristics in the flow cell 1 system to the flow cell 2 system

	Flow Cell 1	Flow Cell 2
Fluid velocities (μm s^{-1})		
Tubing velocity	152.8	24.8
Channel velocity	55.5	55.5
Residence times (min)		
Tubing	9.8	60
Spheroid microwell	2.5	27
Channels	7.5 – 8.3	8.3
Shear stress (dyne cm^2)		
Spheroid microwell	1.34×10^{-3}	3.83×10^{-6}

3.3.2 Viability of spheroids in flow cell 2 system

To assess cell viability in spheroids, FDA staining was used to visualise viable cells. Spheroids kept in static and flow conditions were stained after 72h and images were used to identify the presence of viable cells. Figure 3.3 shows a representative image of a static spheroid (A) and a flow spheroid in the flow cell 2 device (B). Figure 3.4 shows a representative image of MCF7 spheroids in the flow cell 2 chip that were stained with FDA. Viable cells were indicated by the presence of the green fluorescent dye which signifies that cells have metabolised the FDA, converting it to fluorescein (Jones & Senft, 1985). In both panels A and B, the spheroids were green, indicating the presence of viable cells. The image also demonstrates the morphological difference in spheroid edges between the use of Matrigel in the well (B) versus the spheroid in media only (A).

Fluorescence was quantified as described in section 2.2.5 for both static and flow spheroids. Quantified fluorescence is represented in Figure 3.5. The CTCF values for static and flow spheroids were calculated as described previously. Relative fluorescence was determined by dividing flow CTCF values by their static counterparts. The relative fluorescence intensity of flow spheroids was not significantly increased compared to static spheroids. However, a large SEM was present as a result of variation between replicates.

3.3.3 Evaluation of secreted VEGF levels in flow cell 2 system

A VEGF ELISA was also used to assess secreted levels of the protein from static and flow U-87 MG spheroids. These cells are known to secrete high levels of VEGF, therefore providing a benchmark to assess whether spheroids in our flow cell 2 system were reproducing previously characterised traits. Figure 3.6 shows the results of this preliminary test on *n*=1 effluent samples from static and flow U-87 MG spheroids. Statistical testing was not performed due to the low sample size. However, after just 24h in the flow system spheroids secreted 6353 pg/spheroid more VEGF than static counterparts. These levels of secretion were higher than those we reported previously in our lab but confirmed that the spheroids in flow secreted significantly higher levels of VEGF than static counterparts (Collins et al., 2021).

3.3.4 Evaluation of spheroid growth patterns

Spheroids from 3 cell lines were seeded at 5 densities and growth was monitored for a total of 21 days. A logistic growth curve (nonlinear regression) was generated as shown in Figure 3.7. 9.0×10^4 cells/well was chosen as the seeding density for future experiments because MCF7 and MDA-MB-231 spheroids were growing between days 4-7 as evidenced by the upwards line slopes in the charts for those cell types (in green).

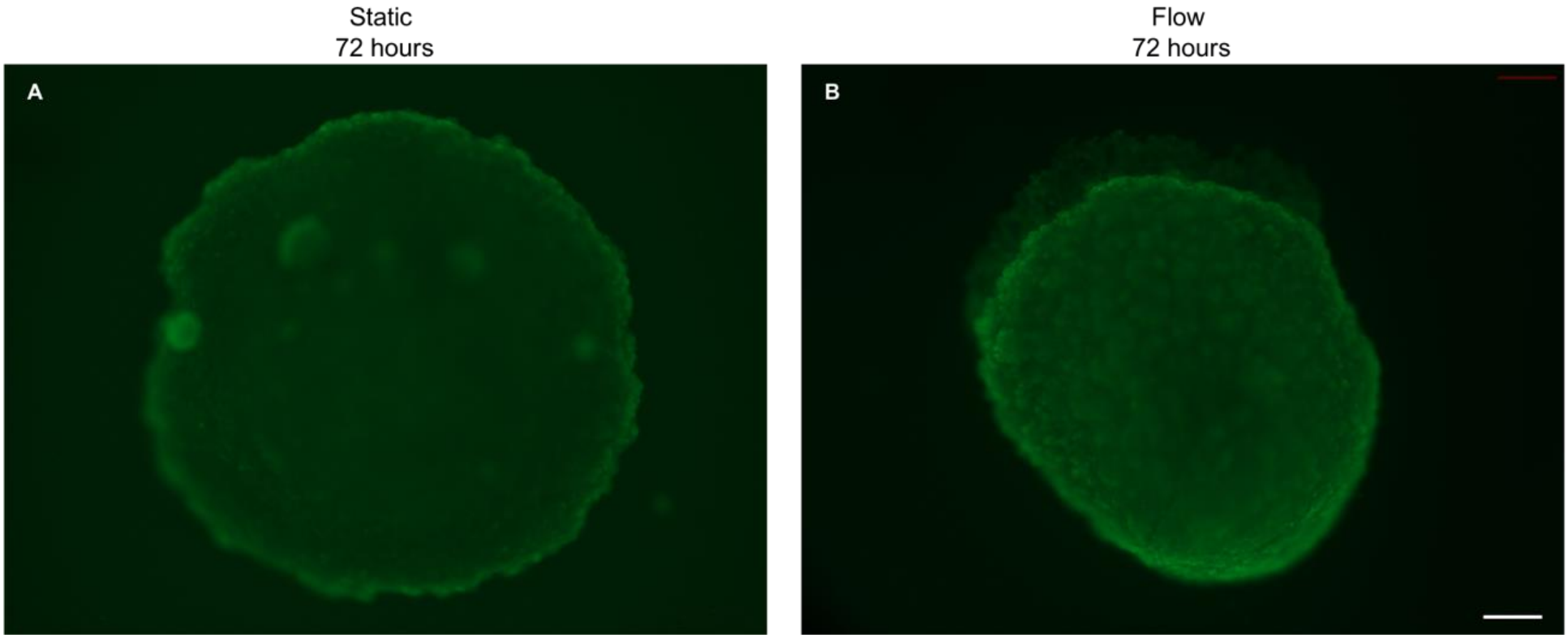

Figure 3.3 Static and flow spheroids stained with FDA

MCF7 spheroids were generated from 9.0 x 10^4 cells seeded in a ULA plate and formed for 96h. Spheroids were then either kept on the ULA plate (static; (A)) or transferred to a flow cell 2 chip (flow; (B)) and kept in Matrigel in these conditions for 72h. At the end of experiments, spheroids were stained with FDA and microscope images were taken at 50x magnification. Scale bar = 200 μm.

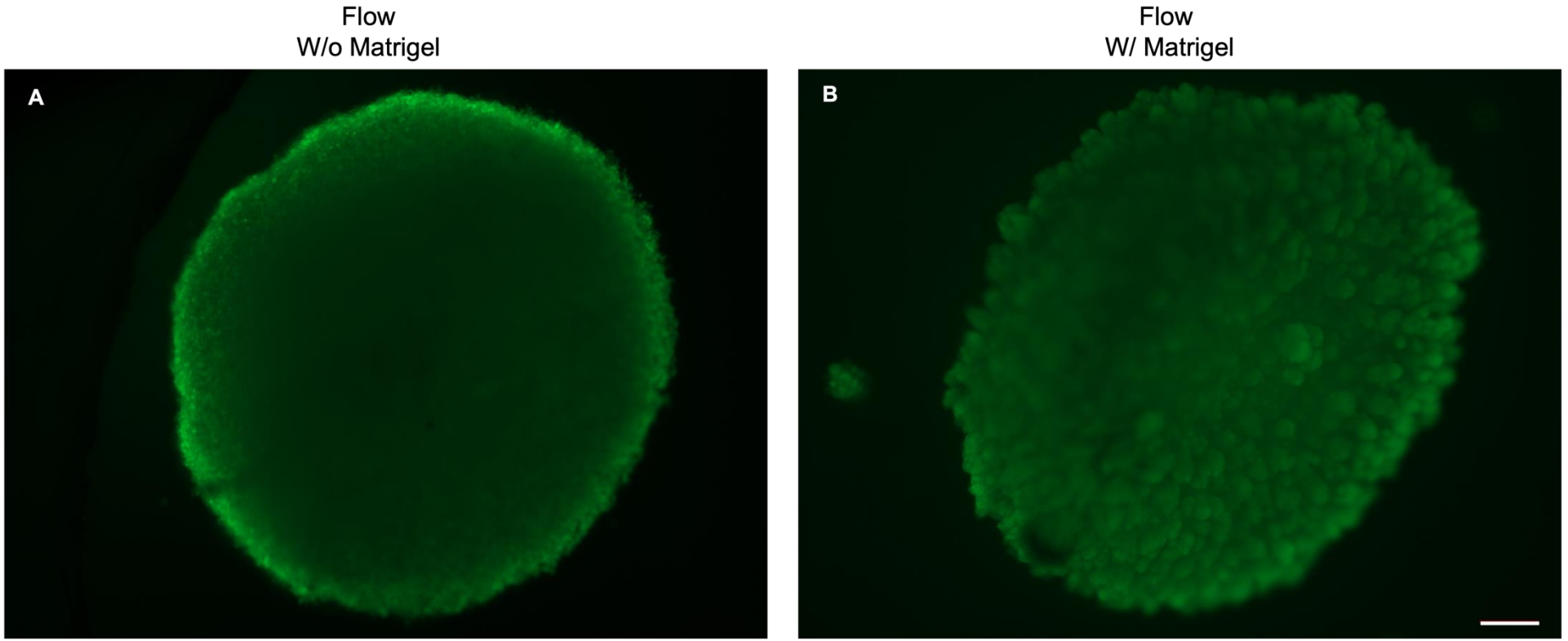

Figure 3.4: FDA stained spheroids in flow

MCF7 spheroids were generated from 9.0 x 10^4 cells seeded in a ULA plate and formed for 96h. Spheroids were then transferred to a flow cell 2 chip with Matrigel (B) or without (A) for 72h. At the end of experiments, spheroids were stained with FDA and microscope images were taken at 50x magnification. Scale bar = 200 μm.

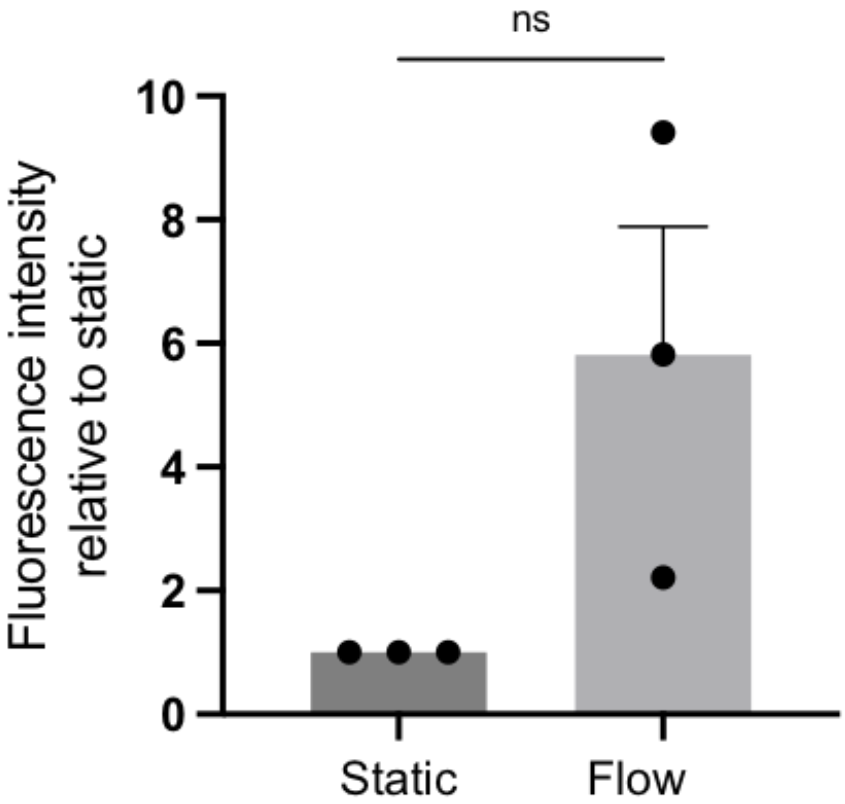

Figure 3.5: FDA fluorescence intensity relative to static

MCF7 spheroids were generated from 9.0 x 10^4 cells seeded in a ULA plate and formed for 96h. Spheroids were then either kept on the ULA plate (static) or transferred to a flow cell 2 chip (flow) and kept in Matrigel in these conditions for 72h. At the end of experiments, spheroids were stained with FDA and microscope images were taken at 50x magnification. Fluorescence quantification was performed as described in 2.2.5 and relative fluorescence was determined for flow compared to static. Statistical significance was determined using student's paired t-tests; ns = not significant.

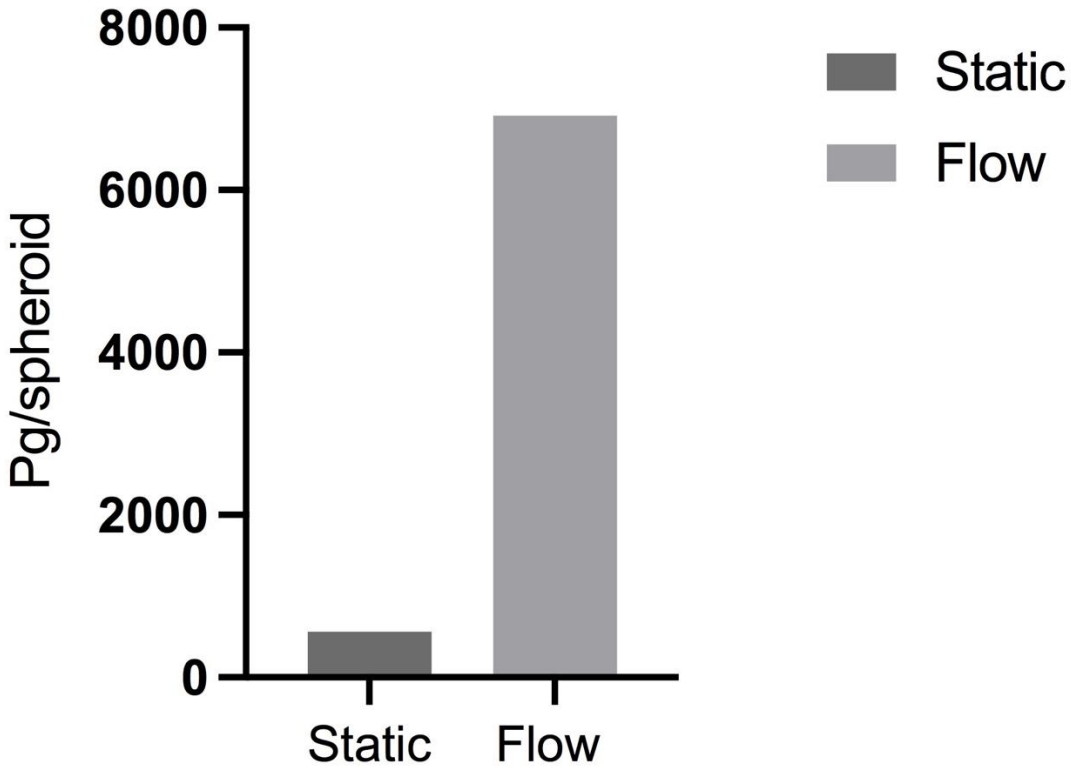

Figure 3.6: VEGF secretion of U-87 MG spheroids in flow cell 2 system

U-87 MG spheroids were generated by seeding 9.0 x 10^4 cells per well in a ULA plate. Spheroids were allowed to form for 96h undisturbed at which point they were either transferred to the flow cell 2 device by incorporation into the spheroid chamber (flow), or they were left in a ULA plate well (static). Spheroids were kept in static or flow conditions for 24h and effluent media was collected from each at the end of experiments. Effluent media samples were used for a VEGF ELISA, performed as described in section 2.9. Chart represents *n* = 1 experiment. Statistical testing was not conducted due to low sample size.

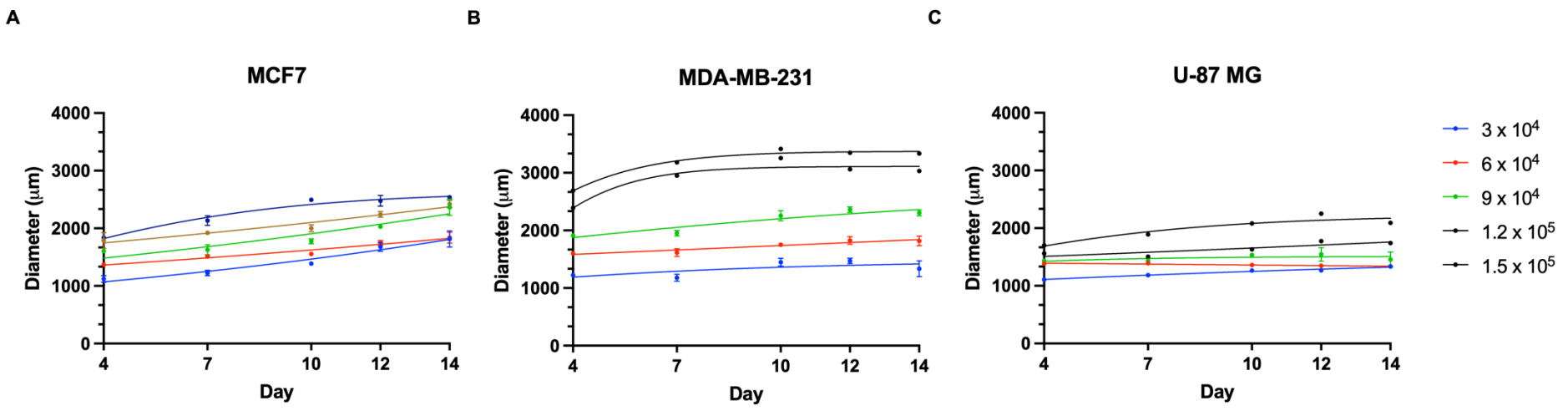

Figure 3.7: Spheroid growth patterns off-chip

MCF7 spheroids (A), MDA-MB-231 spheroids (B), and U-87 MG spheroids (C) were seeded at 5 different densities and grown for 2 weeks (14 days). A nonlinear regression curve was applied. Colours correspond to seeding densities (legend on right side of panel C).

3.3.5 Optimisation of RNA extraction for spheroids on-chip

A series of experiments were conducted to establish RNA yields from various sizes and numbers of spheroids. This was done using spheroids seeded at densities used previously in the flow cell 1 chip to reflect the yields that could be produced from the flow cell 1 experimental setup. At the time of sample collection, spheroids were used for extraction either as a singular spheroid (x 1), in pairs (x 2), or in groups of 3 (x 3). Spheroids were also seeded at 3 different densities. The results are outlined in Table 3.7.

It was envisaged that RNA would be used for qPCR analysis. Therefore, it would need to first be synthesised into cDNA. To do so, 1 μg of starting RNA material was needed in a volume of no more than 11 μL. At this threshold, a yield of 90-91 ng/μL was required. This was determined by dividing 1000 ng (equal to 1 μg) by the yield in ng/μL, resulting in the volume of extracted RNA which is equal to 1μg. Whilst it is possible to synthesise cDNA from smaller quantities of starting RNA, we sought to use this amount for all experiments to maintain consistency. As evidenced by the values in Table 3.7 where the maximum yield achieved was 73.4 ng/μL, the sizes and quantity of spheroids possible for use in the flow cell 1 system were not sufficient for producing enough RNA starting material.

Table 3.7: RNA yields from flow cell 1 sized spheroids

Seeding density	No. of spheroids	A_{260}/A_{280}	RNA yield (ng/μL)
5.0×10^3 cells	1	2.06	10.3
	2	2.09	35.9
	3	2.09	38.4
1.0×10^4 cells	1	2.16	24.4
	2	2.07	36
	3	2.1	46.3
2.5×10^4 cells	1	2.09	43.1
	2	2.08	71
	3	2.05	73.4

Following the advancement from flow cell 1 to flow cell 2, and therefore the use of larger spheroid sizes (9.0×10^4 cells/well at seeding) in the larger microwell, further optimisation experiments were conducted to assess the number of spheroids needed to achieve a minimum yield of 90 ng/μL. In these experiments, spheroids were incorporated into the flow cell 2 system and perfused for 24h before collection and RNA extraction. Table 3.8 summarises the results of

those experiments and outlines the changes to the extraction procedure that were incorporated during the optimisation process. Values in red indicate that the yield was not sufficient.

Table 3.8: RNA yields from spheroids in flow cell 2 system and protocol amendments

No. of spheroids	Timepoint (h)	A_{260}/A_{280}	RNA yield (ng/μL)
1	24	2.1	21.9
1	72	1.89	5.1
1	72	1.98	8.6
Protocol amended: samples collected, lysed, and RNA extracted fresh			
1	24	2.08	42.3
1	24	2.08	57.5
Protocol amended: final elution volume decreased from 40 μL to 30 μL			
1	24	2.06	75
Protocol amended: Corning cell recovery solution used for harvest from Matrigel and harvests done in groups of 3 spheroids			
3	24	2.09	135.9
3	72	2.08	185.7

A test for determining protein extraction yields was also conducted. Similar to the procedure for RNA outlined previously, spheroids were harvested either as a singular spheroid (x 1), in pairs (x 2), or in groups of 3 (x 3). For the purposes of Western blotting, 30 μg of prepared protein would be loaded per well. Ideal loading volumes for a 10-well gel would be no more than 30 μL meaning that protein yields would ideally be greater than 1 mg/mL at a minimum. As shown in Table 3.9 the yields produced by spheroids in the flow cell 2 system were all greater than 1 mg/mL.

Table 3.9: Protein yields from spheroids in flow cell 2 system (average of *n* = 3)

No. of spheroids	Protein yield (mg/mL)
1	4.39
2	5.41
3	6.93

3.3.6 Evaluation of gene expression changes in different incubator environments

The chip setup required that microfluidic devices be housed in an external egg incubator (which we referred to as the flow incubator) during experiments to permit use of a syringe pump. This

meant that static spheroid plates were housed in a standard cell culture incubator whereas flow spheroids on-chip were housed in the egg incubator. A goal of the project for subsequent chapters was to evaluate changes in gene expression, so a qPCR test was used during the optimisation process to determine whether different incubators would introduce variability between the conditions that could affect results. The key variables between incubator environments were the lack of CO_2 and temperature regulation in the egg incubator used for flow compared to the tightly regulated cell culture incubator used for static plates. A preliminary qPCR analysis was performed using static samples collected from 2 conditions: static spheroids kept in the regular cell culture incubator and static spheroids kept in the external flow incubator. The goal was to evaluate changes in gene expression and as part of optimising the conditions for this *VEGFA* was chosen as the transcript as it had been previously used for static vs. flow experiments in our lab. VEGF protein secretion was also shown to be increased in flow in the flow cell 1 system (Collins et al., 2021). The results of these experiments conducted using the flow cell 2 system are shown in Figure 3.8. Flow spheroid transcripts of *VEGFA* were significantly less than static counterparts regardless of the incubator used for housing static plates. In the experimental setup representing the standard protocol for static vs flow, shown in fig. 3.12(B) flow spheroids were the most significantly different to static in their *VEGFA* transcript levels (**p = 0.0028) and transcripts were downregulated by an average of 0.87 fold change (FC). The effect was less pronounced in the comparison to static spheroids in the flow incubator but still observed.

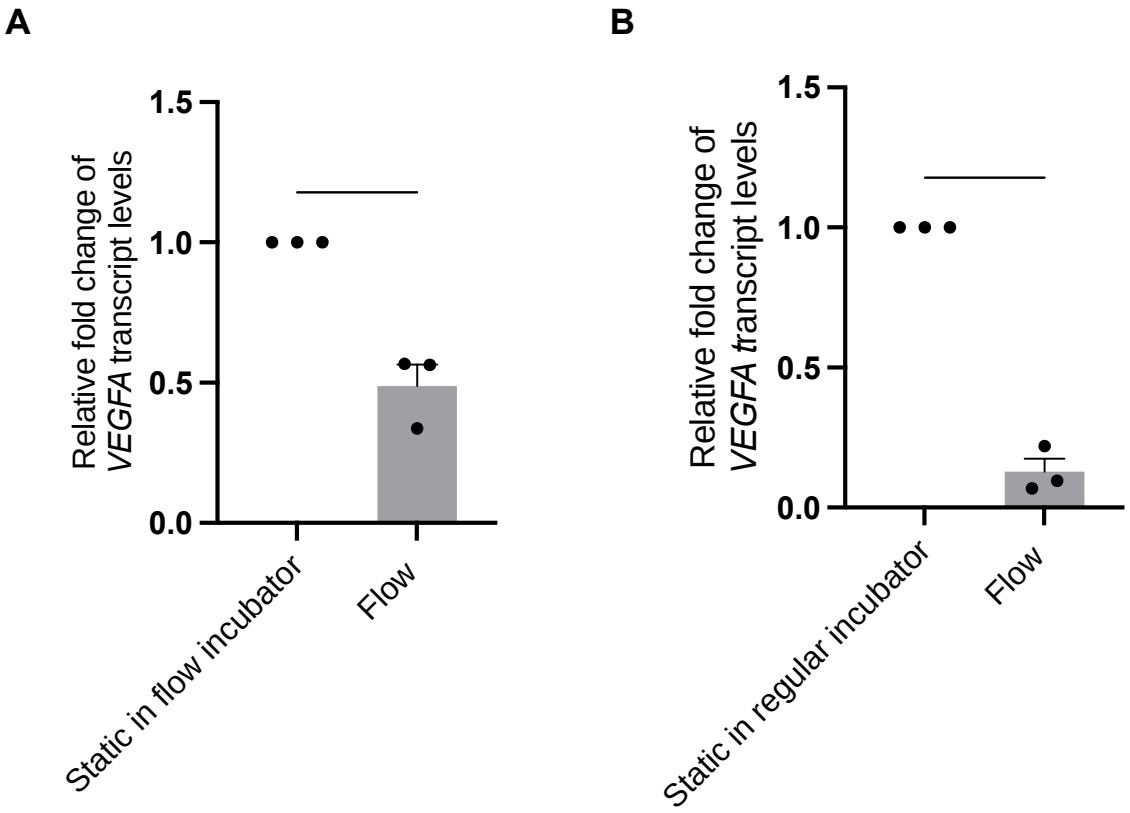

Figure 3.8: Comparison of *VEGFA* transcript levels of spheroids in different incubators

MCF7 spheroids were formed from 9.0 x 10^4 cells seeded in a ULA plate and allowed to form for 96h. Spheroids were kept in a ULA plate, with Matrigel added to reflect standard static v. flow experiments. One plate was placed in the external "flow" incubator and the other kept in the standard cell culture incubator. The flow cell 2 chip was set up in the standard manner described previously Spheroids were kept in these conditions for 72h. Total RNA was extracted and used for qPCR analysis, with *B2M* as the housekeeping gene. Data represent the mean of *n*=3 experiments. Error bars represent mean ± SEM. Statistical significance was determined by paired student's t-tests; *p <0.05; **p<0.01.

3.4 Discussion

Fluid flow is increasingly recognised as a prominent feature of solid tumours but is still poorly understood. We sought to fill this area of unmet need by using a microfluidic device to produce interstitial-like flow in a controlled manner, allowing for study of its effects on cancer cell spheroids in the system. Using a previously designed chip from our lab, the flow cell 1 device, we advanced the design to cater to the experimental needs we envisaged for the overarching aims of this project. The aims of this chapter were to:

1. Identify areas of improvement in the flow cell 1 chip design.
2. Develop a new chip design, the flow cell 2, incorporating the improvements identified in the flow cell 1 design.
3. Establish viability of spheroids in the flow cell 2 system.
4. Optimise the protocols for extracting cellular components, such as RNA, from static and flow spheroid lysate samples.

The following discussion outlines how these aims were achieved and the implications of the results produced.

3.4.1 Evolution from the flow cell 1 to flow cell 2 system

The flow velocities in the flow cell 1 system, particularly in the tubing, were faster than those reported for interstitial flow in the literature. The velocity in the flow cell 1 system was much higher than values reported in the literature at 152.8 $\mu m\ sec^{-1}$ in the tubing. This meant that fluid was entering the chip at a velocity higher than expected for IFF. The flow velocity in the tubing was reduced to 24.8 $\mu m\ sec^{-1}$ in the flow cell 2 system by increasing the diameter of tubing used connecting the syringe to chip, resulting in a velocity closer to ranges reported in the literature. One study reported IFF velocity as low as 0.1 $\mu m\ s^{-1}$ in mice while another study reported velocities as high as 55 $\mu m\ s^{-1}$ (Dafni et al., 2002; Munson & Shieh, 2014). The velocity in the channel component was calculated to be approximately 55 $\mu m\ s^{-1}$ in both of the flow cell systems. However, this did not take into account the velocity of the fluid entering the channel, which was affected by the change in tubing. Computer-based modelling should be used in future work to accurately describe the velocities in the flow cell 2 system.

The residence times were overall increased in the flow cell 2 system compared to the flow cell 1 system as a result of design changes. To the best of our knowledge, there are no defined values for the speed of replenishment of interstitial fluid *in vivo* in normal tissue nor tumour stroma. Thus, a framework for modelling the replenishment of media in the system could not be

followed. Instead, the focus of the work using the flow cell 2 system focused on replicating interstitial flow and investigating how continuous replenishment of media would affect the biology of a spheroid. Tumours do not typically experience high velocities and fluid shear stresses, though research suggests they are subjected to other biomechanical strains and forces caused by overcrowded tissue matrices. Indeed, cancer cells are not usually subjected to high fluid velocities unless they have entered blood circulation, where velocities can reach up to 105 $\mu m\ s^{-1}$ (example given is at the aorta) (Thurston, 1976). Therefore, it was desirable for the flow cell 2 system needed to maintain a low level of shear stress to investigate the effect of slower, interstitial-like flow.

For RNA to be extracted from the flow condition, spheroids also needed to be easily retrieved from the well and without damage. The RNA yield needed to be high enough to perform cDNA synthesis, which required 1 μg of mRNA. Initial tests of RNA extraction using spheroids at the sizes accommodated by the flow cell 1 chip (Table 3.7) were not in range of sufficient RNA. An alternative approach was to increase the size of the spheroids used, but the flow cell 1 chip spheroid well diameter was too narrow to accommodate larger spheroids. Therefore, the diameter of the well was identified as needing to be enlarged.

Additionally, the volume of the flow cell 1 microwell was less than 10 μL, but original protocols called for 20 μL of Matrigel to be loaded. Thus, a contradiction between capacity of the well and volumes required was highlighted. In static wells, 100 μL of Matrigel was added for experiments, further highlighting a major difference between the static and flow conditions. Therefore, enlargement of the spheroid microwell would also serve as a closer comparison to the static condition in regards to environment volume.

A larger well also creates opportunities for future work to involve the use of more than one spheroid in the well at the same time. Due to the variations in flow dynamics that this would cause, we chose to not examine this in the current study as we wanted to examine the isolated effect of interstitial-like flow on cell biology. However, we acknowledge that the design of this chip could be used for alternative experimental designs in the future.

3.4.2 Incorporation of large spheroids into the enlarged flow cell 2 microwell

The experimental design envisaged for understanding how interstitial flow was affecting cell biology was based on the comparisons between static and flow spheroids. Therefore, static spheroids needed to be used in parallel to the flow cell 2 experiments. Whilst growth was measured up to 21 days, static spheroids receiving replenishment of media every 2-3 days were disintegrating as early as 12-14 days. Spheroids in this state would not be able to be collected

for the downstream analyses comparing static and flow. Therefore, in combination with the results established previously in our lab, the growth curve confirmed that 72h (equal to day 7 of the growth curve) was a reliable timepoint for both static and flow spheroids and that a seeding density of 9.0×10^4 cells/well was suitable for maintaining logarithmic growth during that period.

One reason for the importance of the larger spheroid size capacity in the flow cell 2 device was to fully capitalise on the low throughput, precise monitoring system we envisaged. That is, rather than having a focus on a large quantity of smaller sized spheroids for a high throughput approach, we aimed to closely monitor the effects of flow on a physiologically relevant tumouroid without the concern of size constraints in the well. Tumours *in vivo* vary greatly in size and composition and a variety of sizes of spheroids have been used in the literature for TME investigations (Elkin et al., 2005). For example, one group looking at flow and pressure used 50,000 cells/tumouroid to create compressed cell masses infused with collagen to be used on-chip (Azimi et al., 2020). Another study aimed at drug screening used seeding densities in the range of 10,000 – 30,000 cells/well (Monteiro et al., 2020). Others, generally in the case of 96-well, high throughput chip designs, can use seeding densities even lower.

It is also reported that tumours *in vivo* cannot grow beyond 1-2 mm in diameter unless they are vascularized. This is due to the maximum distance that oxygen and nutrients can diffuse without an "active" blood supply (Kimlin et al., 2013). Furthermore, large spheroids (> 500 μm) have an external proliferating zone, an internal quiescent zone (due to limited distribution of oxygen, nutrients, and metabolites), and a necrotic core. This better resembles the cellular heterogeneity of tumours *in vivo* (Daunys et al., 2021). Using spheroids of a larger size was therefore an advantage for better replication of an early stage tumour, prior to angiogenesis and subsequent invasion. The spheroid sizes for all 3 cell lines used in our experiments were established to be between 1000 and 2000 μm between days 4 and 7 in the off-chip growth curve experiment (see Figure 3.7). This indicated that spheroids used in our experiments would be appropriately sized to recapitulate the distinct zones of spheroids (Barisam et al., 2018).

A potential future direction for the use of the flow cell 2 system could be investigations into drug delivery and effects of therapeutic agents on spheroids experiencing IFF. In such a scenario, realistically modelling drug penetration would be lucrative (Minchinton & Tannock, 2006). 2D models are frequently recognised as failing to accurately predict the success of drugs *in vivo* in large part due to the lack of 3D structures and layers present in 2D (Carter et al., 1989; Chambers et al., 2014). Therefore, the use of 3D spheroids at sizes with distinct zones in an IFF environment could provide clearer indications of whether drugs would successfully penetrate the TME *in vivo.*

3.4.3 Viability of spheroids in the flow cell 2 system

The previous sections established that the flow cell 2 system could accommodate larger spheroids and the volumes required for appropriate Matrigel loading. However, we needed to confirm that spheroids of this size and at these timepoints were comprised of viable cells. It is expected that in most spheroids there will be a heterogeneous population of cancer cells, including some that are necrotic depending on the size of the spheroid (Mehta et al., 2012). Indeed, a necrotic core is also common in many tumours (Liu & Jiao, 2019). However, to ensure that spheroids were not dead and did contain viable cells, we used FDA staining to visualise viable cells in static and flow spheroids, seeded at the size selected from the growth curve and at the maximum timepoint of 72h to be used in subsequent experiments. The staining confirmed that viable cells were present in the spheroids in both conditions. Fluorescence was quantified to determine the relative levels of fluorescence intensity. Flow spheroids did not have significantly increased fluorescent intensity compared to static counterparts. In the context of viability though it is biologically relevant that spheroids in flow were not less viable than static as this would suggest that the flow condition diminished viability of cells. Instead, we saw an overall trend of greater FDA fluorescence intensity in flow which correlates to better viability.

A major limitation of this procedure was that a dye for dead cells could not be used as it produced too much background signal. Additionally, using 2D imaging on a 3D mass such as a spheroid inevitably neglects to visualise the entire spheroid. Unfortunately, confocal microscopy was not an option for these experiments due to cost limitations, but we have identified this as an area for future work. Confocal imaging would allow all layers of the spheroids to be visualised.

It was also noted that the appearance of spheroids in flow differed from the appearance of spheroids in static wells. Figure 3.3 shows an example of FDA stained spheroids kept in static and flow conditions for 72h. In panel A, a static spheroid is depicted with a smooth surface and uniform appearance along the perimeter edges. In contrast, panel B shows a spheroid that has been in flow for 72h and has a different surface and edges to that of the static spheroid. The flow spheroid has texture on the surface and the upper edge has protrusions lining the perimeter whereas the static spheroid has a smooth surface and no visible protrusions. This was also demonstrated in Figure 3.4 (B) where the textured surface of a spheroid in flow appears to have small nodules or protrusions forming. Whilst these were only observations, they laid an exciting groundwork for investigation of changes between the conditions at transcript level in the following chapters.

The results of the preliminary test of VEGF secretion by U-87 MG spheroids in flow aligned with previous findings in our lab, establishing that U-87 MG spheroids in flow secrete higher levels of

VEGF (Collins, et al.). However, we wanted to confirm that the use of the external egg incubator for flow experiments was not responsible for changes seen between the static and flow conditions. The external incubator used for flow experiments, referred to as the "flow incubator", was temperature regulated but not humidified like the standard cell culture incubator where static plates were housed. This raised concern in terms of keeping variation between conditions limited to the differences in fluid flow, i.e. static and flow. If the difference in incubator environments was introducing another variable that could be responsible for any changes detected between the conditions in future work, this would need to be addressed. As a test, a static plate of spheroids was kept in the flow incubator for 72h while flow cell 2 chips were also housed there with the continuous perfusion setup, and another static plate was kept in the standard cell culture incubator in parallel. Total RNA was extracted from all 3 conditions and qPCR was used to analyse *VEGFA* transcript levels. As seen in Figure 3.8, there was significant downregulation of *VEGFA* transcripts in the static spheroids kept in the flow incubator compared to those kept in the regular cell culture incubator. However, when transcript levels from static spheroids in the flow incubator were compared to transcripts from flow spheroids (in the same flow incubator during the same experiment), there was still significant downregulation of *VEGFA* in flow compared to static. This suggested that regardless of the incubator environment used, flow spheroids saw decreased *VEGFA* transcript levels compared to static counterparts. Whilst these findings did not align with the high levels of VEGF secreted by U-87 MG spheroids in flow this could have been due to the use of a different cell line (MCF7) for the transcript experiments. Nonetheless, these results laid more groundwork for establishing differences in cell biology between static and flow spheroids, which will be explored in more detail in the next chapter.

3.4.4 RNA and protein can be efficiently extracted from spheroids on-chip

It was envisaged that differences between static and flow spheroids would be evaluated in future work by examining transcriptomic changes. In order to do so, total RNA would need to be extracted from spheroids in both conditions and in quantities sufficient for synthesis of cDNA. Initial experiments using the flow cell 1 device showed even by grouping 3 spheroids together and extracting RNA from the combined sample, yields were low. This contributed to the increased chamber size incorporated into the design of the flow cell 2 device, permitting the use of larger sized spheroids. However, the preliminary experiments using the flow cell 2 device also demonstrated low yields. Through a series of protocol modifications, a method was established to consistently extract RNA from spheroids on-chip to attain yields appropriate for downstream analyses.

Similarly, protein yields were determined for spheroids extracted from the flow cell 2 system. In this case protocol modifications were not required as the yields attained from preliminary

experiments demonstrated that sufficient quantities of protein could be extracted and prepared for further analysis.

3.4.5 Different incubator environments did not significantly impact measured results

An overarching goal of the refinement process from the flow cell 1 system to the flow cell 2 system was to reduce as much variation as possible between the static and flow conditions so that (theoretically) fluid flow would be the only independent variable introduced between spheroids. The flow vs static experimental setup prescribed keeping spheroids in the flow cell 2 system in an external incubator and this contrasted with the use of a temperature regulated, humidified cell culture incubator used to house static spheroid plates. Therefore, we investigated whether being in a different incubator environment would significantly impact an experimental outcomes that we aimed to measure in future work. We planned to do analysis of transcript level changes between static and flow spheroids, so qPCR was chosen as a test. *VEGFA* was chosen as the gene transcript to measure as this had been established in the use of flow protocols in our lab previously. *VEGFA* transcripts were downregulated in flow compared to either static condition (Figure 3.5) but the effect was most significant when static spheroids were kept in the regular cell culture incubator. This demonstrated that changes in transcript levels for flow spheroids compared to static in either incubator were comparable and therefore should not impact experimental outcomes in a significant manner.

3.4.6 Chapter conclusion

In summary, the work in this chapter advanced the flow cell 1 chip to the flow cell 2 chip design. The new chip design made the device fit for purpose by accommodating the size of spheroids needed and the volumes of Matrigel needed to conduct reliable analyses. We confirmed that spheroids in the flow cell 2 system were viable and that sample types such as RNA and could be extracted for further experiments. The optimisation of this system laid the foundation for the work conducted in the following chapters where the interstitial-like flow created in the flow cell 2 system could be used for investigations into cell biology changes.

Chapter 4 Investigating the effects of interstitial flow on cancer cell biology in the TME

4.1 Introduction

The previous chapter established a spheroid-on-chip system, known as the flow cell 2 system, which could house viable spheroids for up to 72h, and which could be harvested for use in downstream analyses. The system produces interstitial-like flow, combined with the use of 3D spheroids embedded in Matrigel, to recapitulate the basis of a tumour microenvironment experiencing interstitial flow. This chapter seeks to use that system to establish an understanding of how interstitial flow may affect cell biology in this environment, as it is an under-researched area.

4.1.1 Interstitial fluid in the TME

Interstitial fluid exists in the interstitial space between tissues, in both normal and tumour tissues. ISF delivers nutrients, removes metabolic wastes, and provides mechanical cues to cells and the ECM. In tumours, tissue structure and the ECM are adversely altered by overcrowded and unorganised blood vessels, which in turn affects the environmental fluid dynamics as well. These changes in tumour stroma have been recognised as clinically important for cancer patient outcomes due to their association with resistance to treatment (Munson & Shieh, 2014). However, despite the significance of biophysical forces in the TME, interstitial fluid flow remains poorly understood in this contest.

4.1.2 Gene expression changes caused by interstitial flow

Studies have started to examine the effects of interstitial fluid flow due to the growing interest in ISF and appreciation for the role it plays in cancer outcomes. For example, Jung Lee and colleagues established YAP1 as a fluid mechanosensor sensitive to changes in fluid shear stresses, and ultimately driving cancer cell migration (Lee et al., 2017). Ground-breaking work by Sheih, Swartz, and Munson has asserted that interstitial flow increases invasion of cancer cells (Shieh et al., 2011; Munson et al., 2013). They have established these outcomes in multiple cancer types but, importantly, none of the studies used 3D aggregates of cancer cells as part of the experimental design (Shah et al., 2015; Kingsmore et al., 2016).

Much more work has been done in the area of endothelial cells and effects of fluid shear stresses, such as those seen in vascular networks, on gene expression changes. Helle and colleagues examined transcriptomic remodelling of endothelial cells induced by flow replicating blood flow-induced shear stress (Helle et al., 2020). Another study using renal epithelial cells also established transcriptomic changes caused by variations in fluid shear stress that lead to upregulation of TGF-B, MAPK, and Wnt signalling pathways (Kunnen et al., 2018). Yang & Xu also

used low shear stresses to analyse gene expression profiles of endothelial cells and found significant differences in their transcriptomes as a result of flow (Yang & Xu, 2021). Whilst these studies did not use cancer cells or indeed even a tumour-like microenvironment, they point to the significant influence that fluid flow is capable of asserting on the gene expression profile of cells.

4.1.3 Hypoxia in the TME

Hypoxia is another physiology that is well established as playing a role in the TME and cancer progression. Breast cancer is reported to generate some of the most hypoxic tumours of all cancer types (Favaro et al., 2011). Irregular and leaky vasculature in tumours leads to poor blood perfusion of the area and as a result, hypoxic regions are commonly observed. Oxygen levels drop below 2% and can even go anoxic in some cases (<0.02% O_2). Somewhat counterintuitively, this lack of oxygen in a primary tumour is often associated with more aggressive tumour types, increased metastasis, and worse overall survival rates (Semenza, 2003; Vaupel et al., 2004). To the best of our knowledge, few studies have examined the specific interaction of hypoxia and interstitial flow in the TME, even though both are prevalent physiologies of tumours (Rofstad et al., 2014).

4.1.4 Chapter specific hypothesis, aims, and objectives

Our spheroid-on-chip model with tight control of interstitial flow rate was well poised to investigate how fluid flow similar to that of ISF in the TME may play a role tumour progression, ultimately leading to metastasis. We hypothesized that based on the literature, where various flow rates were shown to increase expression of EMT markers in cancer cells and dramatically induce genotypic changes in endothelial cells, that breast cancer spheroids in our flow cell 2 chip would follow a similar pattern. The aim of this chapter was to evaluate the effects of interstitial flow on cancer cell biology in the TME. To accomplish that, the following objectives were outlined:

1. Examine how markers of EMT in cancer spheroids are impacted by interstitial flow.
2. Evaluate transcriptomic changes in cancer spheroids caused by interstitial flow.
3. Evaluate whether interstitial flow influenced protein expression profiles of cancer spheroids in interstitial flow.
4. To investigate the relationship between interstitial flow and hypoxia and how they affect cancer spheroid biology in the TME.

4.2 Experimental design

4.2.1 Investigation of changes in EMT markers

Previous studies identified upregulation of EMT markers in cancer cells exposed to fluid flow. Therefore, a panel of genes known to be associated with EMT were used for qPCR analysis (as described in chapter 2 section 2.5.3). MCF7 spheroids were formed as previously described (2.2.1) and exposed to static or flow for either 24h or 72h to investigate the impact of increased duration in a given condition.

Additionally, to query whether differences between static and flow biology relating to EMT might be present in protein expression rather than at transcript level, Western blotting was used to detect expression of E-cadherin in MCF7 spheroids. Spheroids were kept in static or flow conditions as described previously for 24h and 72h. Protein was extracted and analysed as described in section 2.8.1.

4.2.2 Whole transcriptome analysis of static and flow spheroids

The gene expression changes of EMT markers conducted by qPCR analysis were unexpected in the flow cell 2 system and did not provide a clear understanding of how interstitial flow was affecting cell biology. Therefore, an unbiased approach allowing broader evaluation of expression patterns was needed. RNA-seq was used as described in section 2.6 to evaluate the whole transcriptome of MCF7 spheroids. Spheroids were formed as described previously (2.2.1) and kept in static or flow for 24h before total RNA was extracted. A total of 3 independent experiments were conducted in this manner, yielding 3 static samples and 3 flow samples to be sequenced. The 24h timepoint was chosen to represent early stage changes that may be occurring at transcript level in the MCF7 cells. The resulting RNA-seq dataset was analysed using a series of tools, outlined in section 2.7, to identify patterns of expression change at transcript level between the static and flow conditions.

4.2.3 Validation of DEGs and enrichment patterns

The differential expression of genes and associated enriched pathways identified by RNA-seq were evaluated using qPCR analysis, to validate whether they were reproduced in other 24h samples, and to see if they occurred at 72h. The genes selected are described in the following results sections.

4.2.4 Evaluation of changes in protein expression

To investigate whether interstitial flow was also impacting protein expression in cells, Western blotting was used for a selection of proteins. Additionally, to validate the observation of gene

expression change impacts on protein expression, multiple cell lines of different origins were used for some of the proteins evaluated. MDA-MB-231 cells and HEK293T cells represent two distinctly different biologies. MDA-MB-231 cells are a triple negative breast cancer associated with poor patient survival outcomes (Haque et al., 2012). In contrast, HEK293T cells are a non-cancerous, human-derived embryonic kidney cell line. Spheroids were generated from both cell lines as described in section 2.2.1 at 9.0 x 10^4 cells per well and introduced to static or flow conditions as in the experiments using MCF7 spheroids. Protein and effluent media could then be collected and used for analyses.

In addition to Western blotting, ELISA was used to measure the concentration of an analyte in the conditioned media of static and flow spheroids. VEGF ELISA was used as VEGF has been implicated in tumour progression previously and was also upregulated in our lab's previous experiments using the flow cell 1 device (an older iteration of the current chip) (Collins et al., 2021).

4.2.5 Experiments in hypoxia

Experiments comparing static and flow spheroids were conducted in a hypoxia chamber at 1% O_2. The setup and interfacing were the same as described in section 2.3.6 except for a few key adjustments. A smaller syringe pump (Harvard Apparatus, Pump 11 Elite) was used to fit comfortably in the working area of the hypoxia chamber. This pump only accommodated the use of 2 syringes, so 2 microfluidic devices were used instead of 3. Media, tubing, and syringes used in the hypoxia experiments were also passed into the chamber 24h in advance of the experiment start to allow equilibration of materials to the oxygen tension inside the chamber. The glass material of the chips was less permeable to oxygen than the plastic tubing and syringes however, since media was equilibrated in the hypoxic environment for 24h in advance this ensured that hypoxic media was introduced into the flow system (Scott et al., 1971). When experiments were complete, the static ULA plate and flow cell 2 chips were passed out of the chamber and immediately put on ice. Total RNA was then extracted following the same protocol as described in section 2.5.1.

4.3 Results

4.3.1 Evaluation of EMT-associated markers in flow

As noted earlier in this chapter, previous studies have indicated that biomechanical fluid shear stresses in *in vitro* models induce expression changes associated with early metastasis,

specifically, the epithelial to mesenchymal transition. Therefore, a set of EMT-associated genes were evaluated in samples kept in the flow cell 2 chip compared to static controls. Lysyl oxidase (*LOX),* prostaglandin-endoperoxide synthase 2 (*PTGS2)*, zinc finger protein 1 known as *SNA1L,* and vimentin (*VIM*) are canonical EMT genes. Increased expression of all four has been implicated in cancer metastasis (Asting et al., 2011; Wang et al., 2013; Kidd et al., 2014; Wang et al., 2016). In order to see whether IF in our flow cell 2 system reproduced the upregulation of EMT genes seen in other studies, we evaluated transcript levels of these genes at 24h and 72h in MCF7 breast cancer spheroids exposed to static and flow conditions using our microfluidic device characterised in Chapter 3. The initial results are presented in Figure 4.1.

At 24h, *LOX* was significantly upregulated in flow by a fold change (FC) of 1 relative to the static counterpart. However, *PTGS2* and *SNA1L* showed no significant change at 24h, though *PTGS2* did demonstrate an upregulation of 0.5 FC. In contract, *VIM* was significantly downregulated after just 24h by a factor of 0.2. After 72 hours in flow none of the trends present at 24h remained. *LOX* was no longer upregulated, and the average level was almost the same as static, at 1. *PTGS2* saw a small (< 0.2 FC) decrease in expression in flow compared to static after 72h but this was not significant. *SNA1L* and *VIM* also did not yield significantly different levels of expression compared to static at 72h. However, *VIM* was upregulated by 0.25-fold at 72h, whereas it was downregulated (significantly) at 24h.

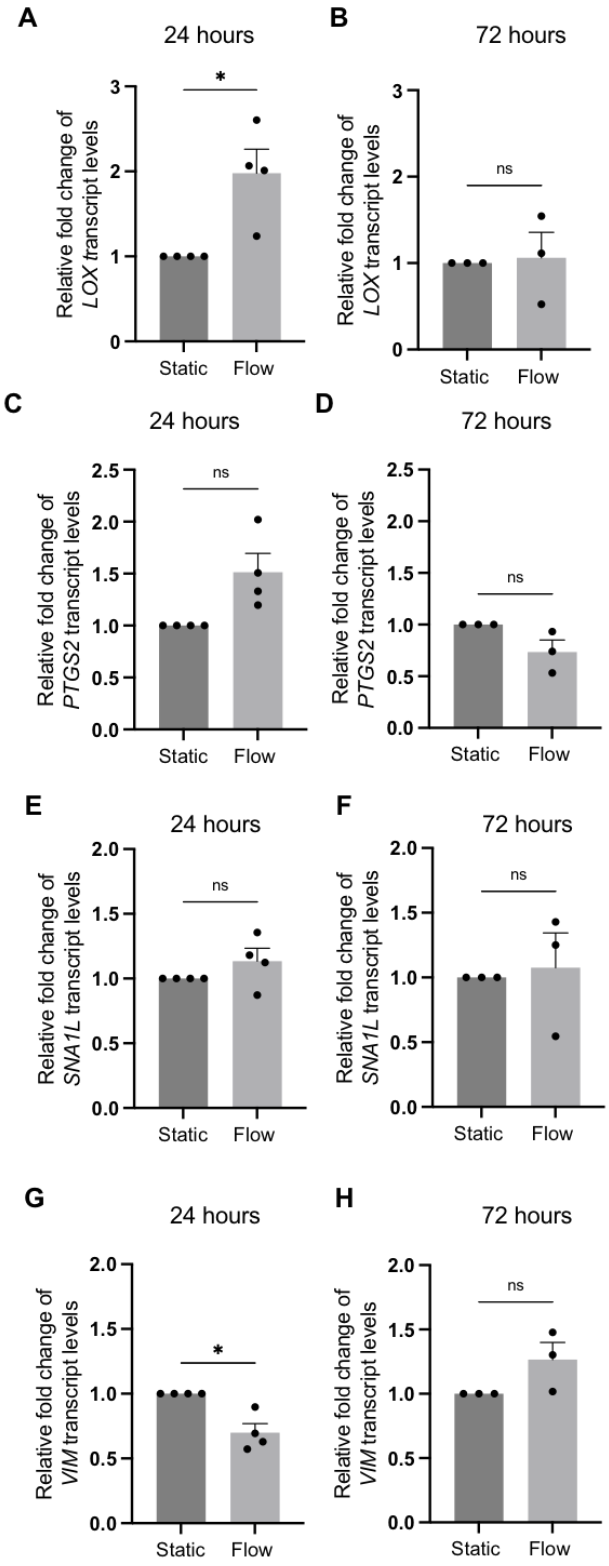

Figure 4.1: Effect of interstitial-like flow on EMT-associated marker transcripts

MCF7 spheroids generated from 9.0 x 10^4 cells were kept in either static or flow conditions (as described in section 2.3.6) for 24h (A, C, E, G) or 72h (B, D, F, H). Total RNA was extracted at the end of experiments and used for qPCR analysis. The housekeeping gene used was *B2M.* Histograms represent the mean of *n*=4 experiments for 24h and *n*=3 for 72h. Dots represent one independent experiment. Error bars represent mean ± SEM. Statistical significance was determined by paired student's t-tests; *p < 0.05, ns = not significant.

A tumour suppressor was selected as the next EMT marker to investigate. E-cadherin is a protein encoded by the *CDH1* gene. It has been established as a tumour suppressor in previous studies, notably for its role in cell-cell adhesion (Kim et al., 2016b). Transcript levels of *CDH1* were evaluated using qPCR analysis (Figure 4.2 A and B). There were not significant differences in relative expression of CDH1 between static and flow spheroids after 24h or 72h, but a small (< 0.25 FC) decrease was evident at both timepoints.

Next, protein expression was analysed by Western blotting to evaluate whether flow induced a change in E-cadherin expression after 24 hours and 72 hours. E-cadherin was chosen as a target representative of EMT. Western blotting did not identify a clear pattern of expression in flow spheroids at either timepoint. Quantification of bands was conducted to analyse differences between static and flow expression of E-cadherin but yielded no statistically significant differences between the two conditions at either timepoint. At 24h there was also a large range of values between the 4 replicates tested and therefore a SEM equal to 0.97. This demonstrated variation between the 24h replicates. The results at 72h were more closely clustered (SEM = 0.18) but still did not show a clear pattern of up or downregulated expression of E-cadherin in MCF7 spheroids in flow.

Finally, two matrix metalloproteinases (MMPs) were investigated in static and flow spheroids. MMPs aid cancer cell invasion into the extracellular matrix, a crucial step of metastasis (Westermarck & Kahari, 1999). qPCR was used to evaluate whether transcript levels of two MMPs, *MMP1* and *MMP14*, were changed by exposure to interstitial flow (Figure 4.3). Transcript levels of *MMP1* showed no significant change after 24h, but after 72h were significantly decreased in flow by a factor 0.8 FC. *MMP14* was not significantly changed at either timepoint, with levels remaining similar between static and flow. It was notable though that the spread of experimental replicates for *MMP14* at 24h were clustered with 2 replicates upregulated by ~0.25 fold and the other 2 downregulated by ~0.25 fold, showing inconsistency between experimental outcomes for this transcript. Further work will need to be conducted to repeat and determine a clear pattern of expression.

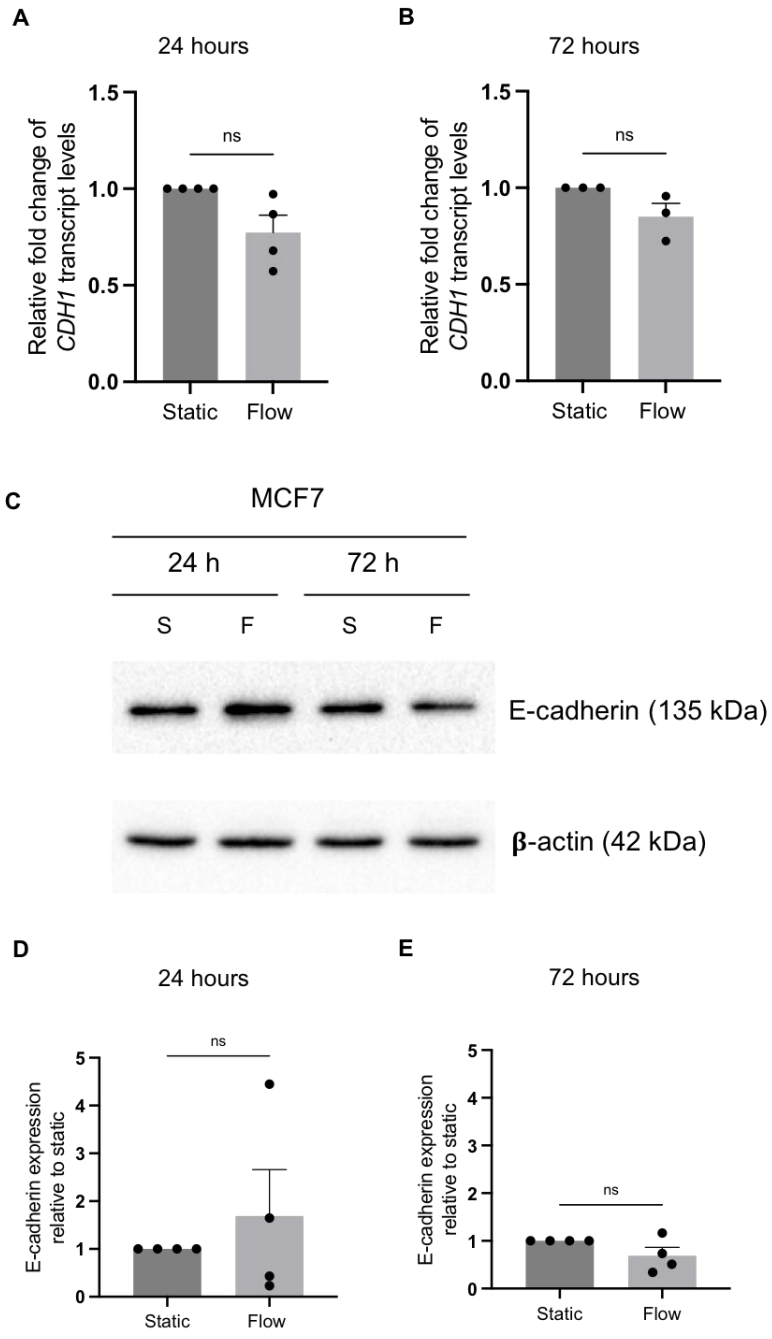

Figure 4.2: Effect of interstitial flow on *CDH1* transcripts and expression of E-cadherin protein

Spheroids were generated from MCF7 cell suspensions of 9.0 x 10^4 cells per well as described in section 2.2.1. After formation, they were kept in static or flow conditions for 24h and. Total RNA was extracted at the end of experiments and used for qPCR analysis (A, B). The housekeeping gene used was *B2M*. Histograms represent the mean of *n*=3 experiments. Error bars represent mean +/- SEM. Statistical significance was determined by paired student's t-tests; ns = not significant. Spheroids were lysed and cell lysates were used for Western blotting to analyse protein expression levels of E-cadherin, with β-actin as a loading control (C). Densitometry was used to quantify bands (D, E). Blots are representative of *n* = 4 experiments.

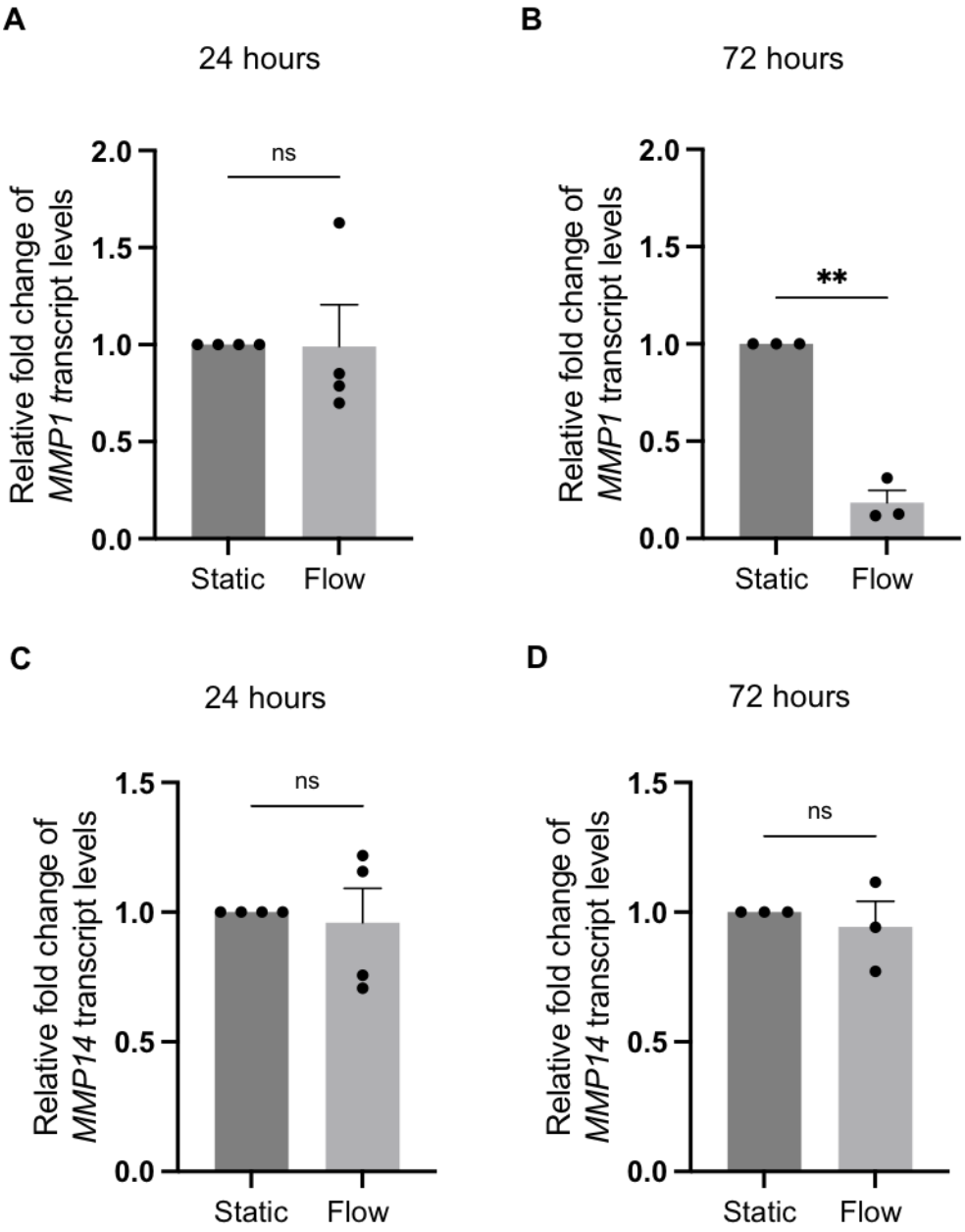

Figure 4.3: Effect of interstitial flow on *MMP* transcript levels

MCF7 spheroids were formed from 9.0 x 10^4 cells and kept in either static or flow conditions for 24h (A and C) or 72h (B and D). Total RNA was extracted at the end of experiments and used for qPCR. The housekeeping gene used was *B2M*. Data represent the mean of *n*=3 experiments. Error bars represent mean +/- SEM. Statistical significance was determined by paired student's t-tests; **p < 0.01, ns = not significant.

4.3.2 Investigation of transcriptomic changes induced by interstitial flow

The results in the previous section were inconclusive as to whether flow was inducing changes in spheroids consistent with early tumour progression and EMT. Both transcript level and protein level analyses did not provide clarity on the effects of flow, so an unbiased approach providing a larger scale picture of changes was needed. RNA-sequencing analyses the entire transcriptome and provides valuable information on differential expression of all genes. Total mRNA samples from MCF7 spheroids in static and flow conditions for 24h were therefore analysed by RNA-seq. Due to cost limitations only one timepoint could be analysed.

The comparison between the transcriptomes of static and flow MCF7 spheroids showed differences in overall expression patterns evident between the two conditions. Figure 4.4 depicts the overall spread of significantly differentially expressed genes present in flow compared to static, represented by the green (downregulated) and red (upregulated) dots. Figure 4.5 summarises the unique expression of genes within each group and the overlap of genes expressed in common. Furthermore, mapping of the differential expression patterns in a heat map (see Figure 4.6) showed that static and flow spheroids expressed unique transcriptomes when mapped with hierarchical clustering.

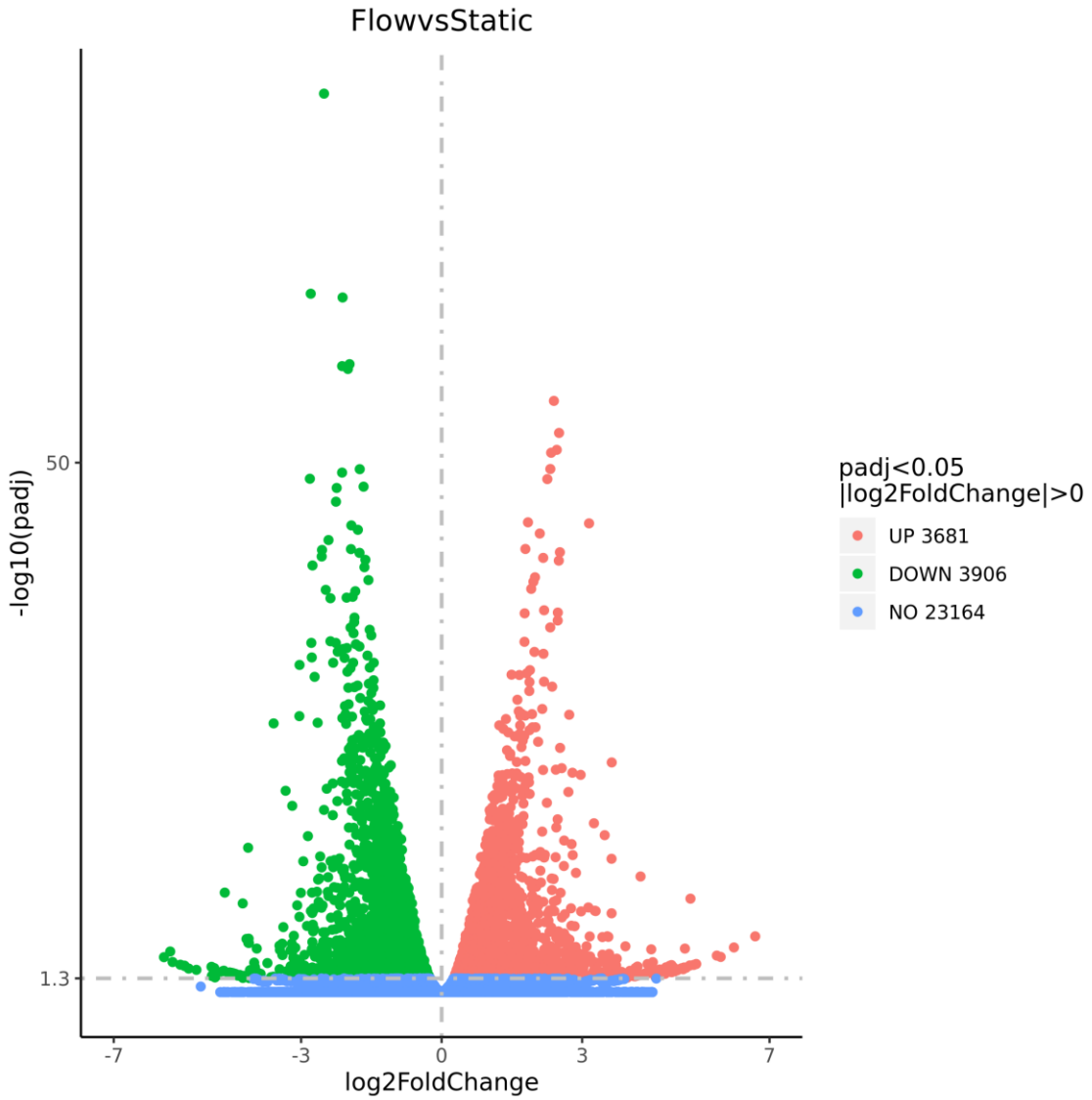

Figure 4.4: Upregulated and downregulated differential expression of genes in flow spheroids compared to static spheroids

MCF7 spheroids were formed by seeding 9.0 x 10^4 cells per well in a ULA plate. After 96h of formation, they were kept in either static or flow conditions for 24h and total RNA was extracted at the end of experiments. Data represent *n* = 3 independent experiments. Here, mRNA extracts were analysed by RNA-seq to evaluate differential expression of > 30,000 genes between static and flow. In the figure above, each dot correlates to a gene analysed; red represents genes upregulated in flow compared to static; green represents genes downregulated in flow compared to static; blue represents genes not significantly differentially expressed between the two conditions. Significance of the expression change is mapped on the y-axis by the adjusted p-value and the level of fold change is mapped on the x-axis by log2FC.

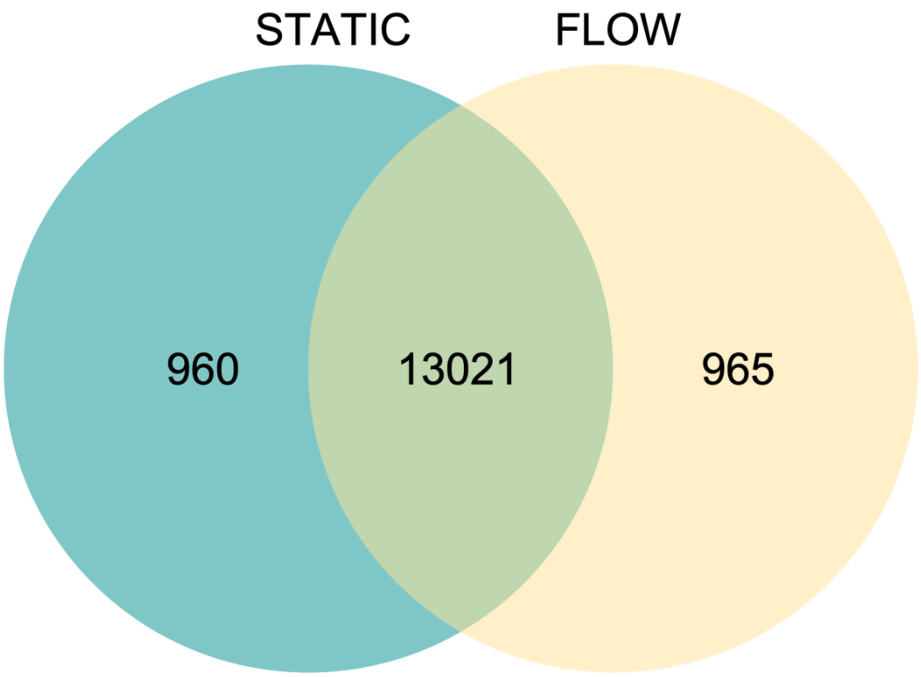

Figure 4.5: Summary of differential expression of genes in static and flow spheroids

MCF7 spheroids were formed by seeding 9.0 x 10^4 cells per well in a ULA plate. After 96h of formation, they were kept in either static or flow conditions for 24h and total RNA was extracted at the end of experiments. Data represent *n* = 3 independent experiments. Here, mRNA extracts were analysed by RNA-seq to evaluate differential expression of > 30,000 genes between static and flow. In the figure above, the unique expression of genes in each condition is summarised numerically. The sum of the numbers in each circle is the total number of genes expressed within a group (condition), and the overlap represents the genes expressed in common between groups.

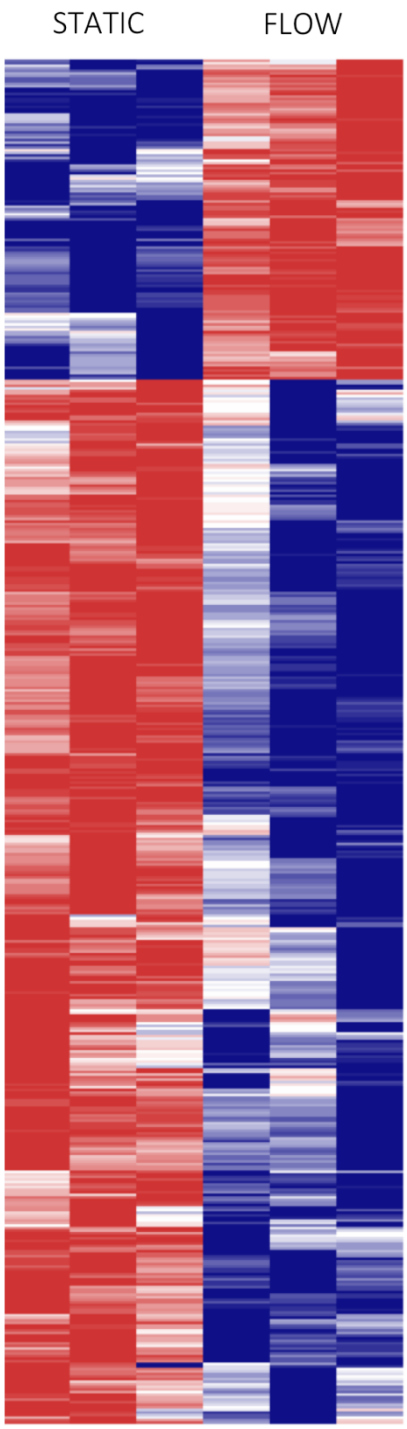

Figure 4.6: Heat map representation of the differential expression of genes in static and flow spheroid samples

MCF7 spheroids formed by seeding 9.0 x 10^4 cells per well in a ULA plate. Once formed, they were kept in either static or flow conditions for 24 h. Total mRNA was extracted and collected for *n* = 3 samples for each condition, which were sent for RNA sequencing analysis. Above, a heat map of differentially expressed genes was generated using the online platform NetworkAnalyst. Each row on the heat map represents one sample, and one columnar line represents a transcript. The 3 leftmost columns are static samples and the 3 rightmost are flow . The whole transcriptome analysed < 30,000 genes, and the top and bottom 600 differentially expressed are represented here. Red corresponds to upregulated expression in flow, and blue corresponds to downregulated expression. The intensity of the colour represents the amplitude of the regulation.

All of the transcripts and their respective fold changes and p-values were entered into IPA software for further analysis of biological processes. A threshold was set so that only transcripts upregulated in flow with a fold change > 2.5 and downregulated with a fold change < -2.5 were analysed. A threshold of significance at $p < 0.01$ was also set. This allowed for analyses to be conducted on the most significantly differentially expressed transcripts. However, because all transcript data was entered into the software before setting a threshold, the software was still able to infer pathway regulation changes using transcripts outside of the threshold cut-off. This allows for more meaningful analyses to be conducted by including whole transcriptome changes for the software to use for downstream and upstream predicted activation or inhibition of pathways. The threshold cutoffs were used for core analyses of the data.

Table 4.1 outlines the top ten transcripts that were the most altered by flow. The highest fold change was present in actin like 8 (*ACTL8*) at 75.6 with strong significance ($p < 0.001$). Next, a gene coding for an integral membrane protein, G protein-coupled receptor 183 (*GPR183*), was found to be upregulated by 37.2 FC compared to static, again with strong significance.

The next most upregulated transcripts had changes in the range of 30 – 36-fold and varied in categories from oncogene family members (*RAB6C*) to SSX family members (*SSX1*). In the downregulated category of transcripts, keratin associated protein 2-4 (*KRTAP2-1*) had the most change relative to static with 0.016 FC (or -5.93 log2 fold change). There were also a variety of novel transcripts downregulated including a PAGE family member, ATP binding cassette subfamily member, and others (outlined in Table 4.1). Colony stimulating factor 2 (*CSF2*), encodes a cytokine that controls the production, differentiation, and function of granulocytes and macrophages, ultimately playing a role in promoting tissue inflammation. *CSF2* is notably situated in the top ten most downregulated genes in flow with a fold change of 0.034 (or -4.85 log2 fold change).

Next, the canonical pathways modulated by the transcript changes found in the dataset were summarised in Figure 4.7, which also depicts the number of molecules involved in a given pathway and the number of molecules from the dataset which were up or downregulated. The associations were compiled using a stringent statistical test (Benjamin-Hochberg) to correct for multiple testing at a threshold of significance $p < 0.01$. Therefore, the seven canonical pathways presented were strongly modulated by the transcripts in the static vs. flow dataset. Cell cycle-associated pathways are heavily represented, including cell cycle control of chromosomal replication, G1/S phase checkpoint regulation, and the role CHK proteins in cell cycle checkpoint control.

Table 4.1: Top upregulated and downregulated molecules in response to interstitial-like flow

Gene name	Full name	Fold change (FC)	Log2 Fold Change (log2 FC)	*p*-value
Upregulated				
ACTL8	Actin like 8	75.56	6.24	6.05×10^{-5}
GPR183	G protein-coupled receptor 183	37.20	5.22	5×10^{-3}
C1QTNF2	C1q and TNF related 2	36.59	5.20	1.08×10^{-5}
RAB6C	RAB6C, member RAS oncogene family	32.66	5.03	2.2×10^{-3}
ERVFRD-1	Endogenous retrovirus group FRD member 1, envelope	31.52	4.98	2.8×10^{-3}
C9orf66	Chromosome 9 open reading frame 66	31.41	4.97	2.6×10^{-3}
FBN2	Fibrillin 2	30.89	4.95	1.1×10^{-3}
SSX1	SSX family member 1	30.45	4.93	3.0×10^{-3}
SLIT3	Slit guidance ligand 3	30.08	4.92	3.5×10^{-3}
LRRC14B	Leucine rich repeat containing 14B	30.00	4.91	6×10^{-4}
Downregulated				
KRTAP2-4	Keratin associated protein 2-4	0.016	-5.93	8.79×10^{-5}
PAGE2B	PAGE family member 2B	0.018	-5.80	2.2×10^{-5}
AC011473.4	Novel transcript	0.021	-5.58	5.5×10^{-4}
AC015813.2	Novel transcript	0.024	-5.40	1.4×10^{-3}
ABCA8	ATP binding cassette subfamily A member 8	0.034	-4.89	7.5×10^{-3}
SLCO1B7	Solute carrier organic anion transporter family member 1B7 (putative)	0.034	-4.85	7.8×10^{-3}
CSF2	Colony stimulating factor 2	0.034	-4.85	1.3×10^{-3}
MIA	MIA SH3 domain containing	0.039	-4.67	2.6×10^{-3}
BARHL1	BarH like homeobox 1	0.052	-4.25	1.1×10^{-2}
BOLA2B	BolA family member 2B	0.053	-4.24	1.6×10^{-2}

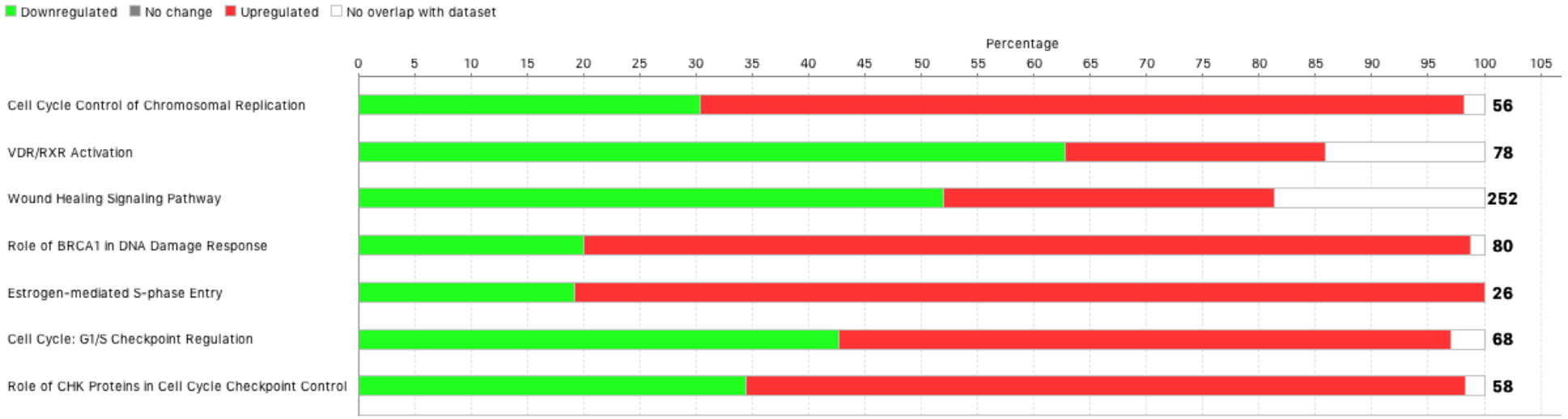

Figure 4.7: Canonical pathways modulated by IFF in flow cell 2 system after 24 hours

MCF7 spheroids were generated from cell suspensions seeded at 9.0 X 10^4 cells per well in a ULA plate. Once formed, spheroids were kept in static or flow conditions for 24h and mRNA samples from n = 3 experiments were collected, prepared, and analysed by RNA-seq. Bar chart represents the statistically significant pathways present within the dataset ($p < 0.01$) , considering only genes for which expression varied greater than 2.5 fold between flow and static samples. Bold figures are the total number of genes in the pathway. Green bar: genes downregulated in flow; red bar: upregulated genes; white bar: no overlap in the dataset

Table 4.2 Top molecular and cellular functions represented by the dataset

Functional Category	*p*-value range	Number of molecules from dataset
DNA Replication, Recombination, and Repair	$1.92 \times 10^{-5} – 3.3 \times 10^{-9}$	76
Cell Morphology	$7.73 \times 10^{-5} – 2.05 \times 10^{-8}$	58
Cell Cycle	$7.25 \times 10^{-5} – 2.73 \times 10^{-8}$	144
Cell Death and Survival	$8.35 \times 10^{-5} – 4.7 \times 10^{-8}$	285
Cellular Development	$8.72 \times 10^{-5} – 6.45 \times 10^{-8}$	278

In all of the cell cycle pathways represented, about 70% of the molecules in the dataset involved in the pathways were upregulated (red bars). Additionally, the role of BRCA1 in DNA damage response pathway and the oestrogen-mediated S-phase entry pathway was associated with upregulation of molecules involved in their respective pathways as a result of flow.

The analysis also revealed specific molecular and cellular functions modulated by interstitial flow, and these corresponded to the canonical pathways represented. Table 4.2 shows the five most represented functions in the dataset, along with the p-value range for each (which corresponds to the range of p-values for even more specific pathway subsets that comprise the functions listed). Cell cycle was listed as the third most represented function which aligns with the canonical pathway analysis. The most strongly represented molecular function was DNA replication, recombination, and repair with 76 molecules from the dataset involved and p-values for the associated subset of pathways being no greater than 1.92×10^{-5}.

Transcription factor enrichment analysis was also conducted using the online platform ENRICHR (Neafsey et al., 1989; Chen et al., 2013; Xie et al., 2021). The top 600 differentially expressed protein-coding genes that were upregulated in flow were entered for analysis. The input list of upregulated genes was compared to the ChIP Enrichment Analysis (ChEA) database to compute over-representation for targets of transcription factors. Figure 4.8 summarises the results. E2F family transcription factors represented half of the top ten enriched terms produced by the analysis, and 4 out of 5 of them were in human sample sets.

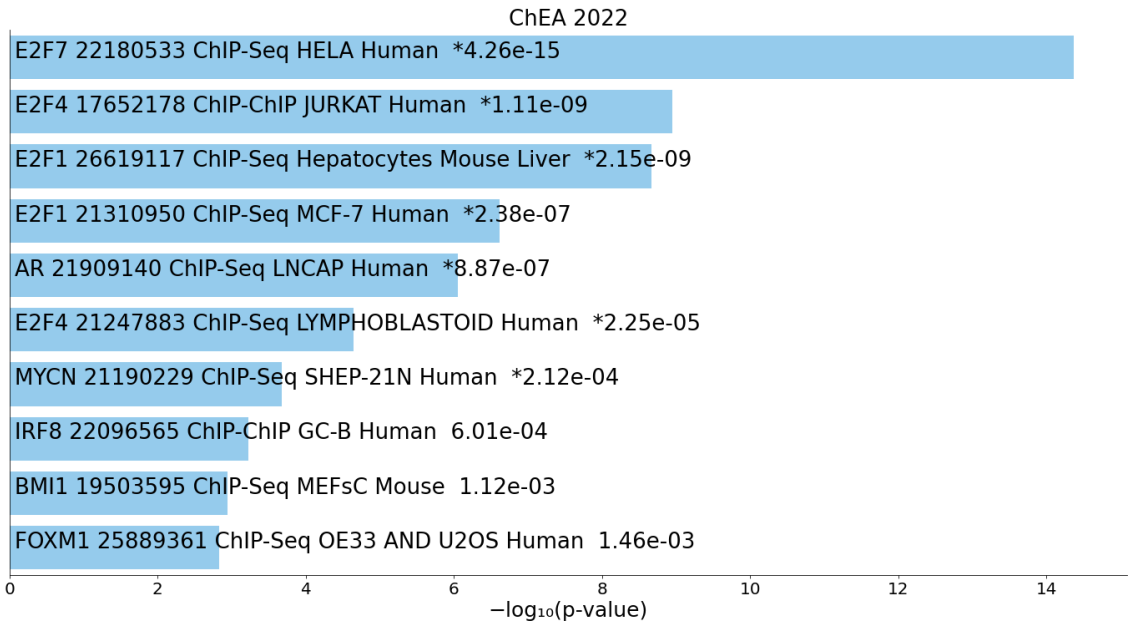

Figure 4.8: Transcription factor target over-representation analysis

MCF7 spheroids were formed from suspensions of 9.0 x 10^4 cells and then kept in static or flow conditions for 24h. Total RNA was extracted and analysed by RNA-seq to compare the conditions. The top 10 enriched transcription factor terms in the ChEA database from entering the 600 most upregulated, differentially expressed genes from RNA-seq analysis are displayed based on the -log10(p-value), along with their corresponding p-values listed next to them. An asterisk (*) next to a p-value indicates the term also has a significant adjusted p-value (<0.05). The term at the top has the most significant overlap with the input query gene set.

4.3.3 Validation of differentially expressed genes and enrichment patterns at transcript level

Panels of gene targets representative of significantly represented pathways and functions identified by RNA-seq were used to validate the patterns with qPCR analysis. Samples from MCF7 spheroids exposed to flow for 24 hours were used again as in the RNA-seq analysis, and 72h samples were also analysed to investigate whether the patterns were maintained with increased duration of exposure to flow.

The panel of genes representative of DNA replication, which included *MCM6*, *RRM1*, and *RRM2*, saw consistent upregulation of gene expression across all of the genes and at both timepoints, as shown in Figure 4.9. *RRM2* levels at 24h were the only category that was not statistically significant, but an increase of 1.8 FC was evident in the chart and there was a large margin of error present within the replicates which could have affected the statistical testing. All three genes remained significantly upregulated at 72 hours, with fold changes relative to static remaining in the range of 2-3 for all. Another three genes selected for their roles in cell cycle regulation (Figure 4.10) were also analysed by qPCR. At both timepoints, all of the genes had increased transcript level expression relative to static, but only one, *E2F1* at 24h, was statistically significant. *ASF1B* and *WEE1* at 72h had large standard errors of the mean due to FC replicate value ranges of 40 – 60. At 24h *WEE1* was not upregulated and at 72 hours the high variability between the replicates skewed the mean, so more repeats are needed to better investigate.

Next, a selection of 4 genes involved in DNA repair pathways (which also overlap with DNA replication pathways) were tested for expression changes between static and flow (see Figure 4.11). These genes included *BLM*, *EXO1*, *FEN1*, and *RAD51*. In alignment with the findings of the RNA-seq where DNA replication and repair pathways were enriched in flow, all 4 genes were upregulated in flow compared to static at both timepoints. *BLM* was most significantly increased after 24h with expression 2.5-fold higher than static on average. It remained significantly upregulated after 72h, ~1 FC increase relative to static. *EXO1* was similar to *BLM* in that it was highly upregulated after 24h. Compared to static counterparts, flow spheroids had an average of 6-fold increase in expression of *EXO1* at 24h, and this dropped slightly at 72h to an average of 2.3 FC but remained statistically significant. *FEN1* relative expression was significantly higher in flow at 24h but not after 72h, though a clear trend of increase was evident from the chart and the average expression was 2-fold higher compared to static spheroids. *RAD51* was the only gene out of the 4 that did not have any significant differences at either timepoint.

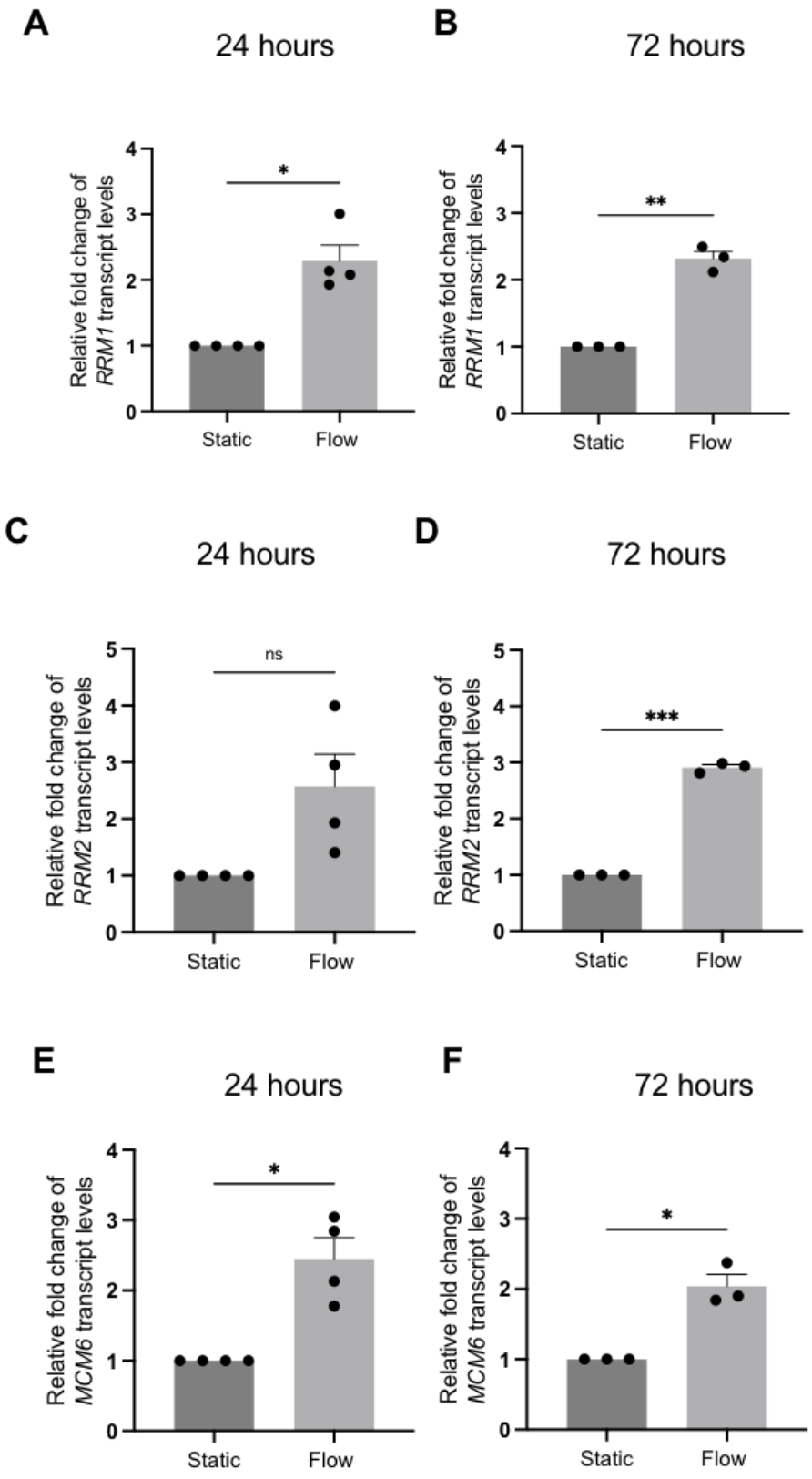

Figure 4.9: Analysis of the transcript levels of DNA replication genes

MCF7 spheroids formed from 9.0 x 10^4 cells were kept in either static or flow conditions for 24h (A, C, E) or 72h (B, D, F). Total RNA was extracted at the end of experiments and used for qPCR analysis. The housekeeping gene used was *B2M*. Data represent the mean of *n*=3 experiments. Error bars represent mean ± SEM. Statistical significance was determined by paired student's t-tests; *$p < 0.05$; **$p < 0.01$; ***p <0.001; ns = not significant.

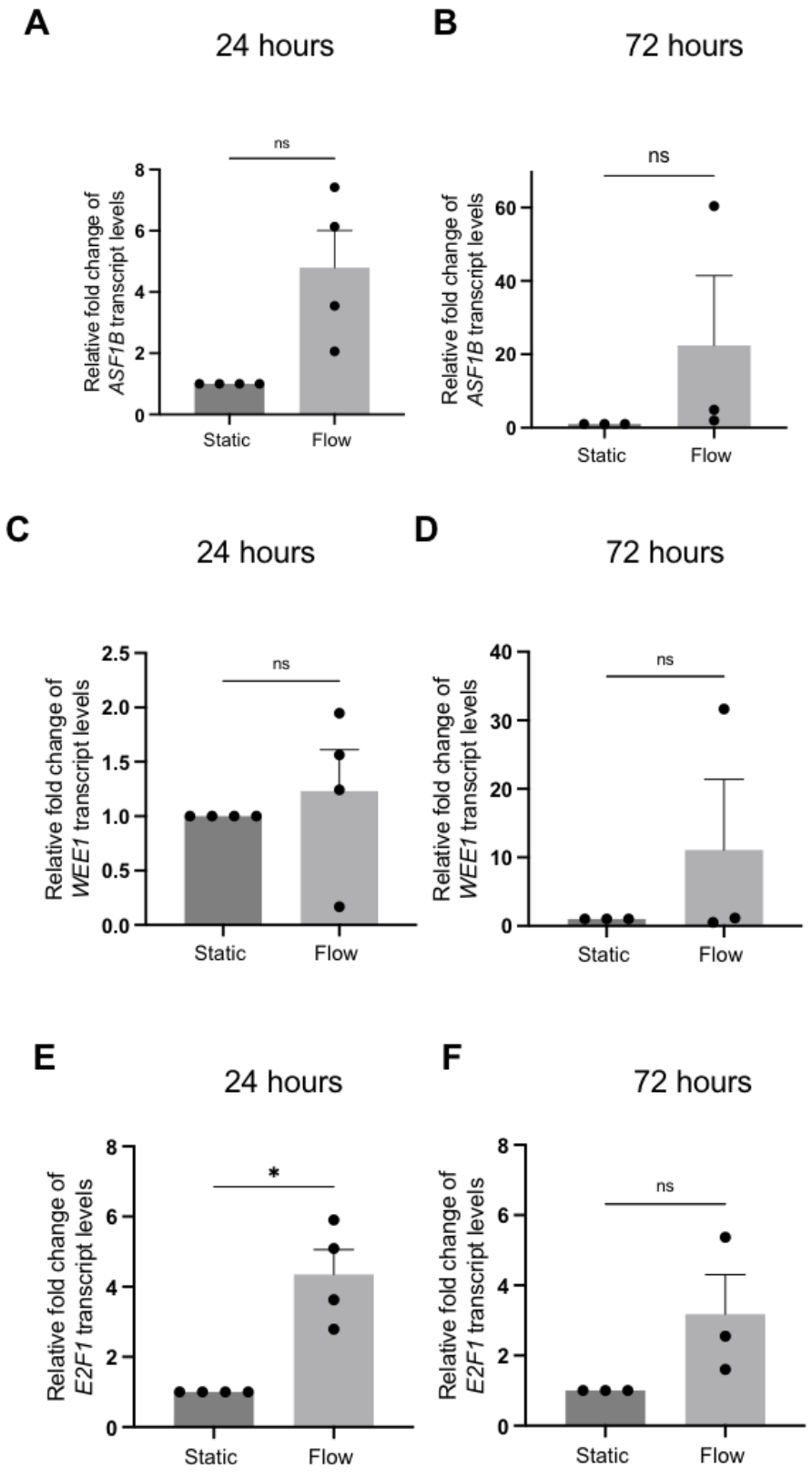

Figure 4.10: Analysis of the transcript levels of cell cycle genes

MCF7 spheroids were generated by seeding 9.0 x 10^4 cells per well in a ULA plate. Spheroids were kept in either static or flow conditions for 24h (A, C, E) or 72h (B, D, F). Total RNA was extracted at the end of experiments and used for qPCR. The housekeeping gene used was *B2M*. Data represent the mean of *n*=3 experiments. Error bars represent mean ± SEM. Statistical significance was determined by paired student's t-tests; *$p < 0.05$; ns = not significant.

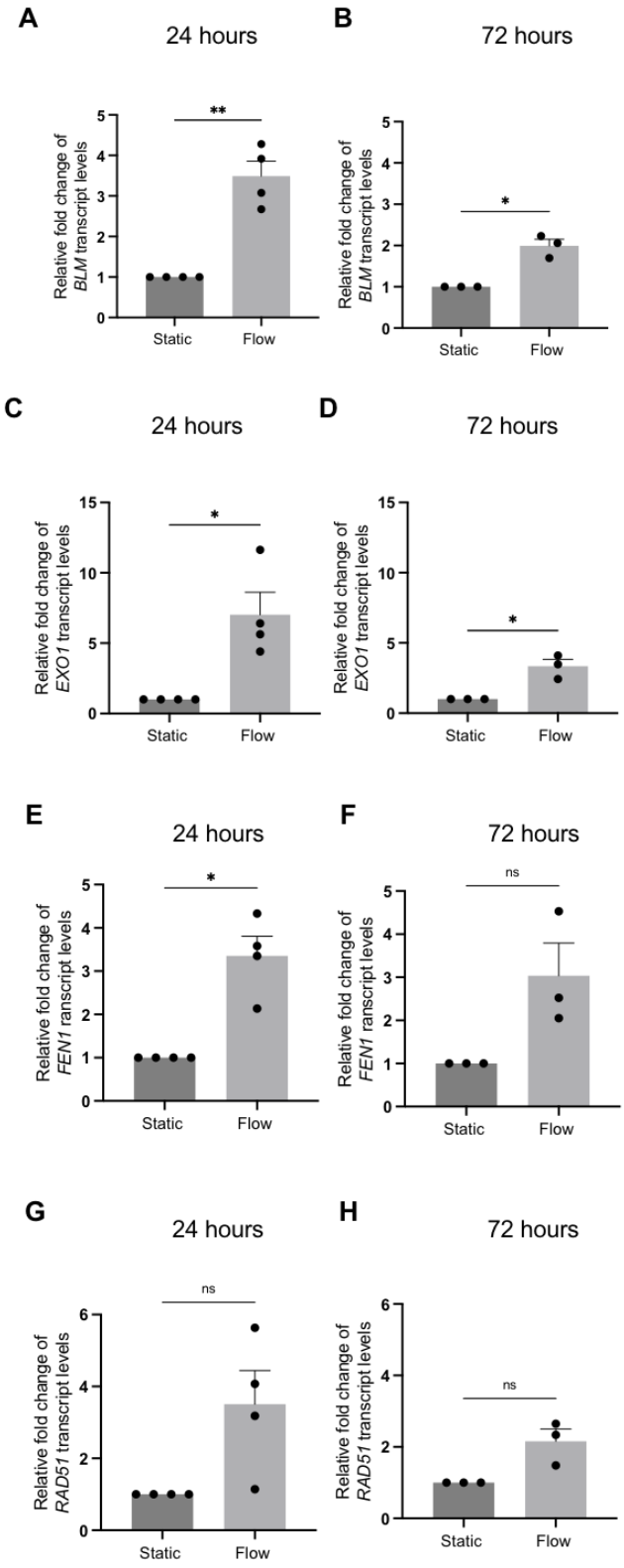

Figure 4.11: Analysis of the transcript levels of DNA repair genes

MCF7 spheroids were formed from suspensions of 9.0 x 10^4 cells and then kept in either static or flow conditions for 24h (A, C, E, G) or 72h (B, D, F, H). Total RNA was extracted at the end of experiments and used for qPCR. The housekeeping gene used was *B2M*. Data represent the mean of *n*=3 experiments. Error bars represent mean ± SEM. Statistical significance was determined by paired student's t-tests; *$p < 0.05$; **$p < 0.01$; ns = not significant.

Lastly, 2 genes involved in DNA repair and specifically implicated in breast cancer, *BRCA1* and *BRCA2*, were evaluated using qPCR analysis. The results are presented below in Figure 4.12, showing the significant upregulation of both genes in flow after both 24h and 72h. The relative expression difference for both genes at both timepoints was < 2 FC and that was sustained for all at 72h.

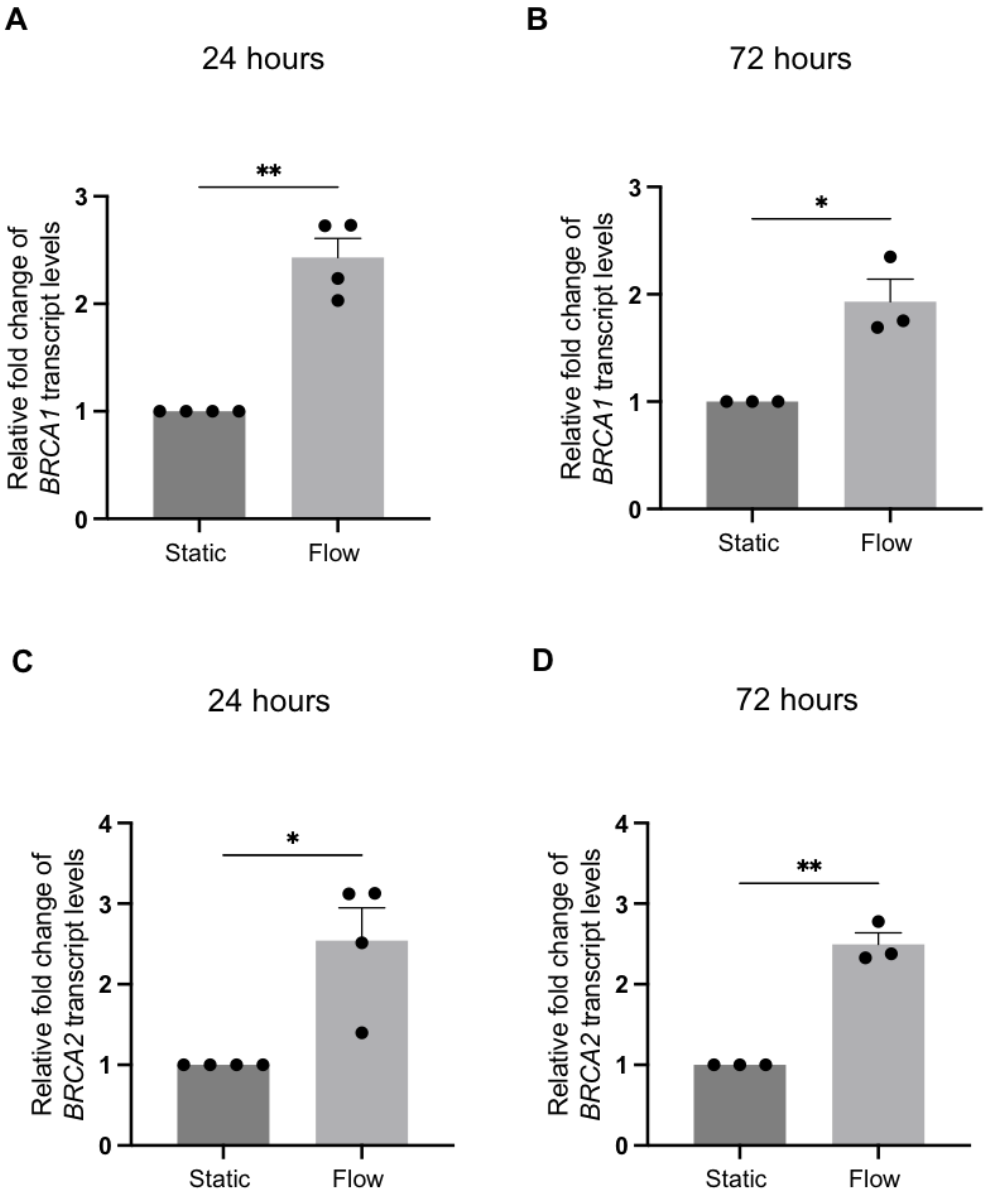

Figure 4.12: Analysis of the transcript levels of *BRCA* genes

MCF7 spheroids were formed from suspensions of 9.0 x 10^4 cells and then kept in either static or flow conditions for 24h (A, C) or 72h (B, D). Total RNA was extracted at the end of experiments and used for qPCR. The housekeeping gene used was *B2M*. Data represent the mean of *n*=3 experiments. Error bars represent mean ± SEM. Statistical significance was determined by paired student's t-tests; *$p < 0.05$; **$p < 0.01$.

4.3.4 Investigation of the relationship between incubator environment and the effect on biological changes in cancer cells

As an additional measure, a plate of static spheroids was placed in the external incubator used for flow experiments, referred to as the "flow incubator". The aim was to test whether the effects identified by RNA-seq and validated in qPCR were simply an artefact of placing spheroids in a different environment. The plate was kept in the flow incubator for 72h with another plate of static spheroids kept in the regular cell culture incubator in parallel. The regular cell culture incubator (which was used for the static condition in all other experiments) was a temperature regulated and humidified environment. Whilst the flow incubator was set to regulate the temperature at 37°C, it was not humidified. The results, shown below in Figure 4.13, demonstrated that there was no significant difference in transcript levels of *MCM6* between static spheroids in either incubator. In the original static v. flow experiments using the external flow incubator for on-chip experiments and the standard cell culture incubator for static plates, *MCM6* was significantly upregulated in flow at both 24h and 72h. While this test was only done for one of the markers of enriched pathways identified in flow, it suggested that the difference in incubators was not a significant contributing factor to the results produced using chips in the flow incubator.

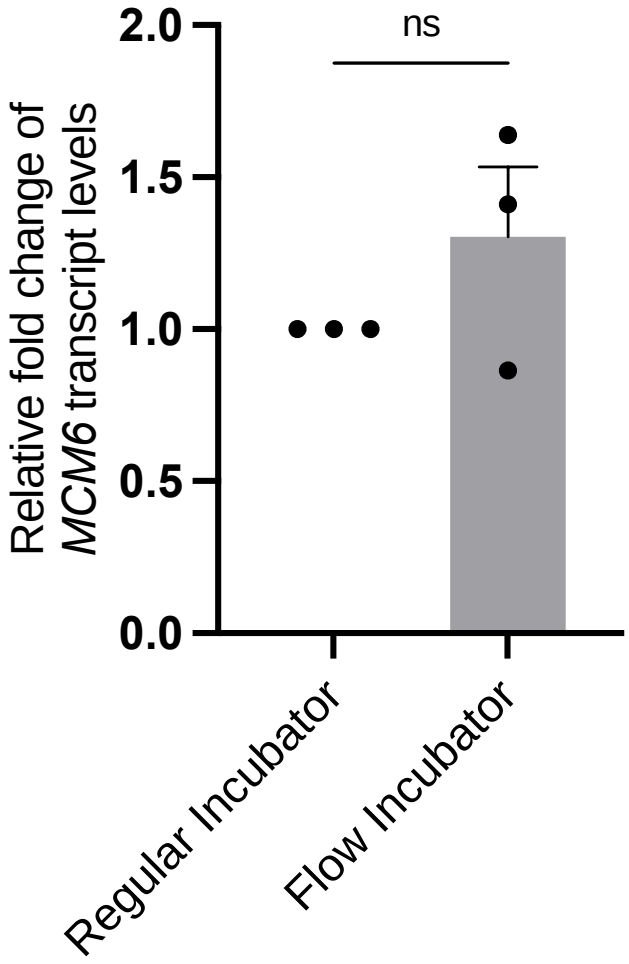

Figure 4.13: MCM6 transcript levels compared between incubator types

MCF7 spheroids were formed from 9.0 x 10^4 cells seeded in a ULA plate and allowed to form for 96h. Spheroids were kept in a ULA plate, with Matrigel added to reflect standard static v. flow experiments. One plate was placed in the external "flow" incubator and the other kept in the standard cell culture incubator. Plates were kept in these conditions for 72h. Total RNA was extracted and used for qPCR analysis, with *B2M* as the housekeeping gene. Data represent the mean of *n*=3 experiments. Error bars represent mean ± SEM. Statistical significance was determined by paired student's t-tests; ns = not significant

4.3.5 Investigating the relationship between hypoxia and interstitial flow and the effect on biological changes in cancer cells

4.3.5.1 Modulation of hypoxia signalling by interstitial flow

Interstitial flow is an important physiology in the TME, but it is not the only one. Hypoxia is also prominent in many solid tumours. Therefore, the interplay between these two TME components was investigated, first by examining hypoxia signalling in spheroids exposed to flow. IPA software was used to infer the activity of molecules involved in hypoxia signalling from the RNA-seq dataset described in section 4.3.2. The analysis software draws from curated databases as well as the fold change data uploaded to extrapolate the activity patterns. In this case, the molecules involved in the canonical hypoxia signalling pathway were matched to the differential expression patterns in the static vs flow dataset, as shown in Figure 4.14. Orange colour in the pathway corresponds to predicted activation, and blue corresponds to predicted inhibition. HIF1alpha and the majority of HIF-1α downstream targets were denoted in blue, indicating an expected inhibition of HIF-1α signalling in the flow condition. Molecules downstream of HIF-1α that were predicted to be downregulated in flow included *SUMO1, LDHA, NOS3, EDN1, EPO, and SLC2A4.*

The results, depicted in Figure 4.15, showed a significant downregulation in expression of *CA9* in flow spheroids at 24h, by ~0.5 FC. However, after 72h there was no significant difference in *CA9* levels between the conditions. *BNIP3* was also not significantly different at either timepoint. *WSB1* on the other hand saw a significant decrease in relative expression in flow at both 24h and 72h. The factor of downregulation was 0.5 – 0.6 FC at both timepoints, demonstrating a sustained lower expression level relative to static counterparts at both times. Finally, *VEGFA* transcripts were significantly decreased in flow spheroids after 24h. The statistically significant downregulation was not sustained at 72h, but a lower level of expression compared to static was evident in all 3 replicates tested, with average FC expression 0.6-fold less than in static.

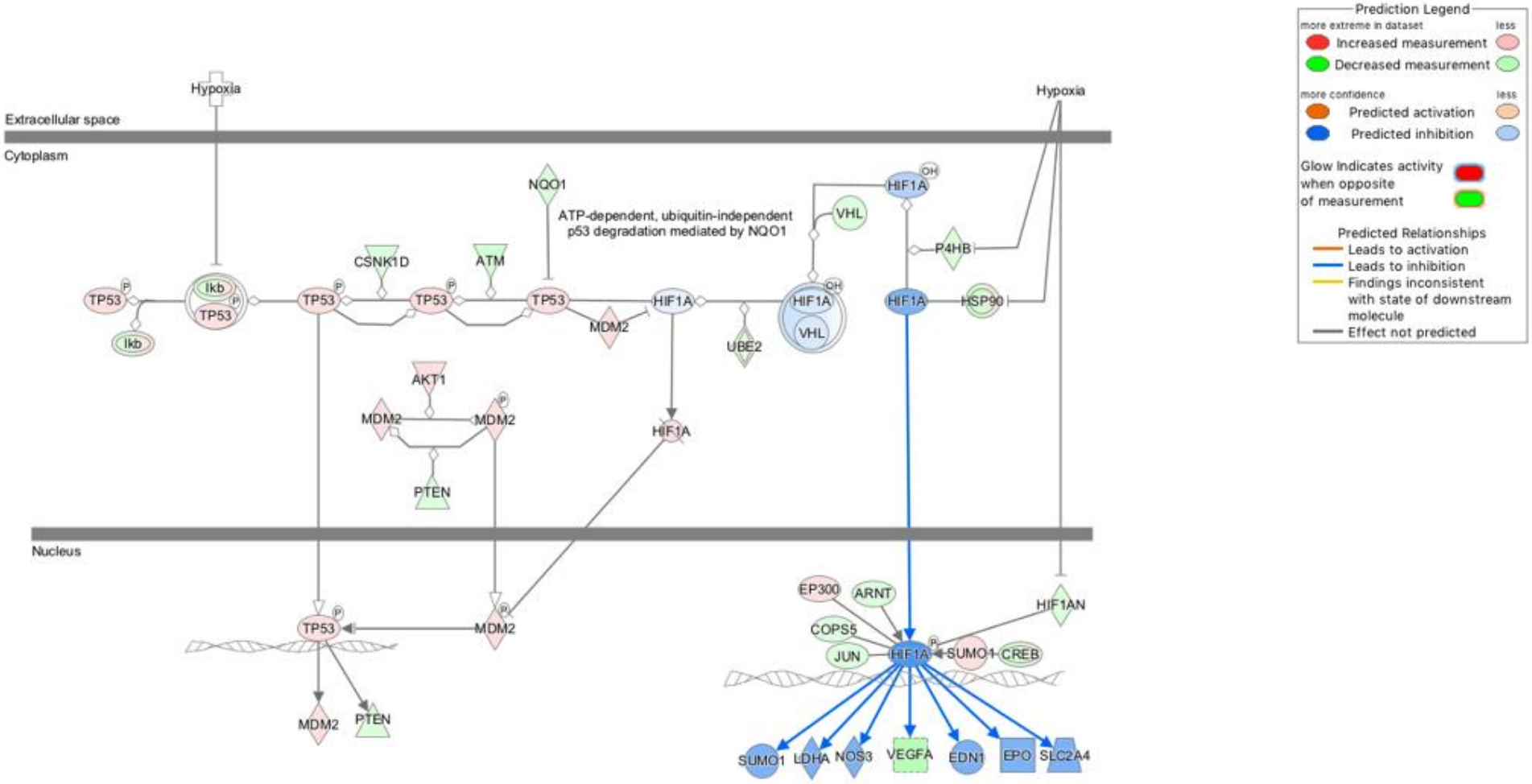

Figure 4.14: Hypoxia signalling pathway with predicted activity of molecules from RNA-seq analysis

The hypoxia signalling pathway with the predicted activity of molecules overlaid in colour. Ingenuity Pathway Analysis software was used to analyse the whole transcriptome of MCF7 spheroids exposed to static or flow for 24h. The software uses input transcript data to infer prediction of molecules involved in the pathway.

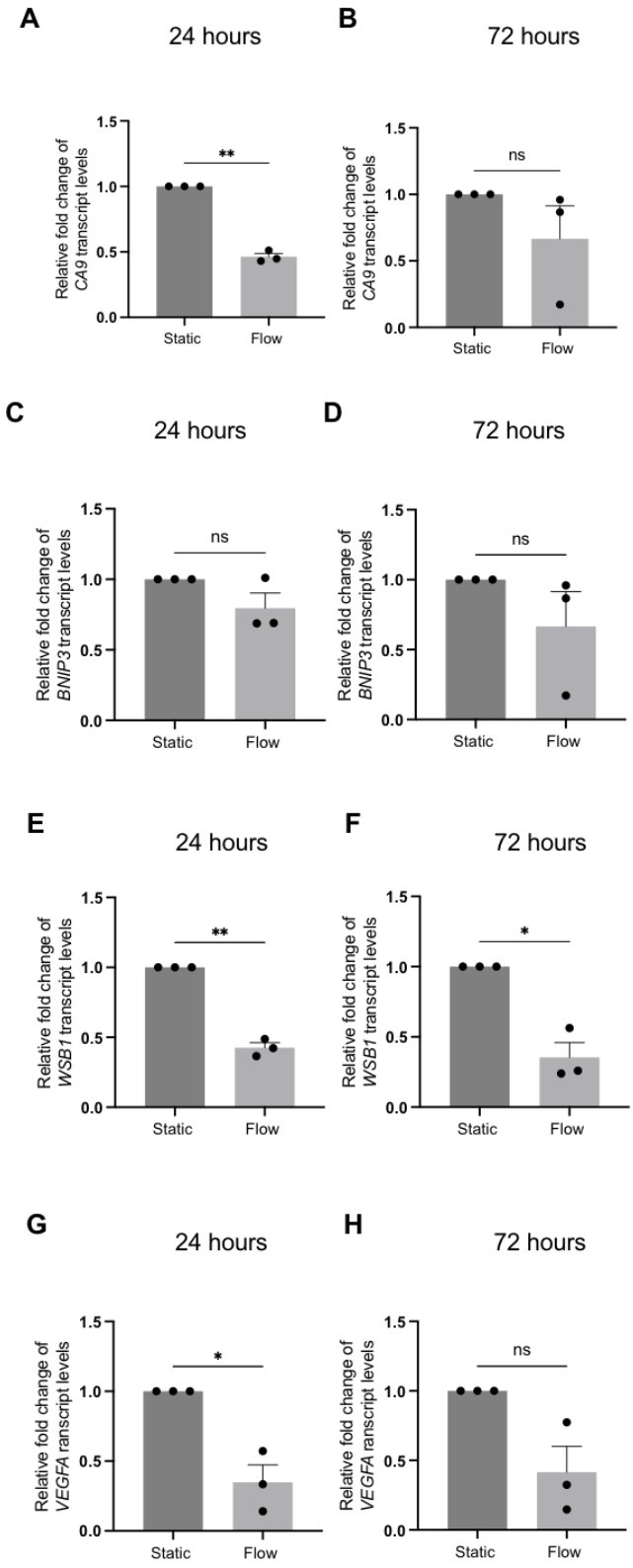

Figure 4.15: Transcript level changes in markers of hypoxia altered by IFF

MCF7 spheroids were formed from suspensions of 9.0 x 10^4 cells and then kept in either static or flow conditions for 24h (A, C, E, G) or 72h (B, D, F, H). Total RNA was extracted at the end of experiments and used for qPCR where *B2M* was the housekeeping gene. Data represent the mean of *n*=3 experiments. Error bars represent mean ± SEM. Statistical significance was determined by paired student's t-tests; *$p < 0.05$, ** $p < 0.01$; ns = not significant

4.3.5.2 Effect of interstitial flow on cancer cells in a hypoxic environment

Static v. flow experiments were also conducted in a hypoxia chamber in an effort to mitigate the effect of better oxygen supply to spheroids in flow, where continuous perfusion of fresh media was suspected to increase oxygen availability. Two panels of genes were used for qPCR to analyse the mRNA extracts of static and flow spheroids kept in hypoxia for 24h. Due to the preliminary nature of these experiments and time constraints, total RNA extracts and their yields were low, limiting the opportunity for extensive subsequent testing on samples.

The first panel used represented markers of hypoxia and included *CA9* and *VEGFA* as in the previous section, and *HK2* was used as a marker of downstream hypoxia signalling (Figure 4.16). *CA9* showed no significant difference in the expression levels between static and flow and there was also a large SEM for flow, due to the large spread of replicate values (0.83, 1.7, and 0.002). *VEGFA* appeared downregulated in flow with the mean of *VEGFA* expression in flow being 0.62 FC less than that of static, but this was not statistically significant. Similarly, *HK2* was not significantly downregulated but the mean FC relative to static was ~0.5 less. Like *VEGFA*, there was also a large SEM for *HK2* due to replicates ranging from as little as 0.02 FC to 0.85.

The second panel used was comprised of three genes involved in a set of functions all related to enriched pathways in flow, identified by RNA-seq and validated by qPCR. These were *MCM6*, *E2F1*, and *BRCA1,* shown in Figure 4.17*. MCM6* transcript levels in flow relative to static were similar and the difference between the means was only 0.04. *E2F1* and *BRCA1* were not statistically significantly upregulated, but the chart depicted an increase in transcript levels of both in flow with ~0.3 FC increase in transcript expression relative to static.

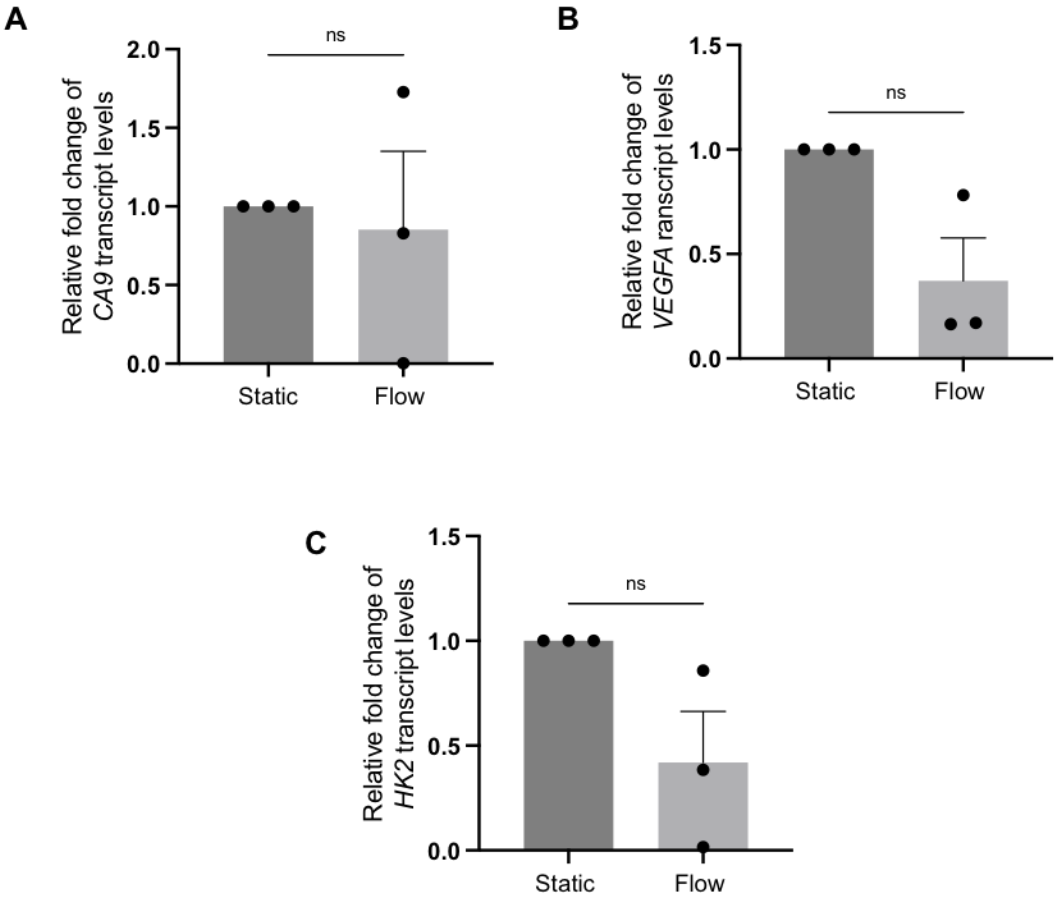

Figure 4.16: Effect of hypoxia on expression of hypoxic markers in interstitial flow

MCF7 spheroids were generated by seeding 9.0 x 10^4 cells per well in a ULA plate. After formation, spheroids were either kept in the plate (static) or transferred to a flow device. Both conditions were kept in 1% O_2 for 24h before spheroids were harvested and total RNA was extracted. qPCR analysis was conducted using *B2M* as the housekeeping gene. Data represent the mean of *n*=3 experiments. Error bars represent mean ± SEM. Statistical significance was determined by paired student's t-tests; *$p < 0.05$, ** $p < 0.01$; ns = not significant

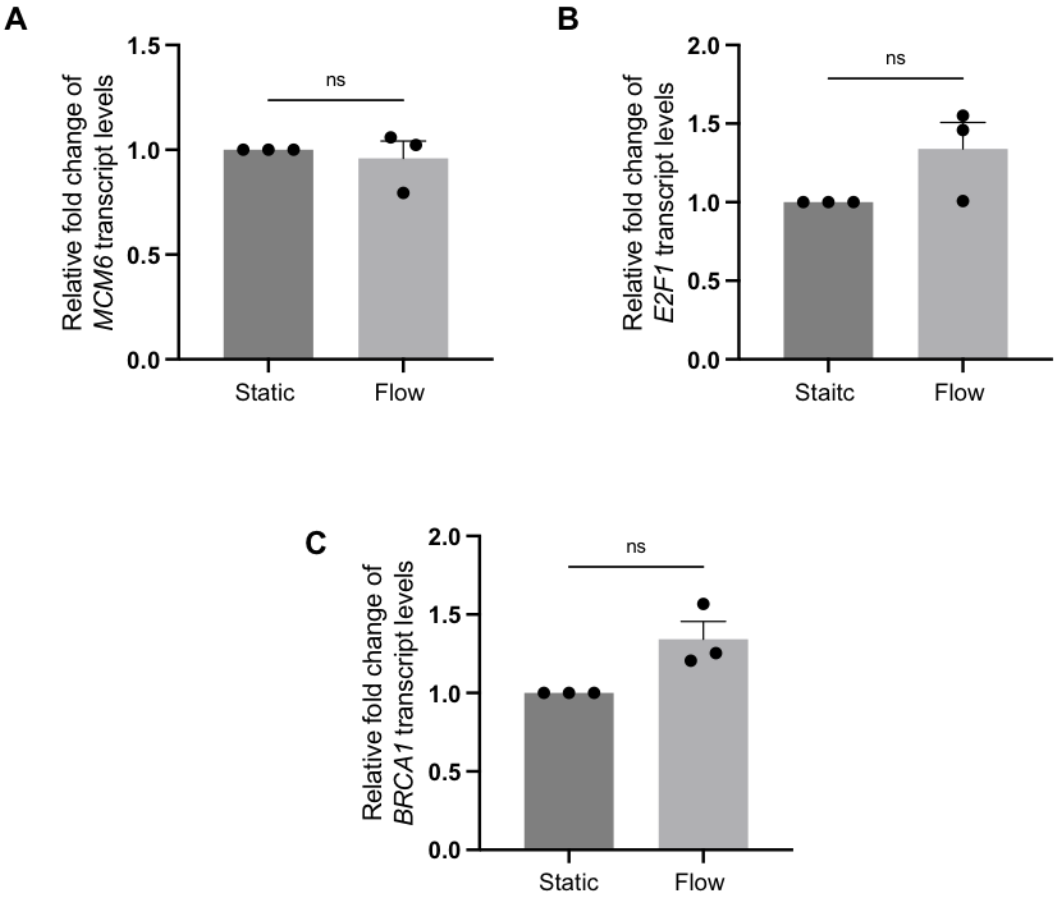

Figure 4.17: Effect of hypoxia on expression of transcripts enriched by flow

MCF7 spheroids were generated by seeding 9.0 x 10^4 cells per well in a ULA plate. After formation, spheroids were either kept in the plate (static) or transferred to a flow device. Both conditions were kept in 1% O_2 for 24h before spheroids were harvested and total RNA was extracted. qPCR analysis was conducted using *B2M* as the housekeeping gene. Data represent the mean of *n*=3 experiments. Error bars represent mean ± SEM. Statistical significance was determined by paired student's t-tests; ns = not significant

4.3.6 Protein expression changes in cells exposed to interstitial flow

4.3.6.1 Western blotting of protein expression levels

Previous analyses identified changes in the transcriptome of static and flow MCF7 spheroids. To investigate whether changes in protein expression were also occurring, Western blotting was used. First, following on from the investigations into hypoxia and interstitial flow, HIF-1α primary antibody was used to visualise expression of this protein (Figure 4.18). Samples from 3D spheroids as well as 2D samples were used. 2D samples were kept in either normoxic (20% O_2) or hypoxic (1% O_2) conditions for 1h and 24h, to provide positive controls showing HIF-1α expression in hypoxic conditions. As seen in the figure below, 3D samples required a longer exposure time to visualize bands compared to the 2D controls. In the 3D samples, bands were present in the static samples but not in flow, and in the 2D control samples HIF-1α bands were present in 1% O_2 samples at both 1h and 24h, but not in the normoxic counterparts.

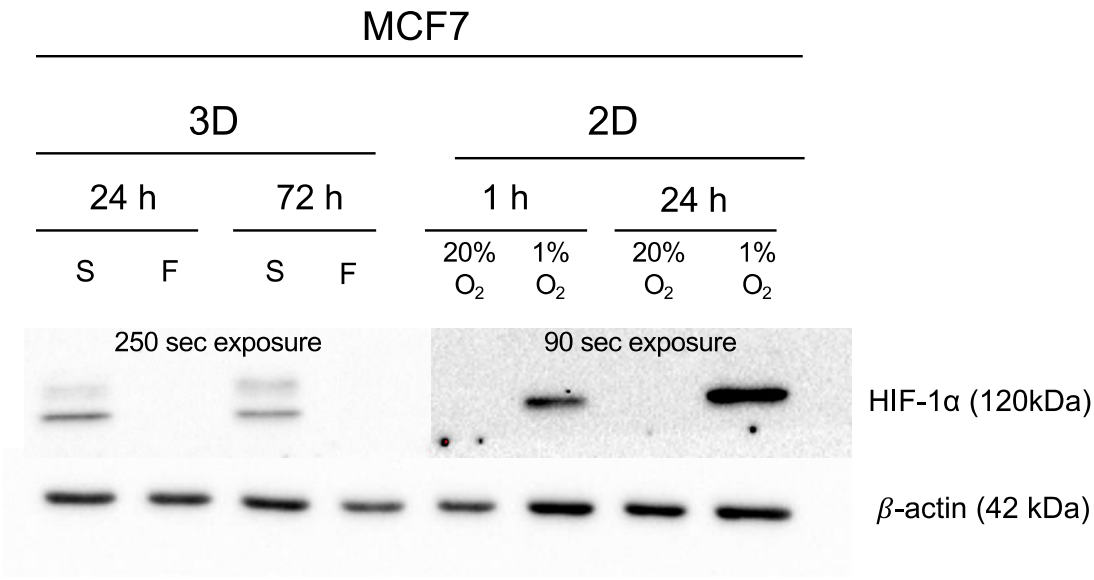

Figure 4.18: HIF-1α expression in MCF7 cells

MCF7 cells were seeded in a ULA plate with 9.0 x 10^4 cells per well. Spheroids (3D) were formed for 96h and then kept in static (S) or flow (F) conditions for 24h and 72h. Additionally, MCF7 cells were seeded in 6mm plastic dishes and allowed to adhere for 24h before either being transferred to a hypoxia chamber (1% O_2) or remaining in a cell culture incubator (20% O_2). Adherent cells (2D) were kept in these conditions for either 1h or 24h. Both 2D and 3D cell lysates were harvested at the end of experiments from their respective conditions and protein was extracted, prepared, and run through an SDS-PAGE gel. 30 μg of protein was loaded per well. Then, Western blotting was used to visualise HIF-1α expression, with β- actin used as a loading control. Blots are representative of *n*=3 experiments.

Next, Hexokinase II levels were evaluated in MCF7 spheroids using Western blotting and densitometry to quantify expression. Hexokinase II is a glycolytic enzyme protein implicated in glucose metabolism. It is known to be upregulated in tumours and is considered a key factor in progression of breast cancer (Patra et al., 2013). It is also important in hypoxic physiology and is considered a downstream target of the HIF-1α signalling pathway. As seen in Figure 4.19 (A), expression levels appear decreased by interstitial flow at both timepoints. However, there was variation amongst the experimental repeats for this protein (B and C). Quantified bands were not significantly different in flow compared to static, but a trend of decreased expression was evident from the charts for both 24h and 72h. At 24h, average expression of HK2 in flow spheroids was 0.53 FC less than static spheroids, and 0.55 FC less after 72h.

To see whether a similar trend could be present in a different cell line, MDA-MB-231 cells were used to generate spheroids and 2D samples and analysed by Western blotting. As with the MCF7s, HK2 appears to be decreased in expression in flow compared to static in the MDA-MB-231 spheroids. It also appears in hypoxia at both the 1h and 24h timepoints in the adherent cells and was overall more highly expressed in both of the 24h adherent samples. The experiment represented in Figure 4.20 is only an n =1, but densitometry was performed for the static and flow 24h samples (data not shown) and the quantification confirmed that there was a 0.46 fold decrease in HK2 expression in the flow sample compared to static.

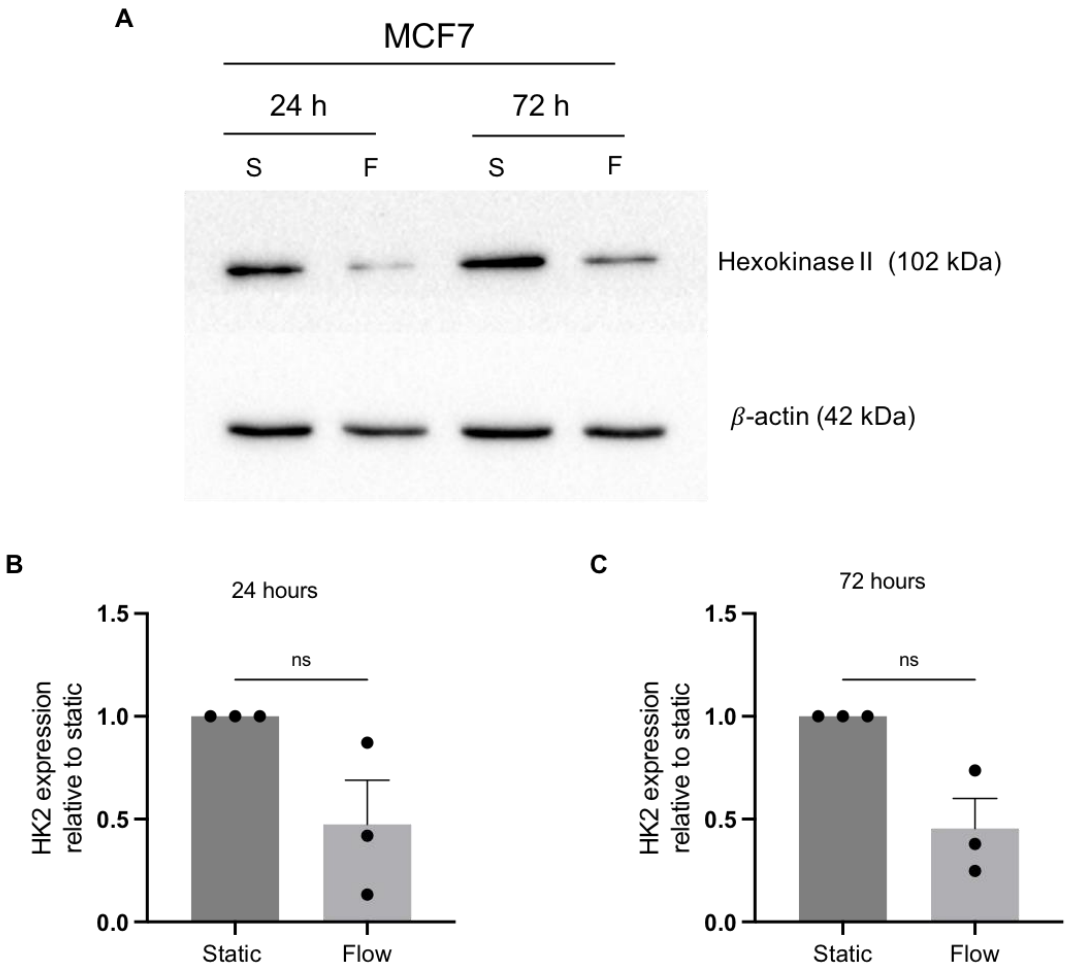

Figure 4.19: Hexokinase II expression in MCF7 spheroids

MCF7 cells were seeded in a ULA plate with 9.0 x 10^4 cells per well. Spheroids were formed for 96h and then kept in static (S) or flow (F) conditions for 24h and 72h. Spheroid cell lysates were harvested at the end of experiments from their respective conditions and protein was extracted, prepared, and run through an SDS-PAGE gel. Then, Western blotting was used to visualise HK2 expression (A), with β- actin used as a loading control. Blots are representative of *n*=3 experiments. Densitometry was performed to quantify band intensity as shown in (B) and (C). Statistical testing was conducted using student's paired *t*-tests; ns = not significant.

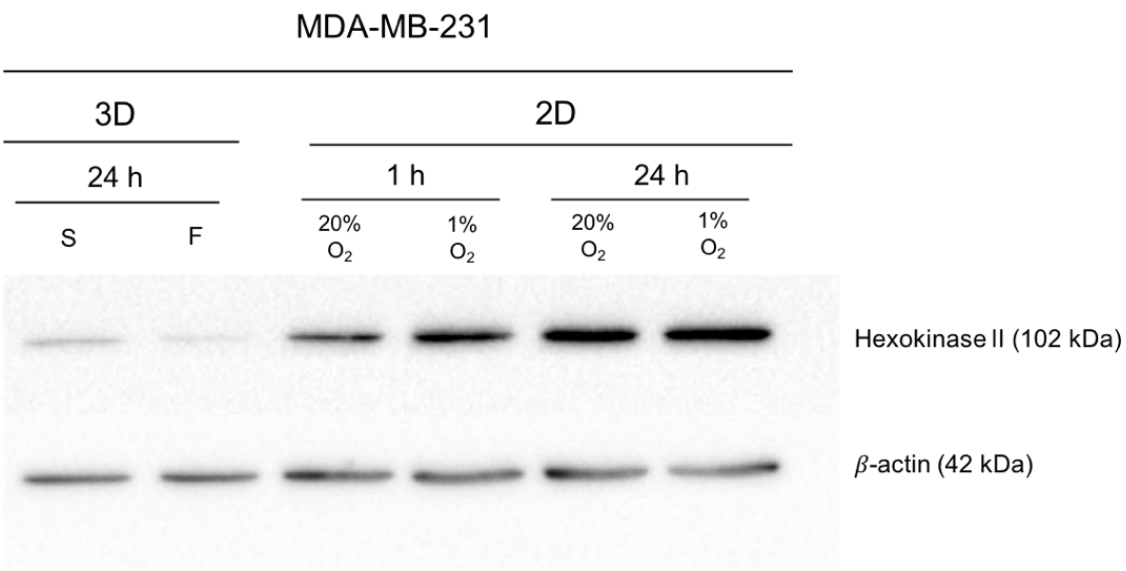

Figure 4.20: Hexokinase II expression in MDA-MB-231 cells

MDA-MB231 cells were seeded in a ULA plate with 9.0 x 10^4 cells per well. Spheroids (3D) were formed for 96h and then kept in static (S) or flow (F) conditions for 24h and 72h. Additionally, MDA-MB-231 cells were seeded in 6mm plastic dishes and allowed to adhere for 24h before either being transferred to a hypoxia chamber (1% O_2) or remaining in a cell culture incubator (20% O_2). Adherent cells (2D) were kept in these conditions for either 1h or 24h. Both 2D and 3D cell lysates were harvested at the end of experiments from their respective conditions and protein was extracted, prepared, and run through an SDS-PAGE gel. Then, Western blotting was used to visualise HK2 expression with β- actin used as a loading control. Blots are representative of *n*=1experiment.

RPA protein (RPA32) expression was also evaluated to follow up on the DNA replication and repair pathways that were shown to be enriched in flow in the RNA-seq dataset (section 4.3.3). In MCF7 spheroids there was no difference evident in RPA expression between static and flow spheroids at 24h or 72h (Figure 4.21 (A)). Densitometry was performed for *n* =3 experiments to quantify band intensities and evaluate whether there was a difference evident from quantification but not visual inspection of bands (Figure 4.21 (B, C)). RPA32 expression was not significantly changed at either timepoint in comparison to static spheroids.

MDA-MB-231 cells and spheroids were also evaluated for the presence of RPA by Western blotting but showed no clear difference between static and flow conditions after 24h (Figure 4.22). RPA band intensity did appear increased in 2D hypoxic samples. Densitometric analysis of *n* =1 experiments with MDA-MB-231 yielded a 1.2 FC in expression of RPA in flow spheroids compared to flow, confirming low levels of change between the two conditions.

Finally, p53 expression was evaluated in MCF7 spheroids (Figure 4.23). Visual inspection of bands did not provide a clear picture of whether changes in expression were occurring. Quantification of bands was used and showed no significant differences in expression of p53 after 24h or 72h. There was a lot of variation between the replicates at 24h (max range of 4.9 FC between highest and lowest replicate). At 72h there was less variation between replicates, but all were close to 1, indicating there was not significant change from static.

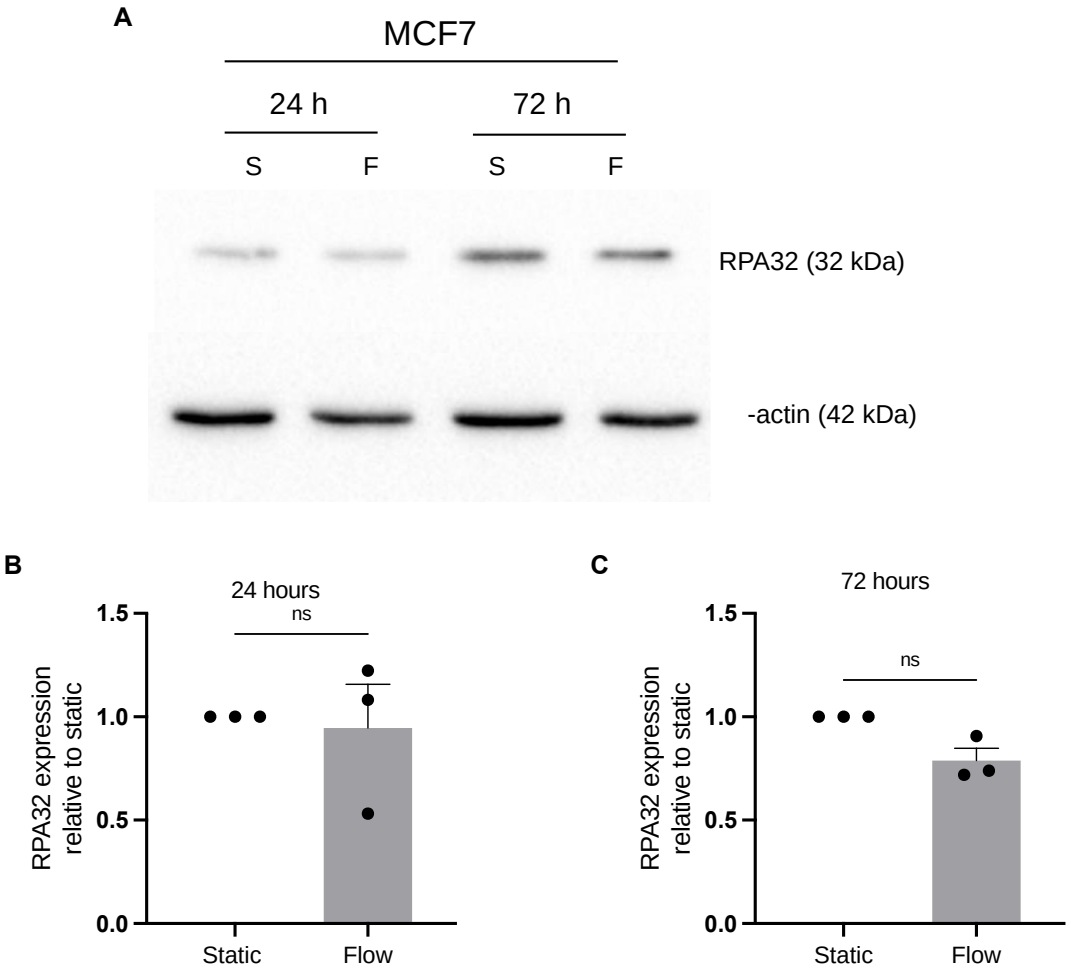

Figure 4.21: RPA32 expression in MCF7 spheroids

MCF7 cells were seeded in a ULA plate with 9.0 x 10^4 cells per well. Spheroids were formed for 96h and then kept in static (S) or flow (F) conditions for 24h and 72h. Spheroid cell lysates were harvested at the end of experiments from their respective conditions and protein was extracted, prepared, and run through an SDS-PAGE gel. Then, Western blotting was used to visualise RPA32 expression (A), with β- actin used as a loading control. Blots are representative of *n*=3 experiments. Densitometry was performed to quantify band intensity as shown in (B) and (C). Statistical testing was conducted using student's paired *t*-tests; ns = not significant.

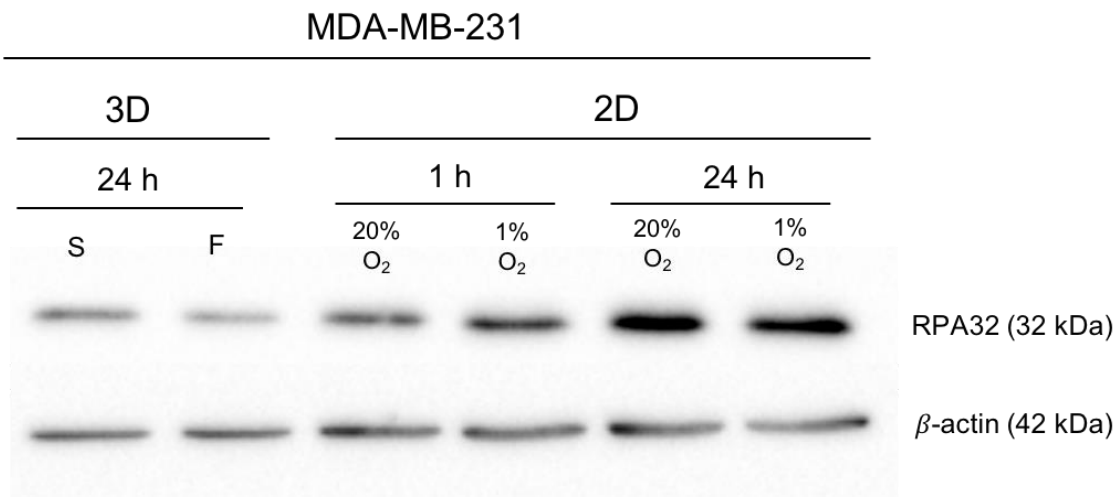

Figure 4.22: RPA32 expression in MDA-MB-231 cells and spheroids

MDA-MB231 cells were seeded in a ULA plate with 9.0 x 10^4 cells per well. Spheroids (3D) were formed for 96h and then kept in static (S) or flow (F) conditions for 24h and 72h. Additionally, MDA-MB-231 cells were seeded in 6mm plastic dishes and allowed to adhere for 24h before either being transferred to a hypoxia chamber (1% O_2) or remaining in a cell culture incubator (20% O_2). Adherent cells (2D) were kept in these conditions for either 1h or 24h. Both 2D and 3D cell lysates were harvested at the end of experiments from their respective conditions and protein was extracted, prepared, and run through an SDS-PAGE gel. Then, Western blotting was used to visualise RPA32 expression with β- actin used as a loading control. Blots are representative of *n*=1experiment

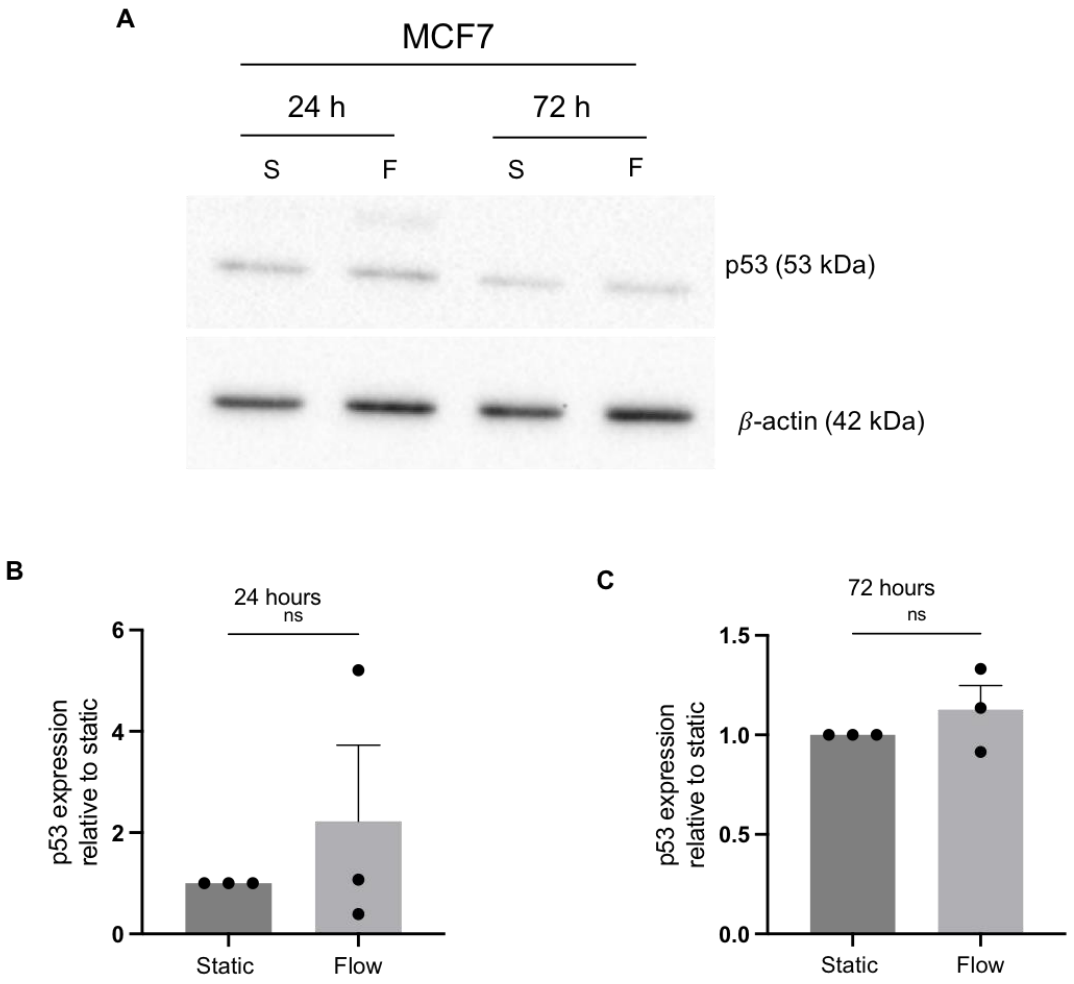

Figure 4.23: p53 expression in MCF7 spheroids

MCF7 cells were seeded in a ULA plate with 9.0 x 10^4 cells per well. Spheroids were formed for 96h and then kept in static (S) or flow (F) conditions for 24h and 72h. Spheroid cell lysates were harvested at the end of experiments from their respective conditions and protein was extracted, prepared, and run through an SDS-PAGE gel. Then, Western blotting was used to visualise p53 expression (A), with β- actin used as a loading control. Blots are representative of *n*=3 experiments. Densitometry was performed to quantify band intensity as shown in (B) and (C). Statistical testing was conducted using student's paired *t*-tests; ns = not significant.

4.3.6.2 Analysis of spheroid secretion levels of VEGFA

Lastly, to examine whether secretion of protein (cytokines) may also be altered by flow, effluent media samples were analysed using a VEGFA ELISA. Conditioned media from MCF7, MDA-MB-231, and HEK293T spheroids kept in static or flow conditions for 24 hours or 72 hours were collected and analysed by ELISA. HEK293T cells are a non-cancerous, human-derived embryonic kidney line and represent a biology different to both the MCF7 and MDA-MB-231 cells. The picograms (pg) per spheroid were calculated and are represented on the y-axis of the charts. The standard curve used for these analyses can be found in appendix 2.

In the MCF7 spheroids after 24 hours, static and flow spheroids were not significantly different in their secretion levels of VEGF. There was variation amongst the experimental repeats in flow increasing the SEM; one replicate had very high levels of over 800 pg/spheroid, while the other two replicates were < 400, and therefore also lower than the levels detected in the static samples. However, after 72 hours a clear and statistically significant difference was evident between static and flow, where flow had significantly lower levels of VEGF (by 272 pg/spheroid) secreted in the media compared to static spheroids.

In contrast, VEGF secretion was significantly increased after 24h in the effluent media of MDA-MB-231 spheroids exposed to flow. The mean of differences between static and flow was 1128 pg/spheroid at 24h. Only an n=1 could be used for 72h. It showed a decreased level of VEGF secretion in flow compared to static by 246 pg/spheroid. HEK293T spheroids in flow secreted significantly higher levels of VEGF compared to static counterparts, but in the sample from 72h flow had less secretion compared to static.

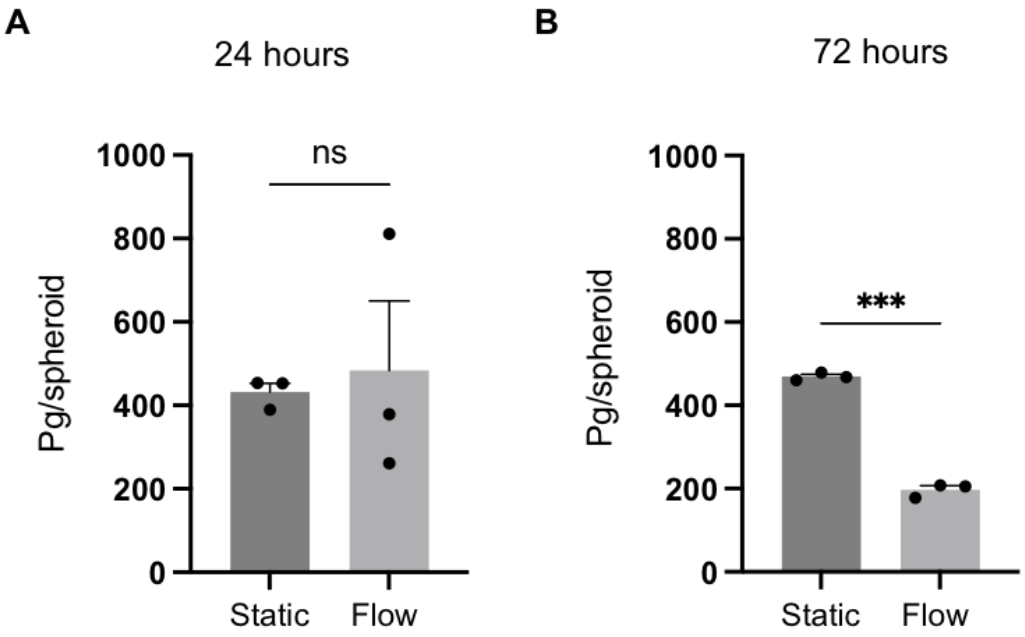

Figure 4.24: MCF7 secreted levels of VEGF

MCF7 spheroids were formed from 9.0 x 10^4 cells and kept in static or flow condition for 24h (A) and 72h (B). Effluent media was collected from both conditions and timepoints and analysed for the presence of secreted VEGF using a VEGF ELISA kit. Each black dot represents the levels detected in an effluent media sample from an independent experiment, and a bar is representative of the average for that condition (*n* = 3 experiments). The amount of VEGF in picograms (pg) per spheroid was calculated for all conditions. Error bars represent the mean ± SEM. Statistical significance was determined using paired student's t-test; ***p < 0.001; ns = not significant.

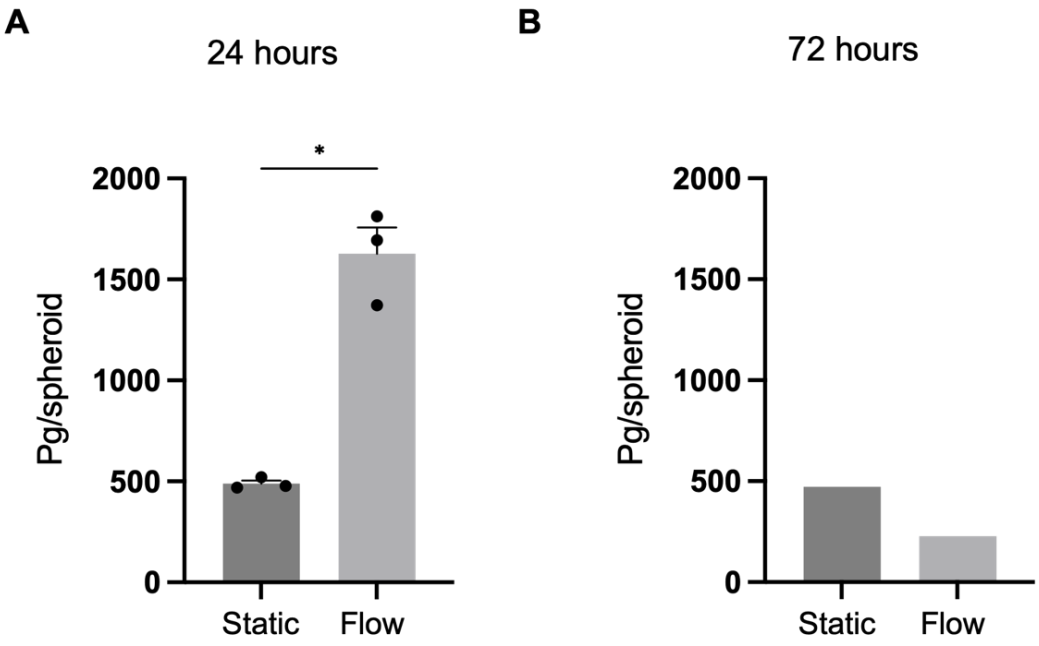

Figure 4.25: MDA-MB-231 secreted levels of VEGF

MDA-MB-231 spheroids were formed from 9.0 x 10^4 cells and kept in static or flow condition for 24h (A) and 72h (B). Effluent media was collected from both conditions and timepoints and analysed for the presence of secreted VEGF using a VEGF ELISA kit. (A) Each black dot represents the levels detected in an effluent media sample from an independent 24h experiment, and a bar is representative of the average of experiments (*n* = 3). Error bars represent the mean ± SEM. Statistical significance was determined using paired student's t-test; *p < 0.05. (B) Values are representative of one independent 72h experiment only. No statistical testing could be conducted.

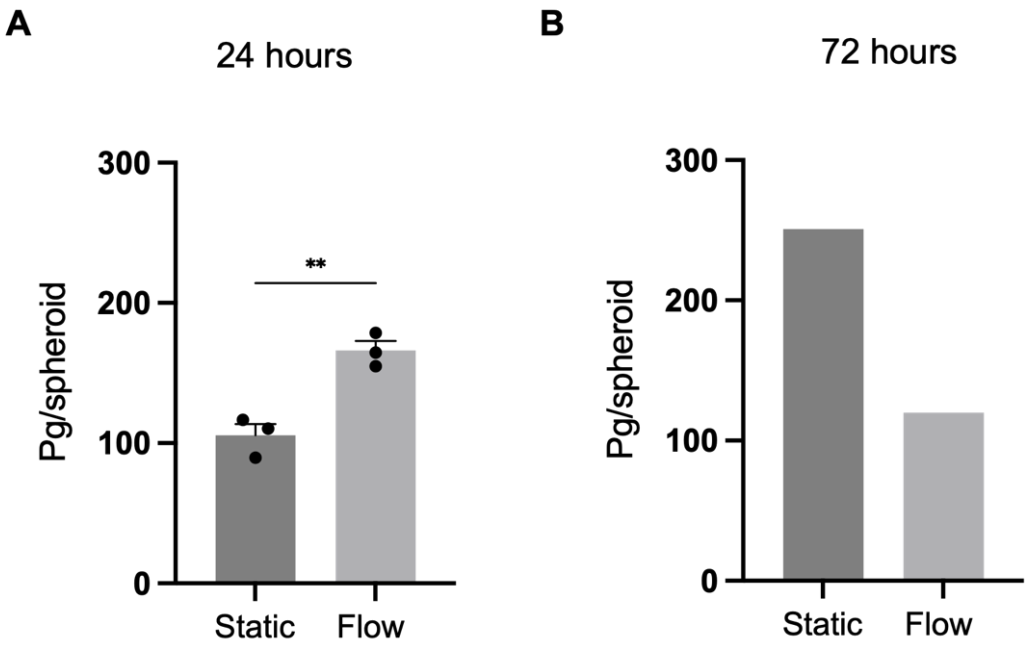

Figure 4.26: HEK293T secreted levels of VEGF

HEK293T spheroids were were formed from 9.0 x 10^4 cells and kept in static or flow condition for 24h (A) and 72h (B). Effluent media was collected from both conditions and timepoints and analysed for the presence of secreted VEGF using a VEGF ELISA kit. (A) Each black dot represents the levels detected in an effluent media sample from an independent 24h experiment, and a bar is representative of the average for that condition (*n* = 3 experiments total for each). Error bars represent the mean ± SEM. Statistical significance was determined using paired student's t-test; **$p < 0.01$. (B) Values are representative of one independent 72h experiment only. No statistical testing could be conducted.

4.3.7 COMSOL modelling of oxygenation in static and flow environments

In collaboration with Dr Martin Christensen at the University of Hull, mathematical, computer-based modelling was used to depict the distribution of oxygen in both static and flow conditions, at various oxygen tensions. The COMSOL modelling software accounted for the chip material (glass), the dimensions of the chip, the PDMS plug sealing the top of the spheroid chamber (although this was not pictured by the software), and the flow rate set by the syringe pump producing continuous perfusion. The kinetics for the basis of the modelling were set from a paper by Grimes and colleagues which described a method for estimating oxygen consumption in spheroids (Grimes et al., 2014) As can be seen in Figure 4.27 panels (A) and (C), computer modelling confirmed that at the flow rate used within the flow cell 2 system (3 μL min^{-1}), the spheroid chamber remained hypoxic at 1% O_2 (represented by blue colour which corresponds to low oxygen concentration). It also demonstrated that the spheroids in flow were better oxygenated than their static counterparts.

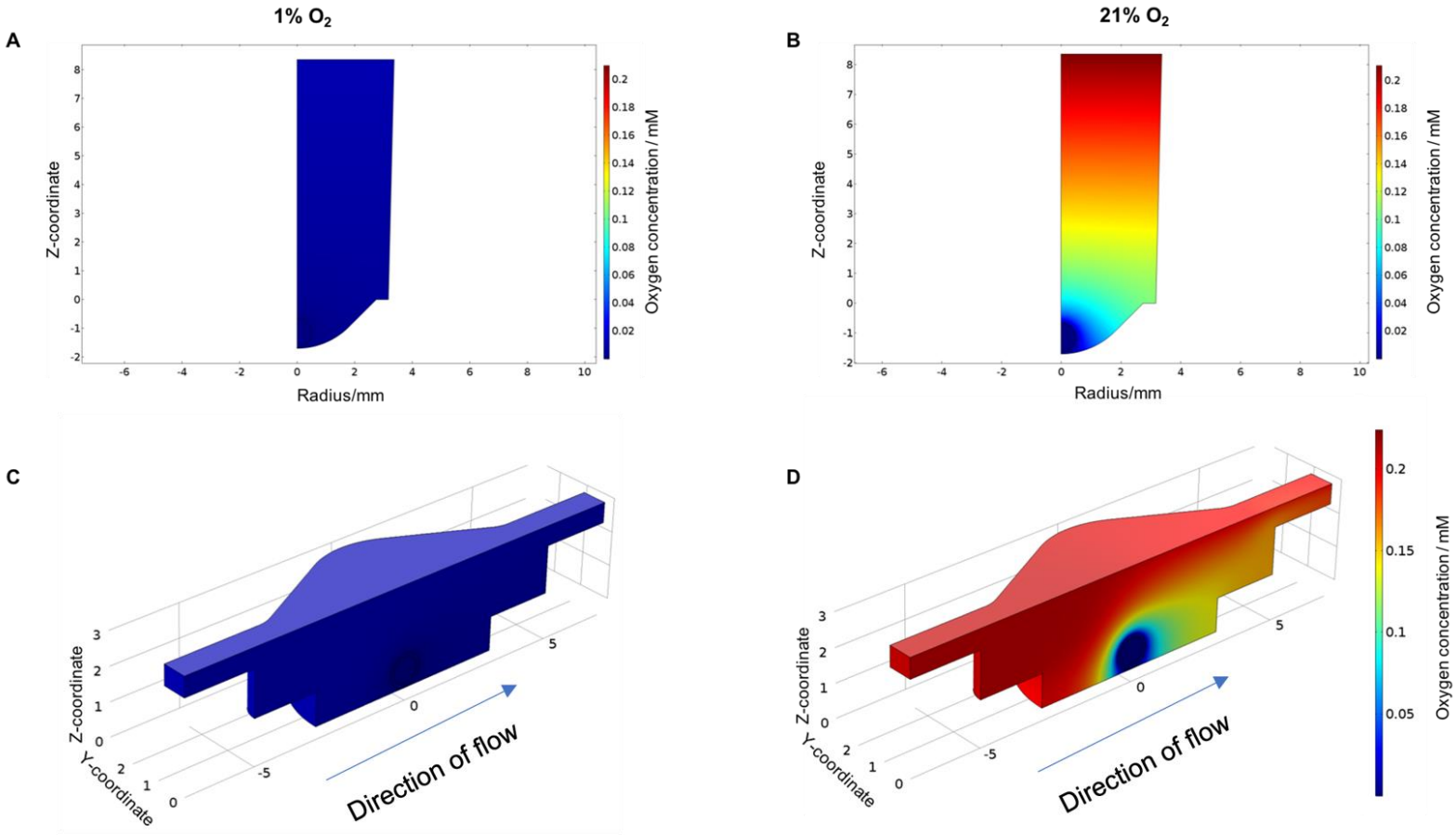

Figure 4.27: COMSOL modelling of oxygen distribution in static and flow environments

Computer-based modelling performed by Dr Martin Christensen as used to visualise oxygen distribution in static (A, B) and flow (C, D) environments at 1% O_2 (A, C) and 21% O_2 (B,D). The diameter of spheroids used for modelling was 1mm. Oxygen concentration is represented by a colour scale, where red correlates to more oxygen and blue correlates to less.

4.4 Discussion

The objective of this chapter was to investigate the effects of interstitial flow on the biology of cells in the TME. The previous chapter refined a microfluidic system for housing viable spheroids in a continuous flow environment for up to 72 hours and established methods for extracting RNA and protein. In this chapter, the goal was to use that spheroid-on-chip device to gain a better understanding of how interstitial flow impacts the biology of cells in the TME. The specific aims of this chapter were to:

1. Examine how markers of EMT in cancer spheroids are impacted by interstitial flow.
2. Evaluate transcriptomic changes in cancer spheroids caused by interstitial flow.
3. Evaluate whether interstitial flow influenced protein expression profiles of cancer spheroids in interstitial flow.
4. To investigate the relationship between interstitial flow and hypoxia and how they affect cancer spheroid biology in the TME.

To do so, a series of experiments evaluating transcriptomic changes and protein expression changes in spheroids exposed to interstitial flow in the flow cell 2 chip were conducted, as well as preliminary experiments conducted in hypoxia. EMT markers were not found to be regulated by interstitial flow in our system, contradicting the findings of other studies. We did, however, identify significant changes between the transcriptomes of spheroids in static and flow by using RNA-seq analysis. This analysis revealed enrichment of pathways related to genome preservation such as DNA replication and repair, as well as cell cycle. Transcription factor enrichment analysis also identified E2F family members as significant targets of highly differentially expressed genes. DNA replication and repair gene transcript levels were validated using qPCR analysis, but cell cycle markers were not conclusively upregulated as they were in RNA-seq. Protein expression analysed by Western blotting did not mimick the pathway enrichment patterns either, however, analysis of secreted VEGF protein did mirror downregulated *VEGFA* transcript levels identified in flow by qPCR.

4.4.1 EMT-associated markers are not significantly altered by interstitial flow

Previous studies have asserted that fluid flow affected cancer cells by causing them to increase expression of EMT markers, increase invasion capacity, and increase their metastatic potential. Tchafa and colleagues showed that interstitial fluid flow induced invasion in breast cancer cells (Tchafa et al., 2015). Another group, Rizvi and colleagues, used a microfluidic device to produce flow shear stresses and found significant upregulation of E-cadherin protein expression as a result, as well an increase in vimentin expression (Rizvi et al., 2013). Following these findings and others, we used EMT as a starting point for investigations of how interstitial flow in our flow

cell 2 system impacted cell biology. qPCR analysis was conducted on static and flow spheroid samples and genes known to be involved in EMT and the metastatic cascade were chosen to reflect the EMT process at a transcript level.

Contrary to the findings of many other studies, our results did not show a clear or conclusive upregulation in EMT markers. This could have been due to the differences in our model (3D spheroids with IFF) compared to previous work (2D or 3D single-cell suspensions). *LOX, PTGS2, SNA1L,* and *VIM* all contribute to tumour progression and were therefore expected to be upregulated in flow compared to static, if flow was indeed inducing changes consistent with EMT. *LOX* was significantly upregulated initially at 24h in flow but the effect was not maintained after 72h. In contrast, *VIM* was actually significantly downregulated in flow after 24h. After 72h that changed, and there was no significant difference between static and flow for *VIM* transcript levels. Meanwhile, *PTGS2* and *SNA1L* were not significantly different for the static and flow conditions at both timepoints. Taken together, these results did not support a clear pattern of upregulation and indeed did not show a clear overall pattern of any kind.

Next, *CDH1* and the protein it codes, E-cadherin, were investigated. E-cadherin expression is often lost in EMT, due to the role that E-cadherin has in maintaining normal epithelial cell adhesion (Baranwal & Alahari, 2009). Results from spheroids in our flow cell 2 device did not show decreases in expression of either *CDH1* at the transcript level or expression of the protein E-cadherin. This further indicated that EMT was not being induced by interstitial flow in our system, contrary to the conclusions drawn by other groups. The working hypothesis we inferred from these results was that the 3D structure of the spheroids used in our work must play a crucial role in the response to flow.

Lastly, two *MMP*s were chosen to evaluate with qPCR. Spheroids in the flow cell 2 system were embedded in Matrigel, an extracellular-like matrix, as described in section 2.3.7. Therefore, we hypothesised that *MMP*s may be a target for change due to the roles they have in cell invasion and degradation of the ECM surrounding a tumour. *MMP14* is known to cleave ECM components and *MMP1* has been specifically implicated in breast cancer invasion capacity (Itoh, 2006; Zhang et al., 2022). However, *MMP1* and *MMP14* were overall not significantly altered by flow – in the one condition that they were significantly different, *MMP1* was *down*regulated in flow after 72h, contrary to what would be expected in cancer cell invasion.

In summary, the results from our flow cell 2 system were not consistent with findings from previous studies where flow appeared to upregulate EMT markers. In fact, our results showed an inconsistent pattern of some markers expected to be upregulated being downregulated in flow, such as *VIM* transcripts after 24h and *MMP1* transcripts after 72h. Importantly, many of

the studies that reported flow causing upregulation of EMT used flow rates which are higher than what has been reported *in vivo*, often using flow velocities closer to the ranges seen in blood vessels (Kutikhin et al., 2018; Yang & Xu, 2021). Interstitial flow velocities *in vivo* are poorly described and vary immensely depending on site, measurement methods, and species. Tumours in mice measured using dynamic contrast-enhanced MRI measurements have reported interstitial flow velocities as low as 0.1 $\mu m\ s^{-1}$ while another study reported velocities as high as 55 $\mu m\ s^{-1}$ in metastatic cases of locally advanced squamous cell carcinoma of the uterine cervix in humans (Dafni et al., 2002; Munson & Shieh, 2014). Furthermore, the studies we are aware of which describe using 3D cell culture actually use suspensions of single cells in a 3D environment (such as inserts) rather than the use of spheroids or 3D masses. This suggests that the organisation of cells in a 3D mass may be important to how cells respond to fluid forces, and that single cells may be more susceptible to the effects of fluid flow than those in aggregates even when they are in an ECM.

4.4.2 Interstitial flow leads to dramatic changes in the transcriptome of MCF7 spheroids

4.4.2.1 RNA-seq and *in silico* analysis

The findings in the previous section did not show a clear pattern of change between static and flow, but only in the scope of EMT. Therefore, we sought to use an unbiased approach that would examine transcriptome-wide changes in static and flow cancer spheroids, and which could identify other functional areas where changes might be occurring. RNA-seq was used to do this, analysing the transcriptomes of MCF7 spheroids kept in static or flow for 24h. The 24h timepoint was chosen to see whether changes could be induced after only 24h, which would indicate a swift and significant influence of IFF on the spheroids. Furthermore, only one timepoint could be examined due to cost limitations but future work will aim to examine 72h and longer in the system.

To the best of our knowledge, this project is one of the first to conduct whole-transcriptome analysis of changes caused by interstitial flow in cancer spheroids. A study by Hoon Cho and colleagues used transcriptome-wide analysis to look at microRNA alterations in breast cancer induced by compression (Kim et al., 2016a). However, the mechanical compression used in their experiments was very different to the interstitial-like flow used in our study, and therefore mechanical forces induced were also different. Additionally, they cited the use of 3D cell culture, but this did not involve spheroids or any type of aggregates, simply cells suspended in extracellular matrix.

The results of the RNA-seq analysis we conducted established that significant differences existed between the transcriptomes of static and flow spheroids. Patterns of differential expression

were evident in the maps of up and downregulated genes (Figure 4.4, Figure 4.6) and the changes were highly significant (Figure 4.4). These unique expression profiles were the first indication that interstitial flow did indeed have an appreciable effect on cells in this condition.

To examine the patterns further, gene-set enrichment analyses were conducted to compare differentially expressed genes against curated databases with canonical pathways. Pathways and functions involved in cell cycle and DNA replication and repair were significantly represented in the results of these analyses (Figure 4.7, Table 4.2). This is particularly interesting given that MCF7 is an ER+ breast cell line, and estrogen receptors exert influence over transcriptional processes and signalling events that affect gene expression ((Fuentes & Silveyra, 2019). More so, transcription factor enrichment analysis (Figure 4.8) revealed that the E2F family of transcription factors represent half of the top ten enriched factors yielded by inputting the 600 most upregulated, protein-coding genes identified by RNA-seq. The E2F family of transcription factors are regulators of genes involved in cell cycle control and cell proliferation (Muller & Helin, 2000). This finding aligned with the pathway enrichment analysis results showing cell cycle pathways to be upregulated. It is also of particular interest because E2F transcription factors have been implicated in cancer because of their roles in regulating cell proliferation. So whilst EMT markers were not affected by flow, it was interesting that another marker associated with cancer progression was increased due to interstitial flow.

It is also worth noting that the RNA-seq analysis yielded a large volume of results, as it analysed over 30,000 genes. We chose not to investigate a large portion of the findings in more detail (mainly due to feasibility and time constraints), such as the role of microRNAs and other non-protein-coding transcripts. These could play important roles in the effect interstitial flow is having on cells and are an excellent target for future work. RNA-seq also laid the foundation for other up- and downstream pathway effects to be analysed further. An interesting example is the upregulation of DNA damage response pathways that was predicted by the enrichment analyses conducted in IPA, shown in Figure 4.28. Potential future work could involve exposing cancer spheroids to radiation and then keeping them in flow conditions to assess whether the predicted upregulation of the DNA damage response pathway improves their ability to recover. As far as we are aware, this is not an area that is well researched. There have been examples of clinical studies examining how high interstitial fluid pressure affects treatment outcomes, such as the use of radiation, for cancer patients (Rofstad et al., 2009). But none to our knowledge have examined how interstitial fluid flow may help cells exposed to radiation - especially in a 3D mass - recover from DNA damage induced by radiation.

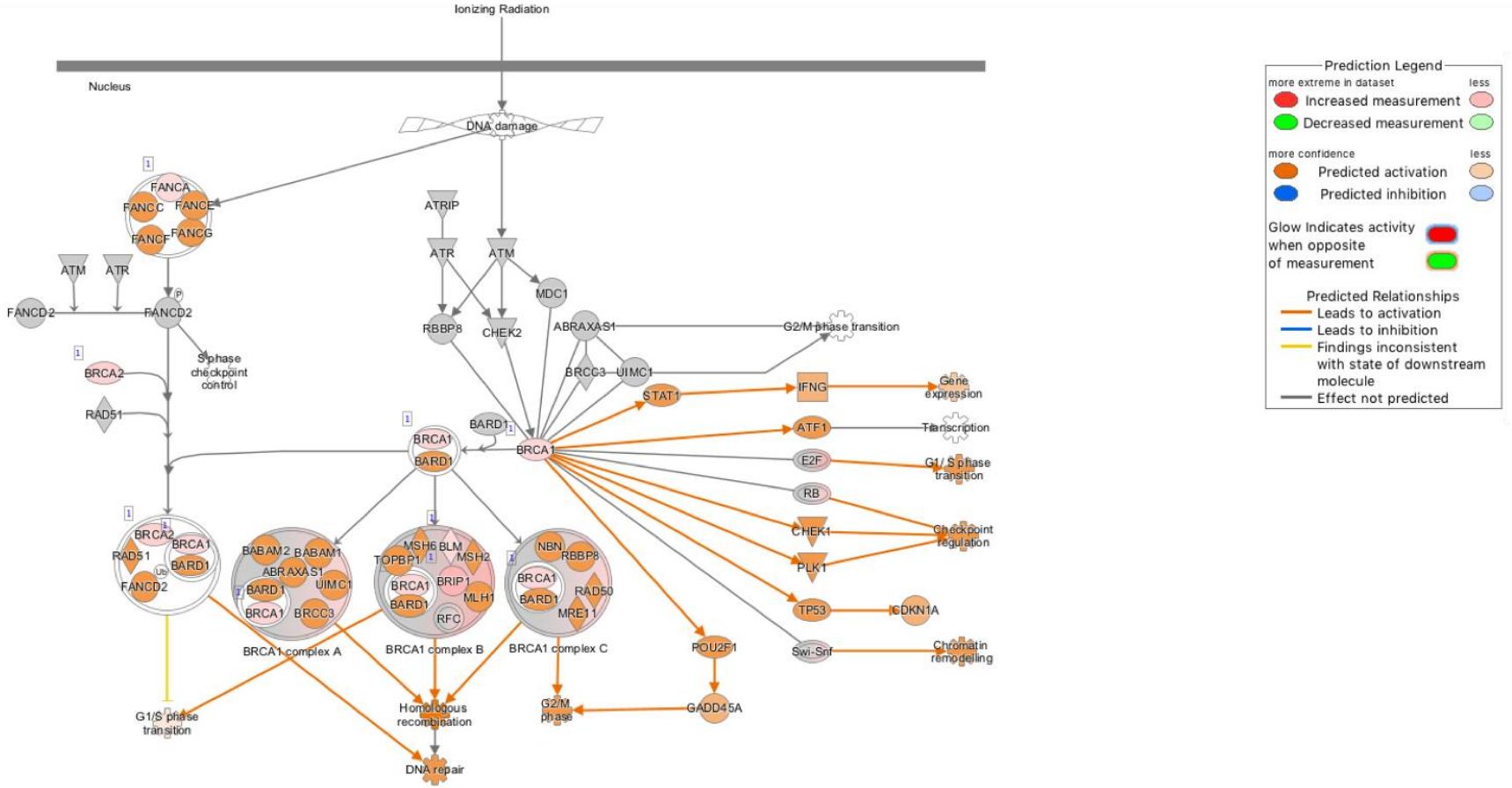

Figure 4.28: DNA damage response pathway with predicted activity of molecules from RNA-seq overlaid

The DNA damage response signalling pathway with the predicted activity of molecules overlaid in colour. Ingenuity Pathway Analysis software was used to analyse the whole transcriptome of MCF7 spheroids exposed to static or flow for 24h. The software uses input transcript data to infer prediction of molecules involved in the pathway

It is possible that more oxygen available to spheroids in flow simply increases production of reactive oxygen species (ROS), which also causes damage to DNA and could therefore be the culprit responsible for triggering the predicted DDR response. The investigations using our flow system in a hypoxic environment (discussed in detail in section 4.3.5 were inconclusive as to whether the DNA repair response was still upregulated in hypoxia (where oxygen availability was not a factor), so this hypothesis would require further work.

4.4.2.2 Validation of enrichment patterns

The RNA-seq analysis provided a broader scope of understanding into how interstitial flow was affecting the transcriptome of cancer spheroids. We sought to validate whether these patterns of enrichment were confirmed by qPCR analysis. Additionally, we used 72h samples as another timepoint to see if enrichment patterns were maintained with extended exposure to flow.

Overall, the genes selected to represent DNA replication saw significantly increased transcript levels relative to static spheroids. Only *RRM2* transcript levels at 24h were not significantly upregulated in flow compared to static, but a trend of increase was noted. The fold changes for the other DNA replication genes were significant but small, in the range of 2 or 3-fold. The findings do suggest that DNA replication pathways were being activated by flow after as little as 24h and for as long as 72h. These results set a framework for looking at extended timepoints for spheroids in flow, perhaps to see if downstream effects of increased DNA replication could be identified.

The results of the cell cycle gene panels were less conclusive, as most results were not significant. Notably though, *E2F1* transcripts were significantly upregulated in flow after 24h. This finding aligned well with the transcription factor enrichment analysis conducted on the gene set of the 600 most upregulated transcripts identified by RNA-seq, where E2F family transcription factors were significantly associated with the input genes. It would be useful to conduct repeats of the static v. flow experiments and repeat the qPCR analysis because there were variations between the experimental repeats used for these analyses. Only 3-4 independent experiments were conducted, making it difficult to identify outliers in such a small sample of replicates where distribution could not be analysed.

The DNA repair response was confirmed by significant upregulation of *BLM*, *EXO1*, and *FEN1* transcripts in flow. It is worth noting that many of the genes selected for the panels and therefore involved in cell cycle, DNA replication, and DNA repair, have roles in more than one pathway and indeed often overlap within these categories. Therefore, it is important to remember that their roles are not restricted to their assigned panel. In the case of DNA repair and replication, this is especially true. *RAD51*, however, is considered a canonical indicator of

DNA damage. Our results showed no significant differences between *RAD51* transcripts in static and flow, but this may demonstrate that DNA damage was not being *caused* by interstitial flow. Rather, DNA replication and replication stress transcripts were upregulated, pointing to those processes being active.

It is also worth noting that experiments conducted by an undergraduate student in our lab using the flow cell 2 system and HEK293T spheroids (a non-cancerous cell line) reported significantly increased transcript levels of *MCM6* as a result of interstitial flow. This finding is interesting because HEK293T cells are non-cancerous, highlighting the potential ability of flow to induce cell biology changes regardless of cell transformation status.

Finally, we evaluated transcript levels of *BRCA1* and *BRCA2* (Figure 4.12). Both are considered canonical breast cancer susceptibility genes but have also been implicated in cell cycle regulation and cell proliferation processes. Interestingly, interstitial flow significantly increased transcript levels of *BRCA1* and *BRCA2* in MCF7 breast cancer spheroids as compared to MCF7 spheroids maintained in static medium. This finding is notable for a couple of reasons: first, breast tissue and tumour microenvironments are reported as having significantly altered ISF pressure and therefore altered flow as well (Nathanson & Nelson, 1994). Identifying an upregulation of *BRCA* transcripts in breast cancer spheroids exposed to interstitial flow *in vitro* aligns with these reports and highlights the potential importance of flow as a feature needed in *in vitro* models. Secondly, *BRCA1* and *BRCA2* have been characterised as key factors in cell cycle and DNA damage response pathways (refer to Figure 4.28, as an example), and cells deficient in *BRCA2* have demonstrated genomic instability and hypersensitivity to DNA damaging agents, such as radiation (Sadeghi et al., 2020). Our results showing increased *BRCA* transcripts indicate that interstitial flow in the TME may contribute to cancer cell progression and capacity to survive by upregulating expression of these genes.

4.4.3 The relationship between interstitial flow, hypoxia, and cell biology in the TME

The results of the analyses at transcript level, described in the previous section, established that interstitial flow was asserting a significant set of changes on the transcriptome of MCF7 spheroids. In addition to interstitial flow, another important (and more established) clinical feature of many solid tumours is hypoxia. In breast cancer, hypoxia has been linked to metastasis (Gilkes & Semenza, 2013). Here, the relationship between interstitial flow and hypoxia was explored to understand how these two physiologies work in early tumour progression.

First, we established that in the flow condition spheroids were better oxygenated and saw decreases in hypoxia signalling (Figure 4.27). A set of hypoxia markers were used for qPCR analysis and all were decreased at transcript level in flow, though not all were statistically

significant, just noted trends of decrease (Figure 4.15). We also collaborated with Dr Martin Christensen to use mathematical, computer-based modelling to depict the distribution of oxygen in both static and flow conditions, at various oxygen tensions. In a normoxic atmosphere of 21% O_2, spheroids did appear to have better oxygenation in the microfluidic chamber than spheroids in static wells, where oxygen concentration is highest at the furthest point from the spheroids (Figure 4.27 (B) and (D)). With continuous perfusion of fresh media there was expected to be an increase in oxygen supply to spheroids in flow and a subsequent downregulation of hypoxia signalling (Figure 4.14) as described above. However, it was unclear whether the novel enrichment patterns identified in flow, such as upregulation of DNA repair and replication pathways, were a by-product of better access to oxygen or a result of fluid flow forces. For example, increased oxygen availability could lead to increased production of ROS, which can also trigger DNA damage and repair responses (Srinivas et al., 2019). In order to discern whether the differential expression of genes in flow was a result of fluid forces, the flow v. static experiment setup was conducted in a hypoxia chamber at 1% O_2. Therefore, the static and flow spheroids would theoretically experience the same level of hypoxia, but only flow spheroids would experience the effect of interstitial fluid flow in their environment.

As can be seen in Figure 4.27 panels (A) and (C), computer modelling confirmed that at the flow rate used within the flow cell 2 system (3 $\mu L\ min^{-1}$), the spheroid chamber remained hypoxic at 1% O_2 (represented by blue colour which corresponds to low oxygen concentration). These results confirmed that as expected, continuous perfusion did not improve oxygen availability to the spheroid chamber on-chip compared to static wells when experiments were conducted in a hypoxia chamber. Therefore, results from experiments conducted in hypoxia where flow was compared to static showed the effect of fluid flow, not the effect of improved oxygen availability in the flow device.

The first panel of genes used to evaluate differences between static and flow in hypoxia represented markers of hypoxia. This was to check whether flow spheroids were still downregulating hypoxia signalling compared to static spheroids, even with both in a hypoxic environment. qPCR analysis of *CA9*, *VEGFA*, and *HK2* showed no significant differences between transcripts, suggesting that flow spheroids were not downregulating hypoxia signalling more than static counterparts when both were in hypoxia. Next, a selection of transcripts that were significantly upregulated in flow and which related to DNA replication, repair, damage response, and cell cycle functions were evaluated. *MCM6, E2F1*, and *BRCA1* were not significantly upregulated by interstitial flow when the experiment was conducted in hypoxia. However, more work is being done in our lab to explore this further, including RNA-seq of static and flow spheroids kept in hypoxia at 1% O_2.

Despite no significant differences detected between static and flow spheroid transcripts in hypoxia, it was notable that *VEGFA* transcripts remained low in flow, by 0.63 FC average less than static. Hypoxia is generally associated with increased VEGF production; however, hypoxia is not the only transcriptional regulator of VEGF (Vaupel, 2004). Other stimuli such as growth factors, hormones, cytokines and cellular stresses have been reported to regulate its expression at the transcriptional level (Pages & Pouyssegur, 2005). Therefore, these preliminary results could indicate that a factor other than hypoxia is regulating *VEGFA* transcripts in the flow cell 2 system.

4.4.4 Interstitial flow does not significantly impact the protein expression profile of cancer spheroids

Expression changes seen at gene or transcript level do not always translate directly to those seen at protein level as a number of processes such as post-translational modifications may affect protein expression. Additionally, the time from transcript level "instructions" to the expression of a protein may be more than what is experimentally tested, and there are other molecular overrides of transcript level changes that could modulate protein expression. Most of the fold changes for gene transcripts discussed in the previous sections were low-grade (less than 10-fold for all). We sought to investigate whether protein expression was influenced by interstitial flow at the timepoints used in our study.

Western blotting was used to confirm that hypoxia was less prevalent in the flow spheroids than in static spheroids. This effect was demonstrated in Figure 4.18, where HIF-1α bands were present in static samples but not flow samples. This confirmed that protein expression associated with hypoxia was downregulated by interstitial flow, as was seen at transcript level previously. HK2 was also blotted for, as it is another downstream marker of hypoxia signalling and has roles in cellular metabolism. No significant differences were detected in HK2 expression levels between static and flow MCF7 spheroids or MDA-MB-231 spheroids, but notable trends of decrease were identified. MDA-MB-231 cells represent a breast cancer biology different to that of MCF7 cells, as they are triple negative (as discussed in section 1.3). Analysing the expression of HK2 in the MDA-MB-231 cells in 2D and in hypoxia served as a method of further comparison. It was not possible to collect sufficient protein from MDA-MB-231 spheroids culture in static and flow for 72 hours, so adherent samples were used instead. Hypoxic samples were also added to the sample panel stratification as a matter of interest, given the relationship between HK2 and hypoxia signalling. Furthermore, since HK2 was expected to be highly expressed in more hypoxic cells, the 24h hypoxic sample served as a positive control to indicate whether the antibody was effectively detecting the protein. RPA expression was also evaluated, as it is a marker of DNA replication stress. However, neither MCF7 nor MDA-MB-231 spheroids

saw significant differences in RPA expression between static and flow conditions. This indicates that DNA replication was upregulated at transcript level, but expression of replication *stress* at the protein level was not occurring. Lastly, the tumour suppressor p53 was also evaluated using Western blotting in MCF7 spheroids, but there were no significant differences detected.

In summary, the protein expression profiles of MCF7 and MDA-MB-231 spheroids were not shown to be significantly different in these experiments. Only the expression of HIF-1α was markedly downregulated by flow. Protein expression experiments may require the use of longer exposures to interstitial flow, to allow changes seen at transcript level to be translated to detectable differences in protein expression. For example, a study by Winkelman and colleagues that reported increased protein expression in a glioblastoma-on-chip model used periods of up to 8 days for experiments (Winkelman et al., 2021).

4.4.5 Chapter conclusion

In summary, this chapter showed that interstitial flow in our flow cell 2 system did not reproduce the upregulation of EMT markers reported by other studies using fluid flow on single cell suspensions in 3D environment. Our results did reveal significant differences between the transcriptomes of static and flow MCF7 spheroids, leading to the novel discovery of upregulated DNA replication and repair transcripts identified by RNA-seq and confirmed by qPCR analysis. This effect was not maintained when static and flow spheroids were kept in hypoxia at 1% O_2, but further work is needed to better understand the effects interstitial flow has on cells in hypoxia.

Chapter 5 Identification of potential interstitial flow biomarkers and evaluation of their clinical relevance

5.1 Introduction

5.1.1 Biomarkers in cancer

Biological markers, known as biomarkers, are broadly defined as biological characteristics that can be objectively measured and evaluated as indicators of normal biological processes, pathogenic processeses, or pharmacological responses to a therapeutic intervention (Naylor, 2003). In more specific terms, biomarkers have been defined as "cellular, biochemical, or molecular alterations that are measurable in biological media such as human tissues, cells, or fluids" (Hulka & Wilcosky, 1988). Further to this definition there are also two major types of biomarkers commonly recognised. The first is biomarkers of exposure, which are used in risk prediction. The second is biomarkers of disease, which are used in the context of screening, diagnosis, and disease progression monitoring. A good biomarker is generally accepted as needing to meet two criteria: sensitivity and specificity. Sensitivity refers to the proportion of individuals with confirmed disease who test positive for the biomarker. This is also known as the true-positive test result. Specificity is the true-negative result, or the proportion of control subjects who test negative for the biomarker (Wagner et al., 2004). Biomarkers can also be either predictive or prognostic, and in some cases may be both. A predictive biomarker is used for predicting patient responses to a treatment or in practice, deciding what treatment measures should be used on a patient. Prognostic biomarkers are used for giving an indication of how the disease will progress and identifying the likelihood of a clinical event, independent of treatment (Das et al., 2017).

In the context of cancer, a biomarker often refers to a substance or process that is indicative of the presence of cancer in the body. However, biomarkers can also be used as tools for cancer risk assessment, screening, accurate diagnosis, patient prognosis, and prediction of response to therapy. In these ways they can serve to optimise decision making in a clinical setting. Given that metastasis is responsible for an overwhelming majority of cancer deaths and significantly depreciates patient outcomes, much of biomarker research in cancer has focused on early detection, prior to the spread of disease throughout the body (Sarhadi & Armengol, 2022). There is also an increasing interest in the use of biomarkers for personalised cancer treatments, often referred to as personalised oncology (Kalia, 2015; Rodriguez-Antona & Taron, 2015).

5.1.2 IFF biomarkers

Tumour ISF is the first point of contact a tumour has with its surrounding environment, bathing the tumour and stroma cells. It follows that interest in ISF has increased, especially for the

potential trove of information it may hold about the tumour it surrounds (Wagner & Wiig, 2015). Indeed, this is where most research on biomarkers and ISF has overlapped; researchers have tried to use ISF as a sampling medium for tumour specific proteins and other biomarker candidates. ISF has even been referred to as the cancer secretome because it is considered by some researchers to be the best medium for studying proteins secreted by cancer cells and other cells in the confined environment of a tumour (Xue et al., 2008; Makridakis & Vlahou, 2010). An example analogous to cancer is work conducted by Sun and colleagues that sought to characterise the proteome of ISF surrounding liver tissue to identify biomarkers of liver disease, highlighting how ISF is gaining notoriety for its direct interactions with pathological sites (Sun et al., 2010)

However, aside from the use of ISF as a sampling medium for cancer-secreted biomarkers, there has been less work on establishing biomarkers of interstitial fluid flow itself. ISF pressure - which has also started to gain clinical relevance for the barriers to treatment it creates – is in some cases considered a predictive biomarker (Lunt et al., 2008; Salavati et al., 2022). That is, a measured increase in ISF pressure equates to poor prognosis (Ferretti et al., 2009). But again, molecular markers of ISF pressure have been examined very little, and to our knowledge no work has been done to specifically establish biomarkers of fluid flow.

5.1.1 Chapter specific hypothesis, aims, and objectives

There remains little understanding of the specific molecular changes associated with changes in fluid flow in tumour microenvironments. Furthermore, even though changes in interstitial fluid flow and pressure are increasingly recognised as important contributors to challenges associated with treatment successes, little research has been done to elucidate the molecular mechanisms by which interstitial fluid influences clinical outcomes. Identifying such mechanisms could provide a better understanding of not only the role that interstitial fluid has in the TME but could also identify biomarkers of altered IFF. We hypothesized that identification of a gene that was significantly differentially expressed in the RNA-seq analysis (conducted in Chapter 4) could be assessed against various clinical outcomes to identify a potential biomarker of IFF in the TME. To accomplish this, the following objectives were outlined:

1. Identify a gene or genes significantly differentially expressed by IFF that could serve as a potential biomarker.
2. Evaluate expression of identified gene(s) in breast cancer patient datasets.
3. Determine whether expression of the identified gene(s) correlates to breast cancer patient outcomes.

5.2 Experimental design

5.2.1 Identification of flow biomarkers – criteria for selection

To identify possible ISF flow biomarkers, the list of differentially expressed genes produced by RNA-seq (as described in chapter 4) was used to identify potential candidates. We used a set of criteria aimed at identifying significantly changed, cancer-relevant genes which would be viable candidates to go on and meet the criteria for a good biomarker outlined in section 5.1.1 above. The 50 most up- and downregulated genes from the DEG lists were evaluated against the following criteria:

- DEG to have $P < 0.01$ reported
- relevance pertaining to cancer in the literature
- no read counts present in one of the conditions (static or flow)

5.2.2 Analysis of potential flow biomarker transcript levels

Potential biomarker candidates identified by RNA-seq as predictive indicators of IFF were initially assessed by qPCR as previously reported (2.5.3). In brief, MCF7 spheroids were kept in static or flow conditions (2.3.6) for 24h and extracted RNA was analysed using qPCR. The 24h timepoint mirrored the experiment duration for the spheroids analysed by RNA-seq and the 72h timepoint was added to investigate whether a longer duration mimicked results at 24h. Transcript levels of the 4 genes selected as described in 5.2.1 were analysed to identify whether the expression pattern demonstrated in the RNA-seq dataset was reproduced when analysed by qPCR for both timepoints.

5.2.3 *In silico* analyses to evaluate the prognostic value of IFF biomarker(s)

The implication of identified IFF biomarker candidate gene expression levels on patient survival was evaluated using online, patient database tools. First, KMplotter (kmplot.com/analysis) was used to assess the correlation between IFF biomarker gene expression and patient survival outcomes (section 2.7.3.2). KMplots provide a visualisation of the effect of high or low expression of the gene of interest on a patient's prognosis (Lanczky & Gyorffy, 2021). Next, TNMplot was used for evaluating differential expression of IFF biomarker candidates in tumour and normal tissues (tnmplot.com/analysis) as described previously (2.7.3.1). This tool uses an integrated database of transcriptome-level patient datasets to evaluate expression levels of genes of interest in tumour, normal, and metastatic tissues (Bartha & Gyorffy, 2021).

5.2.4 *In silico* analyses to evaluate the predictability value of IFF biomarker(s)

ROCplotter was used for validation of identified IFF biomarker candidates as predictive biomarkers in breast cancer (rocplot.org). This online tool links data on patient gene expression levels and responses to therapy to evaluate how predictive the selected gene/biomarker is. An ROC curve plots consist of sensitivity measured on the *y*-axis and 1-specificity on the *x*-axis (Zou et al., 2007). Figure 5.1 shows hypothetical ROC curves representing the diagnostic accuracy. An area under the ROC curve (AUC) is computed which determines the prognostic power of the input gene or "test". AUC values are between 0-1, and the prognostic power is defined as: AUC < 0.6 = effect is small for clinical utility, 0.6 < AUC < 0.7 = cancer biomarker with potential clinical utility, 0.7 < AUC < 0.8 = high quality cancer biomarker, and AUC > 0.8 = best possible biomarker (Fekete & Gyorffy, 2019). AUC is equal to 0.5 when the ROC curve corresponds to random chance and 1.0 corresponds to perfect accuracy. A value less than 0.5 would indicate that the biomarker does worse than random chance at predicting outcomes (Zou et al., 2007).

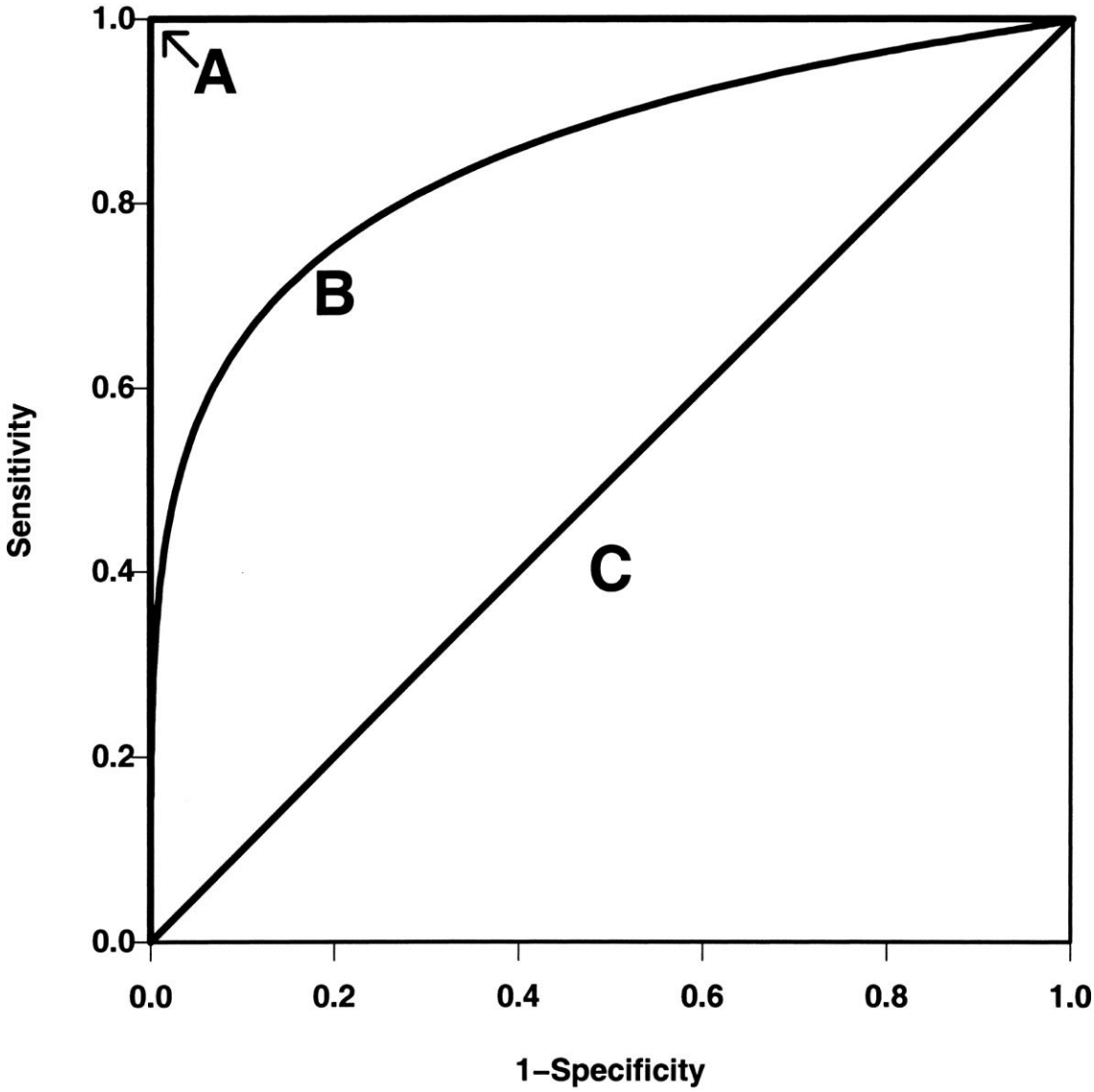

Figure 5.1: Demonstration of hypothetical receiver-operating characteristic analysis

Three hypothetical ROC curves are represented by lines A, B, and C. Line A is in the upper and left axes, representing the "gold standard" of diagnostic accuracy where the AUC = 1. Line B represents a typical ROC curve with an AUC = 0.85. Diagonal line C corresponds to random chance. As the accuracy of a diagnostic test improves, the ROC curve line moves toward position A and the AUC increases, approaching 1. Figure from (Zou et al., 2007).

5.3 Results

5.3.1 Selection of genes of further interest from differentially expressed gene list produced by RNA-seq

A list of differentially expressed genes was obtained by RNA-seq as described in Chapter 4. This list was extensive, with thousands of genes differentially expressed compared to the static condition. To achieve the aim of identifying potential biomarkers of IFF, this list needed to be narrowed down to select genes of interest that could then be further evaluated for potential clinical relevance. Four genes of interest were identified from the list of differentially expressed genes obtained by RNA-seq to further evaluate as potential biomarkers of IFF. *ACTL8* and *RAB6C* were selected from the list of DEGs upregulated in flow and only present in flow samples. *ABCA8* and *BARHL1* were selected as the candidates from the list of downregulated DEGs; because genes selected on the basis of no read counts present in the other condition, this meant that these targets were unique to static spheroids and not expressed in flow. Table 5.1 outlines the targets selected for each category.

5.3.2 Validation of potential IFF biomarkers by qPCR analysis

qPCR was used to determine relative expression level changes of the 4 genes selected in section 5.3.1. Transcript levels were analysed in MCF7 spheroids exposed to flow compared to those in static for 24h and 72h (see section 2.5.3 for detailed methodology).

Of the two genes unique to flow, only one of the genes of interest, *ACTL8*, was significantly upregulated compared to static and this was only at the 72h timepoint. At 24h there was a distinct increase in transcript levels evident in the chart as can be seen in Figure 5.3, panel A. *ACTL8* transcript levels in flow after 24h were an average of 19.5-fold higher relative to static, however, this was not statistically significant. The other gene uniquely present in flow samples was *RAB6C* and the results for this gene are shown in Figure 5.2. Neither timepoint yielded significant differences in *RAB6C* transcript levels between static and flow. There was also a large SEM at both timepoints due to variation between replicates. Both conditions had 1 replicate showing increase relative to static and 1 showing a decrease relative to static, so there was no clear pattern of relative expression.

Table 5.1: Genes selected from RNA-seq dataset as viable biomarker candidates

Present only in flow					
Gene	**Protein**	***p*-value**	**Fold change**	**Protein function**	**Evidence in cancer literature**
ACTL8	Actin like 8	8.3×10^{-6}	75.6	Member of the cancer-testis antigens family. Involved in epithelial cell differentiation.	Previously associated with breast cancer (Yao et al., 2014) Key role in invasion and metastasis of colorectal cancers (Han et al., 2019)
RAB6C	RAB6C, member RAS oncogene family	$2.2. \times 10^{-3}$	32.7	Involved in mitotic cell cycle, regulation of centrosome duplication, and response to xenobiotic stimulus.	Expression may confer a selective advantage to drug-resistant breast cancer cells (Young et al., 2010) Serves as an independent prognostic factor of distant recurrence risk in systemically untreated patients with an ER+/PR− tumor (Fohlin et al., 2020)
Present only in static					
ABCA8	ATP binding cassette subfamily A member 8	7.5×10^{-3}	0.034	Membrane-associated protein in superfamily of ATP binding cassette (ABC) transporters. ABC proteins transport various molecules across intra- and extracellular membranes. May regulate lipid metabolism and be involved in the formation and maintenance of myelin.	Study found (by meta-analysis) significantly lower expression in breast tumors compared to normal breast tissue (Shahan Mamoor, preprint 10.31219/osf.io/8rzk2)
BARHL1	BarH like homeobox 1	0.011	0.052	Enables sequence-specific double-stranded DNA binding activity. Predicted to be involved in reulation of transcription by RNA polymerase II. Considered biomarker of triple-negative breast cancer.	Expression may decelerate tumour growth in human and mouse medulloblastoma; may have tumor suppressive roles (Poschl et al., 2011)
Information in this table was gathered from curated gene databases online; genecards.org and ensembl.org unless cited otherwise.					

Next, the 2 genes uniquely present in static RNA-seq samples, *BARHL1* and *ABCA8*, were assessed. *BARHL1* was not significantly different between static and flow conditions at either timepoint. The mean of differences between conditions at 24h was 2.2 FC and 1.5 FC at 72h, but one replicate in each timepoint dataset was greater than 5 FC whereas the other two were below 1.5, creating variation between replicates. The results did not coincide with the findings of the RNA-seq analysis where *BARHL1* transcripts were differentially expressed between conditions. The next gene examined, *ABCA8*, could not be detected in 2 out of the 3 flow samples used for qPCR and therefore measurable fold changes for 3 independent experiments could not be attained. Thus, statistical testing could not be performed on the fold change data. The mechanism of detection in qPCR is by cycle threshold and if the levels of mRNA *ABCA8* were so low in the flow samples that no read counts were produced during the RNA-seq analysis, it is possible that qPCR was not sensitive enough to detect such low transcript message.

Overall the results of the qPCR analysis for these genes did not align closely with the differential expression detected for them by RNA-seq. *ACTL8* was the only gene of the 4 candidates that saw results consistent with the RNA-seq and had significantly different relative expression of transcripts compared to static after 72h. Therefore, *ACTL8* was selected as the candidate gene for further exploration of biomarker viability.

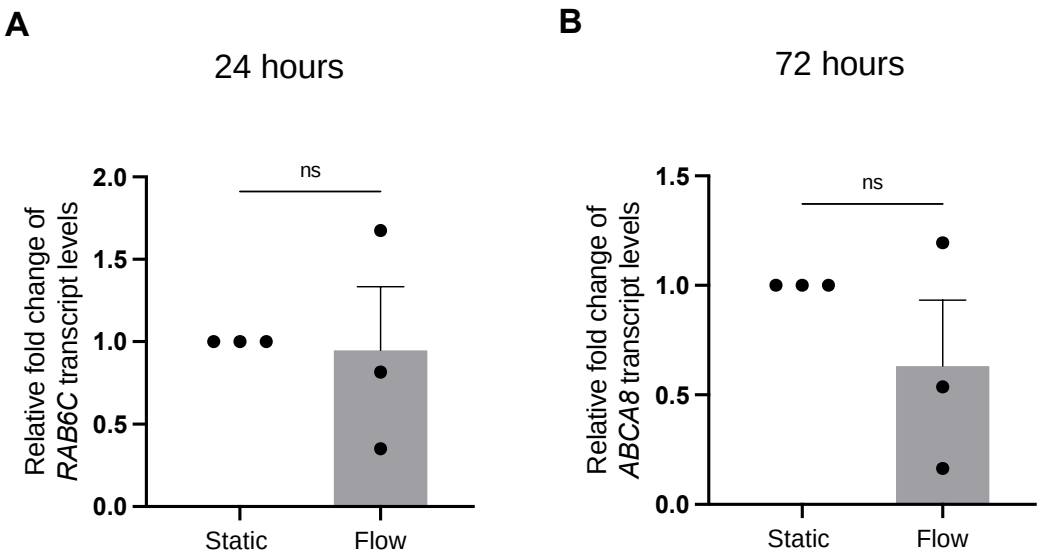

Figure 5.2: *RAB6C* transcript levels in MCF7 spheroids in flow vs static conditions

MCF7 spheroids were formed from 9.0 x 10^4 cells and kept in either static or flow conditions for 24h (A) or 72h (B). Total RNA was extracted from x 3 spheroids at the end of experiments and used for qPCR. The housekeeping gene used was *B2M*. Data represent the mean of *n*=3 experiments. Error bars represent mean +/- SEM. Statistical significance was determined by paired student's t-tests; ns = not significant.

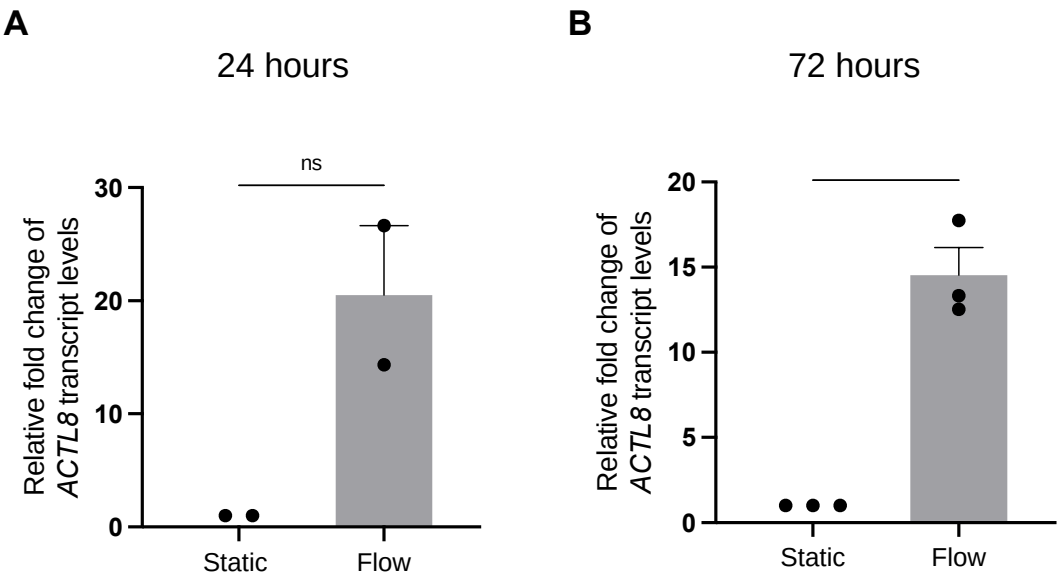

Figure 5.3: *ACTL8* transcript levels in MCF7 spheroids in flow vs static conditions

MCF7 spheroids were formed from 9.0 x 10^4 cells and kept in either static or flow conditions for 24h (A) or 72h (B). Total RNA was extracted from x 3 spheroids at the end of experiments and used for qPCR. The housekeeping gene used was *B2M*. Data represent the mean of *n*=3 experiments. Error bars represent mean +/- SEM. Statistical significance was determined by paired student's t-tests; *p < 0.05; ns = not significant.

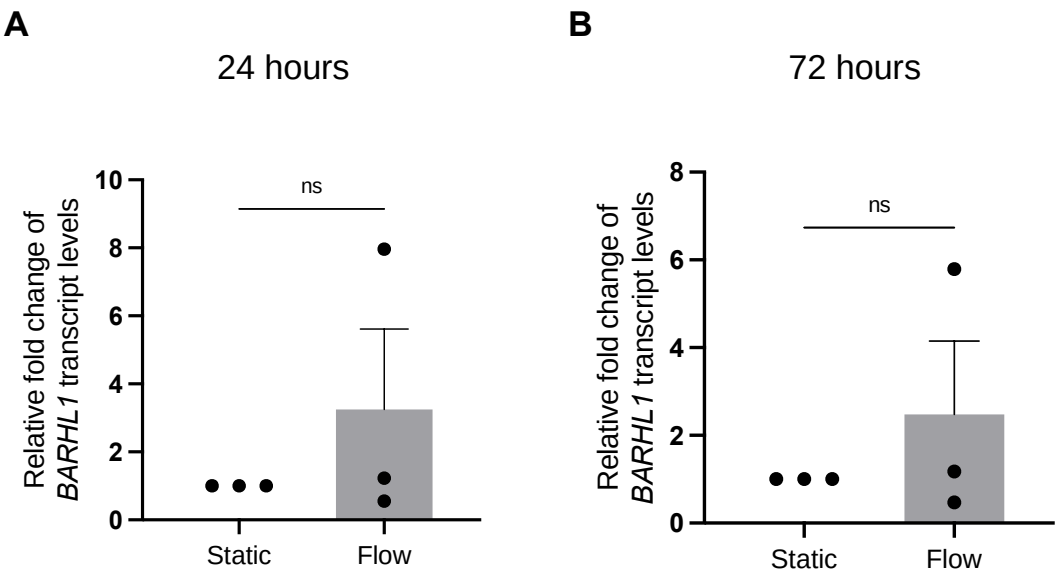

Figure 5.4: *BARHL1* transcript levels in MCF7 spheroids in flow vs static conditions

MCF7 spheroids were formed from 9.0 x 10^4 cells and kept in either static or flow conditions for 24h (A) or 72h (B). Total RNA was extracted from x 3 spheroids at the end of experiments and used for qPCR. The housekeeping gene used was *B2M*. Data represent the mean of *n*=3 experiments. Error bars represent mean +/- SEM. Statistical significance was determined by paired student's t-tests; ns = not significant.

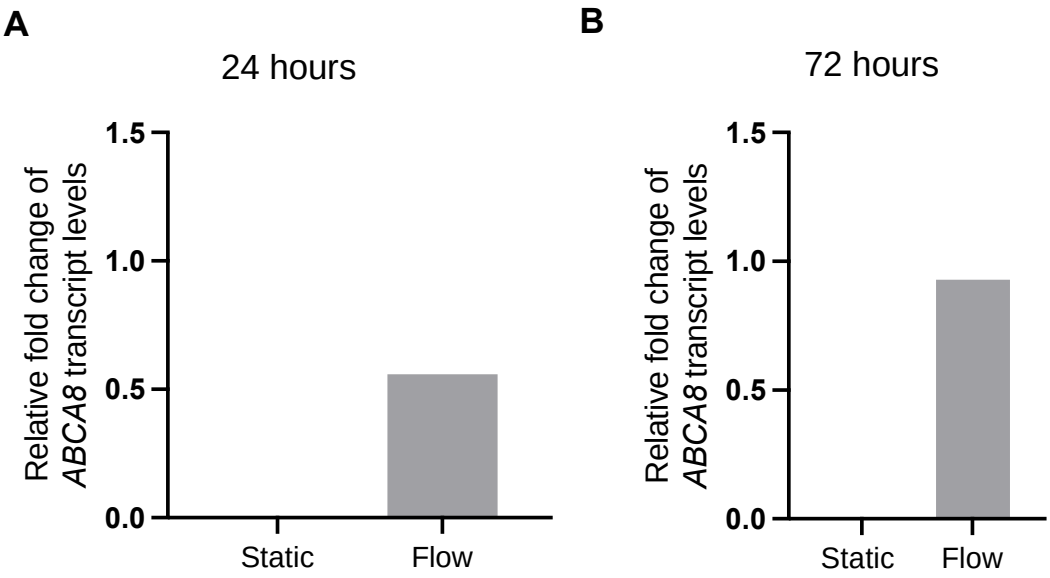

Figure 5.5: *ABCA8* transcript levels in MCF7 spheroids in flow vs static conditions

MCF7 spheroids were formed from 9.0 x 10^4 cells and kept in either static or flow conditions for 24h (A) or 72h (B). Total RNA was extracted from x 3 spheroids at the end of experiments and used for qPCR. Signal was undetectable in n=2 samples and therefore data represent *n*=1 experiments. Statistical significance could not be determined.

5.3.3 Evaluation of expression levels of *ACTL8* in cancer patient tissue

Following the selection of *ACTL8* as the gene of interest to explore further as a potential biomarker of IFF, investigations into expression of this gene in patient tissues were conducted. The online tool TNMplot, which draws from curated patient data repositories, was used to compare expression of *ACTL8* in two ways:

- Between non-paired normal and tumour breast tissue samples
- Between paired normal and tumour tissues, where breast invasive carcinoma (BIC) tumour samples were taken with adjacent normal tissue samples

Figure 5.6 shows the expression of *ACTL8* in unpaired normal and tumour breast samples. The sample size for tumours was much higher than that of the normal tissue samples, with 7569 compared to 242 respectively. Nonetheless, the data demonstrate that tumours showed significantly (p= 1.53 x 10^{-2}) higher relative expression of *ACTL8* compared to normal tissue samples. A similar trend was seen in the paired tumour and normal tissue samples taken from 112 BIC patients (Figure 5.7). *ACTL8* expression in the tumour samples was an average of ~290-fold higher compared to neighbouring, normal tissue and this was highly significant (p = 2.69 x 10^{-14}). These data indicate that tumours express higher levels of *ACTL8* compared to normal tissues. Furthermore, these findings established that expression of *ACTL8* could be important in tumour progression.

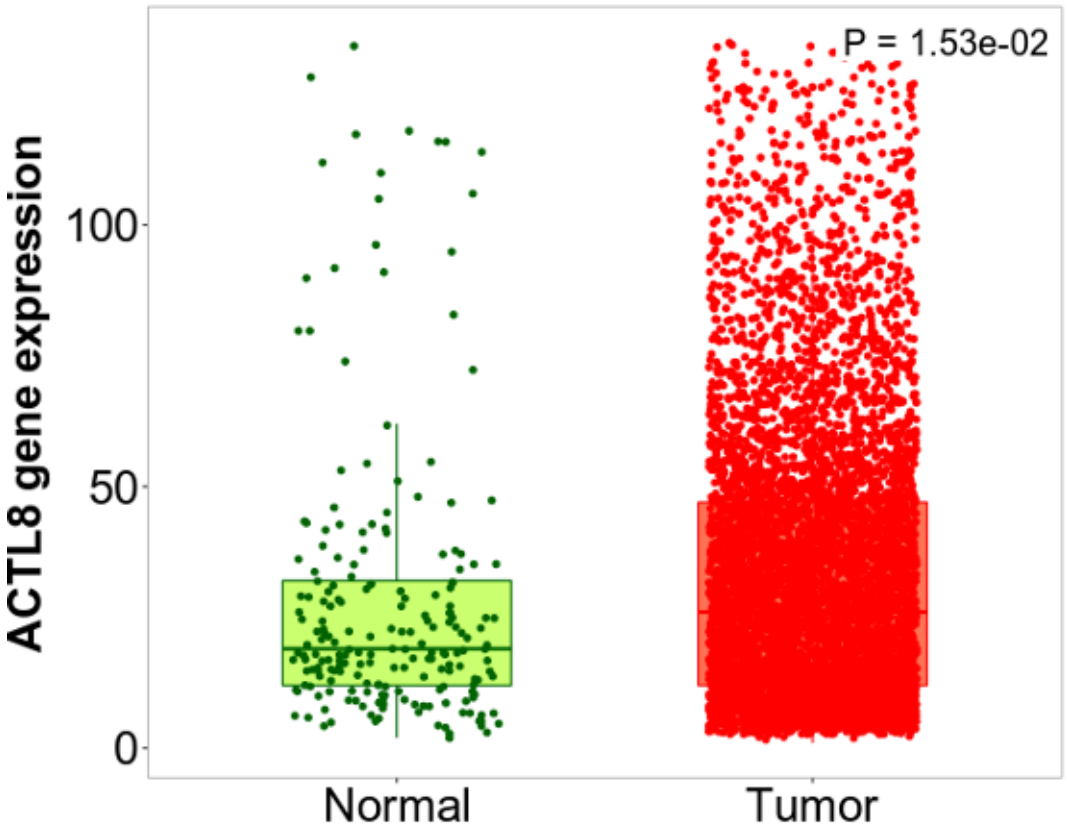

Figure 5.6: *ACTL8* expression in unpaired normal and tumour breast tissue samples

ACTL8 gene expression comparison of non-paired tumour and normal breast tissue patient samples using gene chip array-based data from NCBI GEO (National Center for Biotechnology Information Gene Expression Omnibus). Boxplot was generated using the online analysis platform TNMplot.com. Analysis was run by grouping all specimens of the same category and running a Mann-Whitney U test. Red dots represent expression data from patient breast tumour samples (*n* = 7569) and green dots represent expression data from non-paired normal breast tissue samples (*n* = 242).

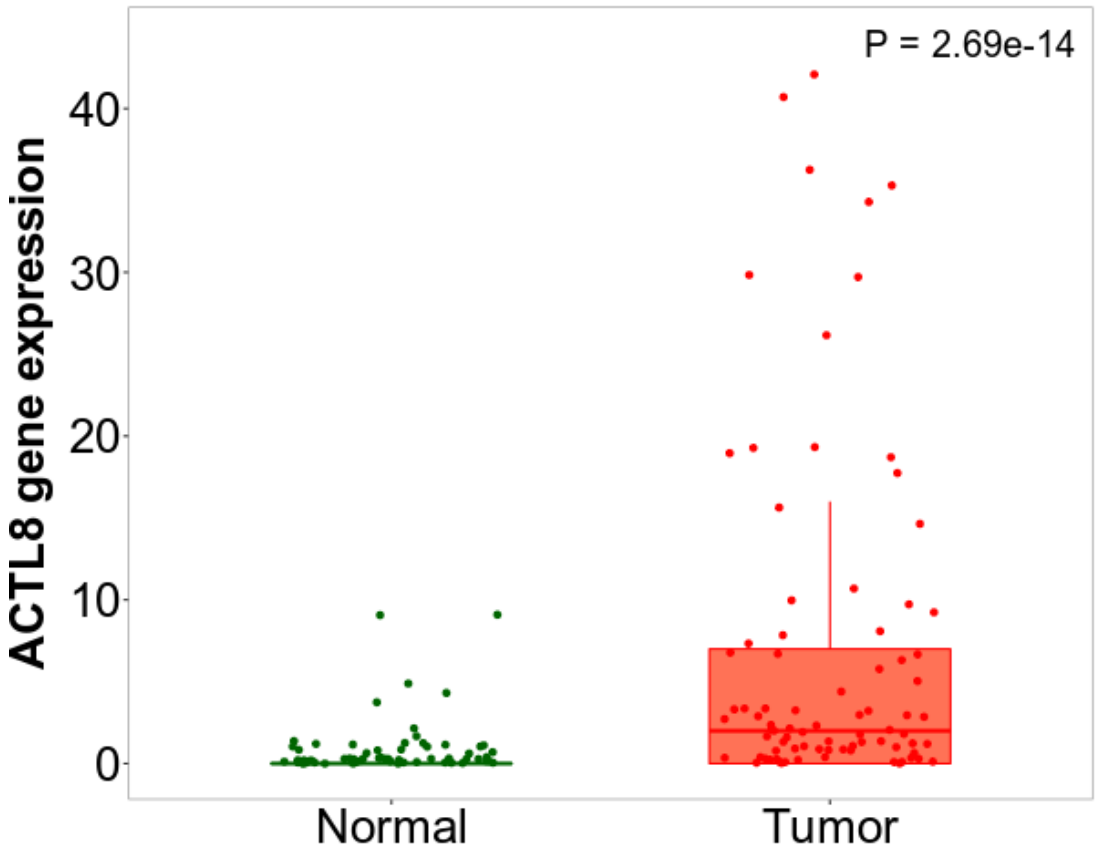

Figure 5.7: *ACTL8* expression in paired normal and tumour adjacent tissues in breast invasive carcinoma patients

ACTL8 gene expression comparison of paired tumour and adjacent normal breast tissue samples from breast invasive carcinoma (BIC) patients (*n* = 112) using RNA-seq based data from The Cancer Genome Atlas (TCGA), Therapeutically Applicable Research to Generate Effective Treatments (TARGET), and The Genotype-Tissue Expression (GTEx) repositories. Boxplot was generated using the online analysis platform TNMplot.com. Statistical analysis was performed using a paired Wilcoxon test. Red dots represent expression data from patient breast tumour samples and green dots represent expression data from non-paired normal breast tissue samples.

5.3.4 Evaluation of *ACTL8* in relation to hypoxia

In chapter 4 the impact of hypoxia on the expression levels of transcripts associated with enriched functions identified by the RNA-seq analysis was assessed. Similarly, *ACTL8* transcripts were measured in static and flow spheroids kept in hypoxia for 24h to determine whether an upregulation of *ACTL8* in flow would still occur in hypoxia. The results shown in Figure 5.8 demonstrate that *ACTL8* was not significantly different between static and flow spheroids when they were kept in hypoxia. However, the data represent only *n*=2 replicates, and both saw an increase in *ACTL8* transcripts in flow compared to static. Further repeats are required to determine if this pattern is statistically significant.

Next, cBioPortal was used for *in silico* analysis of the relationship between *ACTL8* and established hypoxia metagenes expression in a patient dataset. The TCGA, PanCancer Atlas Breast Invasive Carcinoma dataset was used to map *ACTL8* mRNA expression in patients against a hypoxia score. The hypoxia score was drawn from peer-reviewed articles on hypoxia gene expression signatures, referred to as hypoxia metagenes. Two different hypoxia scores were used to assess the relationship of *ACTL8* expression with hypoxia. The first was the Winter hypoxia score, a hypoxia metagene signature derived from head and neck cancer (Winter et al., 2007). The correlation between *ACTL8* and the Winter hypoxia score is shown in Figure 5.9 where mRNA expression of the gene was plotted against the hypoxia metagene score. The $R^2 = 0.14$ and was highly significant (*p*-value = 4.57×10^{-34}). The next hypoxia score used was the Buffa hypoxia score (Buffa et al., 2010). Importantly, this hypoxia metagene signature was derived from multiple cancer types rather than just head and neck cancer. Figure 5.10 shows that *ACTL8* expression in patients was again positively correlated with the hypoxia score ($R^2 = 0.23$) and this was highly significant (Pearson *p*-value = 1.3×10^{-63}).

Taken together, these results demonstrated that *ACTL8* expression in patients was positively correlated with expression of hypoxia metagenes.

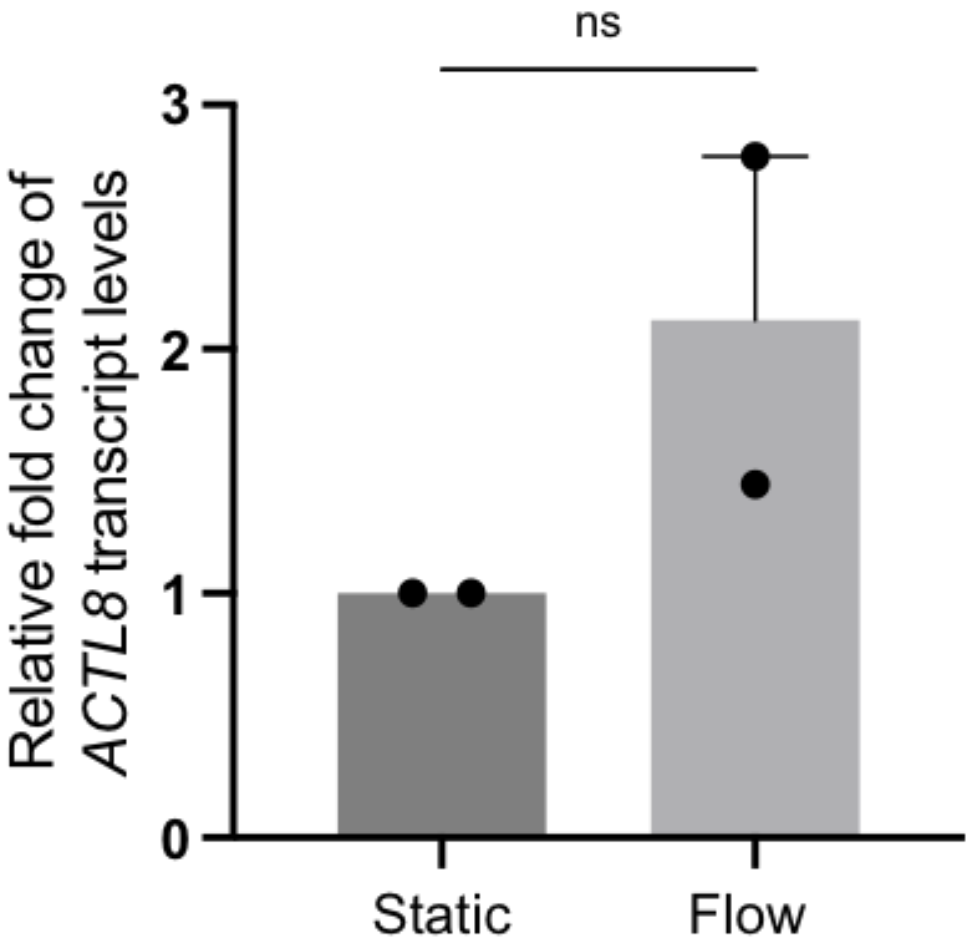

Figure 5.8: *ACTL8* expression levels in static and flow spheroids in hypoxia

MCF7 spheroids were formed from 9.0 x 10^4 cells and kept in either static or flow conditions for 24h at 1% O_2. Total RNA was extracted from x 3 spheroids at the end of experiments and used for qPCR. The housekeeping gene used was *B2M*. Data represent the mean of *n*=2 experiments. Error bars represent mean +/- SEM. Statistical significance was determined by paired student's t-tests; ns = not significant.

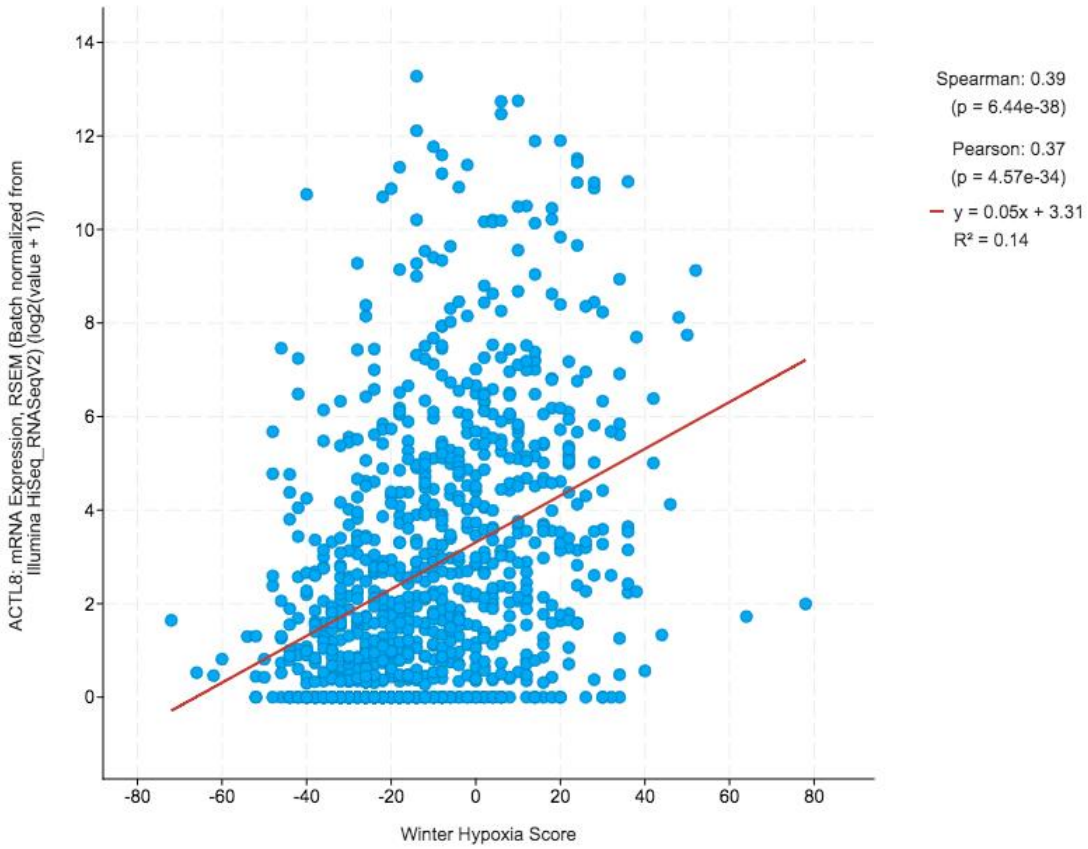

Figure 5.9: *ACTL8* expression in relation to Winter hypoxia score

ACTL8 expression in patients (*n* = 994) from the TCGA PanCancer Atlas Breast Invasive Carcinoma study is plotted on the y-axis against the Winter hypoxia score. The hypoxia score is representative of a hypoxia metagene signature. The expression data was log2 normalised; Pearson *p*-value = 4.57 x 10^{-34}. R^2 represents line of regression correlation value and is equal to 0.14.

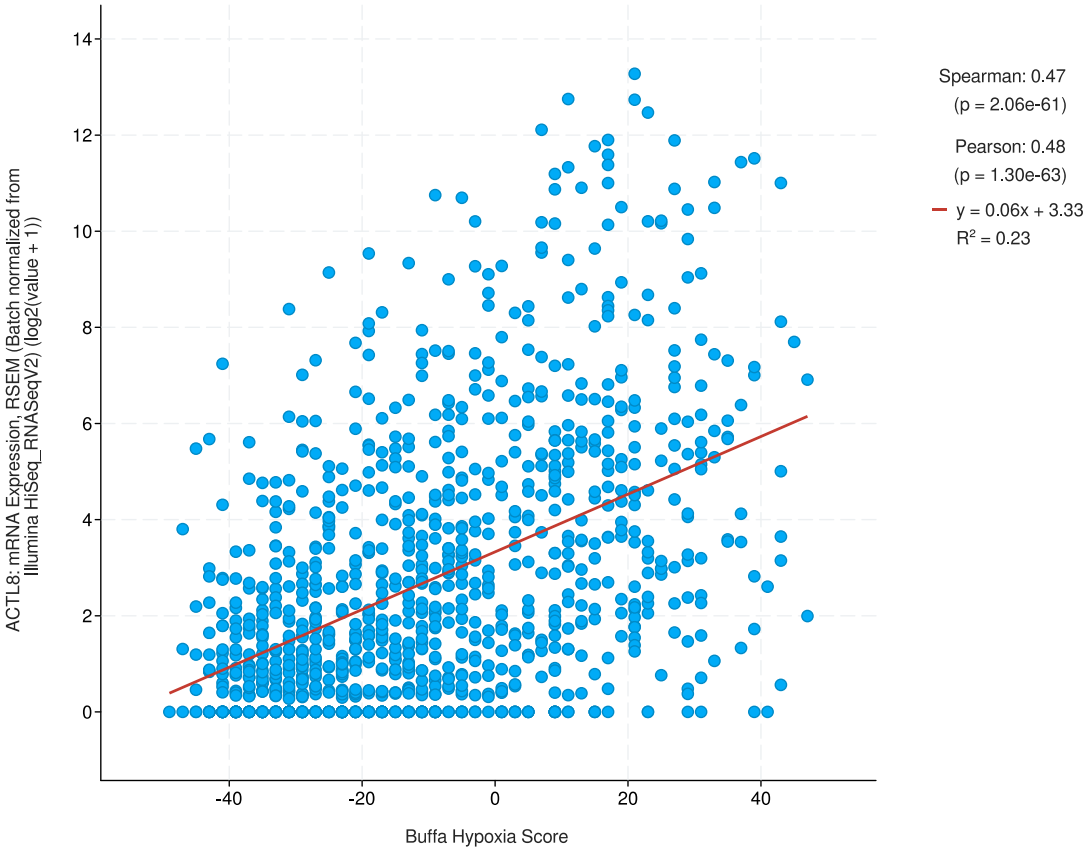

Figure 5.10: *ACTL8* expression in relation to Buffa hypoxia score

ACTL8 expression in patients (*n* = 994) from the TCGA PanCancer Atlas Breast Invasive Carcinoma study is plotted on the y-axis against the Buffa hypoxia score. The hypoxia score is representative of a hypoxia metagene signature. The expression data was log2 normalised; Pearson *p*-value = 1.3×10^{-63}. R^2 represents line of regression correlation value and is equal to 0.23.

5.3.5 Evaluation of *ACTL8* expression levels on breast cancer patient survival

The KMplotter online tool was used next to assess the potential prognostic value of *ACTL8*. As outlined in the introductory portion of this chapter, a prognostic biomarker is one which is useful for giving an indication of disease progression or the likelihood of a clinical event, regardless of treatment. In this case, KMplotter was used to assess the likelihood of survival as the "clinical event" in question. The tool has breast cancer patient datasets derived from both gene chip array-based data and RNA-seq patient data. Gene chip microarray data was examined first and the results are outlined below in Table 5.2. In the analysis, patients were split by median and the analysis was not restricted by subtype or selected sub-cohorts. The samples sizes were indicated by n^{high} and n_{low} where n^{high} corresponds to patients expressing high *ACTL8* levels and n_{low} corresponds to patients expressing low levels of the gene. The total *n* can be determined by adding high and low. This analysis allowed for examination of 3 classifications of survival: relapse-free survival (RFS), overall survival (OS), and distant metastases-free survival (DMFS). RFS relates to the likelihood of a primary tumour reappearing post-treatment, usually referred to as "relapse". OS relates to survival from time of treatment to death, regardless of whether the disease reoccurred or not. And finally, DMFS focuses on the probability that a patient will display distant metastases during progression of the disease. DMFS is particularly useful for indicating the aggressiveness of a tumour, as more aggressive tumours are more likely to metastasise. As shown in the summary of results, DMFS was the only type of survival to be significantly correlated to high *ACTL8* expression and had the highest HR value of the 3 survival outcomes. HR values indicate the prognosis value -- a high *ACTL8* transcript level where HR > 1 signifies high expression of the gene is linked to worse patient prognosis. Conversely, HR < 1 indicates that high expression of the gene of interest is linked to a good patient prognosis (Spruance et al., 2004). The KM plots for this analysis are shown in Figure 5.11. The data depicted in Figure 5.11 demonstrated that after approximately 200 months the number of cases in RFS, OS, and DMFS all dropped to < 20 patients, indicating the low number of surviving patients beyond that time point.

Table 5.2: KMplotter analysis outcomes of mRNA gene chip patient dataset

	p-value	**HR**	**n^{high}**	**n_{low}**
Relapse-free survival	0.18	1.07	2425	2504
Overall survival	0.73	1.03	920	959
DMFS	8.4×10^{-6}	1.42	1374	1391

HR: hazard ratio; n^{high}: number of patients expressing high *ACTL8*; n_{low}: number of patients expressing low *ACTL8*; green: high *ACTL8* indicates good prognosis; red: high *ACTL8* indicates poor prognosis; grey cells: significant *p*-value ($p < 0.05$). The median was used to split patient cohorts into high and low groups.

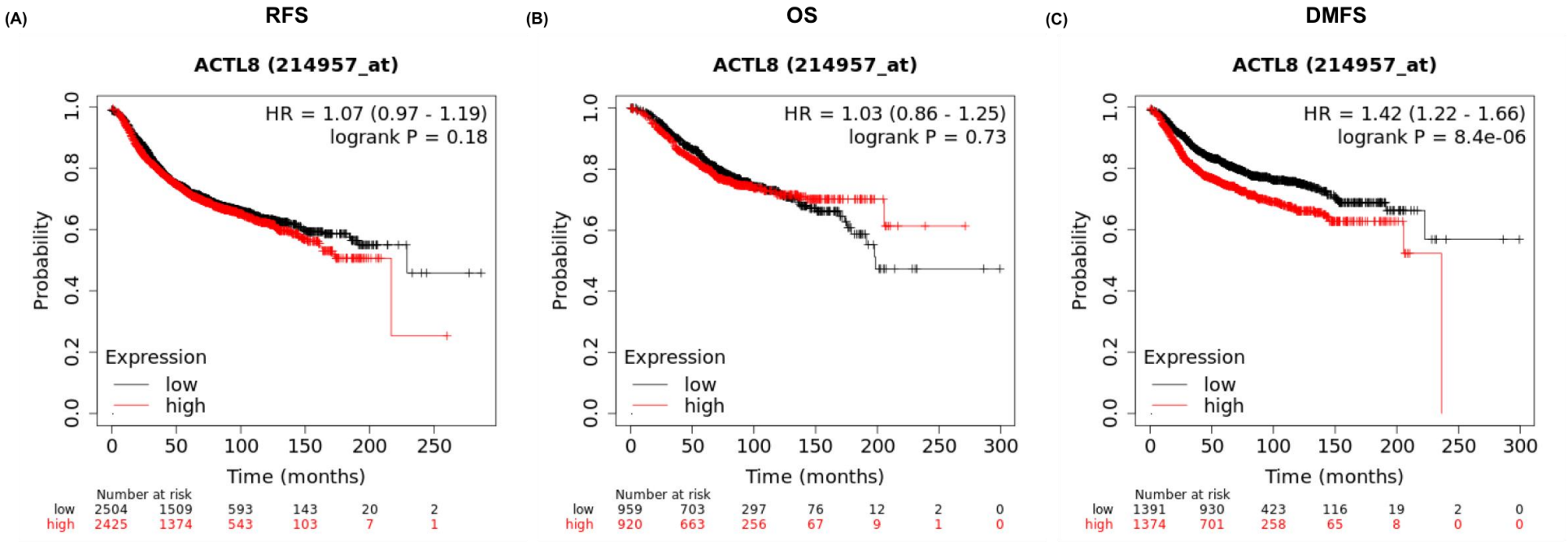

Figure 5.11: KMplots produced from gene chip microarray breast cancer patient data analysis

KMplotter was used to analyse expression levels of *ACTL8* in gene chip array-based patient data and correlate it to 3 survival outcomes: relapse-free survival (RFS) *n* = 4929 (A); overall survival (OS) *n* = 1879 (B), and distant metastases-free survival (DMFS) *n* =2765 (C). Patients were split by median and no other patient selection thresholds were applied. HR = hazard ratio where HR > 1 correlates to poor patient prognosis with high expression of *ACTL8* and HR < 1 correlates to good patient prognosis with high *ACTL8* expression.

Next, breast cancer patient RNA-seq data was used for KMplotter analysis and in this case, the analysis only permitted overall surivival outcomes to be measured. However, the analysis was performed a total of 4 times to examine each breast cancer subtype cohort individually. The summary of these findings is shown in Table 5.3 below. Luminal A breast cancer patients were the only cohort to see both a positive HR value and a significant *p*-value ($p = 0.033$). The KMplot associated with the luminal A subtype analysis is also shown in Figure 5.12. The n^{high} cohort in this analysis consisted of 37 patients whereas the n_{low} cohort was nearly 40 times as large with 1467 patients. This demonstrated the low proportion of patients with the luminal A subtype and a high expression of *ACTL8.* Despite this, the high *ACTL8*-expressing cohort of Luminal A patients saw a hazard ratio correlated to poor overall survival outcomes.

Table 5.3: KMplotter analysis outcomes of mRNA-seq patient dataset in breast cancer subtype cohorts

	p-value	**HR**	**n^{high}**	**n_{low}**
Basal	0.49	0.67	19	290
Luminal A	0.033	2.39	37	1467
Luminal B	0.99	1.01	25	643
HER2 type	0.13	0	13	282

HR: hazard ratio; n^{high}: number of patients expressing high *ACTL8*; n_{low}: number of patients expressing low *ACTL8*; green: high *ACTL8* indicates good prognosis; red: high *ACTL8* indicates poor prognosis; grey cells: significant *p*-value ($p < 0.05$).

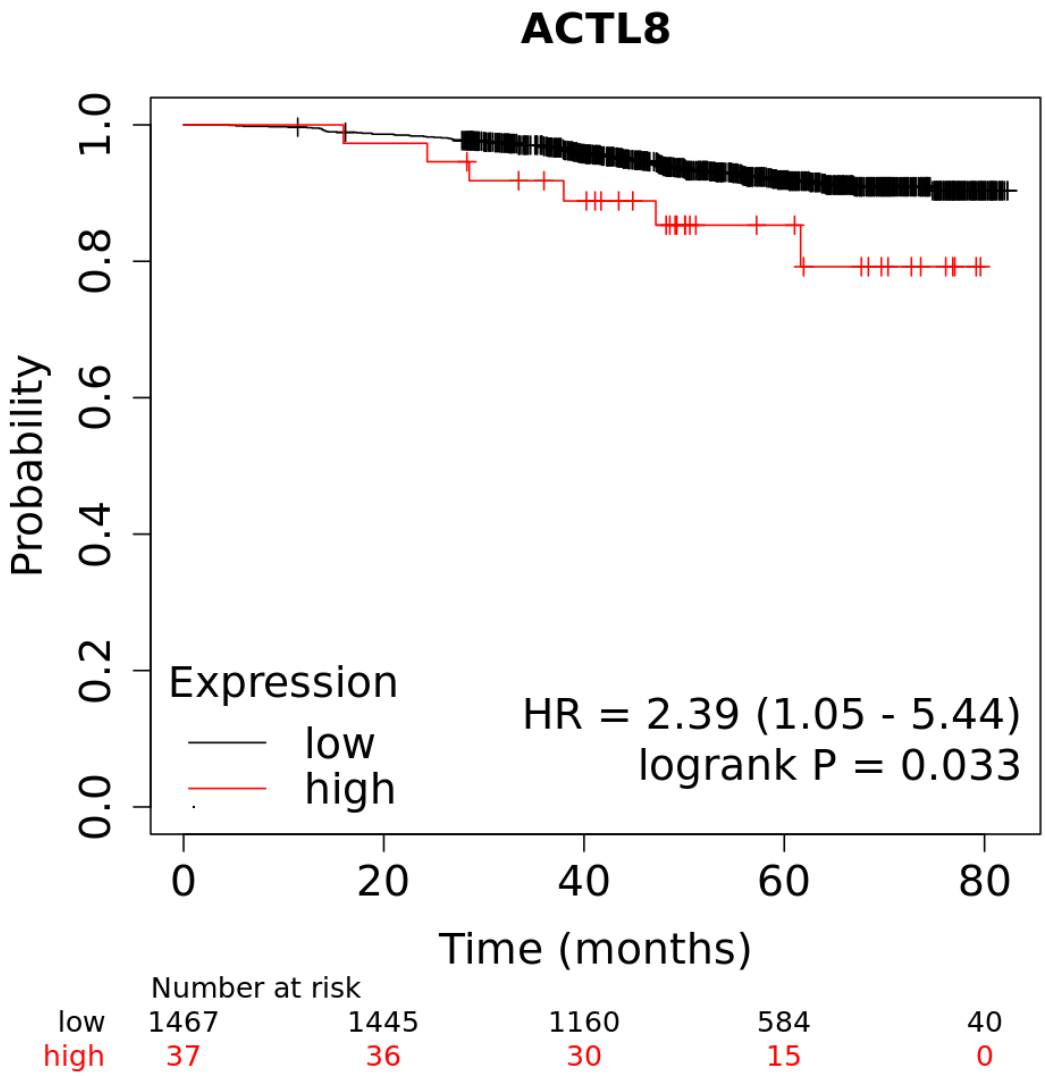

Figure 5.12: Overall survival in luminal A breast cancer patients with high expression of *ACTL8*

KMplotter was used to analyse expression levels of *ACTL8* in RNA-seq-based patient data and correlate it to overall survival in breast cancer subtypes. Above, the correlation between high ACTL8 expression in luminal A type breast cancer patients and overall survival is shown. Patients were split by median and no patient selection thresholds were applied other than subtype = luminal A. HR = hazard ratio where HR > 1 correlates to poor patient prognosis with high expression of *ACTL8* and HR < 1 correlates to good patient prognosis with high *ACTL8* expression. *n* = 1504.

5.3.6 ROC analysis of *ACTL8* as a predictive biomarker

The next analysis used to assess *ACTL8* as a potential biomarker of IFF in cancer was ROCplotter. This is a tool for measuring whether a biomarker is predictive, meaning it correlates to patient responses to therapy which in this case was chemotherapy for the treatment of breast cancer. For the analysis "any chemotherapy" was selected for the analysis. No other filters were applied. This analysed RFS at 5 years for breast cancer patients who had received any type of chemotherapy. The result of the analysis is shown in Figure 5.13.. The key measure computed by the ROC plot is area under the curve or AUC. This is a measure of the prognostic power of the gene of interest. The AUC computed was 0.633 and this was highly significant with a *p*-value of 8.2×10^{-8}. Additionally, Mann-Whitney testing on responder vs. non-responder expression levels yielded a *p*-value of 5.6×10^{-7} and an average 2.4-fold increased level of *ACTL8* expression in non-responder patients. According to ROCplotter, the range of 0.6 – 0.7 AUC is indicative of a "cancer biomarker with potential clinical utility" which is the category that the computed AUC value for *ACTL8* aligned with.

5.3.7 Pan cancer analysis of *ACTL8* patient expression levels

The final analysis used to examine the viability of *ACTL8* as a biomarker of IFF was a pan-cancer analysis of *ACTL8* expression in patients with various forms of cancer. OS and RFS were assessed using KMplotter. A hazard ratio greater than 1 linked *ACTL8* expression to either poor OS or RFS in 15 types of cancer. Of those 15, 3 cancers (breast cancer, kidney renal papillary cell carcinoma, and uterine corpus endometrial carcinoma) had HR's greater than 1 for both OS and RFS and were statistically significantly related to the expression of *ACTL8*. The results of the pan-cancer analysis are summarised in Table 5.4.

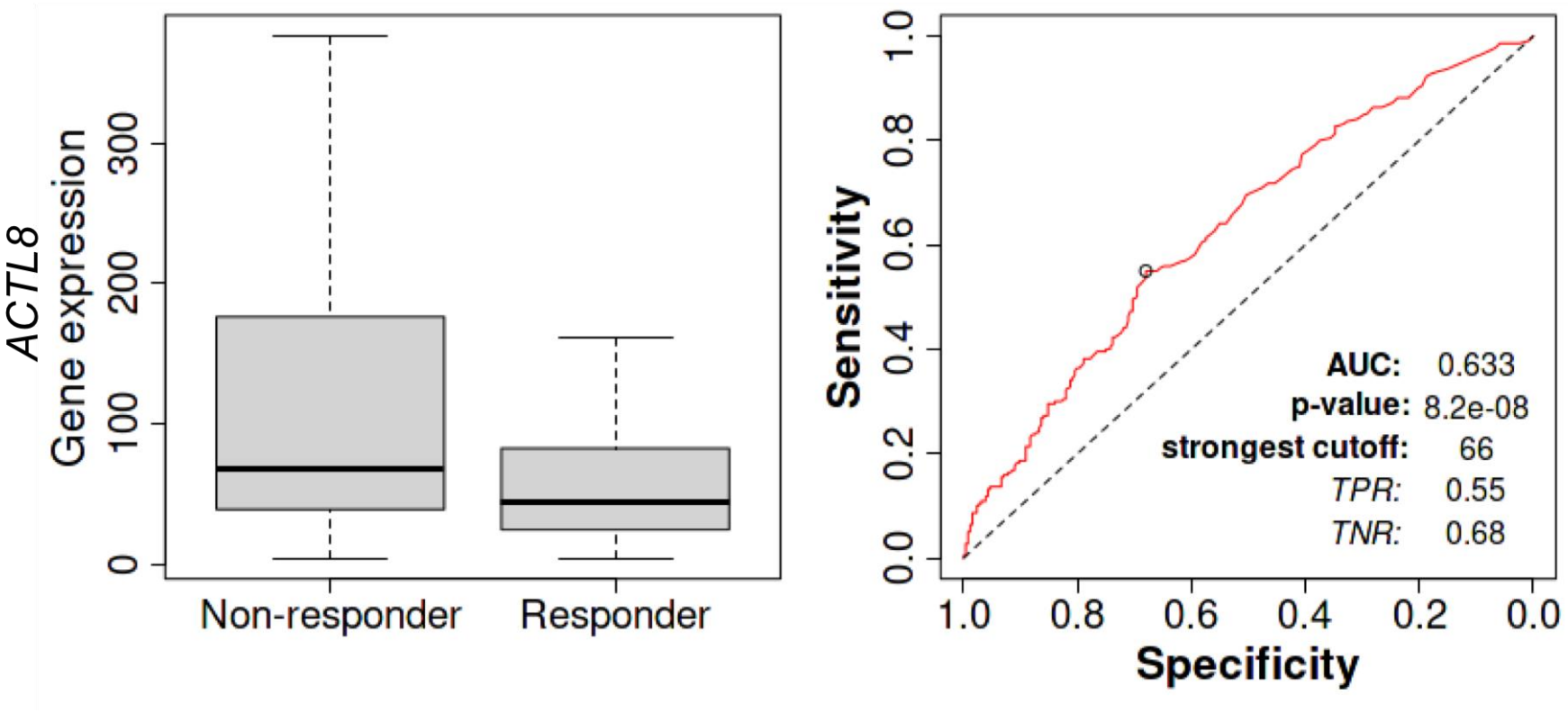

Figure 5.13 Receiver operating characteristic (ROC) plot for *ACTL8*

ROC plotter was used to analyse breast cancer patient *ACTL8* gene expression and responsiveness to any kind of chemotherapeutic treatment to determine predictive biomarker potential. On the left, patient responder and non-responder cohorts and their *ACTL8* gene expression levels are shown with *ACTL8* relative expression mapped on the *y*-axis. Total *n*= 426; non-responders = 197; responders = 229. ROC p-value = 8.2 x 10^{-8} and Mann-Whitney test p-value = 5.6 x 10^{-7}. Computed AUC = 0.633.

Table 5.4 Summary of pan-cancer analysis of *ACTL8* patient expression levels

	Overall survival (OS)				Relapse-free survival (RFS)			
Cancer type	*p*-value	HR	n^{high}	n_{low}	*p*-value	HR	n^{high}	n_{low}
Bladder carcinoma	0.33	1.16	166	238	0.91	0.96	79	108
Breast cancer	$6.1x10^{-3}$	1.57	509	580	0.032	1.6	446	501
Cervical squamous cell carcinoma	0.21	1.36	146	158	0.58	1.24	79	95
Oesophageal adenocarcinoma	0.97	1.01	40	40	0.35	0.35	9	10
Oesophageal squamous cell carcinoma	0.29	0.65	38	43	0.8	1.13	27	27
Head-neck squamous cell carcinoma	0.014	1.4	235	264	0.23	0.61	49	75
Kidney renal clear cell carcinoma	$7.5x10^{-8}$	2.27	134	396	0.67	0.72	22	95
Kidney renal papillary cell carcinoma	$1.6x10^{-4}$	3.02	87	200	$3.7x10^{-4}$	3.93	44	139
Liver hepatocellular carcinoma	0.0072	1.6	148	222	0.89	0.98	126	190
Lung adenocarcinoma	0.22	1.21	157	347	0.69	0.91	88	212
Lung squamous cell carcinoma	0.18	0.83	236	259	0.33	0.78	143	157
Ovarian cancer	0.96	0.99	185	188	0.061	0.72	86	91
Pancreatic ductal adenocarcinoma	0.54	0.85	40	137	0.41	0.66	17	52
Pheochromocytoma and paraganglioma	0.51	0.49	56	122	0.03	8.45	50	109
Rectum adenocarcinoma	0.35	0.69	82	83	0.86	0.87	23	24
Sarcoma	0.2	1.32	82	177	0.52	1.19	48	104
Stomach adenocarcinoma	0.45	1.13	179	192	0.37	1.34	101	114
Testicular germ cell tumour	0.071	0 - Inf	65	69	0.45	1.34	49	56
Thymoma	0.33	0.51	55	63	Sample number too low for meaningful analysis			
Thyroid carcinoma	0.52	0 - Inf	19	483	0.13	2.87	12	341
Uterine corpus endometrial carcinoma	$4.3x10^{-5}$	2.42	261	281	0.0012	2.44	199	223

HR: hazard ratio; n^{high}: number of patients expressing high *ACTL8*; n_{low}: number of patients expressing low *ACTL8*; green: high *ACTL8* indicates good prognosis; red: high *ACTL8* indicates poor prognosis; grey cells: significant *p*-value ($p < 0.05$).

5.4 Discussion

The aim of this chapter was to identify potential biomarkers of IFF in cancer and to assess the potential clinical relevance of any identified candidates. 4 candidate genes were identified from the RNA-seq results using a set of criteria intended to aid in selecting a good biomarker. Of those 4 genes, only one was deemed a viable candidate when analysed further by qPCR at both 24h and 72h. The candidate gene, *ACTL8*, was then evaluated for potential clinical relevance using online database tools and was found to be:

- expressed more highly in breast tumour samples than in normal tissues.
- notably upregulated in flow vs static samples in hypoxia although this was not statistically significant.
- positively correlated to expression of hypoxia metagenes.
- a potential prognostic biomarker of breast cancer DMFS and OS of luminal A breast cancer patients.
- a potential predictive biomarker of RFS at 5 years post chemotherapy treatment in breast cancer patients.

5.4.1 *ACTL8* was identified as a gene of interest for a potential biomarker of IFF

qPCR analysis was used to assess transcript levels of 4 "genes of interest" that were identified from the RNA-seq results as potential biomarker candidates. These represented candidate genes that were altered as a result of the IFF environment on-chip. Only *ACTL8* had significantly different expression in flow vs static samples, so it was chosen as the best candidate to continue exploring for potential clinical relevance. However, these results don't necessarily indicate that the other 3 candidates should be ignored. Due to the high variation between replicates in these experiments it would be beneficial to conduct repeats to better identify patterns of expression in more powerful sample sizes.

Additionally, the mechanism of detection in qPCR is via cycle threshold of signal detection, and given that the levels of mRNA for transcripts such as *ABCA8* were so low in the RNA-seq flow samples that no read counts were detected, it is possible that qPCR was not sensitive enough to detect such low expression levels.

ACTL8 transcripts were also compared in static vs flow spheroids kept in hypoxia to assess whether hypoxia would regulate the change in *ACTL8* identified in flow. Hypoxia is also especially relevant in the clinical context of breast tumours as breast carcinomas are commonly hypoxic (Williams et al., 2001). The results showed no significant difference between static and flow

conditions, but an observed trend of increase was noted in flow replicates. Online database analysis in cBioPortal found expression of *ACTL8* was positively correlated with hypoxia metagene expression. Therefore, in hypoxic conditions hypoxia metagenes upstream of *ACTL8* may have had an effect on transcript levels, but this needs to be investigated further.

ACTL8 was also found to be expressed more in tumour tissues than normal tissues using TNMplot to compare gene expression levels in breast cancer patient datasets. In fact, it was more highly expressed in tumour samples in unpaired sets of tumour and normal tissues as well as paired samples taken from breast tumours and adjacent normal tissues. These results suggested that *ACTL8* was worth exploring further as a potential biomarker of IFF in cancer which could have clinical relevance.

5.4.2 *ACTL8* demonstrated potential as both a prognostic and predictive biomarker

In silico analyses using the online tool KMplotter revealed *ACTL8* to be a prognostic indicator of DMFS in all breast cancer patient types and of OS for luminal A type patients. These results were particularly interesting, firstly for the fact that DMFS is linked to tumour aggressiveness. The findings suggested that increased expression of *ACTL8* in breast cancer patients could be linked to the occurrence of distant metastases and thus poor prognosis. This is important given that metastasis is responsible for the majority of cancer deaths, so knowing more about gene expression profiles linked to poor DMFS outcomes could aid clinicians in anticipating patient prognoses. Secondly, luminal A breast cancer (which is ER+/PR-/HER2-) tends to grow more slowly than other cancers and tends to have a *good* prognosis. This is largely due to advancements in treatments which are able to capitalise on the ER+ hormone receptor expression status for hormonal therapies. Luminal A breast cancers are also thought to be less proliferative than other breast cancer subtypes, which contrasts with finding that DMFS (aggressive, metastatic cancer) was linked to *ACTL8* expression. These findings would benefit from further exploration, perhaps by using more of the patient cohort filters available to elucidate the relationship between *ACTL8* expression and patient outcomes.

The predictive biomarker capacity of ACTL8 was also assessed using ROCplot. This analysis generated an AUC value 0f 0.63 which is widely accepted as good strength for predictive capacity (Fekete & Gyorffy, 2019). *ACTL8* expression was also shown to be an average of 2.4-fold higher in breast cancer patients who were classed as non-responders (RFS < 5 years) relative to responders (RFS > 5 years) and this was statistically significant. These results serve as compelling evidence to continue to investigate *ACTL8* as a biomarker of IFF in cancer.

5.4.3 Potential for investigations in other cancer types

Pan cancer analysis using KMplotter revealed that there are other tumour types where *ACTL8* expression was linked to poor prognosis. These included head neck squamous cell carcinoma, kidney renal clear cell carcinoma, kidney renal papillary cell carcinoma, liver hepatocellular carcinoma, and uterine corpus endometrial cancer. The results of the pan-cancer analysis are summarised in Table 5.4. The tumour types identified by this analysis could serve as interesting cancers to investigate the findings presented in this chapter further.

5.5 Chapter conclusion

ACTL8 was identified as a possible candidate for marking increased ISF flow by passing the series of screenings the gene candidates went through. These included meeting selection criteria from the RNA-seq DEG list, validation of expression levels in static and flow spheroids by qPCR, and evaluation of clinical relevance using publicly available patient datasets. Results from *in silico* analyses were especially compelling for the potential value of ACTL8 as both a prognostic and predictive biomarker. More work is needed to further elucidate the mechanisms by which ACTL8 is linked to the identified patient outcomes.

Chapter 6 General Discussion

6.1 Summary of work presented in previous chapters

After long being overlooked for interest in fluids like blood and lymph, interstitial fluid has started to gain recognition as a key contributor in tumour pathology. Despite this, the mechanisms by which interstitial fluid in the TME contributes to tumour progression are still poorly understood. Where studies have started to examine the relationship more closely, models have been used which don't fully replicate the environment. Whilst acknowledging that a "perfect" model may not be possible to make, we sought to develop a microfluidic spheroid on-chip model which could help to characterise the impacts of interstitial flow on the TME and more specifically, on the biology of cells in the TME. Therefore, the objective of this thesis was to provide a better understanding of the role interstitial flow might have in tumour progression. Thus, each of the chapters focused on accomplishing an aspect of this goal. In **chapter 3**, a spheroid-on-chip microfluidic system was refined from a previous design to replicate interstitial flow in a reliable and reproducible manner, creating a framework for the study of spheroids in the interstitial flow environment. In **chapter 4**, the flow cell 2 system designed in chapter 3 was used to investigate the effects of interstitial flow on cancer cell biology in the TME. Finally, in **chapter 5**, a potential biomarker of interstitial flow was identified and evaluated for its clinical relevance.

6.1.1 Replicating interstitial flow *in vitro* using the flow cell 2 system

The velocity of interstitial fluid *in vivo* is generally accepted as being in the range of 1×10^{-4} – 10 mm s^{-1} (Wiig & Swartz, 2012; Wagner & Wiig, 2015) The velocity for the flow rate used in our system was approximately ~0.05 mm s^{-1}, but this was varied throughout the different components of the system (channels, microwell, tubing) (refer to section 3.2.2). Overall, these were in keeping within the ranges of reported IFF *in vivo* and lower than velocities recorded in the vascular system, often used for studies with endothelial cells in flow (Liu et al., 2015). Our system modelled fluid flow by using a syringe pump to continuously perfuse media over spheroids in the system. Media travelled through a single channel to a spheroid microwell and out through a continuation of the single channel where it could then be collected. The use of continuously perfused media in microfluidic systems and even in cell culture systems is not novel. Additionally, the use of spheroids in microfluidic devices has been used in many applications. However, we identified a gap where continuous flow and 3D spheroids had not been unified extensively to understand how interstitial flow impacts cancer cells. More specifically, transcriptome-wide analyses had not been conducted in cancer cells exposed to IFF to the best of our knowledge.

Studies that have focused on interstitial flow impact on cancer cells have largely been conducted using single cell suspensions in 3D environments. For example, suspending cells in hydrogels (i.e.

Matrigel, collagen, fibronectin) is considered a form of 3D cell culture because cells are not in monolayers and while these methods are an improvement on 2D cells in monolayers on plastic, they still fail to put cells in 3D formations more closely representative of interactions *in vivo*. Indeed, most studies using 3D single cell suspension techniques reported upregulation of EMT or increases in invasion as a result of fluid flow (Shieh et al., 2011; Shah et al., 2015; Tchafa et al., 2015). One study conducted by Rizvi and colleagues did use 3D aggregates (ovarian cancer nodules) in flow and also reported flow induced EMT compared to non-flow (Rizvi et al., 2013). Importantly, the non-flow condition used was a suspension of single cells in 3D matrices. Therefore, comparisons were drawn between 3D single cell suspensions in a static environment and 3D aggregates in flow, rather than 3D aggregates in static (non-flow) and flow conditions.

In contrast, the findings reported in this project did not see the same effect. To our knowledge, one of the only other reports coinciding with our findings is from work reported by Azimi and colleagues (Azimi et al., 2020). Their group used 3D "tumouroids" in which cells were aggregated into compact masses. They induced fluid flow and pressure in a microfluidic system and measured the effects on cells in the tumouroids. Importantly, they did not see overall increases in EMT markers either. In fact, they reported decreased expression of vimentin in MDA-MB-231 tumouroids grown in the flow and pressure environment as well as no increase in snail compared to static. Notably, they did observe a significant increase in *MT1-MMP* transcript, which contrasts with our results. However, some key differences in their experimental design such as the use of collagen rather than Matrigel and the induction of pressure may have been the reason. Regardless, the summary findings of our results and their study warrant further investigation into the impacts of flow on cell biology.

Our study specifically used 3D spheroids in Matrigel in an attempt to better reproduce the 3D nature of the TME in an *in vitro* model. Given that our findings aligned closely with those of Azimi and colleagues and their use of 3D tumouroids, these results may suggest that 3D interactions are an important regulator in the response of cells to interstitial flow. This would not be dissimilar to other reports citing 3D spheroids as being more resistant to chemotherapeutic agents (Chambers et al., 2014). There is ample evidence of cancer cells being less sensitive to drugs when formed as 3D spheroids than when they are grown in 2D (Imamura et al., 2015; Nunes et al., 2019b). Therefore, it may be the case that 3D aggregation is similarly influential in cellular responses to interstitial flow.

Another feature of our model is that it is low throughput. In many cases, where continuous perfusion has been incorporated into the experimental design of studies it was for the utility of high throughput needs (Lanz et al., 2017; Eilenberger et al., 2021). Whereas other studies have

built continuous perfusion in as a design feature for producing high throughput outputs, we sought to identify the effects that flow itself could be having. This necessitated the use of a simplistic, lower-throughput model to insulate the effects of flow from other extraneous factors for flow impacts to be measured. High throughput approaches are useful for running numerous concurrent tests at a time, but our model provided other advantages such as clear imaging of spheroids in IFF, direct comparisons between static and flow conditions, and ability to collect cellular materials such as RNA and protein that could be used for downstream analyses.

Another notable implication of replicating interstitial flow *in vitro* is the possibility of its use in reducing the need for animal models. The UK's National Centre for Replacement, Refinement, and Reduction of Animals in Research (NC3Rs) is one of the leading organisations globally working to develop alternative technologies and platforms, such as microfluidics, to replace animal models. The limited predictability of animal model outcomes is increasingly recognised, highlighting the need for alternative methods of research (Dehne et al., 2017; Meijer et al., 2017). Whilst our system does not represent a method of fully replicating human physiology or even that of an animal, it could serve a purpose in answering specific questions about the TME and flow that would require testing in animals. Alternatively, there is the potential for the use of patient-derived spheroids to be cultured in the flow cell 2 system which would also bypass the need for the use of animal models.

The use of patient-derived materials would introduce a variety of investigative opportunities for the flow cell 2 system, for example determining personalised responses of patient tumours to IFF to better direct drug delivery to a patient's tumour. Indeed, similar approaches have already been undertaken for investigations in lung cancer and glioblastoma multiforme responses to treatment for designing patient therapeutics. Akay and colleagues recently developed a brain cancer chip for the purpose of assessing tumour cell drug response before drug treatments were administered to patients, with the goal of optimising chemotherapeutic cocktails (2018). Another study used a perfused microfluidic platform to culture non-small cell lung adenocarcinoma spheroids derived from patient samples as a chemosensitivity assay (Ruppen et al., 2014; Ruppen et al., 2015). Models such as these demonstrate the potential utility of flow on-chip systems for clinical purposes.

6.1.2 Impacts of interstitial flow on cancer cell biology

Interstitial fluid is present in normal tissues and is recognised for its role in replenishing tissue nutrients and oxygen, as well as removing waste and metabolites. In tumours, abnormal, leaky vasculature paired with altered tissue structures result in poor drainage and thus an increase in the amount of interstitial fluid present (Munson & Shieh, 2014). The role of increased interstitial

fluid present in the TME and the fluid flow associated with it is poorly understood, especially regarding the impacts flow may have on cancer progression.

As described in the previous section, some studies have started to investigate the relationship between flow and cancer cells and reported correlations between fluid flow and EMT, invasion, and overall metastatic potential. However, we did not observe such changes using our flow cell 2 system with 3D spheroids exposed to flow for up to 72h. We therefore decided to take use a broader approach to examine potential changes being caused by flow, opting to analyse the whole transcriptomes of spheroids exposed to either static or flow conditions using RNA-seq. This analysis found significant differential expression of genes between the static and flow conditions. Pathway enrichment analyses of the resulting dataset highlighted cell cycle, DNA replication/repair, and DNA damage response pathways as signalling pathways that were transcriptionally upregulated in flow (Chapter 4). Increase in transcripts associated with DNA replication and repair were confirmed by qPCR analysis and showed similar trends at a longer timepoint of 72h. Analysis of protein expression levels were not significantly conclusive as to whether flow was impacting protein expression, however, notable trends of change were observed. For example, HIF-1α appeared to be downregulated in flow and a downstream target of HIF, HK2, appeared to be downregulated as well. It is possible that longer duration experiments conducted in flow would allow transcriptional changes detected at the timepoints used here to be detected as protein expression changes. Additionally, while some studies have started to examine not only transcriptional or protein expression changes caused by flow but also phenotypic changes, there is still limited understanding of this (Piotrowski-Daspit et al., 2016).

The studies cited previously where 3D single cell cultures were used with flow exposure reported increases in invasion of cells in flow as a phenotypic change (Shieh et al., 2011; Shah et al., 2015; Tchafa et al., 2015). However, as noted before, the 3D spheroid structures may be a key to how cells respond to flow. Thus, experiments examining phenotypic changes in spheroids exposed to flow could help bridge the gap in understanding the scope of interstitial flow impact in the TME. Piotrowski-Daspit and colleagues did examine an EMT invasive phenotype and reported increases in collective invasion using an engineered 3D model of breast tumours exposed to what they described as IF pressure induced flow (Piotrowski-Daspit et al., 2016). However, their study did not cite the use of continuous perfusion or flow anywhere. Rather, pressure was produced in a microfluidic system, resulting in fluid flow. In this context, there was more focus on pressure and importantly, there was not continuous replenishment of media as there is with a perfusion system. These findings combined with those of Azimi and colleagues suggest that pressure and flow may result in different changes to cancer cells. Incorporating the findings from

the work presented in this thesis, these principles of flow and pressure induced changes can direct future investigations into untangling the specific impacts each has. Our system was not designed to measure or investigate flow but this could serve as an important area of interest for future work.

Phenotypes associated with increases in DNA replication and repair and cell cycle would be particularly interesting to examine further, given the enrichment of these pathways identified in the RNA-seq dataset. Cell cycle genes are often upregulated in both highly proliferative cancer cells and those under high replication stress (processes which often occur concurrently and thus see signalling pathway overlaps). Studies have identified that such a signature of gene expression - capturing both replication stress and proliferation – predicted response to ATR (ataxia telangiectasia mutated and Rad3-related) inhibitors with high accuracy (Cuzick et al., 2011; Lundberg et al., 2017; Jo et al., 2021). IFF appears to potentially induce a similar signature of expression, so exploring ATR inhibitor response phenotypes could be a valuable insight into better understanding how IFF impacts tumour cells. This type of future work would also coincide with further exploration of the pathway analysis conducted with IPA on the RNA-seq dataset which predicted activation of the DNA damage response pathway in flow. ATRs are kinases involved in DNA damage repair and ATR inhibitor drugs inhibit the growth of tumour cells by limiting their ability to repair damaged DNA. Given that IFF appears to induce activation of the DNA damage response pathway and subsequently sees predicted activation of ATR, studies examining whether IFF bolsters the ability of cancer cell spheroids to survive ATR inhibitor treatment would be extremely insightful. Understanding whether IFF effectively induces ATR inhibitor drug resistance could yield further insights on how IFF in tumours *in vivo* may contribute to the therapeutic resistant qualities already associated with interstitial fluid pressure (Ferretti et al., 2009).

Lastly, even though our system is not a high throughput design as usually used for drug toxicity screening studies, could use chemotherapeutics. They are also inducers of DNA damage and given that flow upregulated repair, it might be interesting to see if they are more resistant to effects of the drugs in flow.

6.1.3 *ACTL8* as a potential biomarker of IFF

The role of *ACTL8* as a potential biomarker of IFF in cancer was explored using a series of *in silico* analysis tools. A separate study on head and neck squamous cell carcinoma (HNSCC) previously identified *ACTL8* as a prognostic indicator for HNSCC (Li et al., 2019). Indeed, this evidence contributed to our selection of *ACTL8* as a candidate biomarker. Combining this with the findings of *ACTL8* pan-cancer atlas suggests that *ACTL8* may have a wider scope than breast cancer.

Investigating IFF effects using other cell lines and tumour types would benefit our understanding of *ACTL8*'s relationship with IFF specifically.

6.1.4 Caveats and limitations of this study

The TME is highly complex and notoriously difficult to replicate. However, in trying to incorporate too many components of the TME in a model at once there can be a risk of introducing too many variables to decisively draw conclusions of causation or even correlation. In theory, what our model may lack in complexity it compensates for in the simplistic and clear lens it provides for examining IFF effects. However, we acknowledge that the model does not reproduce all components of the TME so future work could incorporate the use of other cell types, alternative hydrogels, and more to build more TME *in vitro* architecture into the system.

Another caveat of the work presented here is that the order of cancer progression events early on is not well defined enough to give significant context to the findings presented here. That is, does ISF cause cancer progression, or is increased IFF caused by the formation of a tumour? Perhaps there is not a definitive answer at all. It may be a feedback loop where, as a tumour grows, over time the ECM will be deformed and become increasing dysregulated, causing changes to the fluid dynamics in the environment. The fluid dynamic changes could then contribute to progression of the tumour, and so on. A feedback system like this would not be new in cancer pathology; hypoxia and the induction of angiogenesis function in a similar manner (Henze & Acker, 2010; Muz et al., 2015).

We also acknowledge that we didn't assess other biomechanical cues such as pressure, only fluid flow. We could have focused more on shear stresses as well; however, at such a low flow velocity it was not our main focus and this could be incorporated into future work instead.

Finally, static spheroids kept in the different incubator environments were compared and saw a significant decrease in relative expression of *VEGFA* transcript in the spheroids kept in the flow incubator compared to the regular incubator (appendix 3). This was concerning as it indicated that just by introducing a change in incubator environment a significant difference in transcript expression could be induced in the spheroids. However, when flow spheroid transcripts were compared to transcripts of static spheroids kept in the flow incubator (simultaneously in the period that the flow spheroids were), there was a significant downregulation of *VEGFA* in flow. In fact, in the standard experimental setup where flow was compared to static spheroids kept in a cell culture incubator, the downregulated effect was most significant. We acknowledge that the effect of different incubators was shown to be significant in static spheroids and that this must be taken into account when considering other results produced using this system. However, given that the effect was replicated and even enhanced when comparing flow to static in

standard incubators, the results suggest that IFF did induce changes at transcript level that were significant and worth exploring further.

6.2 Future directions

The results reported in this project have demonstrated that interstitial fluid flow modifies the biology of cells a in 3D TME chip model. These findings have laid the foundation for a number of other future directions to be pursued with this work.

6.2.1 Co-culture spheroids

Tumours are comprised of heterogeneous populations of cells *in vivo*. It would be useful to generate heterogeneous co-culture spheroids incorporating cell types known to be found tumours. Examples could include fibroblasts, stromal cells, and immune cells. Studies have recognised the impact of heterogeneity on the biology of spheroids in the past, but few have used these spheroids in interstitial flow models. With a newfound understanding of the impacts of flow on the biology of cancer cells gained from this project, it would be interesting to investigate the impacts of incorporation of other cell types in the system as well.

The system presented here could also be used to house patient-derived spheroids. Work such as this would be valuable for further understanding of the potential clinical relevance of these findings.

6.2.2 Other tumour types and cell lines

Our study focused on breast cancer, mainly with the use of MCF7 cells. These represent only a small subset of the types of breast cancer that exist. For future work there is the opportunity to form spheroids from other breast cancer cell lines and investigate whether the transcriptomic changes presented in this project are also observed in different types of breast cancers.

Furthermore, results of pan-cancer analyses conducted in the online KMplotter tool also revealed that increased *ACTL8* expression was strongly correlated with poor patient survival outcomes in some other tumour types. These included: head-neck squamous cell carcinoma (HR = 1.4; p-value = 0.014), kidney renal clear cell carcinoma (HR = 2.27; p-value = 7.5×10^{-8}), kidney renal papillary cell carcinoma (HR = 3.02; p-value = 1.6×10^{-4}), liver hepatocellular carcinoma (HR = 1.6; p-value = 0.007), and uterine corpus endometrial carcinoma (HR = 2.42; p-value = 4.3×10^{-5}) for overall survival outcomes (Table 5.4). These represent viable candidates for other tumour types that could be used for further investigations into impacts of interstitial flow, and also

candidates to confirm whether *ACTL8* transcripts and/or protein expression are upregulated by flow.

6.2.3 Experimental conditions

We conducted experiments in flow up to a timepoint of 72h and even as early as 24h significant transcriptomic changes were identified. Protein expression experiments did not yield significant results but in some cases, trends were evident which may have been biologically significant, if not statistically. It is possible that changes seen at transcript level require more time to be detected as changes translated to protein expression. More so, some of the low-level FC's that were observed for some transcripts examined may be more significantly produced at longer timepoints.

This work has also identified the importance of hypoxia as a physiology that needs to be incorporated into future experimental designs. As described previously, the results of static vs flow experiments conducted in hypoxia were not conclusive and would benefit from larger sample sizes. Therefore, continuing work with the flow cell 2 chip is being conducted in hypoxia to further elucidate the relationship between hypoxia and IFF.

6.2.4 Phenotypic investigations

Investigations into phenotypes that could be linked to IFF were described in section 6.1.2, including the use of ATR inhibitors and other DNA damage inducing agents, such as chemotherapeutics. Recovery from radiation treatment would also be a valuable future direction to pursue to assess whether IFF can aid in radio-resistance. Findings such as these would be clinically relevant for determining treatment options in tumours known to have significantly altered IFF.

6.2.5 Hypoxia, IFF, and associated gene expression

The results of the static vs flow experiments conducted in hypoxia were inconclusive as to whether DNA damage response and upregulation of repair/replication genes was a result of flow or perhaps something else like ROS, involved in HIF signalling pathways. To that end, It would be useful to try harvesting spheroids after exposure to flow and disassociating them to use for FACS analysis, which could help identify ROS levels.

Analysis of ACTL8 expression against hypoxia metagene scores also revealed that *ACTL8* expression was positively correlated with hypoxia gene signatures. This was preliminary, *in silico* work but warrants further investigation.

6.2.6 RNA-seq dataset

As mentioned before, the results produced by RNA-seq analysis of MCF7 static and flow spheroid transcriptomes yielded a high volume of differentially expressed genes and we did not assess all of them extensively. We restricted our focus to protein-coding genes, but there is much more to be explored in the dataset such as differential expression of microRNAs.

6.2.7 Microfluidic device advancements

The flow cell 2 system developed and used in this work served as a useful tool for investigating IFF effects on spheroids. However, as discussed in previous sections it did not address the impact of pressure in the TME or even in the system itself. There are preliminary investigations into the role of pressure in the TME in the literature and our device could be well poised to also examine this area of unmet need (Lunt et al., 2008; Azimi et al., 2020). Therefore, a helpful next step in this work would be to characterise the pressure gradients in the flow cell 2 system, perhaps with the use of computer-based modelling. There are also microfluidic tools such as valves which could be used for controlling pressure in the system through the tubing and these were not explored in the reported work.

6.3 Conclusions

Using a spheroid on-chip microfluidic system refined for the purposes of housing cancer spheroids in a continuous flow environment, a novel set of transcriptomic changes occurring in cancer spheroids exposed to interstitial-like flow were identified. These transcriptomic changes and patterns of differential regulation as a result of flow are the first we know of in cancer cell spheroids. A candidate gene, *ACTL8*, was also identified which could potentially serve as a biomarker of interstitial flow, marking the early changes associated with this physiology in a TME. The predictive and prognostic value of *ACTL8* was shown to be strong in breast cancer, and preliminary pan-cancer analyses identified candidates for other tumour types to explore *ACTL8* expression further. These findings could benefit patient outcomes in the future if *ACTL8* expression is capable of indicating early changes in the TME associated with IFF and ultimately, poor prognoses. Information like this could arm clinicians and patients with prognostic and predictive insights about their disease earlier on. The flow cell 2 system we have developed and the initial findings on the impacts of interstitial flow on cancer cell biology we have presented are the foundation for future work to better our understanding of the role of interstitial fluid in cancer progression.

References

Aceto, N., Bardia, A., Miyamoto, D. T., Donaldson, M. C., Wittner, B. S., Spencer, J. A., Yu, M., Pely, A., Engstrom, A., Zhu, H., Brannigan, B. W., Kapur, R., Stott, S. L., Shioda, T., Ramaswamy, S., Ting, D. T., Lin, C. P., Toner, M., Haber, D. A. & Maheswaran, S. (2014) Circulating tumor cell clusters are oligoclonal precursors of breast cancer metastasis. *Cell*, 158(5), 1110-1122.

Ahmad, A. S., Ormiston-Smith, N. & Sasieni, P. D. (2015) Trends in the lifetime risk of developing cancer in Great Britain: comparison of risk for those born from 1930 to 1960. *Br J Cancer*, 112(5), 943-7.

Akay, M., Hite, J., Avci, N. G., Fan, Y., Akay, Y., Lu, G. & Zhu, J. J. (2018) Drug Screening of Human GBM Spheroids in Brain Cancer Chip. *Sci Rep*, 8(1), 15423.

Akincilar, S. C., Unal, B. & Tergaonkar, V. (2016) Reactivation of telomerase in cancer. *Cell Mol Life Sci*, 73(8), 1659-70.

Amin, A., Karpowicz, P. A., Carey, T. E., Arbiser, J., Nahta, R., Chen, Z. G., Dong, J. T., Kucuk, O., Khan, G. N., Huang, G. S., Mi, S., Lee, H. Y., Reichrath, J., Honoki, K., Georgakilas, A. G., Amedei, A., Amin, A., Helferich, B., Boosani, C. S., Ciriolo, M. R., Chen, S., Mohammed, S. I., Azmi, A. S., Keith, W. N., Bhakta, D., Halicka, D., Niccolai, E., Fujii, H., Aquilano, K., Ashraf, S. S., Nowsheen, S., Yang, X., Bilsland, A. & Shin, D. M. (2015) Evasion of anti-growth signaling: A key step in tumorigenesis and potential target for treatment and prophylaxis by natural compounds. *Semin Cancer Biol*, 35 Suppl, S55-S77.

Asting, A. G., Caren, H., Andersson, M., Lonnroth, C., Lagerstedt, K. & Lundholm, K. (2011) COX-2 gene expression in colon cancer tissue related to regulating factors and promoter methylation status. *BMC Cancer*, 11, 238.

Aukland, K. & Nicolaysen, G. (1981) Interstitial fluid volume: local regulatory mechanisms. *Physiol Rev*, 61(3), 556-643.

Aukland, K. & Reed, R. K. (1993) Interstitial-lymphatic mechanisms in the control of extracellular fluid volume. *Physiol Rev*, 73(1), 1-78.

Azimi, T., Loizidou, M. & Dwek, M. V. (2020) Cancer cells grown in 3D under fluid flow exhibit an aggressive phenotype and reduced responsiveness to the anti-cancer treatment doxorubicin. *Sci Rep*, 10(1), 12020.

Baranwal, S. & Alahari, S. K. (2009) Molecular mechanisms controlling E-cadherin expression in breast cancer. *Biochem Biophys Res Commun*, 384(1), 6-11.

Barisam, M., Saidi, M. S., Kashaninejad, N. & Nguyen, N. T. (2018) Prediction of Necrotic Core and Hypoxic Zone of Multicellular Spheroids in a Microbioreactor with a U-Shaped Barrier. *Micromachines (Basel)*, 9(3).

Bartha, A. & Gyorffy, B. (2021) TNMplot.com: A Web Tool for the Comparison of Gene Expression in Normal, Tumor and Metastatic Tissues. *Int J Mol Sci*, 22(5).

Bhowmick, N. A., Neilson, E. G. & Moses, H. L. (2004) Stromal fibroblasts in cancer initiation and progression. *Nature*, 432(7015), 332-7.

Brinkman, J. E. & Sharma, S. (2019) *Physiology, Body Fluids.* Available online: https://www.ncbi.nlm.nih.gov/books/NBK482447/ [Accessed.

Brown, J. M. & Giaccia, A. J. (1998) The unique physiology of solid tumors: opportunities (and problems) for cancer therapy. *Cancer Res*, 58(7), 1408-16.

Brown, J. M. & Wilson, W. R. (2004) Exploiting tumour hypoxia in cancer treatment. *Nat Rev Cancer*, 4(6), 437-47.

Buffa, F. M., Harris, A. L., West, C. M. & Miller, C. J. (2010) Large meta-analysis of multiple cancers reveals a common, compact and highly prognostic hypoxia metagene. *Br J Cancer*, 102(2), 428-35.

Carmeliet, P., Dor, Y., Herbert, J. M., Fukumura, D., Brusselmans, K., Dewerchin, M., Neeman, M., Bono, F., Abramovitch, R., Maxwell, P., Koch, C. J., Ratcliffe, P., Moons, L., Jain, R. K., Collen, D. & Keshert, E. (1998) Role of HIF-1alpha in hypoxia-mediated apoptosis, cell proliferation and tumour angiogenesis. *Nature*, 394(6692), 485-90.

Carter, C. L., Allen, C. & Henson, D. E. (1989) Relation of tumor size, lymph node status, and survival in 24,740 breast cancer cases. *Cancer*, 63(1), 181-7.

Chambers, K. F., Mosaad, E. M., Russell, P. J., Clements, J. A. & Doran, M. R. (2014) 3D Cultures of prostate cancer cells cultured in a novel high-throughput culture platform are more resistant to chemotherapeutics compared to cells cultured in monolayer. *PLoS One*, 9(11), e111029.

Chen, E. Y., Tan, C. M., Kou, Y., Duan, Q., Wang, Z., Meirelles, G. V., Clark, N. R. & Ma'ayan, A. (2013) Enrichr: interactive and collaborative HTML5 gene list enrichment analysis tool. *BMC Bioinformatics*, 14, 128.

Chen, M. B., Whisler, J. A., Frose, J., Yu, C., Shin, Y. & Kamm, R. D. (2017) On-chip human microvasculature assay for visualization and quantification of tumor cell extravasation dynamics. *Nat Protoc*, 12(5), 865-880.

Chen, Y. C., Lou, X., Zhang, Z., Ingram, P. & Yoon, E. (2015) High-Throughput Cancer Cell Sphere Formation for Characterizing the Efficacy of Photo Dynamic Therapy in 3D Cell Cultures. *Sci Rep*, 5, 12175.

Collins, T., Pyne, E., Christensen, M., Iles, A., Pamme, N. & Pires, I. M. (2021) Spheroid-on-chip microfluidic technology for the evaluation of the impact of continuous flow on metastatic potential in cancer models in vitro. *Biomicrofluidics*, 15(4), 044103.

Collins, T. C. (2019a) *Developing a Novel Spheroid-on-Chip Microfluidic Device for Investigations into Metastasis*. Doctor of Philosophy University of Hull, 05/2019. Available online: https://hydra.hull.ac.uk/resources/hull:17438 [Accessed.

Collins, T. C. (2019b) *Developing a Novel Spheroid-on-Chip Microfluidic Device for Investigations into Metastasis* Doctor of Philosophy University of Hull, 05/2019. Available online: https://hydra.hull.ac.uk/resources/hull:17438 [Accessed.

Cuzick, J., Swanson, G. P., Fisher, G., Brothman, A. R., Berney, D. M., Reid, J. E., Mesher, D., Speights, V. O., Stankiewicz, E., Foster, C. S., Moller, H., Scardino, P., Warren, J. D., Park, J., Younus, A., Flake, D. D., 2nd, Wagner, S., Gutin, A., Lanchbury, J. S., Stone, S. & Transatlantic Prostate, G. (2011) Prognostic value of an RNA expression signature derived from cell cycle proliferation genes in patients with prostate cancer: a retrospective study. *Lancet Oncol*, 12(3), 245-55.

Dafni, H., Israely, T., Bhujwalla, Z. M., Benjamin, L. E. & Neeman, M. (2002) Overexpression of vascular endothelial growth factor 165 drives peritumor interstitial convection and induces lymphatic drain: magnetic resonance imaging, confocal microscopy, and histological tracking of triple-labeled albumin. *Cancer Res*, 62(22), 6731-9.

Das, V., Kalita, J. & Pal, M. (2017) Predictive and prognostic biomarkers in colorectal cancer: A systematic review of recent advances and challenges. *Biomed Pharmacother*, 87, 8-19.

Daunys, S., Janoniene, A., Januskeviciene, I., Paskeviciute, M. & Petrikaite, V. (2021) 3D Tumor Spheroid Models for In Vitro Therapeutic Screening of Nanoparticles. *Adv Exp Med Biol*, 1295, 243-270.

Decker, E. M. (2001) The ability of direct fluorescence-based, two-colour assays to detect different physiological states of oral streptococci. *Lett Appl Microbiol*, 33(3), 188-92.

Dehne, E. M., Hasenberg, T. & Marx, U. (2017) The ascendance of microphysiological systems to solve the drug testing dilemma. *Future Sci OA*, 3(2), FSO185.

Denko, N. C. (2008) Hypoxia, HIF1 and glucose metabolism in the solid tumour. *Nat Rev Cancer*, 8(9), 705-13.

Denton, A. E., Roberts, E. W. & Fearon, D. T. (2018) Stromal Cells in the Tumor Microenvironment. *Adv Exp Med Biol*, 1060, 99-114.

Dydensborg, A. B., Herring, E., Auclair, J., Tremblay, E. & Beaulieu, J. F. (2006) Normalizing genes for quantitative RT-PCR in differentiating human intestinal epithelial cells and adenocarcinomas of the colon. *Am J Physiol Gastrointest Liver Physiol*, 290(5), G1067-74.

Edmondson, R., Broglie, J. J., Adcock, A. F. & Yang, L. (2014) Three-dimensional cell culture systems and their applications in drug discovery and cell-based biosensors. *Assay Drug Dev Technol*, 12(4), 207-18.

Eilenberger, C., Rothbauer, M., Selinger, F., Gerhartl, A., Jordan, C., Harasek, M., Schadl, B., Grillari, J., Weghuber, J., Neuhaus, W., Kupcu, S. & Ertl, P. (2021) A Microfluidic Multisize Spheroid Array for Multiparametric Screening of Anticancer Drugs and Blood-Brain Barrier Transport Properties. *Adv Sci (Weinh)*, 8(11), e2004856.

Elkin, E. B., Hudis, C., Begg, C. B. & Schrag, D. (2005) The effect of changes in tumor size on breast carcinoma survival in the U.S.: 1975-1999. *Cancer*, 104(6), 1149-57.

Fan, Q., Liu, R., Jiao, Y., Tian, C., Farrell, J. D., Diao, W., Wang, X., Zhang, F., Yuan, W., Han, H., Chen, J., Yang, Y., Zhang, X., Ye, F., Li, M., Ouyang, Z. & Liu, L. (2017) A novel 3-D bio-microfluidic system mimicking in vivo heterogeneous tumour microstructures reveals complex tumour-stroma interactions. *Lab Chip*, 17(16), 2852-2860.

Fang, J. H., Zhou, H. C., Zhang, C., Shang, L. R., Zhang, L., Xu, J., Zheng, L., Yuan, Y., Guo, R. P., Jia, W. H., Yun, J. P., Chen, M. S., Zhang, Y. & Zhuang, S. M. (2015) A novel vascular pattern promotes metastasis of hepatocellular carcinoma in an epithelial-mesenchymal transition-independent manner. *Hepatology*, 62(2), 452-65.

Favaro, E., Lord, S., Harris, A. L. & Buffa, F. M. (2011) Gene expression and hypoxia in breast cancer. *Genome Med*, 3(8), 55.

Fekete, J. T. & Gyorffy, B. (2019) ROCplot.org: Validating predictive biomarkers of chemotherapy/hormonal therapy/anti-HER2 therapy using transcriptomic data of 3,104 breast cancer patients. *Int J Cancer*, 145(11), 3140-3151.

Feng, C., Wang, H., Lu, N., Chen, T., He, H., Lu, Y. & Tu, X. M. (2014) Log-transformation and its implications for data analysis. *Shanghai Arch Psychiatry*, 26(2), 105-9.

Ferretti, S., Allegrini, P. R., Becquet, M. M. & McSheehy, P. M. (2009) Tumor interstitial fluid pressure as an early-response marker for anticancer therapeutics. *Neoplasia*, 11(9), 874-81.

Fidler, I. J. (1970) Metastasis: quantitative analysis of distribution and fate of tumor emboli labeled with 125 I-5-iodo-2'-deoxyuridine. *J Natl Cancer Inst*, 45(4), 773-82.

Fohlin, H., Bekkhus, T., Sandstrom, J., Fornander, T., Nordenskjold, B., Carstensen, J. & Stal, O. (2020) RAB6C is an independent prognostic factor of estrogen receptor-positive/progesterone receptor-negative breast cancer. *Oncol Lett*, 19(1), 52-60.

Freitas, I., Baronzio, G. F., Bono, B., Griffini, P., Bertone, V., Sonzini, N., Magrassi, G. R., Bonandrini, L. & Gerzeli, G. (1997) Tumor interstitial fluid: misconsidered component of the internal milieu of a solid tumor. *Anticancer Res*, 17(1A), 165-72.

Freund, J. B., Goetz, J. G., Hill, K. L. & Vermot, J. (2012) Fluid flows and forces in development: functions, features and biophysical principles. *Development*, 139(7), 1229-45.

Frohlich, E., Bonstingl, G., Hofler, A., Meindl, C., Leitinger, G., Pieber, T. R. & Roblegg, E. (2013) Comparison of two in vitro systems to assess cellular effects of nanoparticles-containing aerosols. *Toxicol In Vitro*, 27(1), 409-17.

Fuentes, N. & Silveyra, P. (2019) Estrogen receptor signaling mechanisms. *Adv Protein Chem Struct Biol*, 116, 135-170.

Fuh, K. F., Shepherd, R. D., Withell, J. S., Kooistra, B. K. & Rinker, K. D. (2021) Fluid flow exposure promotes epithelial-to-mesenchymal transition and adhesion of breast cancer cells to endothelial cells. *Breast Cancer Res*, 23(1), 97.

Gaggioli, C., Hooper, S., Hidalgo-Carcedo, C., Grosse, R., Marshall, J. F., Harrington, K. & Sahai, E. (2007) Fibroblast-led collective invasion of carcinoma cells with differing roles for RhoGTPases in leading and following cells. *Nat Cell Biol*, 9(12), 1392-400.

Galuschka, C., Proynova, R., Roth, B., Augustin, H. G. & Muller-Decker, K. (2017) Models in Translational Oncology: A Public Resource Database for Preclinical Cancer Research. *Cancer Res*, 77(10), 2557-2563.

Geiger, F., Schnitzler, L. G., Brugger, M. S., Westerhausen, C. & Engelke, H. (2022) Directed invasion of cancer cell spheroids inside 3D collagen matrices oriented by microfluidic flow in experiment and simulation. *PLoS One*, 17(3), e0264571.

Gilkes, D. M. & Semenza, G. L. (2013) Role of hypoxia-inducible factors in breast cancer metastasis. *Future Oncol*, 9(11), 1623-36.

Gleave, M. E., Hsieh, J. T., Wu, H. C., Hong, S. J., Zhau, H. E., Guthrie, P. D. & Chung, L. W. (1993) Epidermal growth factor receptor-mediated autocrine and paracrine stimulation of human transitional cell carcinoma. *Cancer Res*, 53(21), 5300-7.

Grimes, D. R., Kelly, C., Bloch, K. & Partridge, M. (2014) A method for estimating the oxygen consumption rate in multicellular tumour spheroids. *J R Soc Interface*, 11(92), 20131124.

Gullick, W. J. (1991) Prevalence of aberrant expression of the epidermal growth factor receptor in human cancers. *Br Med Bull*, 47(1), 87-98.

Gupta, G. P. & Massague, J. (2006) Cancer metastasis: building a framework. *Cell*, 127(4), 679-95.

Hamilton, G. (1998) Multicellular spheroids as an in vitro tumor model. *Cancer Lett*, 131(1), 29-34.

Han, Q., Sun, M. L., Liu, W. S., Zhao, H. S., Jiang, L. Y., Yu, Z. J. & Wei, M. J. (2019) Upregulated expression of ACTL8 contributes to invasion and metastasis and indicates poor prognosis in colorectal cancer. *Onco Targets Ther*, 12, 1749-1763.

Hanahan, D. & Weinberg, R. A. (2011) Hallmarks of cancer: the next generation. *Cell*, 144(5), 646-74.

Haque, R., Ahmed, S. A., Inzhakova, G., Shi, J., Avila, C., Polikoff, J., Bernstein, L., Enger, S. M. & Press, M. F. (2012) Impact of breast cancer subtypes and treatment on survival: an analysis spanning two decades. *Cancer Epidemiol Biomarkers Prev*, 21(10), 1848-55.

Heldring, N., Pike, A., Andersson, S., Matthews, J., Cheng, G., Hartman, J., Tujague, M., Strom, A., Treuter, E., Warner, M. & Gustafsson, J. A. (2007) Estrogen receptors: how do they signal and what are their targets. *Physiol Rev*, 87(3), 905-31.

Helle, E., Ampuja, M., Antola, L. & Kivela, R. (2020) Flow-Induced Transcriptomic Remodeling of Endothelial Cells Derived From Human Induced Pluripotent Stem Cells. *Front Physiol*, 11, 591450.

Henze, A. T. & Acker, T. (2010) Feedback regulators of hypoxia-inducible factors and their role in cancer biology. *Cell Cycle*, 9(14), 2749-63.

Herath, S., Razavi Bazaz, S., Monkman, J., Ebrahimi Warkiani, M., Richard, D., O'Byrne, K. & Kulasinghe, A. (2020) Circulating tumor cell clusters: Insights into tumour dissemination and metastasis. *Expert Rev Mol Diagn*, 20(11), 1139-1147.

Hidalgo, M., Amant, F., Biankin, A. V., Budinska, E., Byrne, A. T., Caldas, C., Clarke, R. B., de Jong, S., Jonkers, J., Maelandsmo, G. M., Roman-Roman, S., Seoane, J., Trusolino, L. & Villanueva, A. (2014) Patient-derived xenograft models: an emerging platform for translational cancer research. *Cancer Discov*, 4(9), 998-1013.

Holen, I., Speirs, V., Morrissey, B. & Blyth, K. (2017) In vivo models in breast cancer research: progress, challenges and future directions. *Dis Model Mech*, 10(4), 359-371.

Holliday, D. L. & Speirs, V. (2011) Choosing the right cell line for breast cancer research. *Breast Cancer Res*, 13(4), 215.

Hong, Y., Fang, F. & Zhang, Q. (2016) Circulating tumor cell clusters: What we know and what we expect (Review). *Int J Oncol*, 49(6), 2206-2216.

Huang, C. P., Lu, J., Seon, H., Lee, A. P., Flanagan, L. A., Kim, H. Y., Putnam, A. J. & Jeon, N. L. (2009) Engineering microscale cellular niches for three-dimensional multicellular co-cultures. *Lab Chip*, 9(12), 1740-8.

Hulka, B. S. & Wilcosky, T. (1988) Biological markers in epidemiologic research. *Arch Environ Health*, 43(2), 83-9.

Imamura, Y., Mukohara, T., Shimono, Y., Funakoshi, Y., Chayahara, N., Toyoda, M., Kiyota, N., Takao, S., Kono, S., Nakatsura, T. & Minami, H. (2015) Comparison of 2D- and 3D-culture models as drug-testing platforms in breast cancer. *Oncol Rep*, 33(4), 1837-43.

Itoh, Y. (2006) MT1-MMP: a key regulator of cell migration in tissue. *IUBMB Life*, 58(10), 589-96.

Iversen, P. O., Berggreen, E., Nicolaysen, G. & Heyeraas, K. (2001) Regulation of extracellular volume and interstitial fluid pressure in rat bone marrow. *Am J Physiol Heart Circ Physiol*, 280(4), H1807-13.

Jain, R. K. (1990) Physiological barriers to delivery of monoclonal antibodies and other macromolecules in tumors. *Cancer Res*, 50(3 Suppl), 814s-819s.

Jeon, J. S., Zervantonakis, I. K., Chung, S., Kamm, R. D. & Charest, J. L. (2013) In vitro model of tumor cell extravasation. *PLoS One*, 8(2), e56910.

Jeong, S. Y., Lee, J. H., Shin, Y., Chung, S. & Kuh, H. J. (2016) Co-Culture of Tumor Spheroids and Fibroblasts in a Collagen Matrix-Incorporated Microfluidic Chip Mimics Reciprocal Activation in Solid Tumor Microenvironment. *PLoS One*, 11(7), e0159013.

Jiang, H., Ju, Z. & Rudolph, K. L. (2007) Telomere shortening and ageing. *Z Gerontol Geriatr*, 40(5), 314-24.

Jo, U., Murai, Y., Takebe, N., Thomas, A. & Pommier, Y. (2021) Precision Oncology with Drugs Targeting the Replication Stress, ATR, and Schlafen 11. *Cancers (Basel)*, 13(18).

Jones, K. H. & Senft, J. A. (1985) An improved method to determine cell viability by simultaneous staining with fluorescein diacetate-propidium iodide. *J Histochem Cytochem*, 33(1), 77-9.

Joyce, J. A. & Pollard, J. W. (2009) Microenvironmental regulation of metastasis. *Nat Rev Cancer*, 9(4), 239-52.

Kalia, M. (2015) Biomarkers for personalized oncology: recent advances and future challenges. *Metabolism*, 64(3 Suppl 1), S16-21.

Katt, M. E., Placone, A. L., Wong, A. D., Xu, Z. S. & Searson, P. C. (2016) In Vitro Tumor Models: Advantages, Disadvantages, Variables, and Selecting the Right Platform. *Front Bioeng Biotechnol*, 4, 12.

Kidd, M. E., Shumaker, D. K. & Ridge, K. M. (2014) The role of vimentin intermediate filaments in the progression of lung cancer. *Am J Respir Cell Mol Biol*, 50(1), 1-6.

Kim, B. G., Kang, S., Han, H. H., Lee, J. H., Kim, J. E., Lee, S. H. & Cho, N. H. (2016a) Transcriptome-wide analysis of compression-induced microRNA expression alteration in breast cancer for mining therapeutic targets. *Oncotarget*, 7(19), 27468-78.

Kim, J. & Bae, J. S. (2016) Tumor-Associated Macrophages and Neutrophils in Tumor Microenvironment. *Mediators Inflamm*, 2016, 6058147.

Kim, J., Park, H., Kim, H., Kim, Y., Oh, H. J. & Chung, S. (2022) Microfluidic one-directional interstitial flow generation from cancer to cancer associated fibroblast. *Acta Biomater*, 144, 258-265.

Kim, S., Lee, H., Chung, M. & Jeon, N. L. (2013) Engineering of functional, perfusable 3D microvascular networks on a chip. *Lab Chip*, 13(8), 1489-500.

Kim, S. A., Inamura, K., Yamauchi, M., Nishihara, R., Mima, K., Sukawa, Y., Li, T., Yasunari, M., Morikawa, T., Fitzgerald, K. C., Fuchs, C. S., Wu, K., Chan, A. T., Zhang, X., Ogino, S. & Qian, Z. R. (2016b) Loss of CDH1 (E-cadherin) expression is associated with infiltrative tumour growth and lymph node metastasis. *Br J Cancer*, 114(2), 199-206.

Kimlin, L. C., Casagrande, G. & Virador, V. M. (2013) In vitro three-dimensional (3D) models in cancer research: an update. *Mol Carcinog*, 52(3), 167-82.

Kingsmore, K. M., Logsdon, D. K., Floyd, D. H., Peirce, S. M., Purow, B. W. & Munson, J. M. (2016) Interstitial flow differentially increases patient-derived glioblastoma stem cell invasion via CXCR4, CXCL12, and CD44-mediated mechanisms. *Integr Biol (Camb)*, 8(12), 1246-1260.

Kulic, A., Plavetic, N. D., Gamulin, S., Jakic-Razumovic, J., Vrbanec, D. & Sirotkovic-Skerlev, M. (2016) Telomerase activity in breast cancer patients: association with poor prognosis and more aggressive phenotype. *Med Oncol*, 33(3), 23.

Kunnen, S. J., Malas, T. B., Semeins, C. M., Bakker, A. D. & Peters, D. J. M. (2018) Comprehensive transcriptome analysis of fluid shear stress altered gene expression in renal epithelial cells. *J Cell Physiol*, 233(4), 3615-3628.

Kutikhin, A. G., Sinitsky, M. Y., Yuzhalin, A. E. & Velikanova, E. A. (2018) Shear stress: An essential driver of endothelial progenitor cells. *J Mol Cell Cardiol*, 118, 46-69.

Lanczky, A. & Gyorffy, B. (2021) Web-Based Survival Analysis Tool Tailored for Medical Research (KMplot): Development and Implementation. *J Med Internet Res*, 23(7), e27633.

Lanz, H. L., Saleh, A., Kramer, B., Cairns, J., Ng, C. P., Yu, J., Trietsch, S. J., Hankemeier, T., Joore, J., Vulto, P., Weinshilboum, R. & Wang, L. (2017) Therapy response testing of breast cancer in a 3D high-throughput perfused microfluidic platform. *BMC Cancer*, 17(1), 709.

Lee, H. J., Diaz, M. F., Price, K. M., Ozuna, J. A., Zhang, S., Sevick-Muraca, E. M., Hagan, J. P. & Wenzel, P. L. (2017) Fluid shear stress activates YAP1 to promote cancer cell motility. *Nat Commun*, 8, 14122.

Leong, S. P., Cady, B., Jablons, D. M., Garcia-Aguilar, J., Reintgen, D., Jakub, J., Pendas, S., Duhaime, L., Cassell, R., Gardner, M., Giuliano, R., Archie, V., Calvin, D., Mensha, L., Shivers, S., Cox, C., Werner, J. A., Kitagawa, Y. & Kitajima, M. (2006) Clinical patterns of metastasis. *Cancer Metastasis Rev*, 25(2), 221-32.

Li, B., Zhu, J. & Meng, L. (2019) High expression of ACTL8 is poor prognosis and accelerates cell progression in head and neck squamous cell carcinoma. *Mol Med Rep*, 19(2), 877-884.

Liu, J., Bi, X., Chen, T., Zhang, Q., Wang, S. X., Chiu, J. J., Liu, G. S., Zhang, Y., Bu, P. & Jiang, F. (2015) Shear stress regulates endothelial cell autophagy via redox regulation and Sirt1 expression. *Cell Death Dis*, 6, e1827.

Liu, J., Lichtenberg, T., Hoadley, K. A., Poisson, L. M., Lazar, A. J., Cherniack, A. D., Kovatich, A. J., Benz, C. C., Levine, D. A., Lee, A. V., Omberg, L., Wolf, D. M., Shriver, C. D., Thorsson, V., Cancer Genome Atlas Research, N. & Hu, H. (2018) An Integrated TCGA Pan-Cancer Clinical Data Resource to Drive High-Quality Survival Outcome Analytics. *Cell*, 173(2), 400-416 e11.

Liu, Z. G. & Jiao, D. (2019) Necroptosis, tumor necrosis and tumorigenesis. *Cell Stress*, 4(1), 1-8.

Livak, K. J. & Schmittgen, T. D. (2001) Analysis of relative gene expression data using real-time quantitative PCR and the 2(-Delta Delta C(T)) Method. *Methods*, 25(4), 402-8.

Love, R. R. (2010) Global cancer research initiative. *Cancer Manag Res*, 2, 105-9.

Lu, L., Zeng, H., Gu, X. & Ma, W. (2015) Circulating tumor cell clusters-associated gene plakoglobin and breast cancer survival. *Breast Cancer Res Treat*, 151(3), 491-500.

Luca, A. C., Mersch, S., Deenen, R., Schmidt, S., Messner, I., Schafer, K. L., Baldus, S. E., Huckenbeck, W., Piekorz, R. P., Knoefel, W. T., Krieg, A. & Stoecklein, N. H. (2013) Impact of the 3D microenvironment on phenotype, gene expression, and EGFR inhibition of colorectal cancer cell lines. *PLoS One*, 8(3), e59689.

Lundberg, A., Lindstrom, L. S., Harrell, J. C., Falato, C., Carlson, J. W., Wright, P. K., Foukakis, T., Perou, C. M., Czene, K., Bergh, J. & Tobin, N. P. (2017) Gene Expression Signatures and Immunohistochemical Subtypes Add Prognostic Value to Each Other in Breast Cancer Cohorts. *Clin Cancer Res*, 23(24), 7512-7520.

Lunt, S. J., Fyles, A., Hill, R. P. & Milosevic, M. (2008) Interstitial fluid pressure in tumors: therapeutic barrier and biomarker of angiogenesis. *Future Oncol*, 4(6), 793-802.

Makridakis, M. & Vlahou, A. (2010) Secretome proteomics for discovery of cancer biomarkers. *J Proteomics*, 73(12), 2291-305.

Masters, J. R. & Stacey, G. N. (2007) Changing medium and passaging cell lines. *Nat Protoc*, 2(9), 2276-84.

McCloy, R. A., Rogers, S., Caldon, C. E., Lorca, T., Castro, A. & Burgess, A. (2014) Partial inhibition of Cdk1 in G 2 phase overrides the SAC and decouples mitotic events. *Cell Cycle*, 13, 1400–1412.

McKeown, S. R. (2014) Defining normoxia, physoxia and hypoxia in tumours-implications for treatment response. *Br J Radiol*, 87(1035), 20130676.

Mehlen, P. & Puisieux, A. (2006a) Metastasis: a question of life or death. *Nature reviews cancer*, 6, 449-458.

Mehlen, P. & Puisieux, A. (2006b) Metastasis: a question of life or death. *Nat Rev Cancer*, 6(6), 449-58.

Mehta, G., Hsiao, A. Y., Ingram, M., Luker, G. D. & Takayama, S. (2012) Opportunities and challenges for use of tumor spheroids as models to test drug delivery and efficacy. *J Control Release*, 164(2), 192-204.

Mehta, P., Rahman, Z., Ten Dijke, P. & Boukany, P. E. (2022) Microfluidics meets 3D cancer cell migration. *Trends Cancer*.

Meijer, T. G., Naipal, K. A., Jager, A. & van Gent, D. C. (2017) Ex vivo tumor culture systems for functional drug testing and therapy response prediction. *Future Sci OA*, 3(2), FSO190.

Mentlein, R., Forstreuter, F., Mehdorn, H. M. & Held-Feindt, J. (2004) Functional significance of vascular endothelial growth factor receptor expression on human glioma cells. *J Neurooncol*, 67(1-2), 9-18.

Miki, Y., Swensen, J., Shattuck-Eidens, D., Futreal, P. A., Harshman, K., Tavtigian, S., Liu, Q., Cochran, C., Bennett, L. M., Ding, W. & et al. (1994) A strong candidate for the breast and ovarian cancer susceptibility gene BRCA1. *Science*, 266(5182), 66-71.

Milosevic, M., Fyles, A., Hedley, D. & Hill, R. (2004) The human tumor microenvironment: invasive (needle) measurement of oxygen and interstitial fluid pressure. *Semin Radiat Oncol*, 14(3), 249-58.

Minchinton, A. I. & Tannock, I. F. (2006) Drug penetration in solid tumours. *Nat Rev Cancer*, 6(8), 583-92.

Monteiro, M. V., Gaspar, V. M., Ferreira, L. P. & Mano, J. F. (2020) Hydrogel 3D in vitro tumor models for screening cell aggregation mediated drug response. *Biomater Sci*, 8(7), 1855-1864.

Muller, H. & Helin, K. (2000) The E2F transcription factors: key regulators of cell proliferation. *Biochim Biophys Acta*, 1470(1), M1-12.

Munson, J. M., Bellamkonda, R. V. & Swartz, M. A. (2013) Interstitial flow in a 3D microenvironment increases glioma invasion by a CXCR4-dependent mechanism. *Cancer Res*, 73(5), 1536-46.

Munson, J. M. & Shieh, A. C. (2014) Interstitial fluid flow in cancer: implications for disease progression and treatment. *Cancer Manag Res*, 6, 317-28.

Muz, B., de la Puente, P., Azab, F. & Azab, A. K. (2015) The role of hypoxia in cancer progression, angiogenesis, metastasis, and resistance to therapy. *Hypoxia (Auckl)*, 3, 83-92.

Nathanson, S. D. & Nelson, L. (1994) Interstitial fluid pressure in breast cancer, benign breast conditions, and breast parenchyma. *Ann Surg Oncol*, 1(4), 333-8.

Naylor, S. (2003) Biomarkers: current perspectives and future prospects. *Expert Rev Mol Diagn*, 3(5), 525-9.

Neafsey, P. J., Boxenbaum, H., Ciraulo, D. A. & Fournier, D. J. (1989) A Gompertz age-specific mortality rate model of aging, hormesis, and toxicity: dose-response studies. *Drug Metab Rev*, 20(1), 111-50.

Nistico, P., Bissell, M. J. & Radisky, D. C. (2012) Epithelial-mesenchymal transition: general principles and pathological relevance with special emphasis on the role of matrix metalloproteinases. *Cold Spring Harb Perspect Biol*, 4(2).

Novak, C. M., Horst, E. N., Taylor, C. C., Liu, C. Z. & Mehta, G. (2019) Fluid shear stress stimulates breast cancer cells to display invasive and chemoresistant phenotypes while upregulating PLAU in a 3D bioreactor. *Biotechnol Bioeng*, 116(11), 3084-3097.

Nunes, A. S., Barros, A. S., Costa, E. C., Moreira, A. F. & Correia, I. J. (2019a) 3D tumor spheroids as in vitro models to mimic in vivo human solid tumors resistance to therapeutic drugs. *Biotechnol Bioeng*, 116(1), 206-226.

Nunes, A. S., Costa, E. C., Barros, A. S., de Melo-Diogo, D. & Correia, I. J. (2019b) Establishment of 2D Cell Cultures Derived From 3D MCF-7 Spheroids Displaying a Doxorubicin Resistant Profile. *Biotechnol J*, 14(4), e1800268.

Olumi, A. F., Grossfeld, G. D., Hayward, S. W., Carroll, P. R., Tlsty, T. D. & Cunha, G. R. (1999) Carcinoma-associated fibroblasts direct tumor progression of initiated human prostatic epithelium. *Cancer Res*, 59(19), 5002-11.

Onitilo, A. A., Engel, J. M., Greenlee, R. T. & Mukesh, B. N. (2009) Breast cancer subtypes based on ER/PR and Her2 expression: comparison of clinicopathologic features and survival. *Clin Med Res*, 7(1-2), 4-13.

Orimo, A., Gupta, P. B., Sgroi, D. C., Arenzana-Seisdedos, F., Delaunay, T., Naeem, R., Carey, V. J., Richardson, A. L. & Weinberg, R. A. (2005) Stromal fibroblasts present in invasive human breast carcinomas promote tumor growth and angiogenesis through elevated SDF-1/CXCL12 secretion. *Cell*, 121(3), 335-48.

Pages, G. & Pouyssegur, J. (2005) Transcriptional regulation of the Vascular Endothelial Growth Factor gene--a concert of activating factors. *Cardiovasc Res*, 65(3), 564-73.

Patra, K. C., Wang, Q., Bhaskar, P. T., Miller, L., Wang, Z., Wheaton, W., Chandel, N., Laakso, M., Muller, W. J., Allen, E. L., Jha, A. K., Smolen, G. A., Clasquin, M. F., Robey, B. & Hay, N. (2013) Hexokinase 2 is required for tumor initiation and maintenance and its systemic deletion is therapeutic in mouse models of cancer. *Cancer Cell*, 24(2), 213-228.

Paul-Samojedny, M., Kokocinska, D., Samojedny, A., Mazurek, U., Partyka, R., Lorenz, Z. & Wilczok, T. (2005) Expression of cell survival/death genes: Bcl-2 and Bax at the rate of colon cancer prognosis. *Biochim Biophys Acta*, 1741(1-2), 25-9.

Piotrowski-Daspit, A. S., Tien, J. & Nelson, C. M. (2016) Interstitial fluid pressure regulates collective invasion in engineered human breast tumors via Snail, vimentin, and E-cadherin. *Integr Biol (Camb)*, 8(3), 319-31.

Pires, I. M., Olcina, M. M., Anbalagan, S., Pollard, J. R., Reaper, P. M., Charlton, P. A., McKenna, W. G. & Hammond, E. M. (2012) Targeting radiation-resistant hypoxic tumour cells through ATR inhibition. *Br J Cancer*, 107(2), 291-9.

Poon, C. (2022) Measuring the density and viscosity of culture media for optimized computational fluid dynamics analysis of in vitro devices. *J Mech Behav Biomed Mater*, 126, 105024.

Poschl, J., Lorenz, A., Hartmann, W., von Bueren, A. O., Kool, M., Li, S., Peraud, A., Tonn, J. C., Herms, J., Xiang, M., Rutkowski, S., Kretzschmar, H. A. & Schuller, U. (2011) Expression of BARHL1 in medulloblastoma is associated with prolonged survival in mice and humans. *Oncogene*, 30(47), 4721-30.

Prat, A., Pineda, E., Adamo, B., Galvan, P., Fernandez, A., Gaba, L., Diez, M., Viladot, M., Arance, A. & Munoz, M. (2015) Clinical implications of the intrinsic molecular subtypes of breast cancer. *Breast*, 24 Suppl 2, S26-35.

Qazi, H., Shi, Z. D. & Tarbell, J. M. (2011) Fluid shear stress regulates the invasive potential of glioma cells via modulation of migratory activity and matrix metalloproteinase expression. *PLoS One*, 6(5), e20348.

Randolph, G. J., Angeli, V. & Swartz, M. A. (2005) Dendritic-cell trafficking to lymph nodes through lymphatic vessels. *Nat Rev Immunol*, 5(8), 617-28.

Reed, R. K. & Rubin, K. (2010) Transcapillary exchange: role and importance of the interstitial fluid pressure and the extracellular matrix. *Cardiovasc Res*, 87(2), 211-7.

Rizvi, I., Gurkan, U. A., Tasoglu, S., Alagic, N., Celli, J. P., Mensah, L. B., Mai, Z., Demirci, U. & Hasan, T. (2013) Flow induces epithelial-mesenchymal transition, cellular heterogeneity and biomarker modulation in 3D ovarian cancer nodules. *Proc Natl Acad Sci U S A*, 110(22), E1974-83.

Ro, J., Kim, J. & Cho, Y. K. (2022) Recent advances in spheroid-based microfluidic models to mimic the tumour microenvironment. *Analyst*, 147(10), 2023-2034.

Rodriguez-Antona, C. & Taron, M. (2015) Pharmacogenomic biomarkers for personalized cancer treatment. *J Intern Med*, 277(2), 201-217.

Rofstad, E. K., Galappathi, K. & Mathiesen, B. S. (2014) Tumor interstitial fluid pressure-a link between tumor hypoxia, microvascular density, and lymph node metastasis. *Neoplasia*, 16(7), 586-94.

Rofstad, E. K., Gaustad, J. V., Brurberg, K. G., Mathiesen, B., Galappathi, K. & Simonsen, T. G. (2009) Radiocurability is associated with interstitial fluid pressure in human tumor xenografts. *Neoplasia*, 11(11), 1243-51.

Ruppen, J., Cortes-Dericks, L., Marconi, E., Karoubi, G., Schmid, R. A., Peng, R., Marti, T. M. & Guenat, O. T. (2014) A microfluidic platform for chemoresistive testing of multicellular pleural cancer spheroids. *Lab Chip*, 14(6), 1198-205.

Ruppen, J., Wildhaber, F. D., Strub, C., Hall, S. R., Schmid, R. A., Geiser, T. & Guenat, O. T. (2015) Towards personalized medicine: chemosensitivity assays of patient lung cancer cell spheroids in a perfused microfluidic platform. *Lab Chip*, 15(14), 3076-85.

Sadeghi, F., Asgari, M., Matloubi, M., Ranjbar, M., Karkhaneh Yousefi, N., Azari, T. & Zaki-Dizaji, M. (2020) Molecular contribution of BRCA1 and BRCA2 to genome instability in breast cancer patients: review of radiosensitivity assays. *Biol Proced Online*, 22, 23.

Sakai, Y., Hattori, K., Yanagawa, F., Sugiura, S., Kanamori, T. & Nakazawa, K. (2014) Detachably assembled microfluidic device for perfusion culture and post-culture analysis of a spheroid array. *Biotechnol J*, 9(7), 971-9.

Salavati, H., Debbaut, C., Pullens, P. & Ceelen, W. (2022) Interstitial fluid pressure as an emerging biomarker in solid tumors. *Biochim Biophys Acta Rev Cancer*, 1877(5), 188792.

Sarhadi, V. K. & Armengol, G. (2022) Molecular Biomarkers in Cancer. *Biomolecules*, 12(8).

Schlereth, K., Weichenhan, D., Bauer, T., Heumann, T., Giannakouri, E., Lipka, D., Jaeger, S., Schlesner, M., Aloy, P., Eils, R., Plass, C. & Augustin, H. G. (2018) The transcriptomic and epigenetic map of vascular quiescence in the continuous lung endothelium. *Elife*, 7.

Scott, P. V., Horton, J. N. & Mapleson, W. W. (1971) Leakage of oxygen from blood and water samples stored in plastic and glass syringes. *Br Med J*, 3(5773), 512-6.

Semenza, G. L. (2003) Targeting HIF-1 for cancer therapy. *Nat Rev Cancer*, 3(10), 721-32.

Shah, A. D., Bouchard, M. J. & Shieh, A. C. (2015) Interstitial Fluid Flow Increases Hepatocellular Carcinoma Cell Invasion through CXCR4/CXCL12 and MEK/ERK Signaling. *PLoS One*, 10(11), e0142337.

Shieh, A. C., Rozansky, H. A., Hinz, B. & Swartz, M. A. (2011) Tumor cell invasion is promoted by interstitial flow-induced matrix priming by stromal fibroblasts. *Cancer Res*, 71(3), 790-800.

Shields, J. D., Fleury, M. E., Yong, C., Tomei, A. A., Randolph, G. J. & Swartz, M. A. (2007) Autologous chemotaxis as a mechanism of tumor cell homing to lymphatics via interstitial flow and autocrine CCR7 signaling. *Cancer Cell*, 11(6), 526-38.

Song, J. W. & Munn, L. L. (2011) Fluid forces control endothelial sprouting. *Proc Natl Acad Sci U S A*, 108(37), 15342-7.

Spruance, S. L., Reid, J. E., Grace, M. & Samore, M. (2004) Hazard ratio in clinical trials. *Antimicrob Agents Chemother*, 48(8), 2787-92.

Srinivas, U. S., Tan, B. W. Q., Vellayappan, B. A. & Jeyasekharan, A. D. (2019) ROS and the DNA damage response in cancer. *Redox Biol*, 25, 101084.

Sun, W., Ma, J., Wu, S., Yang, D., Yan, Y., Liu, K., Wang, J., Sun, L., Chen, N., Wei, H., Zhu, Y., Xing, B., Zhao, X., Qian, X., Jiang, Y. & He, F. (2010) Characterization of the liver tissue interstitial fluid (TIF) proteome indicates potential for application in liver disease biomarker discovery. *J Proteome Res*, 9(2), 1020-31.

Sung, H., Ferlay, J., Siegel, R. L., Laversanne, M., Soerjomataram, I., Jemal, A. & Bray, F. (2021) Global Cancer Statistics 2020: GLOBOCAN Estimates of Incidence and Mortality Worldwide for 36 Cancers in 185 Countries. *CA Cancer J Clin*, 71(3), 209-249.

Sung, K. E., Yang, N., Pehlke, C., Keely, P. J., Eliceiri, K. W., Friedl, A. & Beebe, D. J. (2011) Transition to invasion in breast cancer: a microfluidic in vitro model enables examination of spatial and temporal effects. *Integr Biol (Camb)*, 3(4), 439-50.

Tazzyman, S., Niaz, H. & Murdoch, C. (2013) Neutrophil-mediated tumour angiogenesis: subversion of immune responses to promote tumour growth. *Semin Cancer Biol*, 23(3), 149-58.

Tchafa, A. M., Ta, M., Reginato, M. J. & Shieh, A. C. (2015) EMT Transition Alters Interstitial Fluid Flow-Induced Signaling in ERBB2-Positive Breast Cancer Cells. *Mol Cancer Res*, 13(4), 755-64.

Teng, M. W., Swann, J. B., Koebel, C. M., Schreiber, R. D. & Smyth, M. J. (2008) Immune-mediated dormancy: an equilibrium with cancer. *J Leukoc Biol*, 84(4), 988-93.

Thurston, G. (1976) Viscosity and viscoelasticity of blood in small diameter tubes. *Microvasular Research* 11, 133 146

Torisawa, Y. S., Mosadegh, B., Bersano-Begey, T., Steele, J. M., Luker, K. E., Luker, G. D. & Takayama, S. (2010) Microfluidic platform for chemotaxis in gradients formed by CXCL12 source-sink cells. *Integr Biol (Camb)*, 2(11-12), 680-6.

Trujillo-de Santiago, G., Flores-Garza, B. G., Tavares-Negrete, J. A., Lara-Mayorga, I. M., Gonzalez-Gamboa, I., Zhang, Y. S., Rojas-Martinez, A., Ortiz-Lopez, R. & Alvarez, M. M. (2019) The Tumor-on-Chip: Recent Advances in the Development of Microfluidic Systems to Recapitulate the Physiology of Solid Tumors. *Materials (Basel)*, 12(18).

Valastyan, S. & Weinberg, R. A. (2011) Tumor metastasis: molecular insights and evolving paradigms. *Cell*, 147(2), 275-92.

Vaupel, P. (2004) The role of hypoxia-induced factors in tumor progression. *Oncologist*, 9 Suppl 5, 10-7.

Vaupel, P., Mayer, A. & Hockel, M. (2004) Tumor hypoxia and malignant progression. *Methods Enzymol*, 381, 335-54.

Velu, T. J., Beguinot, L., Vass, W. C., Willingham, M. C., Merlino, G. T., Pastan, I. & Lowy, D. R. (1987) Epidermal-growth-factor-dependent transformation by a human EGF receptor proto-oncogene. *Science*, 238(4832), 1408-10.

Vinci, M., Gowan, S., Boxall, F., Patterson, L., Zimmermann, M., Court, W., Lomas, C., Mendiola, M., Hardisson, D. & Eccles, S. A. (2012) Advances in establishment and analysis of three-dimensional tumor spheroid-based functional assays for target validation and drug evaluation. *BMC Biol*, 10, 29.

Wagner, M. & Wiig, H. (2015) Tumor Interstitial Fluid Formation, Characterization, and Clinical Implications. *Front Oncol*, 5, 115.

Wagner, P. D., Verma, M. & Srivastava, S. (2004) Challenges for biomarkers in cancer detection. *Ann N Y Acad Sci*, 1022, 9-16.

Wang, T. H., Hsia, S. M. & Shieh, T. M. (2016) Lysyl Oxidase and the Tumor Microenvironment. *Int J Mol Sci*, 18(1).

Wang, Y., Shi, J., Chai, K., Ying, X. & Zhou, B. P. (2013) The Role of Snail in EMT and Tumorigenesis. *Curr Cancer Drug Targets*, 13(9), 963-972.

Warburg, O. (1956) On respiratory impairment in cancer cells. *Science*, 124(3215), 269-70.

Wculek, S. K. & Malanchi, I. (2015) Neutrophils support lung colonization of metastasis-initiating breast cancer cells. *Nature*, 528(7582), 413-7.

Westermarck, J. & Kahari, V. M. (1999) Regulation of matrix metalloproteinase expression in tumor invasion. *FASEB J*, 13(8), 781-92.

Whitesides, G. M. (2006) The origins and the future of microfluidics. *Nature*, 442(7101), 368-73.

Wiig, H. & Swartz, M. A. (2012) Interstitial fluid and lymph formation and transport: physiological regulation and roles in inflammation and cancer. *Physiol Rev*, 92(3), 1005-60.

Williams, K. J., Cowen, R. L. & Stratford, I. J. (2001) Hypoxia and oxidative stress. Tumour hypoxia--therapeutic considerations. *Breast Cancer Res*, 3(5), 328-31.

Winkelman, M. A., Kim, D. Y., Kakarla, S., Grath, A., Silvia, N. & Dai, G. (2021) Interstitial flow enhances the formation, connectivity, and function of 3D brain microvascular networks generated within a microfluidic device. *Lab Chip*, 22(1), 170-192.

Winter, S. C., Buffa, F. M., Silva, P., Miller, C., Valentine, H. R., Turley, H., Shah, K. A., Cox, G. J., Corbridge, R. J., Homer, J. J., Musgrove, B., Slevin, N., Sloan, P., Price, P., West, C. M. & Harris, A. L. (2007) Relation of a hypoxia metagene derived from head and neck cancer to prognosis of multiple cancers. *Cancer Res*, 67(7), 3441-9.

Wirtz, D., Konstantopoulos, K. & Searson, P. C. (2011) The physics of cancer: the role of physical interactions and mechanical forces in metastasis. *Nat Rev Cancer*, 11(7), 512-22.

Wooster, R., Bignell, G., Lancaster, J., Swift, S., Seal, S., Mangion, J., Collins, N., Gregory, S., Gumbs, C. & Micklem, G. (1995) Identification of the breast cancer susceptibility gene BRCA2. *Nature*, 378(6559), 789-92.

Xie, Z., Bailey, A., Kuleshov, M. V., Clarke, D. J. B., Evangelista, J. E., Jenkins, S. L., Lachmann, A., Wojciechowicz, M. L., Kropiwnicki, E., Jagodnik, K. M., Jeon, M. & Ma'ayan, A. (2021) Gene Set Knowledge Discovery with Enrichr. *Curr Protoc*, 1(3), e90.

Xu, X., Farach-Carson, M. C. & Jia, X. (2014) Three-dimensional in vitro tumor models for cancer research and drug evaluation. *Biotechnol Adv*, 32(7), 1256-1268.

Xu, Z., Gao, Y., Hao, Y., Li, E., Wang, Y., Zhang, J., Wang, W., Gao, Z. & Wang, Q. (2013) Application of a microfluidic chip-based 3D co-culture to test drug sensitivity for individualized treatment of lung cancer. *Biomaterials*, 34(16), 4109-4117.

Xu, Z., Li, E., Guo, Z., Yu, R., Hao, H., Xu, Y., Sun, Z., Li, X., Lyu, J. & Wang, Q. (2016) Design and Construction of a Multi-Organ Microfluidic Chip Mimicking the in vivo Microenvironment of Lung Cancer Metastasis. *ACS Appl Mater Interfaces*, 8(39), 25840-25847.

Xue, H., Lu, B. & Lai, M. (2008) The cancer secretome: a reservoir of biomarkers. *J Transl Med*, 6, 52.

Yang, Y. & Xu, X. (2021) Bioinformatic identification of hub genes and related transcription factors in low shear stress treated endothelial cells. *BMC Med Genomics*, 14(1), 120.

Yao, J., Caballero, O. L., Yung, W. K., Weinstein, J. N., Riggins, G. J., Strausberg, R. L. & Zhao, Q. (2014) Tumor subtype-specific cancer-testis antigens as potential biomarkers and immunotherapeutic targets for cancers. *Cancer Immunol Res*, 2(4), 371-9.

Ye, Y., Hu, Q., Chen, H., Liang, K., Yuan, Y., Xiang, Y., Ruan, H., Zhang, Z., Song, A., Zhang, H., Liu, L., Diao, L., Lou, Y., Zhou, B., Wang, L., Zhou, S., Gao, J., Jonasch, E., Lin, S. H., Xia, Y., Lin, C., Yang, L., Mills, G. B., Liang, H. & Han, L. (2019) Characterization of Hypoxia-associated Molecular Features to Aid Hypoxia-Targeted Therapy. *Nat Metab*, 1(4), 431-444.

Young, J., Menetrey, J. & Goud, B. (2010) RAB6C is a retrogene that encodes a centrosomal protein involved in cell cycle progression. *J Mol Biol*, 397(1), 69-88.

Zervantonakis, I. K., Hughes-Alford, S. K., Charest, J. L., Condeelis, J. S., Gertler, F. B. & Kamm, R. D. (2012) Three-dimensional microfluidic model for tumor cell intravasation and endothelial barrier function. *Proc Natl Acad Sci U S A*, 109(34), 13515-20.

Zhang, W., Huang, X., Huang, R., Zhu, H., Ye, P., Lin, X., Zhang, S., Wu, M. & Jiang, F. (2022) MMP1 Overexpression Promotes Cancer Progression and Associates with Poor Outcome in Head and Neck Carcinoma. *Comput Math Methods Med*, 2022, 3058342.

Zheng, J. (2012) Energy metabolism of cancer: Glycolysis versus oxidative phosphorylation (Review). *Oncol Lett*, 4(6), 1151-1157.

Zou, K. H., O'Malley, A. J. & Mauri, L. (2007) Receiver-operating characteristic analysis for evaluating diagnostic tests and predictive models. *Circulation*, 115(5), 654-7.

Appendix 1

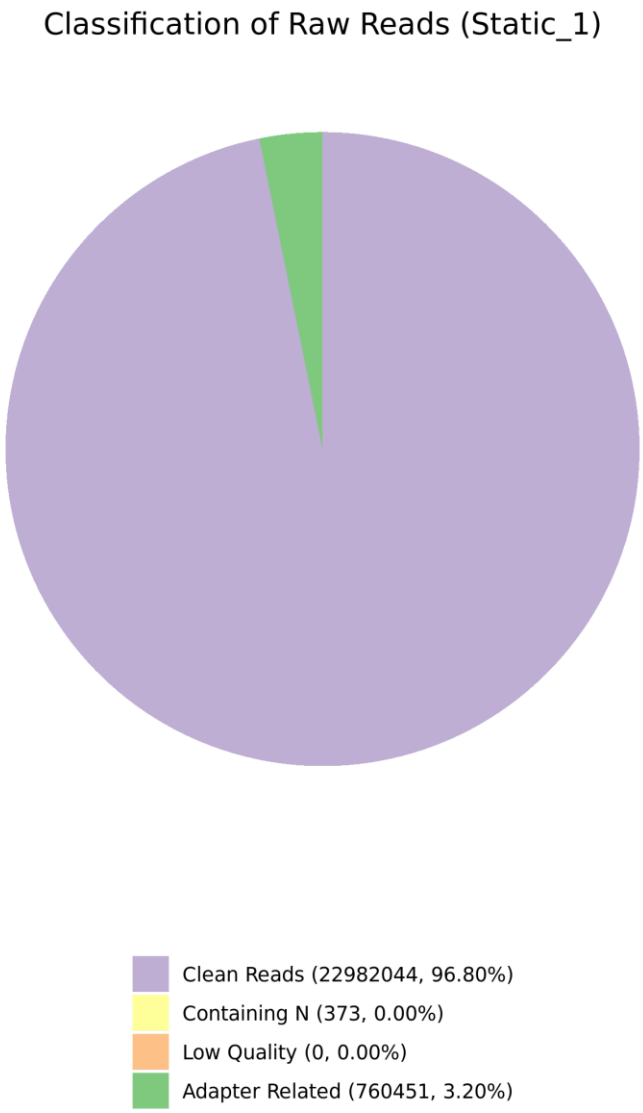

Appendix figure 1: Classification of raw reads in static "1" RNA-seq sample

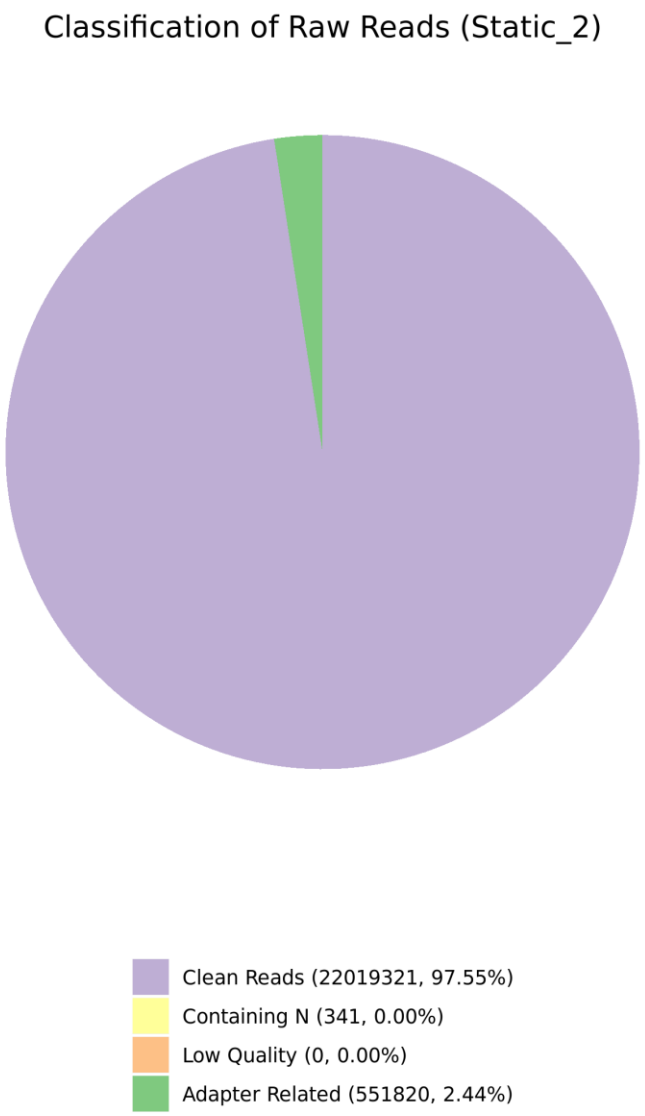

Appendix figure 2: Classification of raw reads in static "2" RNA-seq sample

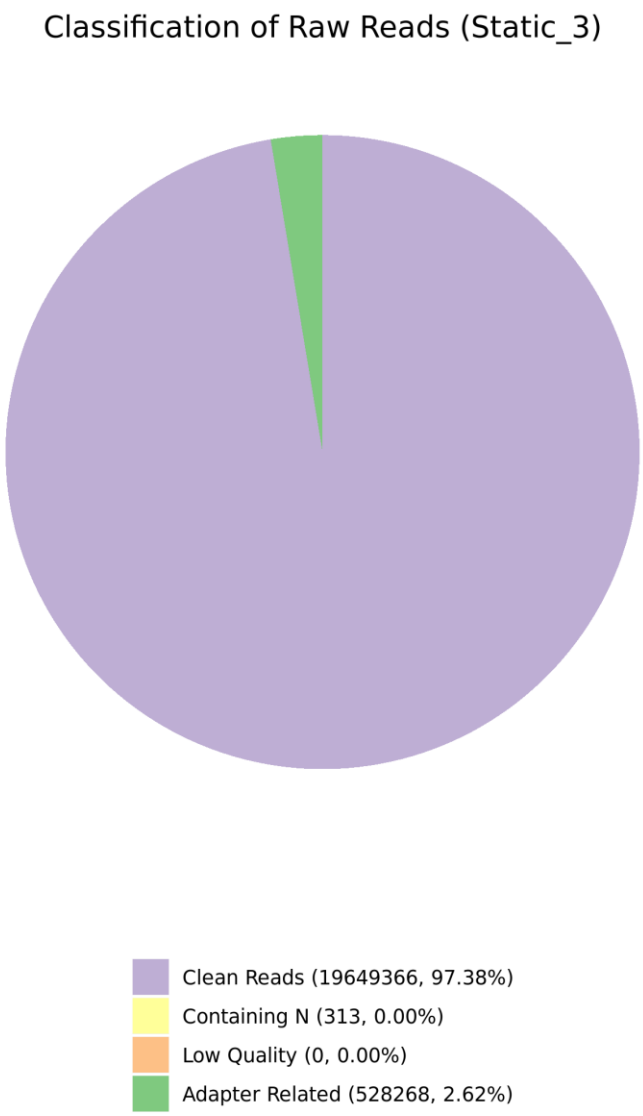

Appendix figure 3: Classification of raw reads in static "3" RNA-seq sample

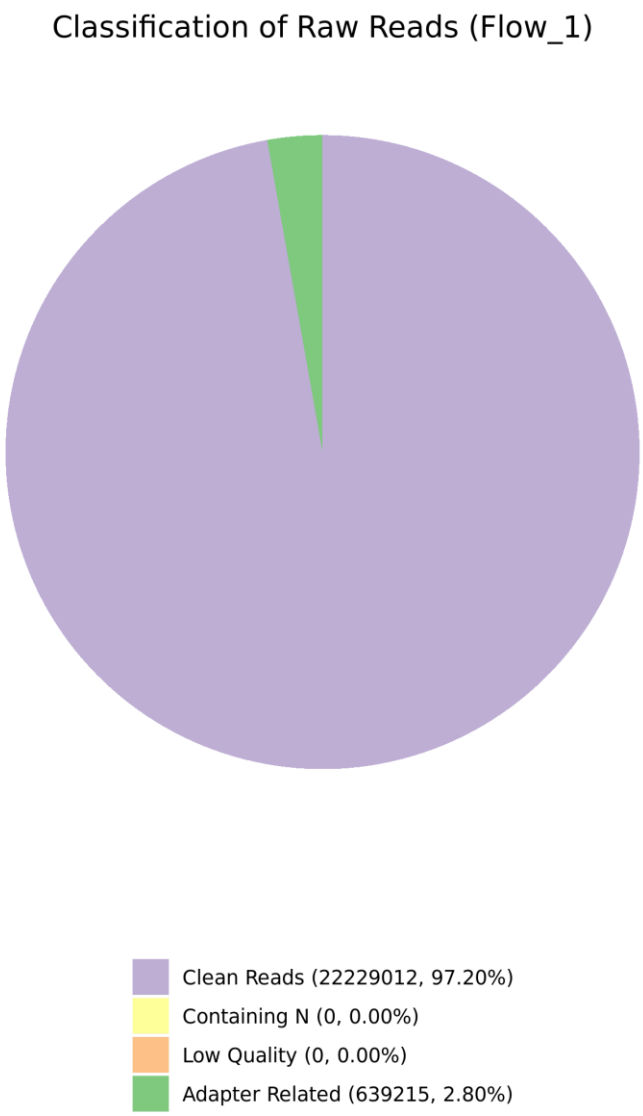

Appendix figure 4: Classification of raw reads in flow "1" RNA-seq sample

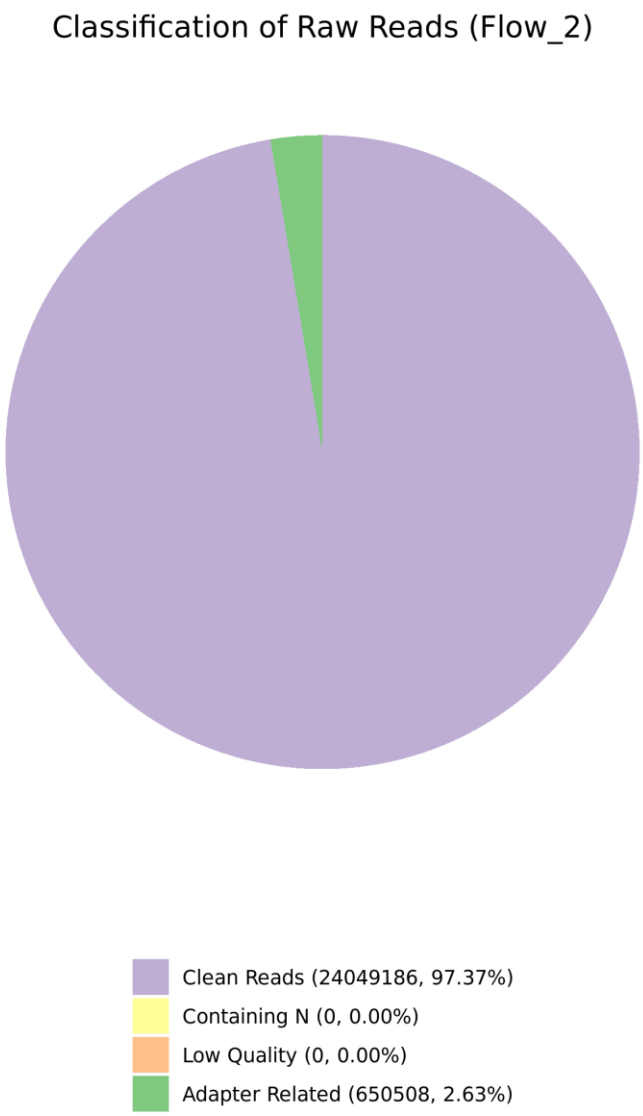

Appendix figure 5: Classification of raw reads in flow "2" RNA-seq sample

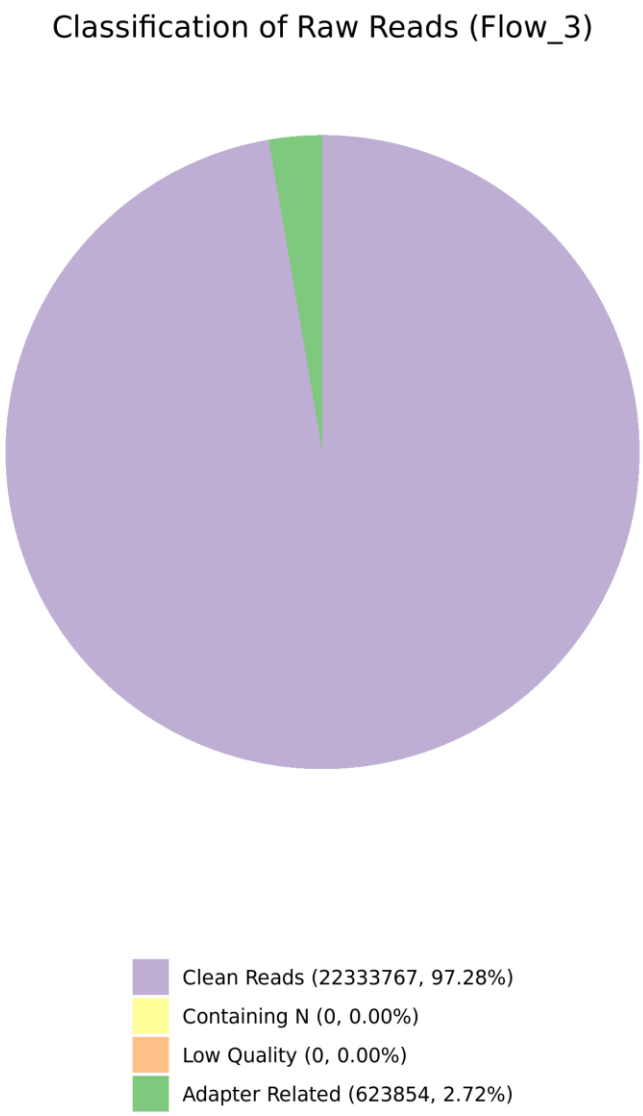

Appendix figure 6: Classification of raw reads in flow "3" RNA-seq sample

Appendix 2

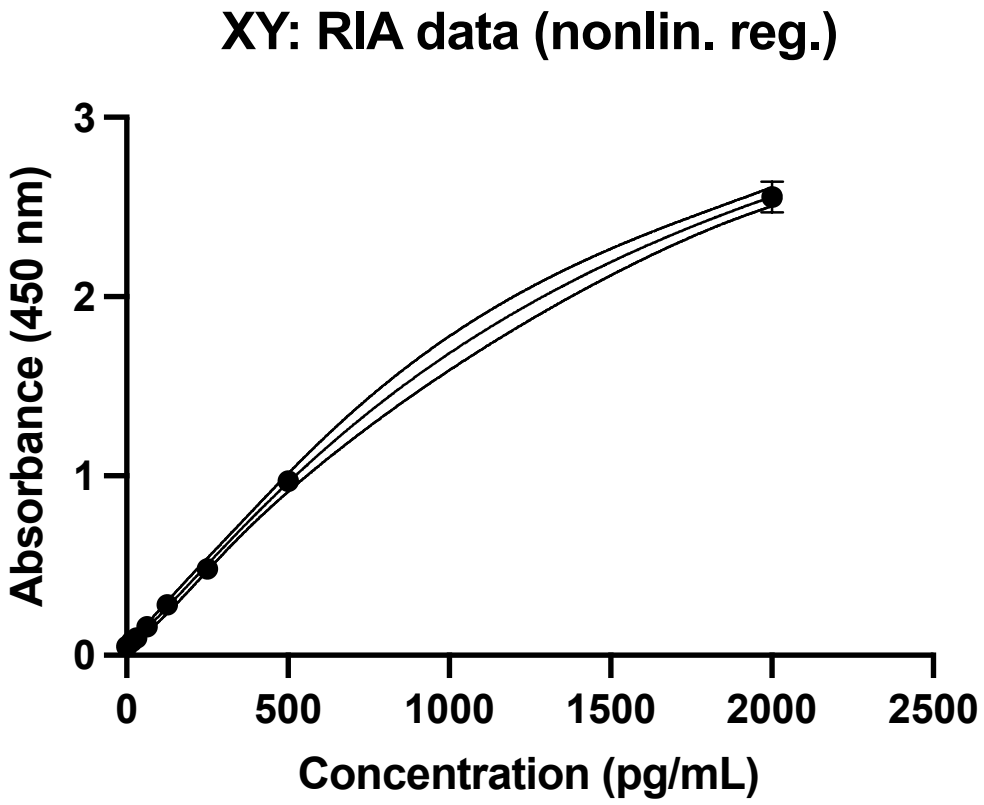

Appendix figure 7: VEGF ELISA standard curve

A standard curve was produced for VEGF, using kit procedures, to determine the levels of absorbance for VEGF present at different concentrations. The straight portion of the sigmoidal curve was used to determine the unknown concentration of VEGF present in effluent samples.

Appendix 3

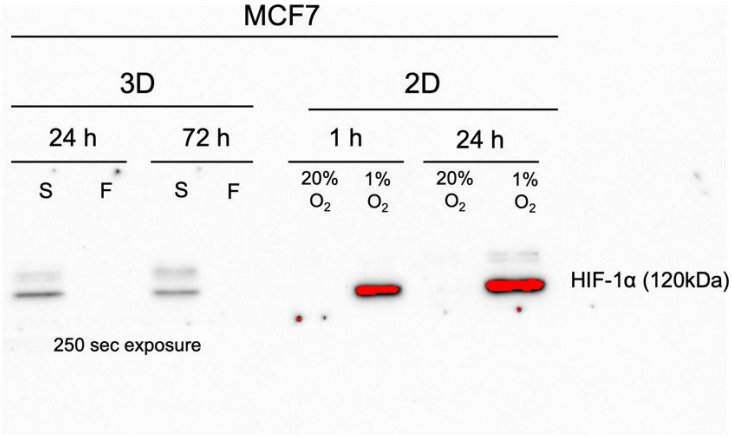

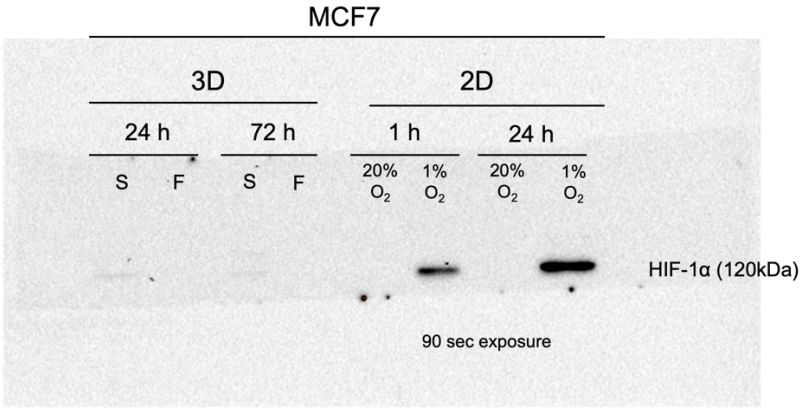

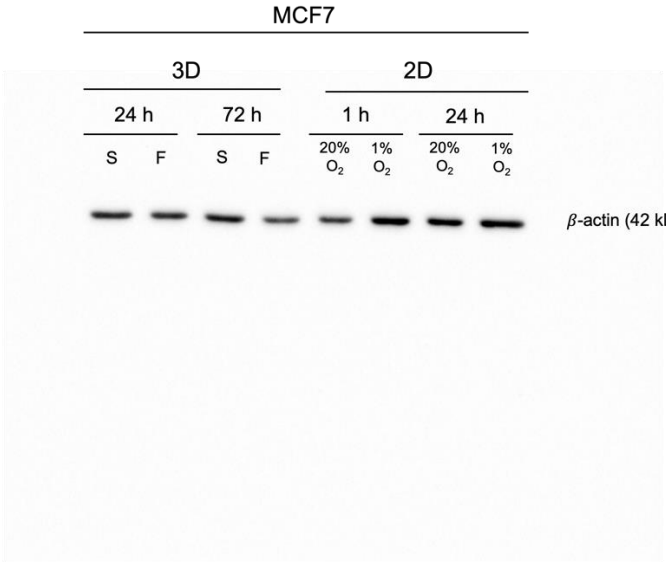

Appendix figure 9: HIF1-α Western blot original images for figure 4.19

MCF7 cells were seeded in a ULA plate with 9.0 x 10^4 cells per well. Spheroids were formed for 96h and kept in static (S) or flow (F) conditions for 24h and 72h. MCF7 cells were seeded in 6mm plastic dishes and allowed to adhere for 24h before either being transferred to a hypoxia chamber (1% O_2) or remaining in a cell culture incubator (20% O_2). Adherent cells (2D) were kept in these conditions for either 1h or 24h. 2D and 3D cell lysates were harvested at the end of experiments and protein was extracted, prepared, and run through an SDS-PAGE gel. 30 μg of protein was loaded per well. Then, Western blotting was used to visualise HIF-1α expression, with β- actin used as a loading control. Blots are representative of *n*=3 experiments.

Appendix 4

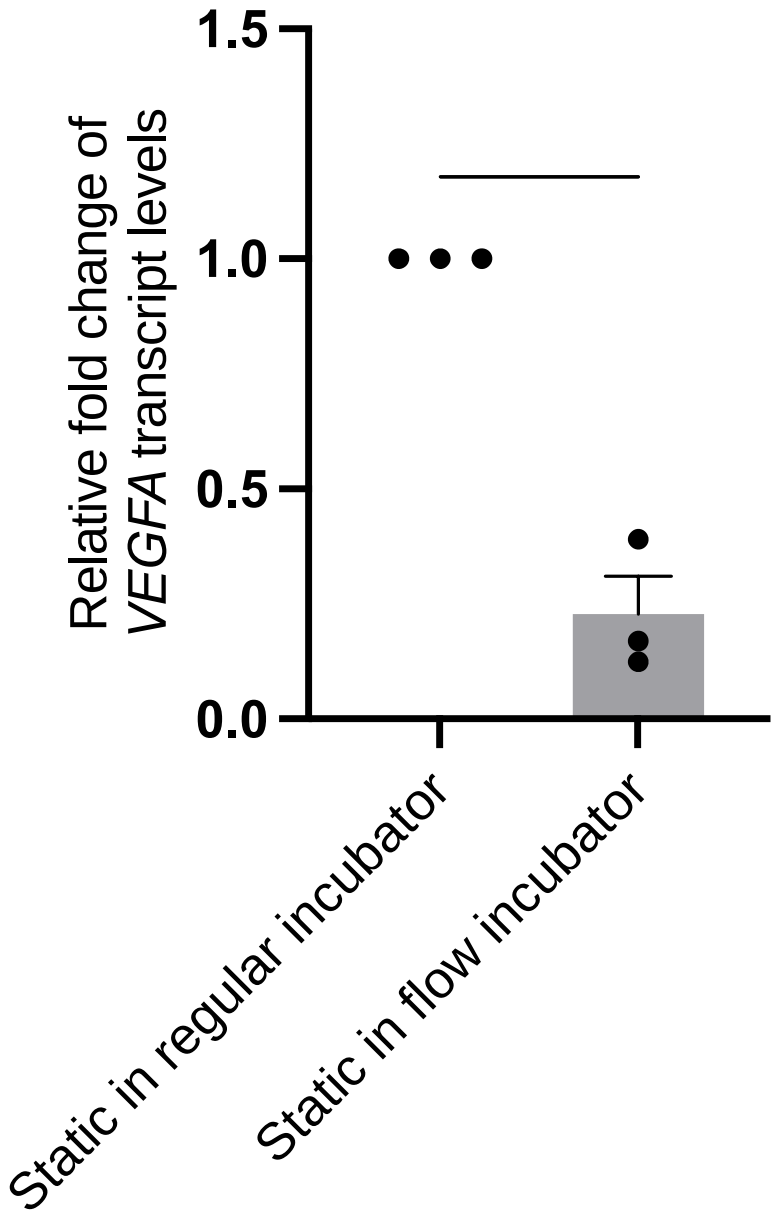

Appendix figure 8: VEGFA transcript levels in static spheroids in different incubators

MCF7 spheroids were formed from 9.0 x 104 cells seeded in a ULA plate and allowed to form for 96h. Spheroids were kept in a ULA plate, with Matrigel added to reflect standard static v. flow experiments. One plate was placed in the external "flow" incubator and the other kept in the standard cell culture incubator. Spheroids were kept in these conditions for 72h. Total RNA was extracted and used for qPCR analysis, with B2M as the housekeeping gene. Data represent the mean of n=3 experiments. Error bars represent mean ± SEM. Statistical significance was determined by paired student's t-tests; *p <0.05.